UNIVERSIDAD COMPLUTENSE DE MADRID
FACULTAD DE PSICOLOGÍA



TESIS DOCTORAL

Modelado computacional de la memoria episódica a nivel neuronal para contrastar la hipótesis de la desconexión en Alzheimer
Computational modeling of the neuronal basis of episodic memory to test the disconnection hypothesis in Alzheimer's

MEMORIA PARA OPTAR AL GRADO DE DOCTOR

PRESENTADA POR

Jesús Cabrera Álvarez

DIRIGIDA POR

Gianluca Susi
Fernando Maestú Unturbe

Madrid

© Jesús Cabrera Álvarez, 2024

UNIVERSIDAD COMPLUTENSE DE MADRID

FACULTAD DE PSICOLOGÍA



TESIS DOCTORAL

Modelado computacional de la memoria episódica a nivel neuronal para contrastar la hipótesis de la desconexión en Alzheimer

Computational modeling of the neuronal basis of episodic memory to test the disconnection hypothesis in Alzheimer's

MEMORIA PARA OPTAR AL GRADO DE DOCTOR

PRESENTADA POR

Jesús Cabrera Álvarez

DIRECTORES

Gianluca Susi y Fernando Maestú Unturbe

UNIVERSIDAD COMPLUTENSE DE MADRID

FACULTAD DE PSICOLOGÍA

PROGRAMA DE DOCTORADO EN PSICOLOGÍA

Modelado computacional de la memoria episódica a nivel neuronal para contrastar la hipótesis de la desconexión en Alzheimer

Computational modeling of the neuronal basis of episodic memory to test the disconnection hypothesis in Alzheimer's

Jesús Cabrera Álvarez

DIRECTORES:

Gianluca Susi y Fernando Maestú Unturbe

Esta tesis doctoral titulada “Modelado computacional de la memoria episódica a nivel neuronal para contrastar la hipótesis de la desconexión en Alzheimer” ha sido financiada por el Ministerio de Universidades a través de un contrato predoctoral de Formación del Profesorado Universitario (FPU19/04251).

This PhD thesis entitled "Computational modeling of the neural basis of episodic memory to test the disconnection hypothesis in Alzheimer’s” was funded by the Spanish Ministry of Universities through a predoctoral FPU grant (FPU2019/04251).

A mi madre, a mi padre,

por enseñarme a volar a fuerza de batir las alas.

Agradecimientos

Una tesis doctoral depende, en parte, de la motivación y el trabajo de un doctorando, pero es inviable llegar a destino si no se cuenta con un buen ambiente de trabajo, una dirección apropiada, el apoyo institucional y los sostenes de la vida personal, que siembran de potencial el proceso. Con más énfasis en estos tiempos en los que la alta competitividad, las presiones por publicar, la corta financiación y los acelerados marcos temporales para el desarrollo de una tesis, llenan de tensión el camino del doctorando debatiéndolo entre la calidad y la cantidad, y somentiéndolo a elevados niveles de estrés. En este marco, pequeños desajustes en el entorno es capaz de desatar problemas de salud mental que, además, entorpecen el proceso y elevan la tensión. Me siento afortunado de haber podido pasar sin tropezar, y me gustaría agradecer a todos los que han hecho el camino transitable.

A **Gianluca Susi** que ha sido el director operativo de este trabajo y sentó las bases para la oportunidad que sería esta tesis. Considerando el reto que suponía acompañar a un psicólogo por el camino de la neurociencia computacional, agradezco su apoyo libre de prejuicios, su esfuerzo y su paciencia. En definitiva, él ha sido la referencia constante para aliviar la incertidumbre, para entender el camino y para caminarlo. Me ha hecho acelerar cuando tocaba y me ha dado oportunidades clave en mi proceso de investigación. Su escucha activa y su consejo me han ayudado a encajar los éxitos en tiempo y forma. Agradezco la franqueza con la que me ha guiado, sin paternalismos ni soberbia, incluso en las contadas y poco significativas discordias. Quizá ahora, que ya me ha enseñado el camino de la ciencia, también me pueda enseñar otros caminos de ritmo y armonía.

Sin la generosidad de **Fernando Maestú** esta tesis no habría tenido lugar. Es incuestionable el éxito de liderar un grupo de investigación con capacidad de trabajo y proyección internacional a base de dar espacio libre y oportunidad a la exploración, la creatividad, y el trabajo autónomo de sus miembros. Agradezco profundamente su estilo de supervisión brillante,

nítido, suave y positivo, que siempre ha conseguido catapultar mi motivación y mi confianza. Conseguía encontrar lo bueno en el trabajo hecho - a veces por encima de uno mismo - y por momentos eso es lo que necesita un doctorando que está entrenado para encontrar los fallos o lo que podría haberse mejorado. No menos importante, agradezco que me enseñara con el ejemplo que en la vida hay otros motivos para la ilusión y el esfuerzo, otras actividades, proyectos y personas que merecen nuestro tiempo tanto como nuestra profesión. Me gusta jugar a los caballeros que suelen ganar, pero solo si se hace de esta manera.

A **Claudio y Jaime,** que aparecieron al principio del camino y engrosaron el horizonte, han sido colaboraciones estupendas que me han divertido y con las que he aprendido mucho. Quiero agradecer al equipo del **C3N,** porque las relaciones interpersonales positivas son centrales para nuestro bienestar y allí siempre me he sentido acogido. A **Martín** por cuidarme, y por mantenerme en su círculo. Porque es una persona profundamente buena, y da cobijo a quien lo necesita. A **Berto** por las discusiones estimulantes, y por la compañía. A **Sandra**, por hacerme agradable el exilio, y a **Inés**, por las confidencias y por enseñarme que trabajar en equipo puede ser eficiente y productivo. A **Bruña** por hacerme sentir que todo está bajo control, que hay soluciones y que no pasa nada. A **Alex** porque marcaste el preludio del camino y así lo guardo. A todos los compañeros que estaban cuando llegué: **Alberto, Alex, Luis, Almu, Fede, Isa, Brenda, Dany, Lucía, Soraya**, y a los que han llegado recientemente para cargar el laboratorio de aire fresco, trabajo duro y motivación: **Marcos, Nacho, Lucía, Adelia, Paula, Noemí, María, Claudia, Adrián, Blanca, Andrea**. También me he divertido escuchando y aprendiendo de las voces de la experiencia: **Pablo y Pacios**. Gracias a todos, qué suerte que este ambiente me haya ayudado a estar bien.

En cualquier caso, siento que esta tesis tiene más de rasgo que de estado, que no es fruto de las circunstancias, sino de las semillas que se sembraron en los momentos adecuados. Agradezco a mi **hermano** por pisar por delante siempre, por abrir camino y por cuidarme. Con una referencia tan generosa y brillante como tú, ¿quién iba a quedarse atrás? Agradezco a mis **padres** por dejarme ser quien soy, y por apoyarme en las decisiones que me han llevado a este punto. Por enseñarme que los esfuerzos tienen sus recompensas, y de esa manera

poder sentir que todo va a estar bien. Esta es la fe que me acompaña. Gracias también por los esfuerzos materiales que ofrecen las oportunidades para poder llegar. Este periodo ha estado lleno de vida gracias a **Alina**, me has arrastrado hacia lo personal insistentemente, me has orientado hacia adelante y hemos crecido. Gracias por señalar el camino y por vivir sin miedo, haces más natural el proceso de hacerse adulto. Al resto de mi **familia** por haberme provisto de un nicho agradable y estimulante en el que crecer.

Gracias a **David Ramos y Omar Batchoula** por los reencuentros y compartir caminos paralelos. Es agradable ver nuestras evoluciones y compartir las incertidumbres, dificultades y éxitos. To **Oleksandr Pashkov and Youssef Lahbabi** for the intense tennis sessions -which were respites in the middle of work storms- and for the stimulating cultural exchange. I'm grateful for the engaging conversations discussing cultural perspectives with mutual respect and joy. In this vast and crowded world, you inspire me to remain open to new experiences and to embrace new people. A mis amigos de Madrid, **Pablo, Adrián, Pablo, Antonio, Lucía** por acompañarme durante tanto tiempo y hacer de una ciudad inmensa un lugar más habitable. A **Marga y Rober**, por ver venir el futuro juntos. A mis amigos de La Línea, **Rober y Sergio**, por ayudarme a volver, por estar abiertos a mí y seguir ahí. A **aquellas que no están porque no pueden**, que las llevo conmigo; a **aquellos que no están porque no quieren**, que los espero.

Agradezco los golpes de suerte, personificados en las decisiones de la oficina de postgrado y en el apoyo de **Luis Enrique López Bascuas**, que además de ser el mejor profesor de mi etapa de grado en psicología, me ayudó cuando más lo necesitaba. Por último, agradezco a aquellos que dejan su impronta en nosotros de maneras sutiles pero realmente significativas. A **Jose Damian Durán**, cuyo manejo de una clase difícil de secundaria fue inspirador tanto en forma como en fondo. Despertó mi interés y redujo el miedo por las formalidades matemáticas, algo que me sería muy útil durante este doctorado. A **Bárbara y Pilar Claro** que, pese a mis resistencias, me prepararon para comunicarme en otro idioma y hoy me es imprescindible. También a **Alexandra Elbakyan** por crear una herramienta justa, pragmática y política, y que nunca he usado.

Contents

Agradecimientos ix

Figures and Tables xix

Abstract xxiii

Resumen xxv

1 Introduction 1

1.1 Episodic memory and its neural correlates . . . 3

1.2 Histopathological biomarkers of Alzheimer's disease . . . 8

1.3 Neuroimaging: a window into the brain . . . 9

1.4 Network neuroscience to characterize the brain . . . 11

1.5 Levels of analysis and reductionism in neuroscience . . . 14

1.6 Computational modelling of brain function . . . 16

1.7 Brain stimulation to intervene in Alzheimer's . . . 19

1.8 Aims and hypotheses . . . 20

I Simulating healthy brain dynamics 23

2 The role of the thalamus in functional connectivity 27

2.1 Introduction . . . 28

2.2 Materials and methods . . . 32

2.2.1 Empirical dataset . . . 32

2.2.2 Functional connectivity . . . 33

2.2.3 Structural connectivity . . . 34

2.2.4 Brain network model . . . 35

2.2.5 Simulations . . . 37
2.2.6 Statistics . . . 39
2.3 Results . . . 40
2.3.1 The thalamus impacts rsFC through its afferences . . . 40
2.3.2 Structure is not the key: comparing thalamocortical and cortico-cerebellar networks . . . 42
2.3.3 Brain dynamics underlying each scenario . . . 43
2.3.4 Thalamic alpha propagates to the cortex within a balanced SNR . . . 44
2.4 Discussion . . . 49

II Integrative model of neurotoxicity in AD **55**

3 A multiscale model of Alzheimer's progression **59**
3.1 Introduction . . . 60
3.2 Methods . . . 62
3.2.1 Data acquisition . . . 62
3.2.2 Structural connectivity . . . 63
3.2.3 Brain network model . . . 63
3.2.4 Closed-loop neurotoxicity model . . . 66
3.2.5 In-silico experiments and simulations . . . 70
3.2.6 Spatiotemporal profile assessment . . . 72
3.2.7 Code Accessibility . . . 73
3.3 Results . . . 73
3.3.1 Single-node experiments favour inhibition over excitation to explain hyperactivity . . . 75
3.3.2 Closed-loop neurotoxicity model: from proteins to neural activity . . . 77
3.3.3 Hyperactivity is not directly linked to hypersynchrony . . . 78
3.3.4 The changes in inhibition lead the evolution of AD . . . 80
3.3.5 Amyloid-beta controls changes in inhibition . . . 83

3.3.6 Toxic seeding determines the spatiotemporal profile of the evolution . 84
3.4 Discussion 86

III Restoring healthy brain function with tACS **93**

4 Understanding the effects of cortical gyrification in tACS **97**
4.1 Introduction 98
4.2 Methods 101
4.2.1 Empirical methods 101
Study design 101
Empirical dataset 101
Neurostimulation 104
Statistical analysis 104
4.2.2 Computational methods 105
Data for simulations 105
Spiking population model 106
Working point simulations 108
From the current propagation model to the stimulation of the SNN . . 110
tACS simulations 111
Statistics 112
4.3 Results 113
4.3.1 Empirical results 113
Participant demographics 113
IAF-tACS did not modulate occipito-parietal activity 114
The stimulation sustained the decay of alpha power in time 114
Neurostimulation effects are highly variable 114
4.3.2 Simulation results 116
Cortical Gyrification Modulates the Effects of tACS: Evidence of Contradictory Outcomes 116

The distribution of normal field components modulates the effects of the stimulation . . . 119
The mean of the distribution is the main predictor of alpha power rise 121
4.4 Discussion . . . 124

5 Reducing fronto-parietal synchrony with tACS **129**
5.1 Introduction . . . 130
5.2 Methods . . . 132
5.2.1 Dataset . . . 132
5.2.2 Functional Connectivity . . . 133
5.2.3 Structural Connectivity . . . 134
5.2.4 Current propagation model . . . 134
5.2.5 Brain network model . . . 136
5.2.6 Stimulus integration and calibration . . . 138
5.2.7 Statistics . . . 139
5.2.8 Network analysis . . . 140
5.3 Results . . . 140
5.3.1 Interindividual variability in response to stimulation during model calibration . . . 140
5.3.2 tACS desynchronization is theoretically feasible . . . 141
5.3.3 High network centrality reduces the impact of stimulation . . . 143
5.3.4 Stimulation effects over the whole network . . . 146
5.4 Discussion . . . 148

Conclusions **153**

6 General discussion **155**
6.1 Is the thalamus key to explain FC disruptions in AD? . . . 157
6.2 Hyperactivity, hypersynchrony and spectral power . . . 159
6.3 The disconnection hypothesis explains AD symptoms . . . 160

6.4 Computational neuroscience and its transference 161
6.5 The quest to understand and treat Alzeimer's 163
6.6 Where is episodic memory in this thesis? 165
6.7 Limitations and future directions 166
6.7.1 Models usefulness 166
6.7.2 Technical limitations 168
6.7.3 Future directions 169
6.8 Concluding remarks 170

Appendix **239**

A1 Supporting information from Chapter 2 241
A2 Extended data from Chapter 3 253
A3 Supplementary data from Chapter 4 260

Figures and Tables

Figures

1.1 Types of memory 5

1.2 Memory nuclei of the Medial Temporal Lobe 7

1.3 Regions of the default mode network 13

2.1 Main schemes of thalamocortical interaction 29

2.2 SC versions 35

2.3 JR model of a cortical column 37

2.4 The bifurcation separates two states. 38

2.5 Thalamocortical experiment 41

2.6 Cortico-cerebellar control experiment 44

2.7 Simulation samples for one subject with parceled thalamus 45

2.8 Parameter space explorations for p_{th} with high thalamic noise 46

2.9 Parameter space explorations over η_{th} to balance SNR in the thalamus 48

2.10 Complementary simulation samples 49

3.1 Modelling framework overview 64

3.2 Single node in-silico experiment 76

3.3 Evolution of the outputs from the closed-loop neurotoxicity model 79

3.4 Functional measures from the closed-loop neurotoxicity model 80

3.5 Parameter spaces for the limits of change of the JR-BNM parameter candidates . 81

3.6 Parameter spaces for C_{ip} isolating the effects of $A\beta$ and hp-tau 83

3.7 Dominance of Braak sequences per seeding strategy 85

3.8 Impact of $A\beta$ and hp-tau seeding on the antero-posterior temporal differentiation for firing rate and FC . . . 86

4.1 Electric field magnitudes computed with ROAST . . . 110
4.2 Estimation of the normal component of the electric field on the white matter surface 112
4.3 Power ratio comparison results through CBPT . . . 115
4.4 Power spectra empirical experiment results . . . 117
4.5 Normal component distributions (i.e., $\underline{E}_{k\perp}$) . . . 118
4.6 Stimulation of a single node with theoretical distributions . . . 120
4.7 Stimulation intensity fitting . . . 122
4.8 Predictors of alpha rise . . . 123

5.1 Scheme of the method to estimate $|E_\perp|$ . . . 135
5.2 Stimulation setups . . . 136
5.3 Simulations for model calibration . . . 141
5.4 Effects of stimulation in the computational model . . . 142
5.5 Network analysis for the average SC of the ten subjects . . . 145
5.6 Disconnection experiment . . . 146
5.7 Baseline vs stimulation metrics . . . 147
5.8 Impact of electric field $E_\perp$ and node strength over nodes' spectral frequency peak 148

6.1 Publication rates in computational neuroscience . . . 162

Tables

2.1 JR parameters used in simulations . . . 38
2.2 Network features for the thalamus and the cerebellum . . . 43

3.1 JR-BNM parameters used in simulations. . . . 66
3.2 Parameters used in the closed-loop neurotoxicity model . . . 70

3.3 Regions of the cingulum bundle included in the BNM 74

4.1 SNN parameters used in simulations 109

4.2 Demographics table for the empirical data 113

5.1 JR parameters used in simulations 138

Abstract

Alzheimer's disease (AD) is a concerning global health problem that tends to worsen with demographic ageing. As more people live longer, the prevalence of AD is expected to rise, imposing substantial health, social, and economic burdens on individuals and societies worldwide. AD is characterized by a cognitive decline that, in its most common clinical manifestation, affects prominently episodic memory limiting progressively the ability to store new information. At the biological level, AD has been classically associated to the abnormal accumulation of two proteins ($A\beta$ and tau) that exert toxic effects on neuronal tissue. This cytotoxicity is believed to disrupt cellular processes, leading to the breakdown of synaptic communication and eventual neuronal death. Despite the pressing epidemiological need, the considerable financial investments, and the research efforts, the understanding of the disease remains limited and treatments scarce.

One parsimonious framework for the understanding of AD is the "disconnection hypothesis". This hypothesis suggests that AD is primarily driven by deficits in neural communication, which are directly related to proteinopathy. According to this theory, the disruption in the communication between brain regions leads to a breakdown in the brain's ability to integrate information across different networks and, therefore, to cognitive and functional impairments.

In this thesis, we approached the study of AD from a computational modelling perspective, with a particular focus on the functional connectivity changes that occur throughout the progression of the disease, and the biological mechanisms that may underlie those changes. We used brain network models constructed from empirical neuroimaging data to simulate brain activity under various conditions. These conditions span from the simulation of healthy brain activity under structural constraints, to the impact of the toxic proteins on neural tissue

through disease development, and to the therapeutic application of transcranial alternating current stimulation (tACS) to modulate brain activity and the intervene in the pathological process. We combined the use of neural mass models and spiking neural networks to adapt the simulations to these requirements of these different applications.

Our findings suggest that disruptions in local neural inhibition, largely due to the widespread accumulation of $A\beta$ proteins, lead the evolution of the disease. As $A\beta$ proteins accumulate, they interfere with normal inhibitory processes in the brain, leading to neuronal hyperactivity and hypersynchrony, particularly in the early stages of the disease. This phenomena foster the propagation and accumulation of tau proteins contributing to the neural disconnection and the cognitive decline seen in AD patients. Additionally, our results highlighted that the location of the early depositions of proteins shapes the spatiotemporal profile of the disease. Furthermore, we explored the potential of tACS as a therapeutic intervention to modulate brain activity and counteract these disruptions. Our results indicated that tACS could potentially help regulate the hypersynchronous neural dynamics associated with early-stage AD which may, in turn, slow down the accumulation of $A\beta$ proteins in the brain.

In conclusion, this thesis provides new insights into the biological mechanisms underlying AD and offers potential therapeutic strategies for mitigating its effects. However, it is important to acknowledge that AD is a complex disorder and that many challenges remain for fully understanding and effectively treating it.

Resumen

La enfermedad de Alzheimer (EA) es un problema de salud global preocupante que tiende a empeorar con el envejecimiento demográfico. A medida que la población se hace más longeva, se espera que la prevalencia de la EA aumente, imponiendo considerables cargas sanitarias, sociales y económicas a individuos y sociedades en todo el mundo. La EA se caracteriza por un deterioro cognitivo que, en su manifestación clínica más común, afecta de manera prominente la memoria episódica, limitando progresivamente la capacidad de almacenar nueva información. A nivel biológico, la EA ha sido clásicamente asociada a la acumulación anormal de dos proteínas ($A\beta$ y tau) que ejercen efectos citotóxicos sobre el tejido neuronal. Se cree que estos efectos interrumpen los procesos celulares normales, lo que conduce a la disrupción de la comunicación sináptica y, eventualmente, a la muerte neuronal. A pesar de la presión epidemiológica, la considerable inversión económica y los esfuerzos de investigación, la comprensión de la enfermedad sigue siendo limitada y los tratamientos escasos.

Una hipótesis parsimoniosa que establece un marco para la comprensión de la EA es la "hipótesis de la desconexión". Esta hipótesis sugiere que la EA es impulsada principalmente por déficits en la comunicación neural, los cuales están directamente relacionados con la proteinopatía. Según esta teoría, la interrupción en la comunicación entre regiones cerebrales lleva a una disrupción en la capacidad del cerebro para integrar información entre redes neuronales, lo que resulta en un deterioro cognitivo y funcional.

En esta tesis, abordamos el estudio de la EA desde una perspectiva de modelado computacional, con especial atención a los cambios en conectividad funcional que ocurren a lo largo del progreso de la enfermedad, y a los mecanismos biológicos que subyacen a esos cambios. Utilizamos modelos de redes cerebrales construidos a partir de datos empíricos de neuroimagen para simular la actividad cerebral bajo diversas condiciones. Estas condiciones abarcan

desde la simulación de la actividad cerebral saludable bajo restricciones estructurales, hasta el impacto de las proteínas tóxicas en el tejido neural durante el desarrollo de la enfermedad, y la aplicación terapéutica de estimulación transcraneal de corriente alterna (tACS por sus siglas en ingles) para modular la actividad cerebral e intervenir en el proceso patológico. Combinamos el uso de modelos de masa neuronal y de redes spiking para adaptar las simulaciones a los requisitos de estas diferentes aplicaciones.

Nuestros hallazgos sugieren que el deterioro de la inhibición neuronal local, en gran medida debido a la acumulación de proteínas $A\beta$, guían la evolución de la enfermedad. Este deterioro en la inhibición conduce tanto a hiperactividad como hipersincronía neuronal, particularmente en las etapas tempranas de la enfermedad. Estos fenómenos favorecen la propagación y acumulación de proteínas tau, que a su vez contribuyen a la desconexión neural y el deterioro cognitivo observado en los pacientes de Alzheimer. Además, nuestros resultados destacaron que la ubicación de las primeras acumulaciones proteicas moldea el perfil espaciotemporal de la enfermedad. También exploramos el potencial de la tACS como una intervención terapéutica para modular la actividad cerebral y contrarrestar estas disrupciones. Nuestros resultados indicaron que la tACS podría ayudar a regular la dinámica neuronal hipersíncrona asociada con la EA en etapas tempranas, lo que, a su vez, podría ralentizar la acumulación de proteínas $A\beta$ en el cerebro y el progreso de la enfermedad.

En conclusión, esta tesis proporciona nuevos conocimientos sobre los mecanismos biológicos subyacentes a la EA y ofrece estrategias terapéuticas potenciales para mitigar sus efectos. Sin embargo, es importante reconocer que la EA es un trastorno complejo y que aún quedan muchos desafíos para comprenderla completamente y tratarla de manera efectiva.

Chapter 1

Introduction

As societies get older, the rates and impact of dementia become increasingly concerning. Since the 1950s, the proportion of people over 65 years has duplicated from 5.10% to 9.63% in the world - from 7.94% to 19.10% in Europe - (Ritchie & Roser, 2019). Dementia refers to a cognitive decline resulting from progressive neurodegeneration that is not part of normal brain ageing although, indeed, age is its main risk factor (Alzheimer's Association, 2019; Knopman et al., 2021; Xia et al., 2018). In dementia, abnormal brain changes disrupt memory, language, reasoning, attention, and perceptual abilities, interfering significantly with patients' daily lives and independence. The most prevalent type of dementia is Alzheimer's disease (AD) which accounts for 50 to 70% of all dementia cases, resulting in approximately 30 million people affected around the world and increasing (X.-X. Zhang et al., 2021). In the most common type of AD, cognitive disruptions primarily affect episodic memory, the ability to recall personal experiences from the past. In the beginning, patients struggle to retain recent information (i.e., anterograde amnesia) while partially preserving their ability to access old memories. As the disease progresses, symptoms intensify generating a more comprehensive cognitive decline, including retrograde amnesia (i.e., difficulties recalling old information), affecting other cognitive modalities (e.g., language, attention, perception) and even leading to apraxias. Despite the severity of the symptoms, the large number of patients affected and the decades of research on the topic, our understanding of AD remains limited and treatments scarce.

A parsimonious theory that has been proposed to explain AD symptoms is *the disconnection hypothesis* (Brier et al., 2014; Delbeuck, 2003). This theory suggests that the cognitive decline arises from the disruption of the communication within brain networks and between brain regions that support cognitive functioning in healthy subjects. During the disease, proteins that are necessary for the normal functioning of the brain begins to accumulate abnormally, generating synaptic changes that affect multiple areas (Knopman et al., 2021) and propagating through the network to disrupt neural function and interregional communication (H. Braak et al., 2011; D. T. Jones et al., 2015; Jucker & Walker, 2018). Although these phenomena have been widely reported in the literature, important questions remain to be answered. Why have most of the clinical trials of pharmacological interventions failed? What are the key elements that should be targeted to stop disease progression? How could we effectively predict the development of the disease in asymptomatic patients? The disease usually manifests its symptoms years after the onset of the pathophysiological process (Amieva et al., 2008; R. Sperling et al., 2014), when symptoms appear, the network has already suffered from a long period of toxic accumulation, propagation, and network degeneration. Therefore, it is relevant to develop diagnostic tools to predict and intervene early in the pathological process. In this thesis, we follow this line of thought to shine a light on the understanding of AD and to contribute to addressing the scientific questions exposed.

In the following, I will introduce key concepts and methodologies that support this thesis. Starting from the exposition of a theoretical framework for memory, followed by an examination of the multiscale neuroscientific evidence on AD, and ending with a discussion of the computational methodologies and brain stimulation techniques that were relevant to the development of this work.

1.1 Episodic memory and its neural correlates

Memory is a cognitive process that allows us to retrieve information from the past. It is of great importance in our daily lives, to know who we are, where we left the keys, how to drive a car, to retain what others are saying in a conversation, and even to be conscious (Ballesteros Jiménez, 2017; Tulving, 1985). There are different types of memory. What we usually refer to as memory are long-term declarative memories, stored for long periods of time and consciously experienced in mind when retrieved, such as remembering the name of your first pet, or recalling what we did for Christmas. However, being able to store and retrieve those memories imply having preserved preceding and more ephemeral forms of memory (Fig 1.1). Just following a sensory input, there is a brief period of information retain (less than a second) called the sensory register (Shiffrin & Atkinson, 1969), where each sensory modality stores information in parallel and without reaching consciousness for a very short time. After that brief time-lapse, information decays and only the attended content is processed further into another short-term type of memory: the working memory (A. D. Baddeley & Hitch, 1974; Broadbent, 1958; G. Sperling, 1960; Treisman & Gelade, 1980). The working memory keeps information active and ready to be used in our minds to perform complex tasks such as comprehension, reasoning, and decision-making (A. Baddeley et al., 1986; A. D. Baddeley & Hitch, 1974). The capacity of this system is limited, between 3 and 5 chunks of information in young adults, and once we have it completely busy with one task (e.g., performing arithmetic operations), it would be tough for us to perform any other (Cowan, 2001, 2010; Cowan et al., 2008). When the information has been used and becomes unattended, it also decays rapidly and leaves the working memory (in the order of seconds). Depending on the processing depth of the information, which is related to the significance of the content, its repetition and integration with previously stored memories, a memory trace could be more or less strongly encoded and stored in long-term memory (A. Baddeley, 2000; Craik & Lockhart, 1972). After storage has occurred, memories are retained for long periods. The strength of the trace and its timely rehearsal determine whether the memory gets weaker until it is forgotten or, by

contrast, strengthened. When the information is still available, cues can activate recall to re-experience consciously the content of the trace (Hayne & Herbert, 2004; Tulving & Osler, 1968). Disruptions on any of these processes could lead to memory impairments as the ones observed in AD.

There is still another dimension that is relevant to conceptualize memory in AD: the level of awareness experienced during the process. Early experiments with amnesic patients showed that although they could not remember having learnt to perform a task in previous sessions, they could actually execute those tasks as if they had learnt. Tasks, for instance, such as drawing on a mirror (Milner et al., 1968) or retrieving words previously learnt (Warrington & Weiskrantz, 1970, 1978). These experiments demonstrated that not all long-term memories are experienced consciously and gave rise to another classification of memory, differentiating between declarative and implicit memories (Squire, 2004; Tulving & Schacter, 1990). While declarative memories appear available to our conscious mind through images or propositions, implicit ones are automatic and do not reach awareness. An implicit memory would be, for example, riding a bike (procedural memory) or recognizing the face of your father (priming). In these situations, we reactivate instantaneously the memory trace without being conscious of the process. Finally, in the case of declarative memories, they can be further divided into episodic and semantic memories (Squire, 2004). The episodic memory is responsible for recalling personal experiences with contextual details such as “where” and “when” the events happened, while semantic memories are related to general knowledge without specific contextual information. For instance, we know that the Earth is spherical, but we probably do not remember the circumstances under which we learnt it.

The course of AD can be divided into three stages: a preclinical stage in which disease-related biological changes began but without a manifestation of cognitive symptoms; a prodromal stage in which mild cognitive impairment emerge due to biological changes; and finally dementia with a more severe cognitive decline and impact on patients’ daily lives. In the prodromal stage, episodic memory tends to appear affected, generating an anterograde amnesia mostly associated with the impairment of consolidation and storage of information

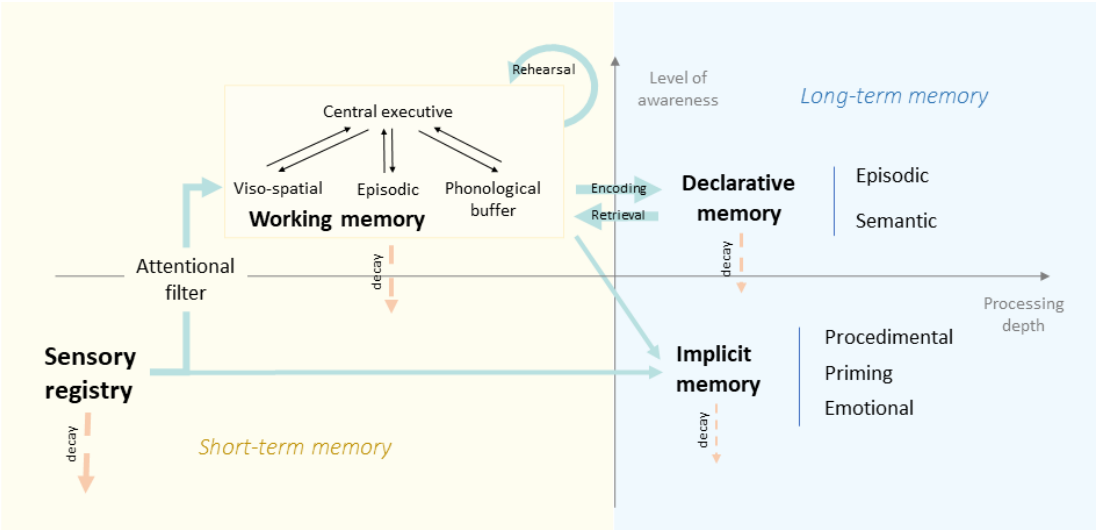


Figure 1.1: Types of memory. Flow-chart relating the systems and processes of memory from sensors to short-term memory to storage and retrieval (processing depth from left to right). The y-axis represents the level of awareness over the information being processed. At every processing stage, information may decay and be lost. Own elaboration based on the works of A. D. Baddeley and Hitch (1974), Broadbent (1958), Craik and Lockhart (1972), Shiffrin and Atkinson (1969), and Tulving and Schacter (1990).

(Becker, 1988; Dubois & Albert, 2004; Morris & Kopelman, 1986; Tounsi et al., 1999). Patients often show impaired free recall with intrusions and false positives in neuropsychological tests (Dubois & Albert, 2004), and progressively the impairment spreads to other memory processes including semantic and working memory. Semantic memory deficits are often manifested through language difficulties in verbal fluency and naming (Chertkow & Bub, 1990; Jahn, 2013; Nebes, 1989), while working memory deficits would arise through distractions during the execution of tasks, and affecting executive functions such as planning, problem-solving and goal-directed behaviour (A. Baddeley et al., 1991; Huntley & Howard, 2009). What started being an anterograde amnesia progresses to a more severe retrograde type and affects other cognitive processes. In sharp contrast, implicit memories tend to be mostly preserved until the very late stages of the disease, even after apraxias may appear (Adam et al., 2005; Knight, 1998; Lesourd et al., 2013).

All these memory processes rely on neurobiological mechanisms within the brain. Some of these mechanisms can be explained in light of the above-mentioned case of an amnesic patient (H.M.) who could not remember having learnt to perform a task. This patient was subject to the resection of its medial temporal lobe (MTL) in order to control his epileptic episodes (Milner et al., 1968). After the surgery, the patient showed a severe degree of anterograde amnesia, losing his ability to build and recall new memories. The MTL includes the hippocampus, entorhinal cortex, parahippocampus and perirhinal cortex, and these regions have since been consistently associated with declarative memory through decades of research (Fig. 1.2).

The hippocampus, a deep brain structure with a seahorse shape, plays a central role in memory formation. Neurons in the hippocampus fire during new experiences and facilitates the strengthening of neuronal connections for the storage of new memories (Buzsáki & Tingley, 2018; Preston & Eichenbaum, 2013; Wood et al., 2000). It works as a temporal hub for memory pattern formation (i.e., engrams) and over time, during the consolidation process, its centrality lowers as memories become distributed across neocortical regions (engram distribution) (Bekinschtein et al., 2007; Kitamura et al., 2017; Roy et al., 2022). Additionally, the hippocampus helps to consolidate the engram traces through sporadic reactivations of memory during sleep and in resting periods (Diekelmann & Born, 2010; Schlichting & Preston, 2014; M. A. Wilson & McNaughton, 1994). Once the long-term memory traces have been fully consolidated, the hippocampus decays in relevance to retrieve the memory content, and it becomes more permanently encoded within the neocortex (Eichenbaum, 2000; Wiltgen et al., 2004). This is why an MTL lesion, such as the one of H.M., does not disrupt the ability to recall remote memories (Kirwan et al., 2008; Rosenbaum et al., 2000).

At a finer scale, the formation of memory engrams relies on a process of synaptic connectivity strengthening called long-term potentiation (LTP) (Bliss & Collingridge, 1993; Josselyn et al., 2015). LTP enhances the communication between neurons that are activated synchronously or within a short time-lapse (i.e., spike timing-dependent plasticity) following the classical hebbian rule "cells that fire together wires together" (Bi & Poo, 2001; Caporale & Dan, 2008;

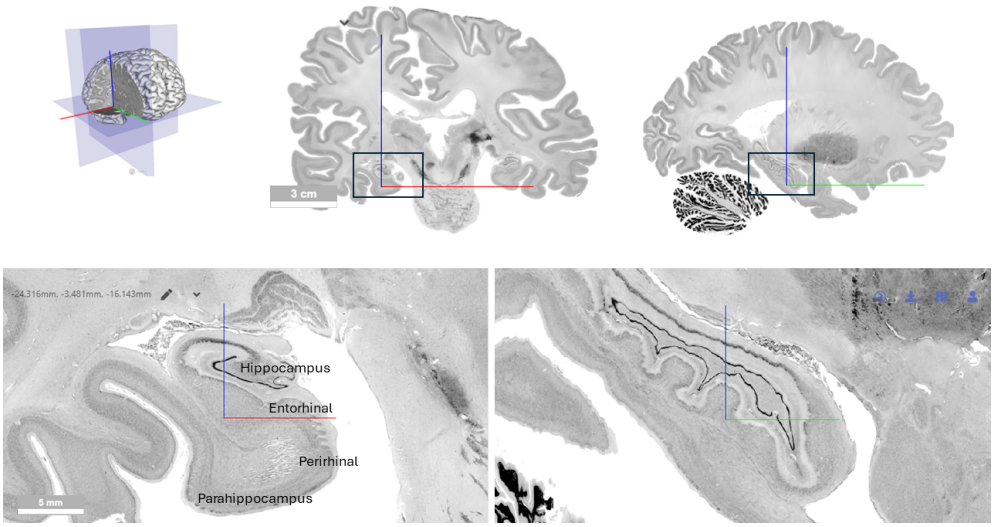


Figure 1.2: Memory nuclei of the Medial Temporal Lobe (MTL) including the hippocampus, entorhinal cortex, perirhinal cortex and parahippocampus. Showing coronal and sagittal views at two resolutions. Slices from the BigBrain (Amunts et al., 2013) accessed at https://www.ebrains.eu/tools/siibra-explorer.

Hebb, 1949). When the postsynaptic neuron fires an action potential, there is a retrograde transmission of the depolarization to the dendrites, then, if the synapse is still active (i.e., there is glutamate in the synaptic cleft), the dendritic depolarization allows opening post-synaptic NMDA channels generating an influx of calcium in the postsynaptic terminal. This influx of calcium triggers structural changes such as the insertion of AMPA receptors in the terminal, the enhancement of protein production, and the stimulation of presynaptic growth, among other processes that contribute to the long-lasting effects of the LTP over the synaptic connection (Nicoll, 2017). Therefore, LTP is a crucial aspect of normal cognitive function and its dysregulation is implicated in various neurological disorders, including AD.

In the following, we will explain how these neurobiological mechanisms of memory may become impaired in AD due to the biological changes happening in the course of the disease.

1.2 Histopathological biomarkers of Alzheimer's disease

From the biological perspective, AD is characterized by a cascade of pathological mechanisms spanning multiple levels of analysis, from molecules to cells to network disruptions. At the molecular level, the two classical histopathological biomarkers of the disease are the accumulations of amyloid-beta ($A\beta$) and tau in the brain (Ballard et al., 2011; Jack et al., 2013). These two proteins are found in healthy brains supporting some of their functionalities: $A\beta$ contributes to protecting neurons from infections, oxidative stress, and metabolic waste, and it also contributes to the regulation of synaptic plasticity; tau is a microtubular protein that gives structure to the cellular bodies (G. F. Chen et al., 2017; Guo et al., 2017; Puzzo et al., 2015). In AD, these two proteins misfold and aggregate becoming toxic for neurons.

$A\beta$ misfolds and aggregates into neuritic plaques in the extracellular space, and its toxic effects include the reduction in the number of GABAergic inhibitory synapses and the disruption of glutamate reuptake from synaptic clefts (Garcia-Marin, 2009; Palop & Mucke, 2010; Zott et al., 2019). These processes trigger neuroinflammation and produce cellular hyperexcitability (M. A. Busche et al., 2008, 2012; Minter et al., 2015) that, in turn, contribute to foster $A\beta$ production, falling into a vicious cycle between $A\beta$ accumulation and hyperactivity (M. A. Busche & Hyman, 2020; Zott et al., 2019). On the other hand, tau gets hyperphosphorylated (hp-tau) and aggregates inside neurons, giving rise to compact structures called neurofibrillary tangles (NFTs) that disrupt neuronal microtubule stability and impair axonal transport (Duquette et al., 2021; Iqbal et al., 2010). The presence of hp-tau leads to the reduction of dendritic spines in pyramidal cells, cellular dysfunction, neuronal death, and brain atrophy (Gómez-Isla et al., 1997; Merino-Serrais et al., 2013; Musi et al., 2018; Schäfer et al., 2021).

The spatio-temporal profile for hp-tau accumulation follows a very well-defined sequence called the Braak stages (H. Braak & Braak, 1991a; H. Braak et al., 2011): the accumulation starts in the entorhinal cortex, propagates across the hippocampal formation, and from there it extends to other regions of the neocortex. It has been proposed that hp-tau propagates within the brain in a prionic fashion: a toxic protein flows to a non-affected region, where it serves as

a template for other tau proteins to hyperphosphorylate and misfold (Jucker & Walker, 2018; Walker, 2018). Importantly, neuronal activity fosters the transportation of hp-tau, and hence, the most hyperactive regions due to $A\beta$ accumulation are likely targets of the propagation of hp-tau (Rodriguez et al., 2020).

These molecular changes start years before the disease manifests clinically (Dubois et al., 2016). While $A\beta$ accumulation starts earlier and more insidiously during the disease, the levels of hp-tau have been strongly associated with the progressive memory impairments observed in AD (Bejanin et al., 2017; Boccalini et al., 2023). Patients would have difficulties consolidating new memories due to the synaptic disruptions provoked by hp-tau in the brain.

Although these molecular changes do not manifest clinically at the beginning of the disease, their impact on brain function at the network level can be observed from very early stages. Being able to record and analyse brain function through non-invasive neuroimaging techniques have opened a great opportunity to foster the understanding of the disease and its early detection.

1.3 Neuroimaging: a window into the brain

Neuroimaging techniques have revolutionized our knowledge about the human brain by providing a window into its structure and function. Among the diverse array of neuroimaging methods, magnetic resonance imaging (MRI) and electrophysiological recordings, such as magnetoencephalography (MEG) and electroencephalography (EEG), stand out as the most widely adopted tools for studying the brain. MRI is capable of generating detailed images of the brain's anatomy, relying on the principles of nuclear magnetic resonance. Through the interaction of radiofrequency pulses and strong magnetic fields, MRI captures high-resolution images in which the signal contrast for soft tissue allows the differentiation of white matter from grey matter from cerebrospinal fluid and the scalp (Grover et al., 2015). The general framework of MRI, allows for several variants, such as diffusion-weighted MRI (dwMRI) and functional MRI (fMRI). dwMRI tracks the movement of water molecules in the brain, getting a

sense of the constriction in the direction of that movement (i.e., anisotropy) that is associated with the integrity of neuronal axons (Beaulieu, 2002; Chilla et al., 2015). Once analysed through tractography techniques, it is taken as a proxy for the location and orientation of white matter tracts in the brain.

Besides the insights provided by MRI, electrophysiological techniques capture the activity generated in the neuronal tissue. MEG is a tool that measures the *magnetic* fields generated by the flow of ions inside neurons, occurring when they get activated after the action potential of an afferent neuron. It is thought that specifically the postsynaptic currents flowing through the apical dendrites of pyramidal cells are the main contributors to the recorded MEG signal (Baillet, 2017) because the voltage dynamics are slower and spatially more distributed than those of action potentials, allowing for the summation of PSPs and collectively generating a stronger magnetic field. It has been proposed that around 10 to 50 thousand neurons might be synchronously activated to generate a detectable MEG signal (Murakami & Okada, 2006). The signal would travel through the air and be captured by an array of coils in a helmet prepared to detect weak magnetic fields in the order of femtoteslas (10^{-15} T). The EEG, instead, measures the *electric* potentials generated by the PSPs currents summation, using electrodes placed directly on the scalp (Lopes da Silva, 2013). MEG tends to obtain better levels of signal-to-noise ratio (MEG$\sim$2.2 dB vs EEG < 1 dB) and to be more spatially accurate than EEG (MEG$\sim$2-3 mm vs EEG$\sim$7-10 mm of resolution) (Fred et al., 2022) while the latter is cheaper and adapts better to different experimental contexts. Both of them provide an excellent temporal resolution in the order of milliseconds, however, they are limited in the spatial domain, particularly for the recording of deep brain structures.

The temporal accuracy of these electrophysiological techniques have allowed the study of brain oscillations. Different configurations of neuronal ensembles and electrophysiological properties give rise to different rhythmic patterns of neural activity that have been associated with cognitive functions (Buzsaaki & Draguhn, 2004). The first rhythmic activity measured and reported in the literature was the alpha rhythm in the seminal work of Hans Berger (Berger, 1929). This German psychiatrist invented the EEG methodology to record the electrical activ-

ity of the brain through electrodes over the scalp. During his recordings, he noticed a regular oscillatory pattern between 8 and 13 Hz, predominant in posterior regions during resting wakefulness with eyes closed (Herrmann et al., 2016). This discovery opened a new line of research in neurophysiology to deepen into the oscillatory behaviour of the brain. These oscillations occur at several frequency bands including delta, theta, alpha, beta, and gamma (i.e., 2-4Hz, 4-8Hz, 8-12Hz, 12-30Hz, 30-45Hz, respectively) and are used as biomarkers of brain health and disease (Buzsaaki & Draguhn, 2004; Llinás, 1988). In AD, electrophysiological investigations have revealed a gradual deceleration of the alpha rhythm during disease evolution (Babiloni et al., 2009; Garcés et al., 2013), accompanied by a fluctuation in relative alpha power that follows a specific spatio-temporal pattern: an initial impact to posterior brain regions, succeeded by the involvement of anterior ones (López-Sanz et al., 2016a; Nakamura et al., 2017, 2018; Pusil et al., 2019).

1.4 Network neuroscience to characterize the brain

In cognitive neuroscience, there used to be a tension between understanding the brain either as a set of distributed regions performing specific tasks (localizationism) or as an integrated network in which the different regions interact to perform those tasks (connexionism) (K. Friston, 2002). Both perspectives have been theorized as principles of brain function: functional segregation and integration, respectively (Sporns & Betzel, 2016). A wide range of examples may explain functional segregation, for instance, the specialization of Broca's area for speech production, the hippocampus for declarative memory consolidation or the visual cortex for visual perception, in which a further specialization can even be raised as specific neurons may respond to different colours, shapes, and motions (Tononi et al., 1994; Wurtz, 2009). In contrast, the integration of those segregated functions is needed to form holistic and coherent representations of the environment and to arrange behaviour in an adaptive way. Moreover, those processes necessarily interact with each other as, for instance, visual

processing may precede the formation of a new episodic memory with visual content. Even localized processes need the interaction with other networks. To study both, the modularity of the brain network (segregation) or its small-worldness (integration), network science provides useful tools to characterize and analyse these properties comprehensively.

Brain networks are usually conceptualized from two complementary perspectives: structure and function. The structural connectivity (SC) of a brain network refers to the physical pathways connecting brain regions. These are called tracts and consist of bundles of white matter fibres composed of myelinated axons that send their projections from one region to the next. This is typically assessed through algorithmic tractography reconstructions based on dwMRI data (Sporns, 2013). On the other hand, the functional connectivity (FC) of a brain network refers to the statistical association of temporal patterns of neural activity between brain regions (K. J. Friston, 1994). It is typically assessed through functional neuroimaging techniques like fMRI, EEG and MEG. FC is interpreted as the integration of brain resources working together to solve brain processing needs, both during tasks and in resting state (K. J. Friston, 2011). It highlights patterns of information exchange and network dynamics of brain function. SC and FC are closely related, in the way that the former supports the emergence of the latter, and the latter mediates changes in the former. However, their match is not complete, there are regions that, although not directly connected physically, could interact functionally through intermediates (Honey et al., 2009).

A key functional network that has been strongly associated with episodic memory is the default mode network (DMN). This network is active during resting wakefulness and gets deactivated when the subject engages in performing a task (Raichle et al., 2001). During resting states, when the brain is not actively engaged in a task, our minds tend to spontaneously retrieve past experiences contributing to their consolidation and accessibility (Humiston et al., 2019; Schlichting & Preston, 2014). Studies have shown that increased DMN activity during rest can

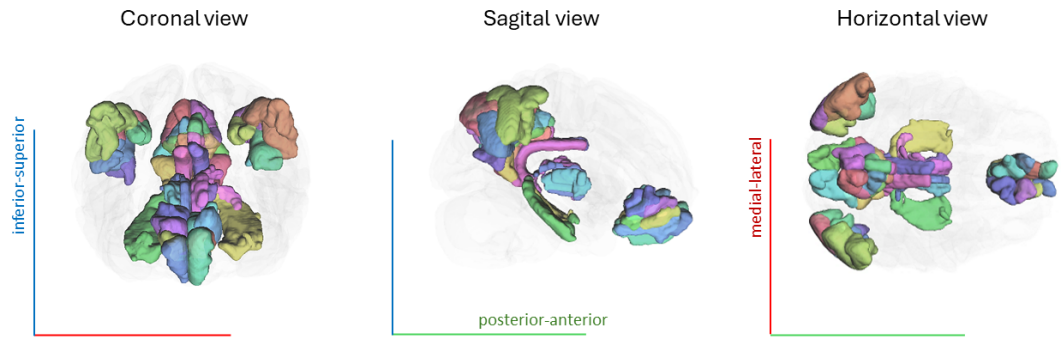


Figure 1.3: Regions of the default mode network including cortical and subcortical areas parcelled with the extended Human Connectome Project (HCPex) atlas (Glasser et al., 2016; C.-C. Huang et al., 2021; Sandhu et al., 2020).

predict enhanced episodic memory performance (Kaefer et al., 2022; Kizilirmak et al., 2023; Smallwood et al., 2021). Furthermore, disruptions in resting-state connectivity within the DMN have been observed in ageing and in individuals with episodic memory impairments (Greicius et al., 2004; Philippi et al., 2014).

The DMN encompasses several brain regions, including the ventromedial prefrontal cortex, dorsomedial prefrontal cortex, posterior cingulate cortex, precuneus, and lateral parietal cortex (Raichle, 2015) (Fig. 1.3). While studies on the DMN have traditionally focused on cortical regions, recent research has shed light on the involvement of deep brain areas. Specifically, T.-W. Lee and Xue (2018) demonstrated significant correlations between DMN activity patterns and those of the thalamus and hippocampus. Similarly, Alves et al. (2019) highlighted the participation of the thalamus and basal forebrain in the DMN, showing high levels of centrality in the network. These regions, particularly the thalamus and hippocampus, may serve as dynamic relay centres (Gollo et al., 2014), fostering synchronization and FC within the DMN.

The thalamus also plays a significant role in supporting episodic memory formation and retrieval. It is responsible for transmitting sensory information to the neocortex, where it can be integrated and processed, ultimately contributing to the encoding and retrieval of episodic memories (S. Sherman, 2016). Research has shown that damage to specific thalamic nuclei,

or dysfunction within the thalamus, can lead to impairments in memory and more specifically in episodic memory (Aggleton et al., 2016; Danet et al., 2015). One of the scientific questions addressed in this thesis is whether a thalamic impairment might be contributing to the functional disruptions observed in FC studies of AD.

In AD, the DMN gets impaired. From a molecular standpoint, the areas involved in that brain network are the ones that exhibit first and more prominently the accumulation of $A\beta$ and the subsequent hyperactivity (Ingala et al., 2021; Palmqvist et al., 2017). It has been proposed that the activity and metabolism patterns of the regions within the DMN may increase the risk for $A\beta$ accumulation (Buckner et al., 2005), getting those regions into the cycle of hyperpexcitability and $A\beta$ accumulation. Furthermore, those regions of the DMN show altered patterns of FC following a sequence of rise and fall affecting first posterior regions and then the anterior ones (Maestú et al., 2021; Nakamura et al., 2017; Pusil et al., 2019). While the rise in FC may be explained by hyperactivity levels, the fall would be caused by the appearance of hp-tau which disrupts synapses and hence inter-regional connectivity (Canuet et al., 2015; Dai et al., 2019; Garcés et al., 2014).

1.5 Levels of analysis and reductionism in neuroscience

To this point, we have mentioned several levels of analysis from which AD can be framed, such as the molecular, cellular, interregional and cognitive levels. This is a transversal issue within science that deserves explicit attention. In the first half of the 19th century appeared the idea of “the unity of scientific laws” claiming that the laws from one discipline could be derivable from those of another (Barendregt & van Rappard, 2004). This is called reductionism (Brigandt & Love, 2023). It proposes that a complete understanding of a system can be achieved by studying its constituent parts and, therefore, higher-level properties and behaviours can be explained by the behaviours and properties of lower-level components

and their interactions (Van Regenmortel, 2004). This approach has powerfully enriched the comprehension of psychological phenomena, fostering the description and explanation of the biological underpinnings of cognition and unlocking potential ways to intervene and change them.

Despite these successes, a caution note might be raised. Different phenomena have different optimal levels of description, where they appear more intuitive for the human mind. Sociology, psychology, biology, chemistry, and physics are scientific disciplines that study phenomena becoming clearer at their specific levels of analysis. Sometimes, a reductionistic approach can unblock the way to further understanding in a discipline but only when optimal-level descriptions and theories are available to serve as the basis for such an endeavour. In the case of psychology, theories describing cognition and behaviour needed to allow for the search and discovery of the underlying biological mechanisms (Krakauer et al., 2017): how could we look for the neuronal basis of memory if we haven't described what memory is at the cognitive level first?

Additionally, each scientific discipline develops its own theoretical framework, language and vocabulary to describe the phenomena studied from their level of analysis. This linguistic and theoretical segregation hampers the communication between areas of knowledge and gives rise to potential misunderstandings between them, especially, when inter-level causal relationships are proposed (Gallagher & Appenzeller, 1999). For instance, it would not be surprising to hear something like "I am stressed *because* I have high cortisol levels". "To be stressed" is a psychological-level statement while "having high cortisol" is a biological-level statement, both are correlated in time but not causally connected. The causes of feeling stressed might be described at the psychological level (e.g., an arousing stimulus), and should not be confused with its correlates (i.e., rising cortisol levels). This bottom-up causality transfer is a widespread problematic understanding that derives from the theoretical segregation and fragmentation of scientific disciplines.

1.6 Computational modelling of brain function

One way to foster the understanding between levels of analysis is to perform research from an integrative perspective, to which computational modelling becomes especially appealing. A computational model is a virtual representation of a complex system that enables us to reproduce its structure and function (Sterratt et al., 2012). These virtual representations are key to explore the relationship between the different scales from which a unique system can be framed. These models are implemented in computational frameworks in which the mathematical expressions are translated into programming languages that can be interpreted and executed by a computer.

Modelling offers several advantages in the study of multiscale phenomena (Dada & Mendes, 2011; Qu et al., 2011). First, they provide a controlled environment where variables can be precisely manipulated, facilitating the exploration of how changes at one level of analysis cascade through the system and affect higher or lower levels. This controllability also allows researchers to conduct experiments that might be impractical or even impossible in the physical world. Second, computational models can accommodate the complexity of real-world systems, capturing non-linear dynamics and emergent properties that often elude traditional analytical methods. Third, they can integrate vast amounts of data from various sources, helping bridge gaps between different scientific disciplines and providing a common platform for interdisciplinary collaboration. Moreover, these models serve as useful tools to validate existing theories, to test and generate new hypotheses and to make predictions of real phenomena.

Within computational neuroscience, one tool that has become widely used to study brain function is the brain network model (BNM), defined as a model that reproduces the activity of an entire brain by incorporating neural mass models (NMM), to simulate neural activity, into an SC network derived from the tractography analysis of dwMRI data (Schirner et al., 2015). Integrating these two elements, we have a framework to virtually experiment with brain structure and function in health and disease, even in a personalized way (V. Jirsa et al., 2023).

To build a SC network, dwMRI measuring the anisotropy of water diffusion in the brain are reconstructed. Different algorithms associate a probability distribution of the orientation of fibres to each voxel of the dwMRI volume (Sinke et al., 2018). Then, a fibre tracking strategy constructs streamlines connecting the different regions of the brain (Gutierrez et al., 2020; Jeurissen et al., 2017). These streamlines are built by following the most likely trajectory of the white matter tract from randomly located seeds, given the previous reconstruction probabilities. Specific rules are used to determine when the algorithm stops, where the streamline ends, and whether the result is valid (F.-C. Yeh et al., 2013). These reconstructions provide insights into the organization and integrity of white matter tracts. Once tractography is completed, the resulting set of streamlines generated can be interpolated within a parcellation atlas of the brain to obtain an SC matrix that quantifies how many streamlines connect two brain regions and what is the length of those pathways (C.-H. Yeh et al., 2020). These maps are symmetric, as only the orientation (but not the direction) of the diffusion of water molecules is captured in the dwMRI image.

NMM are sets of differential equations that reproduce key features of the oscillatory dynamics of neuronal populations. There are different types of NMMs depending on their provenance including phenomenological, biological and reduced models. Phenomenological models (e.g., Kuramoto), come from the field of physics and were developed to study natural phenomena such as synchronization or bifurcations, usually without neuronal activity as target (Kuramoto, 1975; Landau, 1944; Stuart, 1960). Biologically-inspired models (e.g., Wilson-Cowan), are developed to integrate features of actual neural tissue, for instance, the presence of different types of cells and their specific electrophysiological behaviours (H. Wilson & Cowan, 1973; Zetterberg et al., 1978). Finally, reduced models (e.g., Wong-Wang) are developed through the mathematical simplification (i.e., mean-field reduction) of spiking neural network models in which neuronal populations are described through the interactions of individual neurons (Stefanescu & Jirsa, 2008; Wong & Wang, 2006). In this thesis, we used a biological model proposed by Jansen and Rit (1995) to take advantage of the biologically plausible definition of parameters, which becomes essential to link the model to the empirical evidence in AD.

BNMs have already been used to model AD at the mesoscale level. Some studies have adjusted model parameters to get insights about different aspects of the disease such as Zimmermann et al. (2018) that adjusted the synaptic connectivity parameters of the model to match empirical FC matrices in different AD stages finding significant correlations between the fitted parameters and cognitive performance. Similarly, Ranasinghe et al. (2022) optimized parameters to adjust spectral data in a model that included the effects of toxic AD proteins. They showed a link between the accumulation of $A\beta$ and hp-tau with the excitatory and inhibitory time constants of the NMM, respectively. Other studies have tried to explain the oscillatory slowing observed in AD. van Nifterick et al. (2022) explored different excitatory-inhibitory mechanisms that could lead to the slowing of AD using NMMs, proposing that both hyperexcitation and disinhibition could produce the oscillatory slowing. Alexandersen et al. (2023) integrated a model of toxic protein propagation in the brain with a BNM of neural activity that evolved over years of the disease. They showed that the oscillatory changes in the AD continuum could be more related to local neurodegeneration than to the disruption of interregional SC. From a similar approach, de Haan et al. (2012) proposed a model of activity-dependent degeneration to explain why central regions of the brain (i.e., network hubs) get disrupted earlier during the disease. Finally, these types of models have also been used to investigate the potential effects of AD interventions over neural activity, for instance, Stefanovski et al. (2019) modelled the disruption of inhibitory synapses in AD through changes in the inhibitory time constants linked to $A\beta$ accumulation and explored the potential of memantine for restoring healthy brain dynamics. Also, de Haan et al. (2017) tested several intervention targets on excitation-inhibition balance to protect the AD networks from neurodegeneration.

While BNMs are defined at the mesoscale level, sometimes it is necessary to model with finer detail, including neuron-specific electrophysiological dynamics. In that case, spiking neural networks (SNN) are at the right scale, modelling regions as interconnected sets of individual neurons simulated through their own sets of differential equations (Deco et al., 2008). These models allow defining parameters at the cellular level including the conductance of ion chan-

nels, membrane resting potentials, or activation thresholds, to name a few. These networks should not be confused with artificial neural networks (ANN) (Yamazaki et al., 2022) whose aims are clearly different: the latter are intended to serve machine learning applications while the former are intended to reproduce a biological phenomenon as accurately as possible.

1.7 Brain stimulation to intervene in Alzheimer's

In AD, intense efforts have been delivered to develop effective treatments. For many years, the only available medications were designed to alleviate cognitive symptoms and improve the patient's daily lives, such as cholinesterase inhibitors and NMDA receptor antagonists (Ajenikoko et al., 2023; Conti Filho et al., 2023). Just recently, a brand new disease-modifying immunotherapy targeting to reduce $A\beta$ deposition called Lecanemab was approved by the FDA (U.S. Food and Drug Administration) showing to slow down cognitive decline after 18 months of administration (van Dyck et al., 2023). While promising, the drug does not halt or revert the pathological process, underscoring the need to explore and design further and complementary intervention approaches.

Non-invasive brain stimulation (NIBS) techniques, such as transcranial magnetic stimulation (TMS) and transcranial electric stimulation (tES), hold promise as treatment for AD (Chang et al., 2018). These methods involve the application of targeted electric or magnetic fields over the scalp to modulate brain activity. NIBS are currently under intense investigation testing different protocols and their immediate to long-term effects on cognition to understand their potential to intervene in AD and to enhance cognition (Dong et al., 2018; Koch et al., 2022; Y. Liu et al., 2023; Matzen et al., 2015; Nissim et al., 2023).

Among these techniques, transcranial alternating current stimulation (tACS) is a type of tES that consists in applying weak alternating electrical currents to the scalp to entrain or modulate neural oscillations. By delivering these oscillatory currents at specific frequencies and amplitudes, tACS can temporarily shape brain activity and synchronization patterns (Herrmann et al., 2013; A. Liu, Vöröslakos, Kronberg, Henin, Krause, et al., 2018). This technique holds the

potential to intervene in one of the key early changes of brain activity in AD: hypersynchrony. Reducing levels of hypersynchrony in AD could be a proxy to slow down the vicious cycle established between cellular hyperactivity and the production and accumulation of $A\beta$ (Maestú et al., 2021).

These interventions can (and should) be tested through computational modelling before their application in experimental contexts. By integrating the modelling of current propagation (Y. Huang et al., 2018) with models of brain activity as BNMs, it is possible to explore *in-silico* the effects of stimulation. This poses a good opportunity to guide the application of the technique by exploring different stimulation setups and parameterizations for specific problems. Research in this line have already started to emerge. Merlet et al. (2013) tested the effects of tACS at the individual alpha frequency of a subject to increase the power in the alpha band. Luppi et al. (2024) optimized a tDCS stimulation protocol to protect the brain from the disruptions related to AD, applying in-silico stimulation to a model of the neurodegeneration process. Other studies with a higher level of detail have shown how the morphology and the orientation of neurons relative to the induced electromagnetic field could determine the effects generated on the underlying tissue (Aberra et al., 2020; Tran et al., 2022).

1.8 Aims and hypotheses

The overarching aim of this thesis is to build a computational framework that: 1) enhances the mechanistic comprehension of connectivity changes related to episodic memory occurring in AD, and 2) offers an in-silico tool to test potential interventions. We divided the project into three main objectives: first, modelling and simulating healthy brain resting-state to reproduce the network activity associated with the consolidation of episodic memory; second, modelling the impact of AD neurobiological changes over neural activity and network integrity; and finally, exploring from a computational perspective the potential of tACS as a therapeutic intervention to restore a healthy functioning of brain networks in AD. Following these objectives, the manuscript is structured into three parts, one part per objective that may include one or more research studies.

In the first part (chapter 2), we approached the building of BNMs from healthy patients' neuroimaging data (first objective), and we used them to evaluate the role of the thalamus in shaping resting-state FC. The preliminary outline of this thesis was intended to evaluate the impact of subcortical disconnections on AD, and more specially, the impact of thalamic disruptions. Therefore, we studied whether including/excluding the thalamus from the simulations would change the emergent FC in healthy networks. This would be a first step towards understanding how the thalamus could be involved in shaping neural networks supporting episodic memory, and serving to better understand dysfunction in AD. However, the unexpected results shifted our focus towards a more distributed approach.

The second part (chapter 3) presents a multiscale model of AD progression that integrates the type of BNM built in the previous part with a model of protein propagation that simulates the diffusion of toxic proteins in AD ($A\beta$ and tau) across the network. Within the framework of this integrative model, we explored a set of causal hypotheses on the evolution of AD, shining light on the contribution of different factors at several levels of analysis.

The final part investigates the potential of tACS in restoring healthy brain function. This part contains two pieces of research. The first one (chapter 4) presents a technical look into the effect that cortical morphology may have to determine the impact of stimulation over network function. In this study, we lowered the level of analysis in our simulations to cells building a SNN model, and evaluating the relevance of the relative orientation of pyramidal cells with respect to the orientation of the electric field generated by the stimulation.

The insights from chapter 4 supported the modelling framework presented in the last piece of research in chapter 5. In this study, we modelled the application of tACS to try to reduce the front-parietal hypersynchronization observed in the early stages of AD evolution. This intervention could be a potential therapeutical approach to retain or slow down the pace of the disease evolution.

The last chapter (chapter 6) includes an overarching discussion of the presented work and final remarks.

PART I

Simulating healthy brain dynamics

"All models are wrong, but some are useful"

George E. P. Box

The first aim of this thesis was to build a model of healthy brain function as a first step towards investigating the impact of structural disconnections happening in AD. As mentioned above, the preliminary outline of this thesis included a special interest on the effects of subcortical disconnections, and specially, of the thalamus as a relay node involved in the DMN (Alves et al., 2019; S. M. Sherman & Guillery, 2011). Therefore, we used the healthy brain models to perform a set of computational experiments in which we evaluated the impact of the thalamic SC to shape cortical resting state FC.

Chapter 2

Modeling the role of thalamus in resting state functional connectivity

The thalamus is a central brain structure that serves as a relay station for sensory inputs from the periphery to the cortex and regulates cortical arousal. Traditionally, it has been regarded as a passive relay that transmits information between brain regions. However, recent studies have suggested that the thalamus may also play a role in shaping functional connectivity (FC) in a task-based context. Based on this idea, we hypothesized that due to its centrality in the network and its involvement in cortical activation, the thalamus may also contribute to resting-state FC, a key neurological biomarker widely used to characterize brain function in health and disease. To investigate this hypothesis, we constructed[1] ten in-silico brain network models based on neuroimaging data (MEG, MRI, and dwMRI), and simulated them including and excluding the thalamus, and raising the noise into thalamus to represent the afferences related to the reticular activating system (RAS) and the relay of peripheral sensory inputs. We simulated brain activity and compared the resulting FC to their empirical MEG counterparts to evaluate model's performance. Results showed that a parceled version of the thalamus with higher noise, able to drive damped cortical oscillators, enhanced the match to empirical FC. However, with an already active self-oscillatory cortex, no impact on the dynamics was observed when introducing the thalamus. We also demonstrated that the enhanced performance was not related to the structural connectivity of the thalamus, but to its higher noisy inputs.

1. Work in this chapter can be found in Cabrera-Álvarez J, Doorn N, Maestú F, Susi G (2023) Modeling the role of the thalamus in resting-state functional connectivity: Nature or structure. *PLOS Computational Biology* 19(8): e1011007.

Additionally, we highlighted the relevance of a balanced signal-to-noise ratio in thalamus to allow it to propagate its own dynamics. In conclusion, our study sheds light on the role of the thalamus in shaping brain dynamics and FC in resting-state and allowed us to discuss the general role of criticality in the brain at the mesoscale level.

2.1 Introduction

In humans, the thalamus is a nut size structure near the center of the brain that relays sensory inputs traveling to the cortex (Guillery & Sherman, 2002), fosters cortico-cortical communication through transthalamic pathways (Kato, 1990; S. M. Sherman & Guillery, 2011), and controls cortical arousal through the reticular activating system (RAS) (Garcia-Rill, 2009). To carry out these tasks, it contains three functionally distinct parts (E. G. Jones, 1985): dorsal, ventral, and intralaminar. The dorsal part communicates bidirectionally with the cortex establishing two schemes of information exchange (Halassa & Sherman, 2019; S. Sherman, 2016) (see Fig 2.1): first-order relay, in which the thalamus receives subcortical and sensory inputs (i.e., driving inputs), relays them to the cortex through excitatory thalamocortical cells and gets back modulatory feedback from layer 6 pyramidal neurons (i.e., modulatory inputs); and higher order relay, in which the thalamus receives inputs from layer 5 pyramidal cells of a cortical region and relays them to another location in the cortex, creating a transthalamic pathway for cortico-cortical connections (Kato, 1990; S. M. Sherman & Guillery, 2011). In the ventral part, the reticular nucleus' inhibitory neurons establish connections both with each other and with neurons in the dorsal nuclei, to regulate and foster communication inside the thalamus (Crabtree, 2018; S. M. Sherman & Guillery, 2005). The interactions between the dorsal and ventral parts of the thalamus allow for the generation of sustainable oscillations of neural activity, such as delta oscillations, sleep spindles, and slow waves, that may propagate to the cortex and influence its dynamics (David & Friston, 2003; Fogerson & Huguenard,

2016; Fuentealba & Steriade, 2005; Huguenard & McCormick, 2007; Lopes da Silva, 1991; Schreiner et al., 2022). The intralaminar part is involved in the RAS (Steriade, 1996) delivering cholinergic and monoaminergic neurotransmission diffusely to the cortex and controlling arousal (Garcia-Rill, 2009).

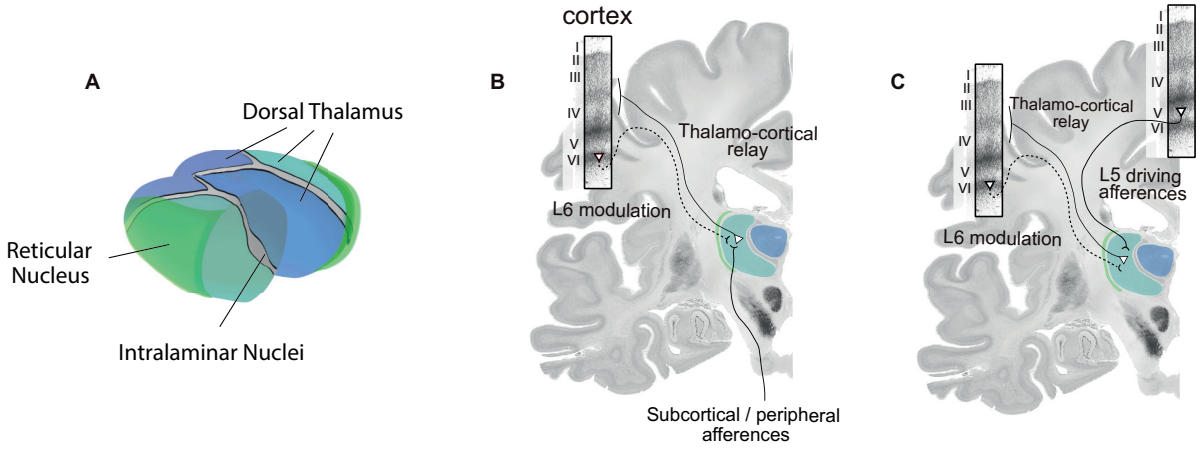


Figure 2.1: Main schemes of thalamocortical interaction. A) Functionally distinct parts of the thalamus including the dorsal thalamus with its anterior, lateral, and medial regions, the reticular nucleus as the main component of the ventral thalamus in green, and the intralaminar nuclei in grey. B) First-order relay scheme in which the subcortical/peripheral afferences are relayed to the cortex generally to layers 3 and 4. C) High-order relay scheme in which afferences from a cortical region are relayed to another. Coronal slices were acquired from the Big Brain project (Amunts et al., 2013) using ebrains platform.

Through these pathways, the thalamus connects to a widespread set of cortical regions (Behrens et al., 2003; Hwang et al., 2017; Iturria-Medina et al., 2007), playing a role in different psychological processes such as sleep (Jan et al., 2009; Schreiner et al., 2022; Vantomme et al., 2019), pain (Jin et al., 2020; Vartiainen et al., 2016), memory and learning (Wolff & Vann, 2018), attention (Portas et al., 1998; Schmitt et al., 2017; Wimmer et al., 2015), motor and sensory processing (Huguenard & McCormick, 2007; S. M. Sherman & Guillery, 2005; Torrico & Munakomi, 2021), and consciousness (Alkire et al., 2008; Laureys, 2005; Redinbaugh et al., 2020; Schiff, 2010; Tasserie et al., 2022). This role of the thalamus has been classically depicted as a passive relay that transfers information between brain regions (S. M. Sherman, 2007; Wolff & Vann, 2018), however recent findings are challenging this view (Barson et al., 2020; Dehghani & Wimmer, 2019; Hwang et al., 2017; Nakajima & Halassa, 2017; Wolff & Vann, 2018). Specifically, Schmitt et al. (2017) showed that the mediodorsal thalamus was

amplifying a FC pattern supporting the representation of specific task-related rules. All the thalamocortical mechanisms described above (i.e., the dorsal relay of peripheral sensory inputs, the transthalamic pathways for cortico-cortical communication, and the RAS neurotransmission that activates the cortex) may contribute to define the FC in the brain. Our study is aimed at understanding how.

FC is defined as a correlation between spatially distant neurophysiological signals (K. J. Friston, 1994) representing the functional integration of psychological processes in distributed brain networks (K. J. Friston, 2011). Early neuroimaging studies were focused on revealing the activity patterns underlying cognitive processes during task execution, using resting-state as a control condition (Raichle, 2010). However, later findings showed that the brain in resting-state has a rich intrinsic activity (Mason et al., 2007; Raichle et al., 2001) related to automatic and unconscious cognitive processing (Christoff et al., 2009; Raichle, 2015). Since then, resting-state FC (rsFC) has been used to characterize brain function in health and disease (Hausman et al., 2020; Spinosa et al., 2022; Tang et al., 2022) usually considering it as a static measure. More recently, this approach has been extended to capture the temporal richness of the activity patterns in resting-state through the concept of dynamical FC (dFC) (Hutchison et al., 2013; Preti et al., 2017) which has been suggested to reflect ongoing cognitive processing and that may be more informative of brain function and dysfunction than the static form (Cohen, 2018; Gonzalez-Castillo et al., 2015; Petkoski et al., 2023; Sadaghiani et al., 2015). Both metrics support the characterization of healthy aging, for which a general decrease in static FC, complemented by a slowing and less complex dFC has been shown and related to changes in cognitive performance (Battaglia et al., 2020; Betzel et al., 2014; Fjell et al., 2015; Sala-Llonch et al., 2015). Interestingly, some authors have proposed that changes in the thalamocortical network may contribute substantially to the disruptions in FC and cognition during aging (Fama & Sullivan, 2015; Goldstone et al., 2018). Understanding the mechanisms

that underlie and control (d)FC is an important research question that is still undisclosed, especially in aging. Here, we hypothesize that a similar thalamic mechanism that has been shown to be involved in defining FC during task execution (Schmitt et al., 2017) might also be active in resting-state.

Computational modeling allows for the generation of in-silico versions of real brains and personalized brain dynamics (Schirner et al., 2015) employing brain network models (BNM). A BNM is based on: a structural connectivity (SC) network derived from diffusion-weighted MRI that captures how brain regions are wired together, and a set of neural mass models (NMM) that reproduce the electrophysiological dynamics of each brain region. A widely studied NMM is the Jansen-Rit (JR) (Jansen & Rit, 1995), a biologically-inspired model of a cortical column that implements excitatory and inhibitory subpopulations to produce oscillatory activity. This model shows a bifurcation over a parameter representing the strength of its inputs (Grimbert & Faugeras, 2006; Spiegler et al., 2010) that will be used in our work to reproduce different modes of the thalamocortical interaction. In a system, a bifurcation occurs when a change in the value of a parameter (i.e., bifurcation parameter) produces a qualitative change in the behavior of the system. For the JR model, the bifurcation separates two different states: a fixed point state, where the model behaves as a damped oscillator (prebifurcation), and a limit cycle state, where the model autonomously oscillates (postbifurcation). These two states turned out to be relevant to understand our findings.

To investigate the potential contribution of the thalamus to rsFC, we built ten in-silico BNMs based on healthy subjects' neuroimaging data (MEG, MRI, dwMRI) using JR NMMs. We simulated them using: 1) three SC versions (i.e., parceled thalamus, pTh; thalamus as a single node, Th; without thalamus, woTh) to explore the effect of both the parcellation and the mere presence of cortico-cortical transthalamic pathways and 2) implementing a higher noisy input to the thalamus to reproduce its participation in RAS and the presence of peripheral sensory relays. We compared the simulated FC and dynamical FC (dFC) to their empirical MEG counterparts to evaluate performance. Additionally, we performed further simulations to explore under which conditions the thalamus contributes to the rsFC, including a control

experiment using the cortico-cerebellar network instead of the thalamocortical one, and a set of parameter explorations over the intrinsic thalamic oscillatory behavior and the magnitude of the implemented noise. Our results showed that a limited set of driving nodes leading cortical activity was a plausible scenario in rsFC, where the thalamus would play a major role due to its nature: involved in the RAS system, and projecting sensory relays. These results contribute to the understanding of the basic principles of whole-brain function in health and disease, and to enrich the current picture of criticality behavior in the brain.

2.2 Materials and methods

2.2.1 Empirical dataset

MRI (T1 and DWI) scans and MEG recordings were acquired from 10 healthy participants in resting-state, with ages between 62 and 77 years old (mean 69, sd 4.17, 3 males, 7 females) from a dataset owned by the Centre of Cognitive and Computational Neuroscience, UCM, Madrid.

MRI-T1 scans were recorded in a General Electric 1.5 Tesla magnetic resonance scanner, using a high-resolution antenna and a homogenization PURE filter (fast spoiled gradient echo sequence, with parameters: repetition time/echo time/inversion time=11.2/4.2/450 ms; flip angle=12°; slice thickness=1 mm, 256×256 matrix, and field of view=256 mm).

Diffusion-weighted images (dw-MRI) were acquired with a single-shot echo-planar imaging sequence with the parameters: echo time/repetition time=96.1/12,000 ms; NEX 3 for increasing the SNR; slice thickness=2.4 mm, 128×128 matrix, and field of view=30.7 cm yielding an isotropic voxel of 2.4 mm; 1 image with no diffusion sensitization (i.e., T2-weighted b0 images) and 25 dw-MRI (b=900 s/mm2).

MEG recordings were acquired with an Elekta-Neuromag MEG system with 306 channels at 1000Hz sampling frequency and an online band-pass filtered between 0.1 and 330Hz. MEG protocol consisted of 5 min resting-state eyes closed.

All participants provided informed consent.

2.2.2 Functional connectivity

MEG recordings were preprocessed offline using the spatiotemporal signal space separation (tSSS) filtering algorithm (Taulu & Hari, 2009), embedded in the Maxfilter Software v2.2 (correlation limit of 0.9 and correlation window of 10 seconds), to eliminate magnetic noise and compensate for head movements during the recording. Continuous MEG data were preprocessed using the Fieldtrip Toolbox (Oostenveld et al., 2011), where an independent component-based algorithm was applied to remove the effects of ocular and cardiac signals from the data, together with external noise.

Source reconstruction was performed using the software Brainstorm (Tadel et al., 2011), anatomically informed by the MRI scans of each subject. We employed the minimum norm estimates method (M. Hämäläinen & Ilmoniemi, 1994), with the *constrained dipoles* variant, by which the current dipoles are oriented normally to the cortical surface, to model the orientation of the macrocolumns of pyramidal neurons, perpendicular to the cortex (Tadel et al., 2019)

Source-space signals were then filtered in the alpha band (8-12 Hz) to calculate FC between the time series using the Phase Locking Value (PLV(α)) (Lachaux et al., 1999), and the resulting matrices were averaged into the AAL2 parcellation scheme (Rolls et al., 2015). We restricted the analysis to 1) cortical regions, to avoid the limitations of MEG recordings regarding deep brain signals (Bénar et al., 2021); and 2) the alpha band, for computational simplicity and being aware that it dominates MEG resting-state recordings. In addition, we computed dynamical functional connectivity matrices by extracting PLV(α) on consecutive intervals of 4 seconds of length with the sliding window approach and 50% of overlapping (Liuzzi et al., 2019), and evaluating the correlation between these PLV(α) matrices.

2.2.3 Structural connectivity

Diffusion-weighted images were processed using DSI Studio (http://dsi-studio.labsolver.org). The quality of the images was checked before fiber tracking and corrected for motion artifacts, eddy currents, and phase distortions. Then, tensor metrics were calculated. To improve reproducibility, we used a deterministic fiber tracking algorithm with augmented tracking strategies (F.-C. Yeh, 2020; F.-C. Yeh et al., 2013; F. Yeh et al., 2010). The whole brain volume was used as seeding region. Both the anisotropy and angular thresholds were randomly selected (the latter, from 15 degrees to 90 degrees). The step size was randomly selected from 0.5 voxels to 1.5 voxels. A total of 5 million seeds were placed and tracks with lengths shorter than 15 or longer than 180 mm were discarded.

To explore the impact of including/excluding the thalamus in simulations, we performed a first experiment comparing three different structural connectivity (SC) versions of each subject brains': woTh, Th, and pTh. pTh consists of a brain network with 148 regions extracted from AAL3 atlas from which we kept the thalamic parcellation and, removed and merged the other areas to make it comparable to AAL2 scheme; Th consists of the 120 regions from AAL2; same for woTh in which we removed thalamic nuclei (118 regions). These three versions of the structural connectomes are represented in Fig 2.2 and included the cerebellum parceled into its nuclei. A list with all ROIs included can be found in S1 Table. Two connectivity matrices were calculated per SC version: counting the number of tracts connecting (i.e., passing through) each pair of brain regions, and the average length of those tracts.

As a control experiment, we applied the same process to the cerebellum as it is a brain region with similar network characteristics (see Tables 2.2 and S1), and it can also be modeled as a parceled structure and a single node. We extracted three SC versions per brain using AAL3 atlas: parceled cerebellum (pCer), cerebellum as a single node (Cer), and without cerebellum (woCer). The thalamus was modeled as parceled through all these versions, and therefore the resulting SCs were composed of 148, 122 and 120 regions, respectively.

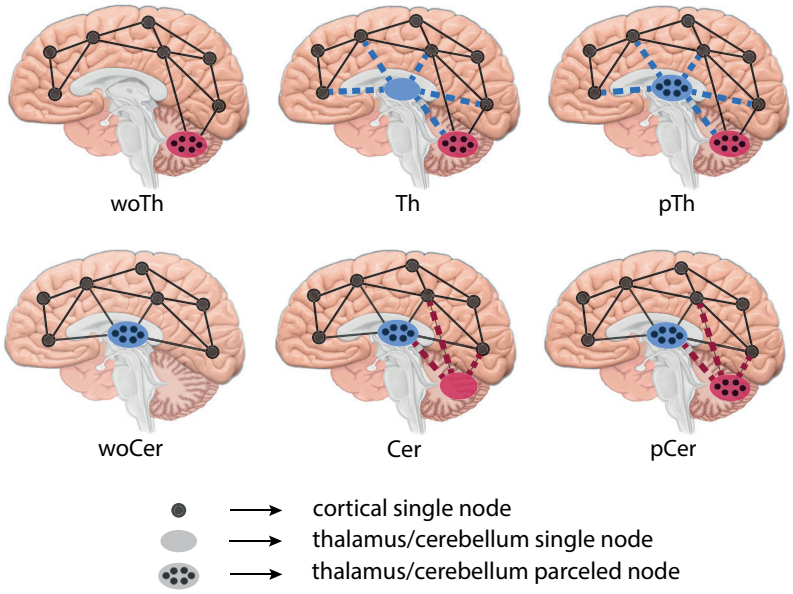


Figure 2.2: SC versions. First line shows the SC versions for the thalamocortical experiment: woTh, Th, pTh. The second line shows the SC versions for the cortico-cerebellar control experiment. Dashed lines representing driver connections.

2.2.4 Brain network model

SC matrices served as the skeleton for the BNMs implemented in TVB (Sanz-Leon et al., 2015) where regional signals were simulated using JR NMMs (Jansen & Rit, 1995). This is a biologically inspired model of a cortical column capable of reproducing alpha oscillations through a system of second-order coupled differential equations:

$$\dot{y}_{0_i}(t) = y_{3_i}(t) \tag{2.1}$$

$$\dot{y}_{1_i}(t) = y_{4_i}(t) \tag{2.2}$$

$$\dot{y}_{2_i}(t) = y_{5_i}(t) \tag{2.3}$$

$$\dot{y}_{3_i}(t) = AaS[y_{1_i}(t) - y_{2_i}(t)] - 2ay_{3_i}(t) - a^2 y_{0_i}(t) \tag{2.4}$$

$$\dot{y}_{4_i}(t) = Aa(input(t) + C_2 S[C_1 y_{0_i}(t)]) - 2ay_{4_i}(t) - a^2 y_{1_i}(t) \tag{2.5}$$

$$\dot{y}_{5_i}(t) = Bb(C_4 S[C_3 y_{0_i}(t)]) - 2by_{5_i}(t) - b^2 y_{2_i}(t) \tag{2.6}$$

Where:

$$S[v] \;=\; \frac{(2 \;\cdot\; v_{\max})}{1 \;+\; \exp^{r(v_0 - v)}} \tag{2.7}$$

The inter-regional communication introduces heterogeneity in terms of connection strength w_{ji}, and conduction delays d_{ji} (i.e., tract length / conduction speed) between nodes i and j, where:

$$input(t) = p_i + \eta_i(t) + g \sum_{j=1}^{n} w_{ji} \cdot S[y_{1_j}(t - d_{ji}) - y_{2_j}(t - d_{ji})] \tag{2.8}$$

It represents the electrophysiological activity (in voltage) from three subpopulations of neurons: pyramidal neurons (y_0), excitatory interneurons (y_1), and inhibitory interneurons (y_2). These subpopulations are interconnected (Fig 2.3) and integrate external inputs from other cortical columns. The communication is implemented in terms of firing rate (Eqs. 2.1 to 2.6) and a sigmoidal function (Eq. 2.7) stands for the conversion from voltage to firing rate.

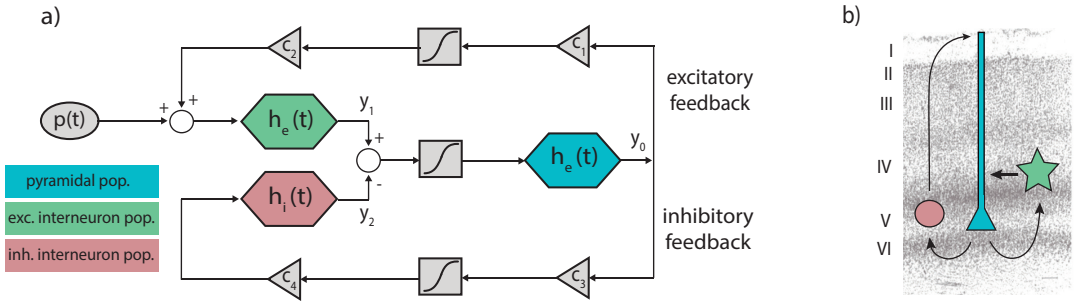


Figure 2.3: JR model of a cortical column. a) Block diagram depicting JR operators and modules where each color is associated with a different neural population: pyramidal (cyan), excitatory interneurons (green) and inhibitory interneuron (red). b) Histological contextualization of the cortical layers. Modified from Jansen and Rit (1995) and Stefanovski et al. (2019)

The input represents two main drivers of activity in the NMMs: inter-regional communication and intrinsic input. The former consists of the signal transmission between nodes through the SC of the brain in which weights are linearly scaled by a global coupling factor g, and tract lengths are divided by conduction speed to define d_{ji}. Conduction speed was set to 15 m/s given the low impact shown in previous parameter space explorations done in this project (see Fig S5). The latter is defined by a Gaussian noise with p mean and η std. Parameter values are described in Table 2.1.

The JR model shows two supercritical hopf bifurcations for the parameter p (Grimbert & Faugeras, 2006). When JR NMMs are implemented in a connected network, the parameter g scales the inter-regional input to nodes, becoming a bifurcation parameter. We used the first bifurcation to separate two NMM's behaviors (Fig 2.4): damped oscillator in the *prebifurcation* range where nodes tend to a fixed point in voltage, and limit cycle in the *postbifurcation* range where nodes self-oscillate in the alpha frequency.

2.2.5 Simulations

In the first experiment, simulations were performed varying two parameters: the standard deviation of the input to the thalamus (i.e., noise, η_{th}=[0.022, 2.2x10^{-8}]) representing the presence/absence of subcortical and peripheral inputs; and the thalamic structure (woTh, Th, pTh). The higher noise level was determined following previous research (David & Friston,

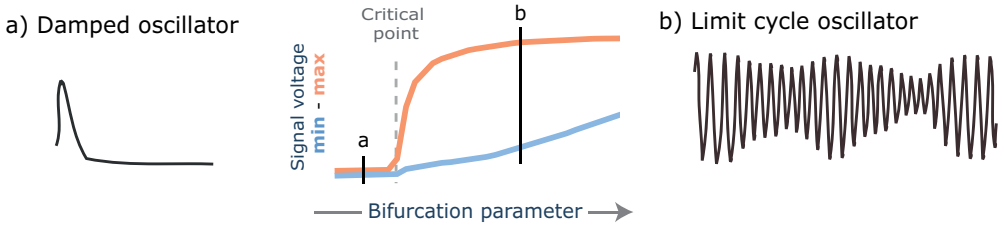


Figure 2.4: The bifurcation separates two states. In the center, a bifurcation diagram shows the minimum and maximum voltage for each value of the bifurcation parameter. At the critical point (dashed line), the bifurcation occurs and separates two states of the system: a) damped oscillator, whose activity tends to decay to a fixed point; and b) limit cycle oscillator, whose activity is a self-sustained oscillation.

Table 2.1: JR parameters used in simulations.

Parameter	Value	Unit	Description
A	3.25	mV	Average excitatory synaptic gain
B	22	mV	Average inhibitory synaptic gain
a	0.1	ms^{-1}	Time Constant of excitatory PSP
b	0.05	ms^{-1}	Time Constant of inhibitory PSP
C1	135		Average synaptic contacts: pyramidals to excitatory interneurons
C2	108		Average synaptic contacts: excitatory interneurons to pyramidals
C3	33.75		Average synaptic contacts: pyramidals to inhibitory interneurons
C4	33.75		Average synaptic contacts: inhibitory interneurons to pyramidals
v_{max}	0.0025	ms^{-1}	Half the maximum firing rate
r	0.56	mV^{-1}	Slope of the presynaptic function at v_0
v_0	6	mV	Potential when half the maximum firing rate is achieved
p	variable	ms^{-1}	Mean of random Gaussian intrinsic input
η	variable	ms^{-1}	Standard deviation of random Gaussian intrinsic input (noise)
g	variable		Coupling factor for inter-regional communication -multiplier of weights-
s	15	mm/ms	Conduction speed for inter-regional communication

Unless otherwise stated, we used default values for parameters p=0.09 and η=2.2x10^{-8}. Note that along the study, we introduce bimodalities in those parameters p_{th} and η_{th}).

2003), while the lower was chosen to avoid flat signals in the fixed state of the JR model. Additionally, we explored the parameter space for coupling factor (g=[0-60]). These models were simulated with the parameter p set to 0.09. We performed three simulations of 60 seconds (removing the initial 4 seconds to avoid transients) per model and computed two

metrics: the Pearson's correlation coefficient between the vectorized upper triangular matrices of the simulated and empirical FC (i.e., $r_{PLV(\alpha)}$); and the KSD(α) between the distributions of correlations in the dFC matrices (empirical and simulated). The same configuration was used in the control experiment with the cerebellum.

For further explorations, we simulated for 10 seconds (omitting the initial 2 seconds to avoid transients) different ranges of the mean intrinsic input to the thalamus (p_{th}) and its standard deviation (η_{th}). Besides the $r_{PLV(\alpha)}$ and KSD(α) metrics, we show 1) *bifurcation diagrams* capturing the averaged maximum and minimum signal's voltage per simulated ROI at each point in the parameter space. In the case of exploring 2 parameters at the same time (e.g., g and p_{th}), bifurcations are presented in heatmaps conveying information about the difference between the maximum and minimum signal voltage; 2) *signal-to-noise ratio* (SNR) in the thalamus that is computed by dividing the amplitude of simulated signals by the standard deviation of the Gaussian noise used for the thalamus; 3) *relative power* between cortex and thalamus calculated by dividing the averaged area of cortical spectra by the averaged area of thalamic spectra.

2.2.6 Statistics

We averaged the results of the 3 sets of simulations (i.e., repetitions) and performed statistical analysis for the group of 10 subjects. For the first experiment, we considered the maximum $r_{PLV(\alpha)}$ and minimum KSD(α) per subject, thalamic SC version and scenario. The effects of thalamic SC version and noise levels were evaluated using four two-way repeated measures ANOVA: two comparing maximum $r_{PLV(\alpha)}$ in prebifurcation and postbifurcation; and another two comparing minimum KSD; after checking for the statistical assumptions of normality (Shapiro's test) and sphericity (Mauchly's test). Pairwise comparisons for thalamic structure and thalamic noise were evaluated using Wilcoxon test, correcting for multiple comparisons using FDR Benjamini-Hochberg method. The same procedure was applied in the control experiment with the cerebro-cerebellar network to maximum $r_{PLV(\alpha)}$ comparisons.

2.3 Results

2.3.1 The thalamus impacts rsFC through its afferences

To explore the role of the thalamus in rsFC, we used two features of our in-silico BNMs: its structure, by simulating three different SC versions per subject (pTh, Th, woTh), and the NMMs noisy input by implementing higher than cortex thalamic noise (η_{th}=[0.022, 2.2x10^{-8}], η_{cx}=[2.2x10^{-8}]) to represent thalamic RAS system and peripheral first-order relays. We used the coupling parameter (*g*) to scale connectivity weights looking for the best match to empirical rsFC (i.e., the working point), as usual in whole-brain modeling (Deco & Jirsa, 2012; Deco et al., 2017; Deco et al., 2018; Palesi et al., 2020). Given that *g* acts as a bifurcation parameter, the simulated activity could be categorized into two regimes: prebifurcation, in which nodes operate as damped oscillators, and postbifurcation, in which nodes operate as autonomous oscillators. We simulated 60 seconds of brain activity per model and measured FC and dFC in the alpha band to compare to their empirical counterparts using Pearson's correlation ($r_{PLV(\alpha)}$) and Kolmogorov-Smirnov distance (KSD), respectively. We will show statistical comparisons using the best values of those metrics per subject and bifurcation side.

Results on $r_{PLV(\alpha)}$ showed a significant impact for both the structure [F(2, 18)=191.77, η_g^2=0.77, eps=0.55, p<0.0001], noise [F(1, 9)=178.25, η_g^2=0.87, eps=1, p<0.0001], and their interaction [F(2, 18)=172.12, η_g^2=0.77, eps=0.55, p<0.0001] in *prebifurcation*. In contrast, in *postbifurcation*, we did not find significant differences for structure [F(2, 18)=1.29, η_g^2=0.013, eps=0.76, p=0.29] or the interaction [F(2, 18)=1.74, η_g^2=0.004, eps=0.65, p=0.21] while a weak effect was found for noise [F(1, 9)=5.89, η_g^2=0.006, eps=1, p=0.038].

In prebifurcation, implementing high thalamic noise raised significantly $r_{PLV(\alpha)}$ values from close to zero to $r_{PLV(\alpha)}\approx$0.33 for Th [W=0, Cohen's d=5.09, p-corr=0.005], and $r_{PLV(\alpha)}\approx$0.45 for pTh [W=0, Cohen's d=6.8, p-corr=0.005] (see Fig 2.5). The resulting correlation values with high noise differed significantly between the implementations of the thalamic structure [F(2,

18)=186, η_g^2=0.87, eps=0.53, p-corr<0.0001], and pTh showed a global peak of $r_{PLV(\alpha)}$ that unexpectedly overcame the values observed in postbifurcation in 8 out of 10 subjects (see Fig S1) although the differences were not statistically significant [W=18, Cohen's d=0.142, p=0.375].

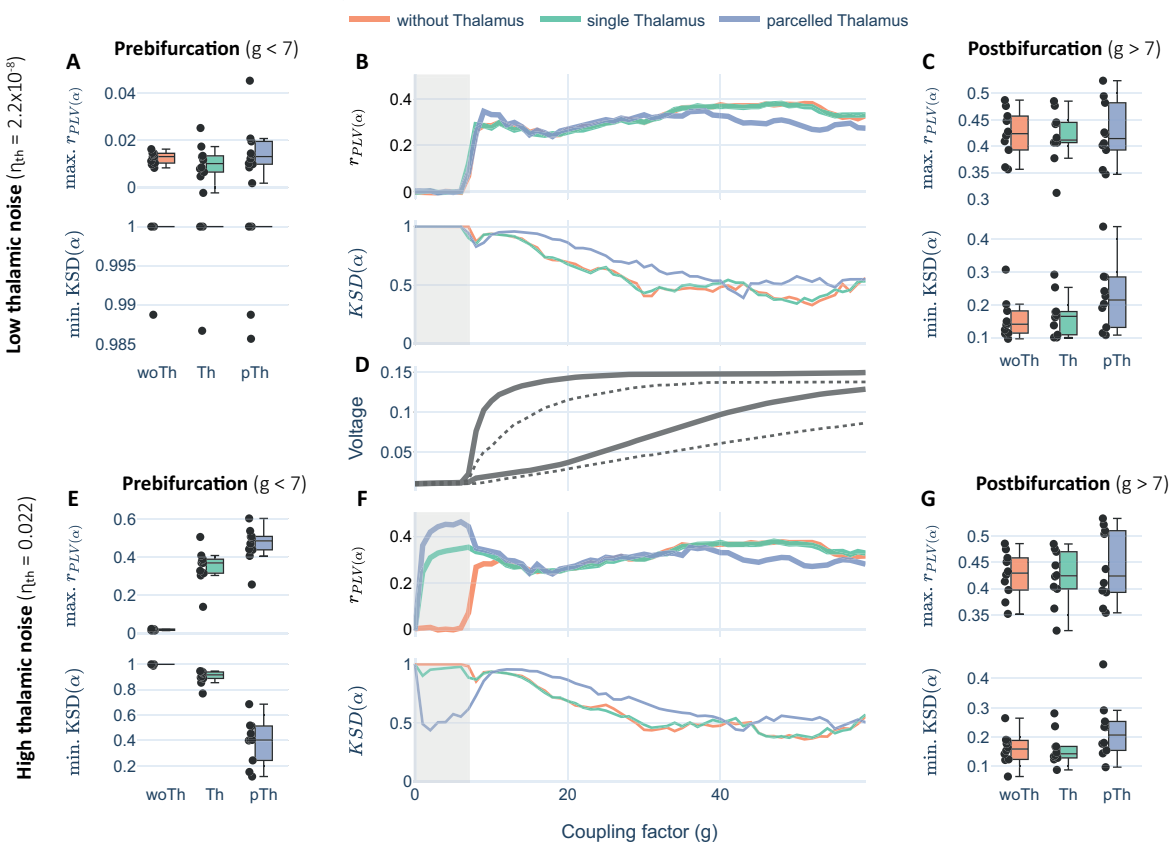


Figure 2.5: Thalamocortical experiment. Simulations for two levels of thalamic noise (low noise in A, B, C; high noise in E, F, G), three implementations of thalamocortical SC (in colours), and exploring the parameter space for coupling factor (g) divided into prebifurcation (g < 7 shadowed regions in B and F) and postbifurcation (g > 7). B, F shows group averaged $r_{PLV(\alpha)}$ and KSD(α) metrics. In the margins, boxplots show maximum values for those metrics per subject in prebifurcation (A, E) and postbifurcation (C, G). D shows the averaged bifurcation diagrams consisting of the maximum and minimum voltages per simulation for the cortex (thick line) and the thalamus (dashed line).

Regarding dFC, the results followed a similar trend in which thalamic structure [F(2, 18)=119.95, η_g^2=0.77, eps=0.56, p<0.0001], the thalamic noise [F(1, 9)=106.3, η_g^2=0.73, eps=1, p<0.0001] and the interaction [F(2, 18)=111.66, η_g^2=0.77, eps=0.55, p<0.0001] were statistically significant factors only in prebifurcation. In that range, high thalamic noise enhanced performance

for pTh [W=0, Cohen's d=4.89, p-corr=0.0029] showing a local KSD(α) minimum, and also slightly for Th [W=0, Cohen's d=2.5, p-corr=0.0029] (see Fig 2.5). Interestingly, we noticed that high values of KSD(α) for woTh and Th were due to opposite underlying dFC distributions. woTh correlations were centered near r=0 implying that FC matrices in time changed randomly, while Th correlations were centered near r=1 implying that FC matrices in time were quasistatic (see S2).

In summary, the inclusion of the thalamus in the model had an impact just in prebifurcation range (in which nodes operate as damped oscillators), and only when implementing a high thalamic noise. For pTh, this condition overcame the performance of any other model. In postbifurcation range (in which nodes autonomously oscillate) the values for $r_{PLV(\alpha)}$ were also high, however, the thalamus did not show a significant impact. The slight differences observed in the boxplots may be related to a higher number of autonomous oscillators trying to impose their own dynamics that may make it more difficult to establish stable functional interactions between the nodes.

2.3.2 Structure is not the key: comparing thalamocortical and cortico-cerebellar networks

We wondered whether the observed improvement of $r_{PLV(\alpha)}$ with high thalamic noise in prebifurcation could be explained by the specific characteristics of the SC pattern of the thalamus. To test this, we performed a control experiment comparing the thalamocortical network to another with similar properties: the cortico-cerebellar network (see Table 2.2). We built three SC versions per subject: parceled cerebellum (pCer), single node cerebellum (Cer) and without cerebellum (woCer), all of them including the thalamus parceled. We simulated them implementing high noise into the cerebellum to compare the model performance to the thalamocortical network.

Table 2.2: Network features for the thalamus and the cerebellum.

	Degree	Node strength	Betweenness	Path Length
Global average	0.827	0.231	0.00119	1.165
Thalamus average	0.851	0.111	0.00125	1.141
Cerebellum average	0.883	0.224	0.00132	1.110

Averaged network metrics for the thalamus, the cerebellum, and the global average of all regions. Similar relation to average was observed between regions in all metrics (degree, betweenness, and path length) except for node strength. For more details on the network analysis, see S1 Table.

We observed that the general trend found with the thalamocortical networks persisted. woCer simulations showed close to zero $r_{PLV(\alpha)}$ values in prebifurcation range with high noise, while Cer and pCer increased significantly their maximum correlations [F(2, 18)=148.39, η_g^2=0.895, eps=0.75, p-corr<0.0001] up to similar values obtained with the thalamocortical network (see Fig 2.6). Moreover, pCer in prebifurcation also resulted in a global maximum in $r_{PLV(\alpha)}$compared to postbifurcation values. Interestingly, Cer changed the underlying bifurcation diagram of the model, moving it toward higher values of coupling. This was reflected by the peak of $r_{PLV(\alpha)}$ in higher g values.

These results suggest that the specific thalamocortical SC pattern is not a major determinant of the thalamic contribution to rsFC.

2.3.3 Brain dynamics underlying each scenario

To understand the dynamics that underlie the observed values of $r_{PLV(\alpha)}$ and KSD, we extracted a simulation sample per model condition with pTh (i.e., high/low thalamic noise, and pre- / post-bifurcation; see Fig 2.7).

The dynamics in the prebifurcation range with high and low noise showed 1/f pink noise pattern. This is the result of a damped JR node processing a Gaussian noise as shown in previous literature (Kiebel et al., 2008; Wendling et al., 2002). High and low noise conditions in prebifurcation could be differentiated by their spectral powers and by the differences in FC matrices: with low noise, nodes are not powerful enough to interact, producing a functional

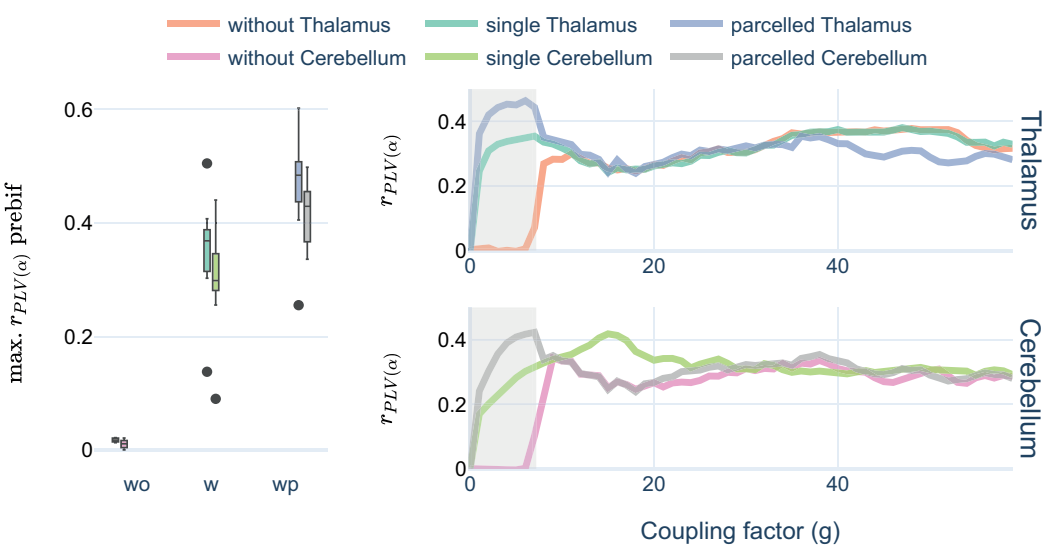


Figure 2.6: Cortico-cerebellar control experiment. Comparing the simulations implementing high noise in thalamus and in cerebellum with three versions of their structure. Left, boxplot showing maximum $r_{PLV(\alpha)}$ values per subject in the prebifurcation space for both experiments. Right, lineplots conveying averaged values of $r_{PLV(\alpha)}$ per value of coupling factor, and SC version. Shadowed areas covering the prebifurcation range.

disconnection that was captured by the FC and dFC matrices. In sharp contrast, in postbifurcation, nodes were self-oscillating in alpha frequency around 10Hz. Note the similarity between high and low noise to the thalamus in postbifurcation range, supporting the results reported in previous sections.

2.3.4 Thalamic alpha propagates to the cortex within a balanced SNR

The best-performing thalamocortical model was the one in prebifurcation that integrated high thalamic noise and pTh. Looking at its underlying dynamics, we observed that the spectrum was showing a 1/f shape. As we are trying to reproduce MEG FC, in which a predominant alpha frequency is usually observed, we wondered whether a spectral change towards alpha would impact the model performance. In this section, we manipulated the oscillatory frequency of the thalamus making it surpass bifurcation and self-oscillate in alpha by varying its average input, p_{th}. These simulations were performed with pTh structure and η_{th} = 0.022.

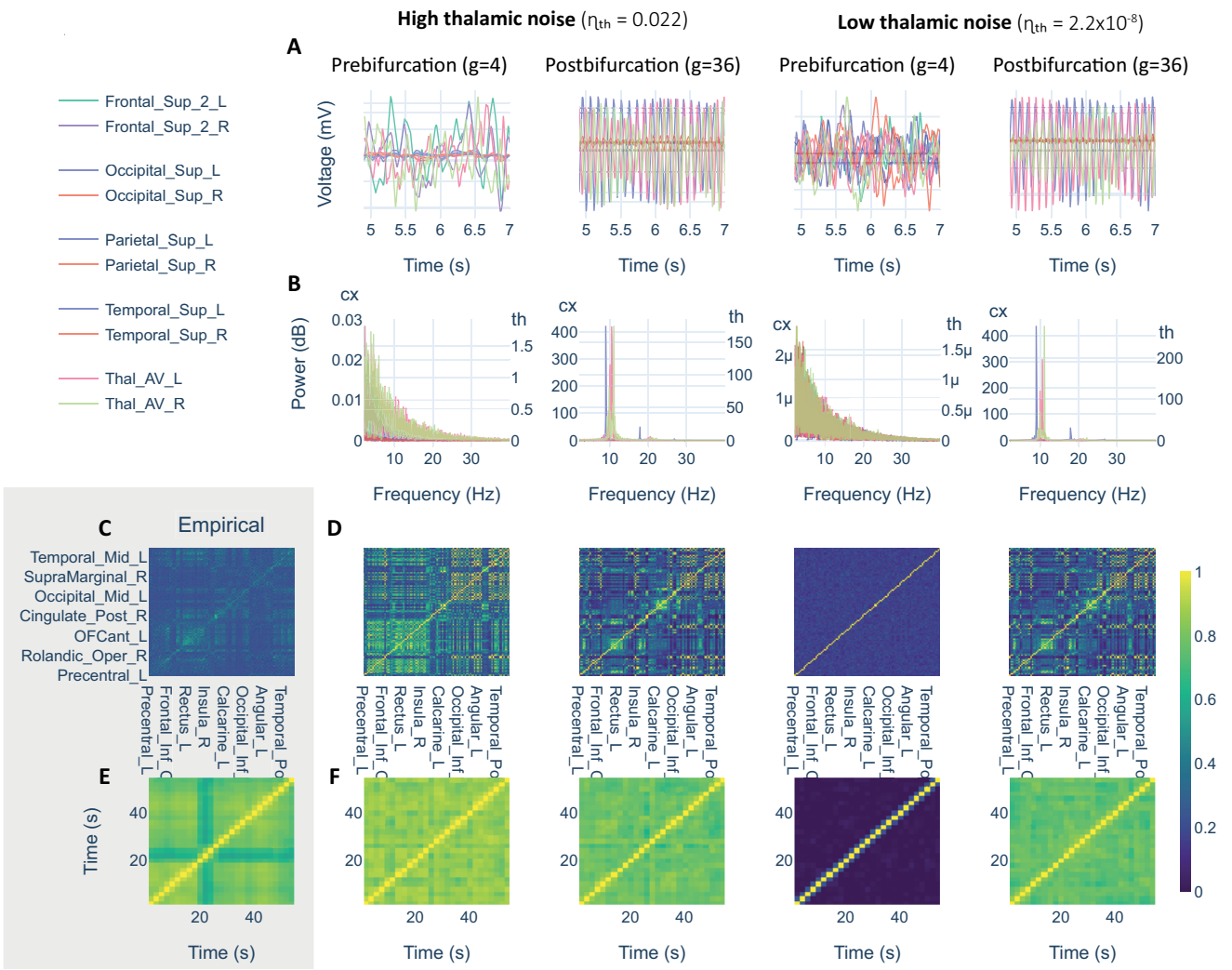


Figure 2.7: Simulation samples for one subject with parceled thalamus. In columns, simulation samples combining low/high thalamic noise with coupling values from pre/post- bifurcation. We selected g=4 to simulate prebifurcation and g=36 to simulate postbifurcation. First two rows show samples from the simulated signals (A), and their corresponding spectra (B). Last two rows showing PLV(α) (C, D) and dFC(α) (E, F). C and E showing empirical references for PLV(α) and dFC(α), respectively.

Simulations rising p_{th} in prebifurcation (g<7), resulted in a transition of thalamic nodes from the noisy 1/f pink noise spectra to an alpha oscillation (see Fig 2.8, FFT peak), passing first through the slow and high amplitude limit cycle of the JR model (Grimbert & Faugeras, 2006; Spiegler et al., 2010) at p_{th}=[0.11 - 0.13] (see the dark orange spot in Fig 2.8 SNR). In this transition along the bifurcation, $r_{PLV(\alpha)}$ lowered down right after the high power and slow limit cycle (p_{th} > 0.13). This could be due to a high SNR $\approx$ 6 producing hypersynchronization (mean

PLV≈0.7; see Fig 2.8 mean PLV). However, we did not find this phenomenon with the slow limit cycle (PLV(α)mean ≈0.5) even though it showed a higher SNR. This might be explained by the alpha band filtering that leaves out of the analysis the potentially hypersynchronizing oscillations of the slow limit cycle.

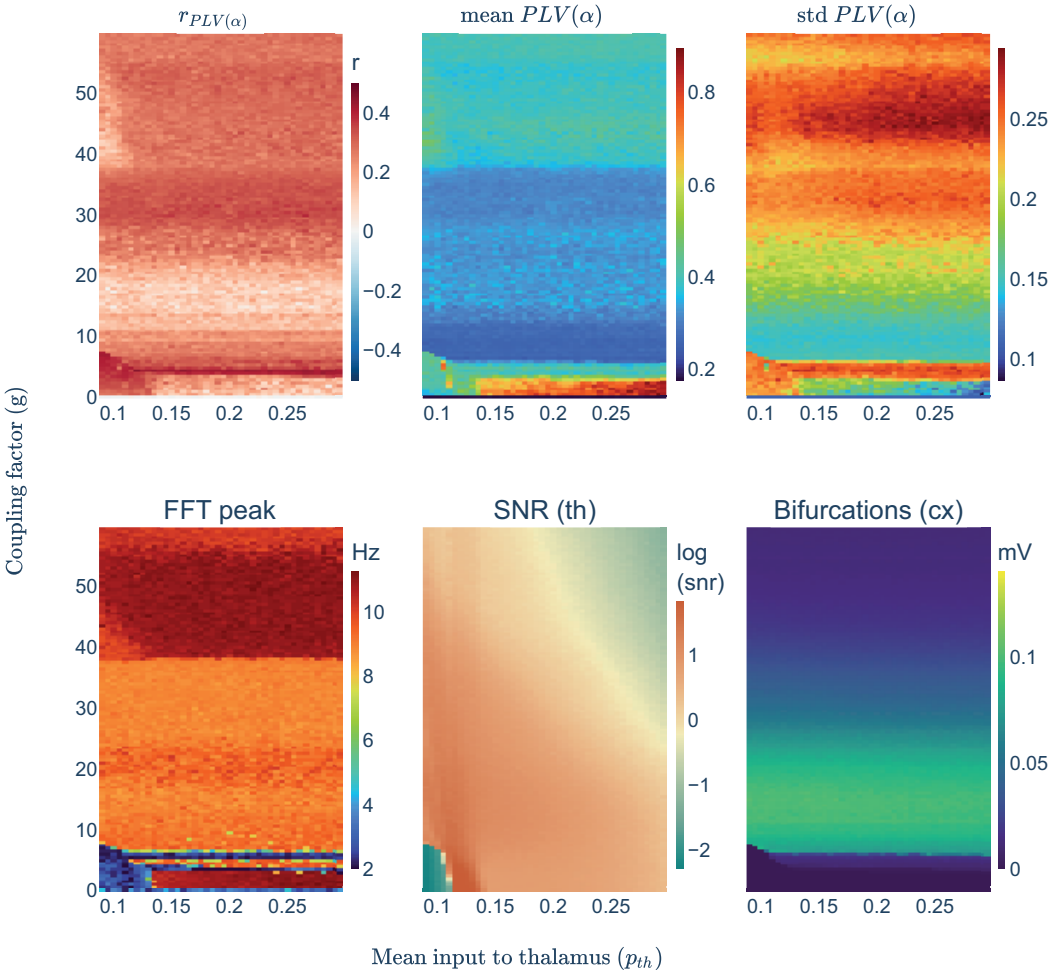


Figure 2.8: Parameter space explorations for p_{th} with high thalamic noise. Sets of three simulations averaged for subject one and parceled thalamus. Heatmaps showing different metrics from the same each simulation: the empirical-simulated correlation of PLV in alpha band ($r_{PLV(\alpha)}$), the simulated mean and std. of the PLV(α) values, the frequency peak of the nodes' averaged spectra (FFT peak), the signal to noise ratio in thalamic nodes computed as the amplitude of simulated signals divided by the standard deviation of the Gaussian noise used for the thalamus (SNR(th)), and the bifurcation of cortical signals using the averaged maximum-minimum signals' voltage.

Interestingly, the changes in thalamic activity indirectly increased the inter-regional inputs to cortical nodes, making some of them pass bifurcation at g≈3 and g≈6 (see the horizontal blue lines in Fig 2.8, FFT peak). These nodes produced a further rise in $r_{PLV(\alpha)}$ (see the horizontal red line in Fig 2.8, $r_{PLV(\alpha)}$) suggesting two important things for prebifurcation simulations: 1) that every node is a potential contributor of a general driving mechanism that we have located in the thalamus (through a high noise), and 2) that the number of drivers participating in that mechanism matters.

In the range of p_{th}=[0.13-0.3], where we observed alpha oscillations, $r_{PLV(\alpha)}$ decreased. We wondered whether this effect could be related to the rise in SNR after setting the thalamus to oscillate in the alpha band. Therefore, we fixed p_{th}=0.15, and we varied the noisy input to the thalamus (η_{th}) to explore its impact on model performance. We found an optimal balance for SNR at η_{th}=[0.05-0.15] in which the noisy inputs to the thalamus were enough to avoid hypersynchronization (see Fig 2.9 mean PLV) and low enough to maintain the intrinsic dynamics produced by the thalamus (i.e., alpha oscillations, see Fig 2.9 FFT peak). Further increases in noise would replace progressively the alpha oscillatory behavior by a 1/f spectra without reducing $r_{PLV(\alpha)}$.

From these observations, it could be thought that a general rise of noise in the model (i.e., to all nodes) would lead to better performance, however, in our modeling framework this is only true when the noise is implemented into a limited number of nodes. Independent noise into all cortical nodes is not linked to an enhancement of $r_{PLV(\alpha)}$ (see Fig S3).

From these parameter explorations, we extracted four additional models of interest to explore their underlying dynamics (see Fig 2.10). Two of them related to the exploration of p_{th}: one for the hypersynchrony situation (p_{th}=0.15, η_{th}=0.022), another for the slow JR limit cycle (p_{th}=0.12, η_{th}=0.022); and another two regarding the exploration of SNR: one for the optimal SNR (p_{th}=0.15, η_{th}=0.09), and another for a higher noise than the optimal range (p_{th}=0.15, η_{th}=0.5). Fig 2.10 shows the underlying dynamics for each of the additional model scenarios simulated with g=2.

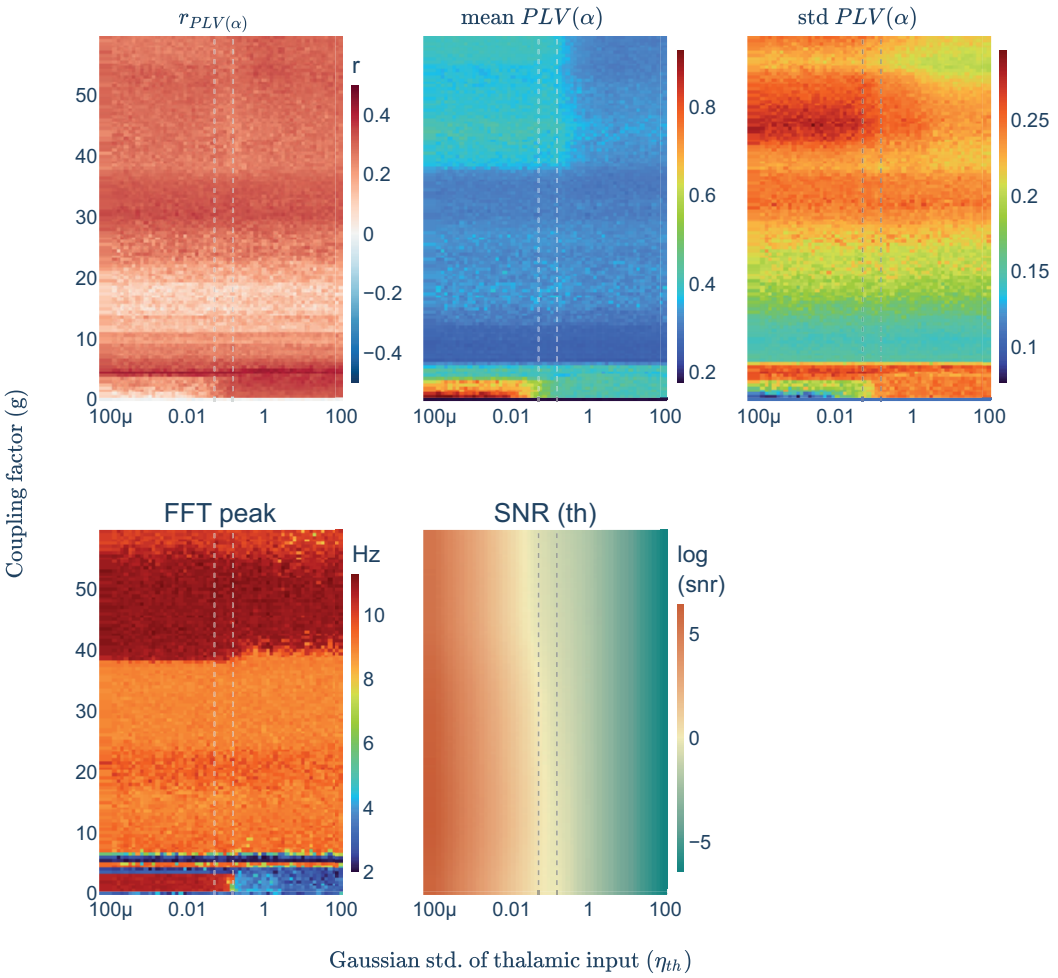


Figure 2.9: Parameter space explorations over η_{th} to balance SNR in the thalamus. Sets of three simulations averaged for subject one and parceled thalamus. Heatmaps showing different metrics from the same each simulation: the empirical-simulated correlation of PLV in alpha band ($r_{PLV(\alpha)}$), the simulated mean and std of the PLV(α) values, the frequency peak of the nodes' averaged spectra (FFT peak), the signal to noise ratio in thalamic nodes computed as the amplitude of simulated signals divided by the standard deviation of the Gaussian noise used for the thalamus (SNR(th)), and the bifurcation of cortical signals using the averaged maximum-minimum signals' voltage. Vertical dashed lines define the optimal SNR range.

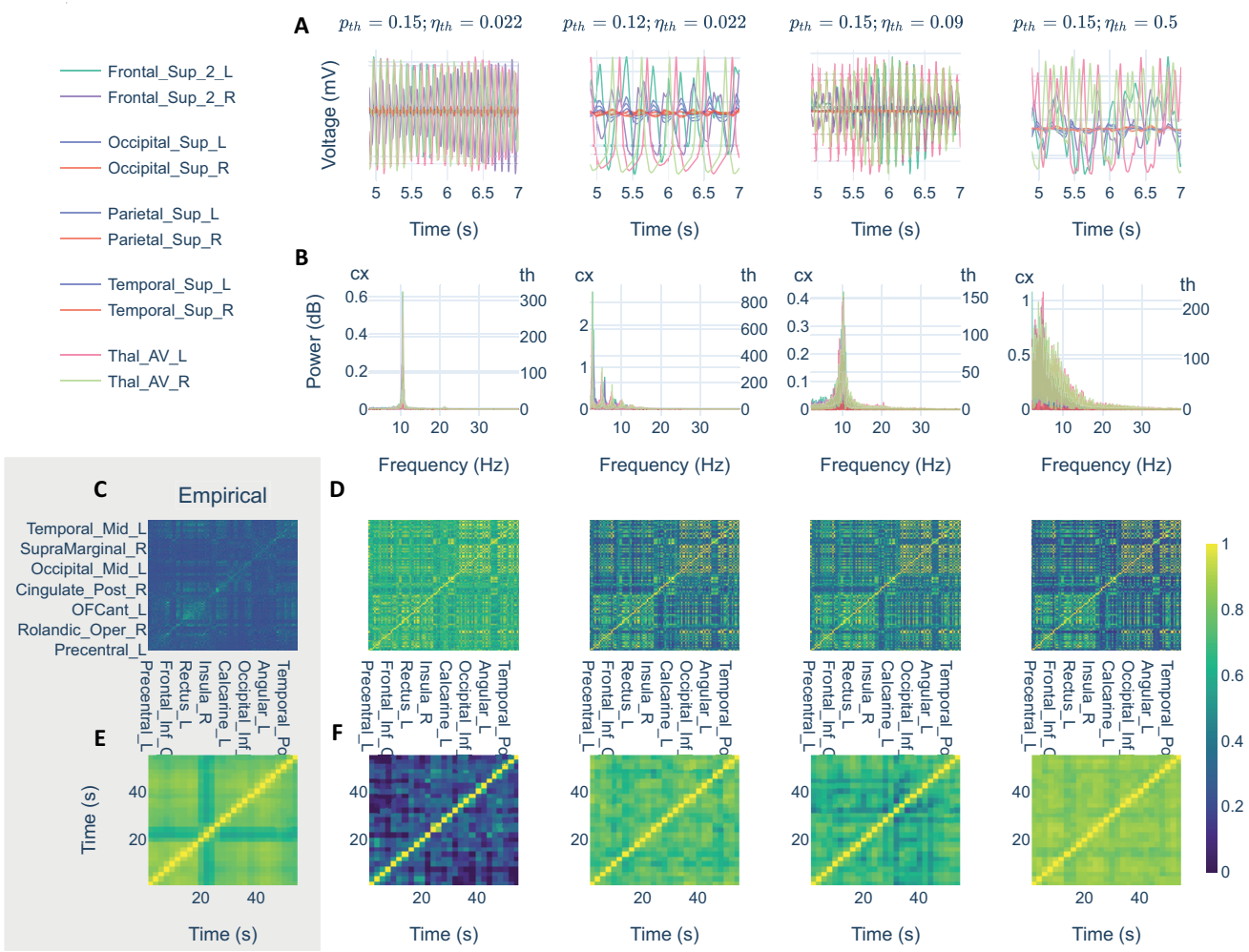


Figure 2.10: Complementary simulation samples. Simulation samples derived from the parameter explorations with parceled thalamus and cortical nodes in prebifurcation (g=2). In columns, simulation samples in which the thalamus drives cortical activity with different levels of noise (η_{th}=[0.022, 0.09, 0.5]) and at two different points of the thalamic bifurcation determined by $p_{th} = [0.12, 0.15]$, the former corresponds to the slow limit cycle of JR. First two rows show samples from the simulated signals (A), and their corresponding spectra (B). Last two rows showing PLV(α) (C, D) and dFC(α) (E, F). C and E showing empirical references for PLV(α) and dFC(α), respectively.

2.4 Discussion

Understanding thalamocortical networks is crucial for unraveling the complex dynamics of the human brain. These networks are essential for transmitting sensory information from the periphery to the cortex and regulating cortical arousal, which are fundamental processes for perception, attention, and cognition. In this study, we aimed to gain a deeper understanding

of the role of the thalamus in rsFC by utilizing computational brain models. Our experiments focused on testing two key features of thalamocortical networks: the presence of thalamic afferences related to the RAS and first-order sensory relays, and the structure of the thalamus. Interestingly, we found that only when we raised thalamic noisy inputs to represent the RAS and peripheral afferences activating a damped cortex, its presence affected the simulated dynamics. To validate our findings, we performed a control experiment using the cerebro-cerebellar network and showed that implementing high noise into the cerebellum could replicate the results observed in the thalamocortical network. Finally, we explored how the oscillatory behavior of thalamic nodes, specifically their frequency and SNR, could shape the emergent rsFC. Our study provides novel insights into the role of thalamocortical networks in shaping brain dynamics and highlights the relevance of balanced SNR activity for the propagation of alpha rhythms from the thalamus.

We expected that introducing the thalamus in our simulations would have generated a difference in model performance in postbifurcation, where the best correlations are usually found. However, this was not the case, as implementing the thalamus in our model only affected results in prebifurcation and when introducing a high thalamic noise to represent afferences from RAS system and peripheral sensory relays. In prebifurcation, nodes are operating as damped oscillators tending to relaxation at a fixed point. When we introduced high noise in the thalamus, its afferences to cortex rose cortical activation levels allowing for functional interactions. In this situation, the thalamus is driving cortical activation. Additionally, the best model performance was observed within this parametrization and including the thalamus with its dorsal nuclei divisions (pTh). More importantly, the postbifurcation range has been often associated with a state of generalized epileptic seizure (Breakspear et al., 2005; Wendling et al., 2016) due to its highly synchronized intra-node oscillatory activity (see the spectra at postbifurcation in Fig 4B) that is not the empirical target of this study (i.e., MEG resting state). Taken together, these ideas led us to focus on the prebifurcation range.

A further control experiment demonstrated that this mechanism was not directly related to thalamic SC. This was ascertained by embedding the driver mechanism into another hub-like region (i.e., cerebellum) and obtaining equivalent results for the match to empirical rsFC. This would mean that in our model, where all neural masses are functionally equal, any node could theoretically play the role of the thalamus. In this line, during parameter explorations, some isolated cortical nodes passing bifurcation would contribute to enhance performance by being part of that driving mechanism. This would add up to the observation that parceled structures (i.e., thalamus and cerebellum) performed better than their single node versions, indicating that the number of driver nodes matters. In further research, it should be explored whether there is a computational optimum number of drivers to reproduce rsFC that could be subject or session-specific, and whether these differences may be linked to differences in brain and cognitive functioning.

Taken together, our main conclusion is that *a limited set of driving nodes is likely to underlie the dynamics of rsFC*. We believe that those drivers might be linked both to the regions participating in the RAS system (Intralaminar Thalamus, Raphe Nuclei, and Locus Coeruleus) (Garcia-Rill, 2009; Steriade, 1996) and to the dorsal nuclei of the thalamus that are implicated in the relay of sensory information and have also been tightly linked to the generation of oscillatory behavior in the cortex in slow waves (Crunelli & Hughes, 2010; Rigas & Castro-Alamancos, 2007; Sanchez-Vives, 2020; Sheroziya & Timofeev, 2014). This would support the view of the thalamus as a driver and controller of cortical dynamics (Alonso & Swadlow, 2015; Logiaco et al., 2021; Mofakham et al., 2021; Schmitt et al., 2017; S. Sherman, 2016).

Further explorations on the spectral characteristics of the drivers showed that the thalamus could propagate its own intrinsic alpha dynamics when a balanced SNR was achieved. This feature represents the interaction between thalamocortical pacemaker neurons (Fogerson & Huguenard, 2016) and peripheral sensory inputs reaching the system and provoking event-related desynchronization (Palva & Palva, 2007; Pfurtscheller et al., 1994). The model showed a good performance for reproducing empirical rsFC in that optimal range and with additional noise, generating a 1/f spectra. However, lower levels of noise with an alpha-oscillating tha-

lamus reduced performance and led to a hypersynchronization situation transmitted from the thalamus to the cortex, generating an epileptic-like dynamic (Jiruska et al., 2013; Mishra et al., 2013). In line with these results, the thalamus has been proposed to be involved in the onset of temporal lobe epileptic seizures, transmitting more regular patterns of activity to the hippocampus (Y.-H. Li et al., 2014; C. H. Zhang et al., 2015).

From the computational perspective, previous work has shown that BNMs may reproduce better empirical rsFC when the models operate at the edge of bifurcation (Deco et al., 2017), the critical point. At this point, noisy excursions or the effect of nodes' interaction can lead the masses to behave in any of the two regimes separated by the critical point. This phenomenon, referred to as criticality (Deco & Jirsa, 2012), has been proposed to enhance the capacity of brain systems to convey information (Cocchi et al., 2017). However, in our study, we showed an equivalent performance both at the edge of bifurcation and over the whole prebifurcation range. This contrast might be explained by the different cortical and thalamic parametrization implemented in our nodes. Our thalamic driving nodes feed the cortex, leading the dynamics. In the cited study Deco et al. (2017), the nodes that randomly switch between states would represent the same driving mechanism as in our model. Interestingly though, our approach would suggest that criticality is not a necessary feature in the dynamics of a resting brain at the mesoscale level.

Many studies in the field have explicitly (Cabral et al., 2011; David et al., 2005; Demirtaş et al., 2017) or implicitly (Aerts et al., 2020; Courtiol et al., 2020; Deco & Jirsa, 2012; Stefanovski et al., 2019) excluded subcortical regions from their BNMs. This could be due to the technical limitations of recording deep brain signals and/or to the complexity of reconstructing SC schemes for small, deep crossing-fibers regions. But, more importantly, it could be due to the unknown role that these regions may play in shaping simulated whole brain dynamics. Some studies have attempted to unravel these mechanisms, showing the importance of the cerebellum for brain dynamics (Palesi et al., 2020), the relevance of cortico-subcortical interaction for shaping dynamical functional connectivity (Favaretto et al., 2022) and the relevance of neurotransmission (Deco et al., 2018; Kringelbach et al., 2020). Additionally, other studies

are paving the way towards multiscale computational models in which subcortical areas are implemented with a further spatiotemporal level of detail (Betzel & Bassett, 2017; D'Angelo & Jirsa, 2022; Meier et al., 2022a; Shaheen et al., 2022). These approaches could be an interesting path to extend our knowledge regarding the potential role of the thalamus (and other activating brain regions) in whole brain simulations.

In conclusion, our study provides novel insights into the role of thalamocortical networks in shaping brain dynamics. We demonstrate that a limited set of driving nodes leading cortical activation may better describe resting-state activity. The thalamus would be a relevant part in this mechanism due to its participation in the RAS system and through its peripheral sensory relays being delivered from its multiple dorsal nuclei. In this type of architecture, driving nodes might show a balanced SNR to avoid hypersynchronization in the network. Although it is still debated whether the thalamus has an active role in cognition (S. Sherman, 2016; Sieveritz & Raghavan, 2021; Wolff & Vann, 2018), our study strongly suggests its active participation in driving cortical dynamics and shaping FC in resting-state. These findings may contribute to a better understanding of brain function and dysfunction, fostering the development of new therapeutic approaches targeting thalamocortical circuits.

PART II

Integrative model of neurotoxicity in AD

"Knowing why is more important than learning what"

Watson (2010)

In the previous chapter, we showed how the thalamus could shape FC through its involvement in the RAS system and its relay function, but not through its specific SC pattern. These conclusions led us to reconsider the focus on thalamocortical SC as the aim for the following research step: modelling AD. We decided instead to focus on a wider approach to SC deficits linked to the proteinopathy and its spreading dynamics along the disease evolution. Therefore, in the next chapter, we present a multiscale model of AD that integrates proteinopathy dynamics and the BNM previously built to explore what alterations in AD are responsible for the observed electrophysiological changes reported in literature.

Chapter 3

A multiscale closed-loop neurotoxicity model of Alzheimer's disease progression explains functional connectivity alterations

The accumulation of amyloid-beta ($A\beta$) and hyperphosphorylated-tau (hp-tau) are two classical histopathological biomarkers in Alzheimer's disease (AD). However, their detailed interactions with the electrophysiological changes at the meso- and macroscale are not yet fully understood. We developed a mechanistic multiscale model of AD progression[1], linking proteinopathy to its effects on neural activity and vice-versa. We integrated a heterodimer model of prion-like protein propagation, and a brain network model of Jansen-Rit neural masses derived from human neuroimaging data whose parameters varied due to neurotoxicity. Results showed that changes in inhibition guided the electrophysiological alterations found in AD, and these changes were mainly attributed to $A\beta$ effects. Additionally, we found a causal disconnection between cellular hyperactivity and interregional hypersynchrony contrary to previous beliefs. Finally, we demonstrated that early $A\beta$ and hp-tau depositions' location determine the spatiotemporal profile of the proteinopathy. The presented model combines

1. Work in this Chapter can be found in Cabrera-Álvarez, J., Stefanovski, L., Martin, L., Susi, G., Maestú, F., & Ritter, P. (2024). A multiscale closed-loop neurotoxicity model of Alzheimer's disease progression explains functional connectivity alterations. eNeuro, 11(4), ENEURO.0345-23.2023.

the molecular effects of both $A\beta$ and hp-tau together with a mechanistic protein propagation model and network effects within a closed-loop model. This holds the potential to enlighten the interplay between AD mechanisms on various scales, aiming to develop and test novel hypotheses on the contribution of different AD-related variables to the disease evolution.

3.1 Introduction

Alzheimer's disease (AD) is a progressive neurodegenerative disorder widely characterized at several levels of analysis from molecules to cells to the whole brain. The interactions between these levels of analysis remain poorly understood, contributing to the limited treatment options (Breijyeh & Karaman, 2020; van Dyck et al., 2023). A mechanistic understanding of AD is essential for developing novel therapeutic interventions.

The main pathophysiological changes in AD involve the misfolding and accumulation of amyloid-β ($A\beta$) and a hyperphosphorylated version of the tau protein (hp-tau) in the brain (Masters et al., 2015). These two proteins have different toxic effects, while $A\beta$ generates hyperactivity through the disruption of GABAergic inhibitory synapses (Palop & Mucke, 2010) and the reduction of glutamate reuptake (Zott et al., 2019), hp-tau disrupts the synaptic connectivity of neurons by reducing the number of dendritic spines in pyramidal cells (Merino-Serrais et al., 2013). $A\beta$ tends to aggregate into plaques, while hp-tau aggregates into neurofibrillary tangles (NFTs). Following the prion hypothesis of AD, misfolded $A\beta$ and hp-tau propagate through the brain acting as seeds (i.e., prions) that trigger the misfolding and aggregation of their normal counterparts (Frost & Diamond, 2009; Gomez-Gutierrez & Morales, 2020; Walker, 2018). It has been shown that the hyperactivity produced by $A\beta$ orients the prionic propagation of hp-tau in the brain (Rodriguez et al., 2020) following the Braak stages from the entorhinal cortex to the neocortex, producing a network disruption that has been linked to cognitive decline (H. Braak & Braak, 1991a; H. Braak et al., 2011; Therriault et al., 2022). The higher the activity levels in a region, the faster the propagation of hp-tau to those regions. Additionally,

hyperactivation has also been linked to an enhanced extracellular secretion and deposition of $A\beta$ generating a cyclical phenomenon that reinforces bidirectionally neural hyperactivity and $A\beta$ concentration (M. A. Busche & Hyman, 2020; Cirrito et al., 2005; Kamenetz et al., 2003; Stargardt et al., 2015; K. Yamamoto et al., 2015).

At the whole brain level, electrophysiological recordings have shown a slowing of alpha frequency peak along the disease evolution (Babiloni et al., 2009; Garcés et al., 2013). Additionally, several studies have reported an early increase in alpha power and hypersynchrony between parietal regions (Nakamura et al., 2017, 2018), followed by a disruption in those network's functional connectivity (FC) and a rise in anterior hypersynchrony (López-Sanz et al., 2016b; Pusil et al., 2019). These observations suggest a temporal dissociation between anterior and posterior in the electrophysiological changes that occur in AD (Maestú et al., 2021). Finally, the whole network gets disrupted due to the effect of hp-tau accumulation and further generation of NFTs (Ahnaou et al., 2017; Palop et al., 2006; Pereira et al., 2019; Ranasinghe et al., 2014). Whether the hypersynchronization is linked to the previously mentioned cellular hyperactivity remains unknown (Maestú et al., 2021). Here, we hypothesize that hyperactivity causes an increase in interregional synchrony (i.e., FC) due to a higher rate of neural communication that enhances the coordination of distant neuronal groups.

In recent years, significant computational modelling efforts have employed brain network models (BNMs) to investigate neural activity and its relationship to several aspects of the disease (Alexandersen et al., 2023; Ranasinghe et al., 2022; Stefanovski et al., 2019; Stefanovski et al., 2021; van Nifterick et al., 2022). These models reproduce neural activity by using sets of differential equations known as neural mass models (NMMs) that are interconnected through empirically-derived structural connectivity (SC) networks based on tractography. These models are expected to serve as a tool for getting deeper insights into the mechanisms of AD and to be able to predict its appearance and evolution.

In this study, we extended a previously published multiscale model of AD evolution based on neuroimaging data that includes molecular, cellular, and interregional features of the brain (Alexandersen et al., 2023). Specifically, it integrates a heterodimer model for the generation and propagation of AD-related proteins, neuronal population activity, and interregional synaptic coupling. We aimed to explore the mechanisms that give rise to the observed neurophysiological changes in AD and to evaluate the relative impact of the different proteins involved. To pursue these goals, first, we explored an isolated neural population and the effects produced by changing the parameter candidates affected by AD (i.e., excitation and inhibition-related parameters). Second, we simulated the neurotoxicity model and adjusted its parameters to reproduce the empirically observed phenomena in AD (i.e., frequency slowing, relative alpha decrease, increase/decrease in excitation, and increase/decrease in functional connectivity). Finally, we use the resulting network model to analyze the impact of different biological mechanisms giving rise to AD progression. The mechanistic explanations derived from the model are key to understanding the effects of delivered treatments, fostering the development of new ones, and enhancing early detection methods.

3.2 Methods

3.2.1 Data acquisition

Magnetic resonance imaging (MRI) scans were acquired for 20 healthy participants (17 females) with mean age 60.5 (sd 4.17) at the Centre for Cognitive and Computational Neuroscience, Complutense University of Madrid. Diffusion-weighted images (dw-MRI) were acquired with a single-shot echo-planar imaging sequence with the parameters: echo time/repetition time = 96.1/12,000 ms; NEX 3 for increasing the SNR; slice thickness = 2.4 mm, 128×128 matrix, and field of view = 30.7 cm yielding an isotropic voxel of 2.4 mm; 1 image with no diffusion sensitization (i.e., T2-weighted b0 images) and 25 dw-MRI (b = 900 s/mm2).

All participants provided informed consent.

3.2.2 Structural connectivity

In a preprocessing stage, FSL eddy was used to correct for eddy current distortion. The correction was conducted through the integrated interface in DSI Studio (http://dsi-studio.labsolver.org). Then, the eddy-corrected dw-MRI data was rotated to align with the AC-PC line. The restricted diffusion was quantified using restricted diffusion imaging (F.-C. Yeh et al., 2016). The diffusion data were reconstructed using generalized q-sampling imaging (F. Yeh et al., 2010) with a diffusion sampling length ratio of 1.25. The tensor metrics were calculated using dw-MRI with a b-value lower than 1750 s/mm². A deterministic fibre tracking algorithm (F.-C. Yeh et al., 2013) was used with augmented tracking strategies (F.-C. Yeh, 2020) to improve reproducibility. The whole brain was used as seeding region. The anisotropy threshold was randomly selected. The angular threshold was randomly selected from 15 degrees to 90 degrees. The step size was randomly selected from 0.5 voxels to 1.5 voxels. Tracks with lengths shorter than 15 or longer than 300 mm were discarded. A total of 5 million seeds were placed.

A combination of Desikan-Killiany (Desikan et al., 2006) and ASEG (Fischl et al., 2002) atlases were used as a volume parcellation atlas, and two SC matrices were calculated (see Figure 3.1D): weights by using the count of the connecting tracks, and tract length by using the average length of the streamlines connecting two regions. The final SC consisted of a subset of these networks including 40 regions (see Table 3.3) representing the cingulum bundle (Bubb et al., 2018b), one of the most prominent white matter structures that interconnect frontal, parietal, temporal and subcortical regions, and whose impairment has been related to AD and cognitive decline (Bubb et al., 2018b; Y. Chen et al., 2023; Yu et al., 2017).

3.2.3 Brain network model

SC matrices served as the skeleton for the BNMs implemented in The Virtual Brain (Sanz-Leon et al., 2015) where regional signals were simulated using Jansen-Rit (JR) NMMs (Jansen & Rit, 1995). The JR is a biologically inspired model of a cortical column capable of reproducing alpha oscillations through a system of second-order coupled differential equations (see

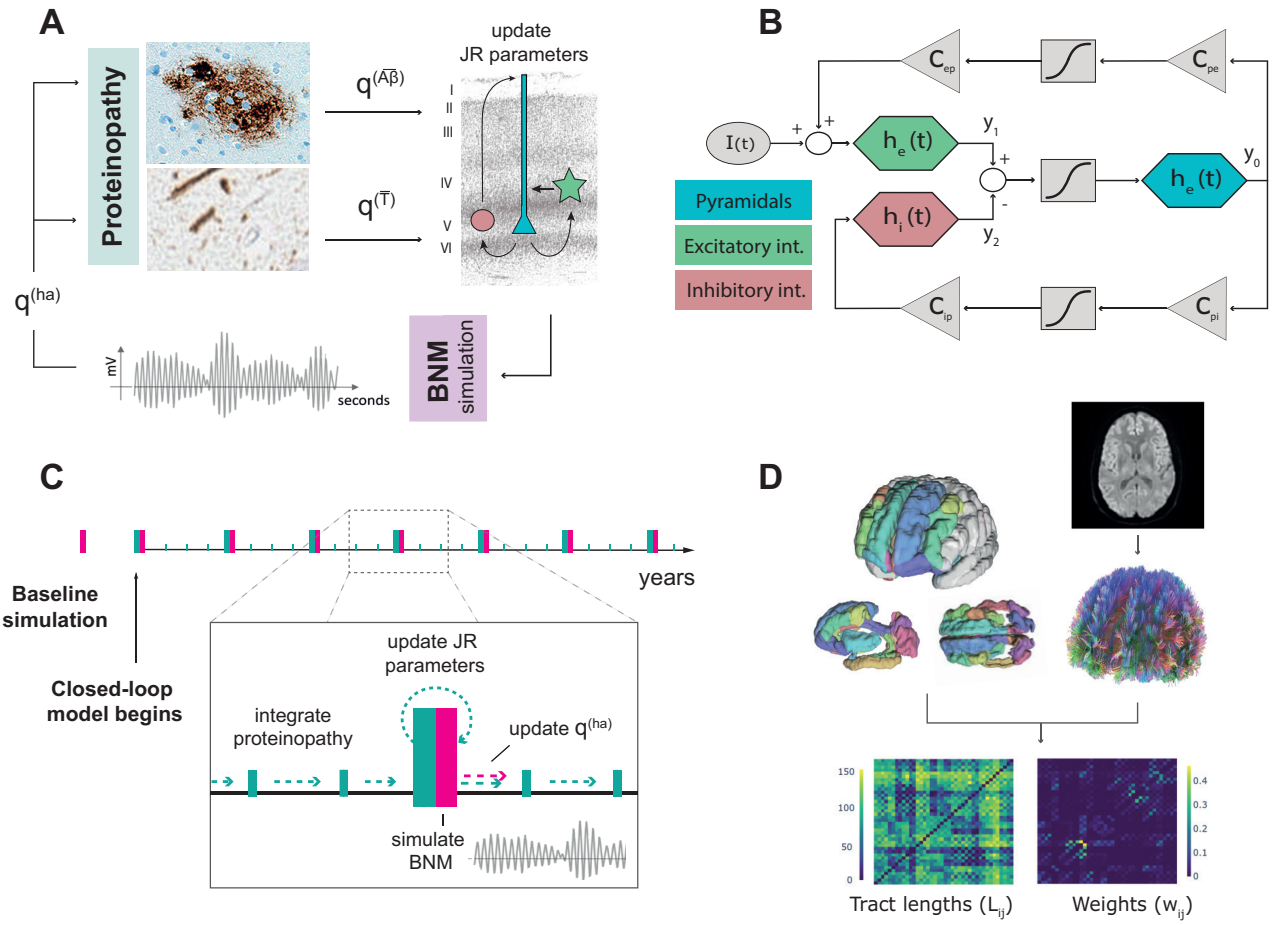


Figure 3.1: Modelling framework overview. A) The closed-loop neurotoxicity model integrates a model of proteinopathy dynamics and a BNM to simulate neural activity, interacting in a closed-loop: proteinopathy affects neural activity and vice-versa. B) Scheme of the JR NMM with three interacting subpopulations where triangles represent synaptic contacts between subpopulations, boxes represent the sigmoidal transformation of voltage into firing rate and coloured hexagons represent the transformation of firing rate into voltage. C) Implementation timeline for the closed-loop model. First, a baseline simulation is gathered to get a baseline firing rate. Then, the closed-loop model simulation begins by integrating the proteinopathy with dt=0.25 (years) and simulating the BNM to update hyperactivity damage ($q_i^{(ha)}$) with dt=1 (year). D) Pipeline to extract SC matrices. Tractography is performed on dw-MRI data, and SC matrices are extracted using a customized version of the DK atlas. The histological image for the $A\beta$ plaque in panel A was distributed by Michael Bonert, under a CC BY-SA 3.0 license. The NFT image was taken from Moloney et al. (2021).

Table 3.1 for a description of parameters; Figure 3.1B):

$$\dot{y}_{0_i} = y_{3_i} \tag{3.1}$$

$$\dot{y}_{1_i} = y_{4_i} \tag{3.2}$$

$$\dot{y}_{2_i} = y_{5_i} \tag{3.3}$$

$$\dot{y}_{3_i} = \frac{H_e}{\tau_e}\, S[y_{1_i} - y_{2_i}] - \frac{2}{\tau_e} y_{3_i} - \frac{1}{\tau_e^2} y_{0_i} \tag{3.4}$$

$$\dot{y}_{4_i} = \frac{H_e}{\tau_e}\, \{I_i(t) + C_{ep}\, S[C_{pe}\, y_{0_i}]\} - \frac{2}{\tau_e} y_{4_i} - \frac{1}{\tau_e^2} y_{1_i} \tag{3.5}$$

$$\dot{y}_{5_i} = \frac{H_i}{\tau_i}\, C_{ip}\, S[C_{pi}\, y_{0_i}] - \frac{2}{\tau_i} y_{5_i} - \frac{1}{\tau_i^2} y_{2_i} \tag{3.6}$$

Where:

$$S[v] = \frac{2\, e_0}{1 + e^{r(v_0 - v)}} \tag{3.7}$$

$$I_i(t) = \eta_i(t) + g \sum_{j=1}^{n} w_{ji}\, S[y_{1_j}(t - d_{ji}) - y_{2_j}(t - d_{ji})] \tag{3.8}$$

for i=1,...,N with N as the number of simulated regions. The inter-regional communication introduces heterogeneity in terms of connection strength w_{ji}, and conduction delays d_{ji} between nodes i and j where: $d_{ji} = \frac{L_{ji}}{s}$, with L_{ji} being the length of the tract from node i to node j, and s representing the conduction speed.

This model represents the electrophysiological activity (in voltage) of three subpopulations of neurons: pyramidal neurons (y_0), excitatory interneurons (y_1), and inhibitory interneurons (y_2) and their derivatives (y_3, y_4, and y_5, respectively). These subpopulations are interconnected through an average number of synaptic contacts (C_{ep}, C_{ip}, C_{pe} and C_{pi}), and integrate external inputs from other cortical columns. The communication is implemented in terms of firing rate, using a sigmoidal function for the conversion of the voltage inputs (eq. 3.7). Parameters regarding postsynaptic potential amplitudes (H_e, H_i), and time constants (τ_e, τ_i) shape the oscillatory behaviour of subpopulations' voltages.

Table 3.1: JR-BNM parameters used in simulations.

Parameter	Value	Unit	Description
H_e	3.25	mV	Average excitatory synaptic gain
H_i	22	mV	Average inhibitory synaptic gain
τ_e	10	ms	Time Constant of excitatory PSP
τ_i	20	ms	Time Constant of inhibitory PSP
C_{pe}	135		Average synaptic contacts: pyramidals to excitatory interneurons
C_{ep}	108		Average synaptic contacts: excitatory interneurons to pyramidals
C_{pi}	33.75		Average synaptic contacts: pyramidals to inhibitory interneurons
C_{ip}	33.75		Average synaptic contacts: inhibitory interneurons to pyramidals
e_0	0.0025	ms^{-1}	Half the maximum firing rate
r	0.56	mV^{-1}	Slope of the presynaptic function at v0
v_0	6	mV	Potential when half the maximum firing rate is achieved
p	0.1085	ms^{-1}	Mean of random gaussian intrinsic noisy input
σ	0.022	ms^{-1}	Standard deviation of random gaussian intrinsic noisy input
g	25		Coupling factor for inter-regional communication
s	20	m/s	Conduction speed for inter-regional communication

The input ($I_i(t)$) represents two main drivers of activity in the NMMs: inter-regional communication and an intrinsic noisy input. The latter is defined as a local and independent Gaussian noise $\eta_i(t) \sim \mathcal{N}(p, \sigma)$.

A global coupling factor g is implemented to scale linearly tracts' weights. Both, g and s are scaling factors that apply to all nodes and were adjusted to reproduce the qualitative features of the AD evolution.

3.2.4 Closed-loop neurotoxicity model

We have adapted an already published model for AD protein propagation, first shown by Thompson et al. (2020) that reproduces the evolution of tau and $A\beta$ concentrations in the AD brain, and a further extension by Alexandersen et al. (2023) that linked this evolution to changes in neural activity patterns using NMMs. Here, we adapt this latter model by implementing a JR NMM and introducing a feedback mechanism that connects the NMMs' activity to the production and diffusion of toxic proteins in the AD brain (Figure 3.1A).

Proteinopathy dynamics are described by the heterodimer model, one of the most common hypotheses that describe the prion-like spreading of toxic proteins. This hypothesis suggests that a healthy (properly folded) protein misfolds when it interacts with a toxic version of itself (misfolded; the prion/seed) following the latter's structure as a template (Garzón et al., 2021). Therefore, this model includes healthy and toxic versions of amyloid-beta ($A\beta$, $\tilde{A\beta}$) and tau (T, $\tilde{T}$) that are produced, cleared, transformed (from healthy to toxic), and propagated in the SC with N nodes. The proteinopathy dynamics for i $\in$ [1, N] were adapted from Alexandersen et al. (2023) to include the effect of hyperactivity on the enhanced production of $A\beta$ (M. A. Busche & Hyman, 2020; Cirrito et al., 2005; Kamenetz et al., 2003; Stargardt et al., 2015; K. Yamamoto et al., 2015) and on the biased prion-like propagation of $\tilde{T}$ to hyperactive regions (Rodriguez et al., 2020); see Table 3.2 for a description of parameters):

$$\dot{A\beta_i} = -\rho \sum_{j=1}^{N} L_{ij}\, A\beta_j + \text{prod}_{A\beta}\, q_i^{(ha)} - \text{clear}_{A\beta}\, A\beta_i - \text{trans}_{A\beta}\, A\beta_i\, \tilde{A\beta_i} \tag{3.9}$$

$$\dot{\tilde{A\beta}_i} = -\rho \sum_{j=1}^{N} L_{ij}\, \tilde{A\beta}_j - \text{clear}_{\tilde{A\beta}}\, \tilde{A\beta}_i + \text{trans}_{A\beta}\, A\beta_i\, \tilde{A\beta}_i \tag{3.10}$$

$$\dot{T}_i = -\rho \sum_{j=1}^{N} L_{ij}\, T_j + \text{prod}_T - \text{clear}_T\, T_i - \text{trans}_T\, T_i\, \tilde{T}_i - \text{syn}\, \tilde{A\beta}_i\, T_i\, \tilde{T}_i \tag{3.11}$$

$$\dot{\tilde{T}}_i = -\rho \sum_{j=1}^{N} L_{ij}\, \tilde{T}_j\, q_i^{(ha)} - \text{clear}_{\tilde{T}}\, \tilde{T}_i + \text{trans}_T\, T_i\, \tilde{T}_i + \text{syn}\, \tilde{A\beta}_i\, T_i\, \tilde{T}_i \tag{3.12}$$

Where *prod*, *clear* and *trans* stand for rates of protein production, clearance, and transformation from a healthy isoform to a toxic one. *syn* stands for the synergistic effect between $A\beta$ and tau that fosters the conversion of the latter into its toxic isoform (M. A. Busche & Hyman, 2020). $q_i^{(ha)}$ represents the effect of hyperactivity on the production of $A\beta$ and the propagation of tau (further details below). ρ stands for a diffusion constant, and L_{ij} for the laplacian diffusion term:

$$L_{ij} = -w_{ij}(t) + \delta_{ij} \sum_{j=1}^{N} w_{ij}(t) \tag{3.13}$$

where δ_{ij} stands for the Kronecker delta (representing the NxN identity matrix).

The impact of protein concentration on the brain network model is established through two sets of transfer functions. First, a set of damage functions that are used to translate the concentration of toxic proteins into damage variables (Alexandersen et al., 2023):

$$\dot{q}_i^{(\tilde{A\beta})} = c_q^{(\tilde{A\beta})}\, \tilde{A\beta}_i\, (1 - q_i^{(\tilde{A\beta})}) \tag{3.14}$$

$$\dot{q}_i^{(\tilde{T})} = c_q^{(\tilde{T})}\, \tilde{T}_i\, (1 - q_i^{(\tilde{T})}) \tag{3.15}$$

where $c_q^{(\tilde{A\beta})}$ and $c_q^{(\tilde{T})}$ are damage constants for $A\beta$ and hp-tau, respectively.

Second, a set of equations that translate the damage just mentioned into NMM parameter changes. We adapted these equations to the JR NMM. It was assumed that each protein ($\tilde{A\beta}$ and $\tilde{T}$) impacts the excitation/inhibition balance in different ways:

- $\tilde{A\beta}$ generates neuronal hyperactivity through the impairment of GABAergic synapses (Garcia-Marin, 2009; Limon et al., 2012; Ulrich, 2015; Verret et al., 2012) and through the disruption of glutamate re-uptake (Zott et al., 2019).
- Soluble hp-tau ($\tilde{T}$) has been shown to change significantly the number and morphology of dendritic spines in pyramidal cells, producing neural silencing that dominates over the $\tilde{A\beta}$ hyperactivation (M. Busche et al., 2019; Merino-Serrais et al., 2013).

The effects of $\tilde{A\beta}$ will be modelled through changes in the local parameters of the JR NMM including an increase in the amplitude of the excitatory postsynaptic potential (H_e) related to the disruption of glutamate reuptake (3.16), and a reduction of the number of inhibitory synapses to pyramidal cells (C_{ip}) related to GABAergic deficits (eq. 3.17). The silencing effects of $\tilde{T}$ will be modelled through a reduction in the number of excitatory interneurons' synapses to pyramidal cells (C_{ep}), a reduction of interregional wights (w_{ij}), and to C_{ip}.

$$\dot{H_{e_i}} = c_{exc}^{(\tilde{A\beta})}\; q_i^{(\tilde{A\beta})}\; (H_{e_{max}} - H_{e_i}) \tag{3.16}$$

$$\dot{C_{ip_i}} = -c_{inh}^{(\tilde{A\beta})}\; q_i^{(\tilde{A\beta})}\; (C_{ip_i} - C_{ip_{min}}) - c_{inh}^{(\tilde{T})}\; q_i^{(\tilde{T})}\; (C_{ip_i} - C_{ip_{min}}) \tag{3.17}$$

$$\dot{C_{ep_i}} = -c_{exc}^{(\tilde{T})}\; q_i^{(\tilde{T})}\; (C_{ep_i} - C_{ep_{min}}) \tag{3.18}$$

$$\dot{w}_{ij} = -c_{sc}^{\tilde{T}}\; (q_i^{(\tilde{T})} + q_j^{(\tilde{T})})\; (w_{ij} - w_{ij_{min}}) \tag{3.19}$$

Where:

$$w_{ij_{min}} = w_{ij_0}\ (1 - sc_{dam}) \tag{3.20}$$

$H_{e_{max}}$, $C_{ip_{min}}$, $C_{ep_{min}}$, sc_{dam} determine the maximum change allowed per parameter candidate. $c_{exc}^{(\tilde{A\beta})}$, $c_{inh}^{(\tilde{A\beta})}$, $c_{exc}^{(\tilde{T})}$, $c_{inh}^{(\tilde{T})}$ stand for constants calibrating the effects of $A\beta$ and hp-tau over excitation and inhibition variables.

To this point, we have completed half of the closed-loop model. The second half regards the impact of the simulated neural activity on protein propagation. Neural hyperactivity fosters extracellular secretion and deposition of $A\beta$ generating a cyclical phenomenon that reinforces bidirectionally neural hyperactivity and $A\beta$ concentration (M. A. Busche & Hyman, 2020; Cirrito et al., 2005; Kamenetz et al., 2003; Stargardt et al., 2015; K. Yamamoto et al., 2015). Additionally, hyperactivity orients the prionic propagation of $\tilde{T}$ in the brain (Rodriguez et al., 2020) following the Braak stages (H. Braak & Braak, 1991a).

To capture these effects in our model, we introduced an additional damage variable for hyperactivity (eq. 3.21), based on the averaged increase in firing rate per region compared to baseline:

$$\dot{q}_i^{(ha)} = c_q^{(ha)}\ (-q_i^{(ha)} + \Delta ha_i)\ (q_{max}^{(ha)} - q_i^{(ha)})\ q_i^{(ha)} \tag{3.21}$$

Where:

$$\Delta ha_i = ha_i \,/\, ha_{i_0} \tag{3.22}$$

The firing rate (ha_i) was evaluated as the sigmoidal transformation of incoming afferences to the pyramidal subpopulation (i.e., $S[y_{1_i}(t) - y_{2_i}(t)]$) and the baseline ($ha_{i_0}$) was defined as the regional firing rate measured in a whole brain simulation free from the impact of proteinopathy (eq. 3.22). The damage variable $q_i^{(ha)} \in (0, q_{max}^{(ha)})$ was implemented as a factor in equations 3.9 and 3.12 multiplying the production of $A\beta$ and biasing the Laplacian term for $\tilde{T}$ distribution. When $ha_i \approx ha_{i_0}$, $q_i^{(ha)}$ tends to one and, therefore, it would not affect the proteinopathy dynamics. $c_q^{(ha)}$ stands for the damage rate for hyperactivity.

Table 3.2: Parameters used in the closed-loop neurotoxicity model. $A\beta$ and T stands for healthy amyloid-beta and tau proteins while $\tilde{A\beta}$ and $\tilde{T}$ stand for their toxic isoforms.

Parameter	Value	Unit	Description
$\text{prod}_{A\beta}$	3	M · years^{-1}	Production rate for $A\beta$
$\text{clear}_{A\beta}$	3	years^{-1}	Clearance rate for $A\beta$
$\text{trans}_{A\beta}$	3	M^{-1} · years^{-1}	Transformation constant of $A\beta$ into its toxic isoform $\tilde{A\beta}$
$\text{clear}_{\tilde{A\beta}}$	2.4	years^{-1}	Clearance rate for $\tilde{A\beta}$
prod_{T}	3	M · years^{-1}	Production rate for T
clear_{T}	3	years^{-1}	Clearance rate for T
trans_{T}	3	M^{-1} · years^{-1}	Transformation of tau into its toxic isoform $\tilde{T}$
$\text{clear}_{\tilde{T}}$	2.55	years^{-1}	Clearance rate for $\tilde{T}$
syn	0.4	M^{-2}·years	Synergistic effect between $\tilde{A\beta}$ and $\tilde{T}$
ρ	50	cm · years^{-1}	Effective diffusion constant
$c_q^{(\tilde{A\beta})}$	1	M^{-1} · years^{-1}	Damage rate for $\tilde{A\beta}$
$c_q^{(\tilde{T})}$	1	M^{-1} · years^{-1}	Damage rate for $\tilde{T}$
$c_q^{(ha)}$	0.01		Damage rate for hyperactivity
$c_{exc}^{(\tilde{A\beta})}$	0.8	years^{-1}	Constant for the effect of $\tilde{A\beta}$ on excitation locally
$c_{inh}^{(\tilde{A\beta})}$	0.4	years^{-1}	Constant for the effect of $\tilde{A\beta}$ on inhibition locally
$c_{exc}^{(\tilde{T})}$	1.8	years^{-1}	Constant for the effect of $\tilde{T}$ on excitatory local connectivity
$c_{inh}^{(\tilde{T})}$	1.8	years^{-1}	Constant for the effect of $\tilde{T}$ on inhibitory local connectivity
$c_{sc}^{(\tilde{T})}$	0.05	years^{-1}	Constant for the effect of $\tilde{T}$ on interregional connectivity
$\text{H}_{\text{e}_{\text{max}}}$	3.65		Maximum value allowed for H_e parameter change
$\text{C}_{\text{ip}_{\text{min}}}$	13.25		Minimum value allowed for C_{ip} parameter change
$\text{C}_{\text{ep}_{\text{min}}}$	28		Minimum value allowed for C_{ep} parameter change
sc_{dam}	0.3		Maximum damage of $\tilde{T}$ on interregional connectivity
$q_{max}^{(ha)}$	2		Maximum damage value for hyperactivity

3.2.5 In-silico experiments and simulations

In this work, we performed simulations for several complementary in-silico experiments. First, we explored the parameter spaces of a single JR NMM to evaluate the effects of proteinopathy on neural activity, by varying the AD parameter candidates (H_e, C_{ip}, C_{ep}, and w_{ij}). As this first experiment's simulations were performed with a single node, we accounted for the reduction of interregional connectivity (w_{ij}) produced by hp-tau using the mean of the intrinsic noisy input to the node (p), a JR variable that substitutes the interregional afferences not being considered

in the simulation. In total, we performed four sets of simulations in this in-silico experiment: the first one focused on the parameters related to $A\beta$ effects, and the remaining three focused on parameters related to tau effects. The simulations were performed for 20 seconds of neural activity discarding the initial 12 to avoid transients, and we recorded information regarding the spectral frequency peak, spectral power in different frequency bands, and firing rate.

Second, we built and simulated the neurotoxicity model to deepen the mechanisms of AD progression. The initial conditions of the proteinopathy dynamics were fixed using a toxic protein seeding following literature on AD staging: the entorhinal cortex for tau (H. Braak & Braak, 1991a) with an initial $\tilde{T}$=0.0025 per region; and insula, precuneus, posterior and isthmus cingulate cortices, and orbitofrontal cortex for $A\beta$ (Palmqvist et al., 2017) with an initial $\tilde{A\beta}$=0.0125. Two different integration timelines coexist within the closed-loop model: an integration over the years of AD evolution, and an integration over seconds when simulating the neuronal activity (see Figure 3.1C). The former implies integrating the proteinopathy dynamics each dt=0.25 (yrs) and evaluating the BNM with the updated parameters due to proteinopathy effects each dt=1 (yrs). The evaluation of the BNM executes a neural activity simulation for 10 seconds out of which the initial 2 seconds are discarded to avoid initial-conditions' transients. Once the BNM is evaluated, the proteinopathy continues to be integrated with updated parameters given the simulated levels of neural activity. We decided to implement two different integration times over years for the proteinopathy and the BNM (i.e., dt=0.25 and dt=1 yrs., respectively) to reduce the computational load.

We used the neurotoxicity model in several ways: first, we adjusted the model by exploring the impact of the limits of change for the parameter candidates $(H_{e_{max}}, C_{ip_{min}}, C_{ep_{min}}, sc_{dam})$ and two BNM free parameters (g and s) on the temporal evolution of the model, in terms of averaged frequency peak, relative alpha power, firing rate, and FC. The latter was calculated using the Phase Locking Value (PLV; (Bruña et al., 2018; Lachaux et al., 1999)) between signals filtered in the alpha band (8 - 12 Hz):

$$PLV_{jk} = \frac{1}{T}\left|\sum_{t=1}^{T} e^{i(\phi_j(t)-\phi_k(t))}\right| \tag{3.23}$$

Where ϕ stands for the instantaneous phase of the signals via the Hilbert transform and i for the imaginary unit.

The limits of change for the model parameters determine the extent of the proteinopathy's impact on JR parameters and, therefore, on the neural activity. We explored those parameter spaces to select a set of values that could reproduce qualitatively the empirical observations reported in the AD continuum: the slowing of alpha frequency, and the rise and decay of relative alpha power, cellular firing rate and FC. The adjusted parameters are used here as the default values for our model and are included in Tables 3.1 and 3.2. Second, we described the outputs of the model with the default parameters including an averaged description of parameter trajectories (eqs. 3.16-3.19), spectra, firing rate, and PLV of the simulated brain regions; third, we disentangled the contribution of $A\beta$ and hp-tau to the changes in inhibition by isolating their respective effects on the model evolution. This was achieved by setting to zero alternatively the parameters that define the impact of $A\beta$ and hp-tau on inhibition in our model (i.e., $c_{inh}^{(A\beta)}$ and $c_{inh}^{(T)}$) and re-computing and comparing the parameter space for the limit of change of C_{ip} with the original situation. Finally, we used it to evaluate the spatiotemporal evolution of the model with the Braak stages as a reference (see below).

3.2.6 Spatiotemporal profile assessment

We evaluated the spatial propagation of hp-tau using the Braak stages as a reference and the impact of $A\beta$ seeding over the temporal antero-posterior differentiation in terms of firing rate and FC. Braak stages were adapted from (Therriault et al., 2022) considering the regions included in our cingulum bundle network (see Table 3.3): *stage one (rI)* included the entorhinal cortex; *stage two (rII)* included the hippocampus; *stage three (rIII)* included the parahippocampus and amygdala; *stage four (rIV)* included insula, posterior cingulate, inferior temporal, and inferior parietal; *stage five (rV)* included other cortical regions.

We simulated our closed-loop neurotoxicity model by implementing different seeding strategies. The baseline seeding (i.e., fixed strategy) was the same used in previous studies (Alexandersen et al., 2023; Thompson et al., 2020) as stated above. The remaining strategies consisted in randomizing the seeding of $A\beta$, randomizing the seeding of hp-tau, and randomizing both. The randomization respected two conditions: the number of seeded regions had to be the same as in the fixed strategy, and the seeding had to be symmetrical between hemispheres. For the antero-posterior differentiation, we also limited the randomization of $A\beta$ seeding to posterior areas or anterior areas.

One hundred simulations were performed per seeding strategy. For each timestep, we averaged the concentration of hp-tau in the regions of the Braak stages to determine what Braak regions were presenting higher levels of the protein, and we sorted them into Braak sequences following Putra et al. (2021). Then, we extracted the dominant Braak sequence per simulation as the most repeated sequence in time. For the antero-posterior differentiation, we averaged posterior and anterior neural dynamics and we extracted the time to peak (given the rise and decay in the metrics) of each average.

3.2.7 Code Accessibility

The models described above were implemented in Python 3.9, and executed in a Surface Pro 7 (8Gb RAM) running Windows 11 and a HPC cluster. The code used in the paper is freely available online at github.com/jescab01/ADprogress_2023 and as Extended Data in this manuscript.

3.3 Results

The proposed model for the physiological changes in AD is based on extensive literature that describes the effects of $A\beta$ and hp-tau on neural tissue. These changes include the disruption of glutamate reuptake, the reduction of GABAergic synapses, and the reduction of pyramidal dendritic spines. To effectively model these changes, we proposed four parameter candidates

Table 3.3: Regions of the cingulum bundle included in the BNM Bubb et al. (2018b). $A\beta$ and tau superscripts denote the regions used as seeding (H. Braak & Braak, 1991a; Palmqvist et al., 2017). I, II, III, and IV superscripts denote the regions included in the Braak stages (Therriault et al., 2022).

Left Frontal Pole	Right Frontal Pole
Left Rostral Middle Frontal	Right Rostral Middle Frontal
Left Caudal Middle Frontal	Right Caudal Middle Frontal
Left Superior Frontal	Right Superior Frontal
Left Lateral Orbitofrontal $^{A\beta}$	Right Lateral Orbitofrontal $^{A\beta}$
Left Medial Orbitofrontal $^{A\beta}$	Right Medial Orbitofrontal $^{A\beta}$
Left Insula $^{A\beta;\,\mathrm{IV}}$	Right Insula $^{A\beta;\,\mathrm{IV}}$
Left Caudal Anterior Cingulate	Right Caudal Anterior Cingulate
Left Rostral Anterior Cingulate	Right Rostral Anterior Cingulate
Left Posterior Cingulate $^{A\beta;\mathrm{IV}}$	Right Posterior Cingulate $^{A\beta;\mathrm{IV}}$
Left Isthmus Cingulate $^{A\beta}$	Right Isthmus Cingulate $^{A\beta}$
Left Superior Parietal	Right Superior Parietal
Left Inferior Parietal $^{\mathrm{IV}}$	Right Inferior Parietal
Left Precuneus $^{A\beta}$	Right Precuneus $^{A\beta}$
Left Inferior Temporal $^{\mathrm{IV}}$	Right Inferior Temporal $^{\mathrm{IV}}$
Left Parahippocampal $^{\mathrm{III}}$	Right Parahippocampal $^{\mathrm{III}}$
Left Hippocampus $^{\mathrm{II}}$	Right Hippocampus $^{\mathrm{II}}$
Left Thalamus	Right Thalamus
Left Amygdala $^{\mathrm{III}}$	Right Amygdala $^{\mathrm{III}}$
Left Entorhinal cortex $^{\mathrm{tau;\,I}}$	Right Entorhinal cortex $^{\mathrm{tau;\,I}}$

that could account for the observed effects. Specifically, we selected two parameters to model the effects of $A\beta$ on neural activity including the amplitude of the excitatory postsynaptic potential (H_e) to account for the disruption of glutamate reuptake, and the number of local synaptic contacts from inhibitory interneurons to pyramidal neurons (C_{ip}) to account for the reduction of GABAergic synapses. Regarding the effects of tau, we selected three parameter candidates that could effectively model the disruption of pyramidal dendritic spines: C_{ip} mentioned above, C_{ep} as the local synaptic contacts from excitatory interneurons to pyramidal neurons, and w_{ij} as the interregional SC weights.

3.3.1 Single-node experiments favour inhibition over excitation to explain hyperactivity

In order to gain a better understanding of the impact of toxic proteins on neural behaviour, we explored the parameter spaces of the proposed candidates (H_e, C_{ip}, C_{ep}, and w_{ij}) through single-node NMM simulations. Note that we used the mean of the intrinsic noisy input to the node (p) to account for the reduction of w_{ij} as simulations were performed with a single node.

In general terms, and in line with previous analysis of the JR model (Grimbert & Faugeras, 2006; Spiegler et al., 2010), results showed two main patterns of oscillation: a fast limit cycle in the alpha frequency band (8-12 Hz), and a slow limit cycle in theta frequency band (4-8 Hz). These two behaviours were categorically separated in the parameter spaces as can be observed in the frequency and relative power charts of Figure 3.2. The noisy regions surrounding the main limit cycles correspond to the fixed point states of JR that are found at both extremes of the excitation-inhibition continuum. In these states, the model might not have enough activation to give rise to an oscillatory behaviour, or it might be saturated by a too-high excitation. In both states, the noise acts as a driver giving rise to low-amplitude and low-frequency noisy oscillations, and the more stable the fixed point (i.e., more extreme excitation-inhibition balance) the lower the frequency and amplitude. Accordingly, note that the noisy regions coincide with the low-power regions in the absolute power plots of Figure 3.2.

Focusing on the limit cycle regions, the parameter candidates related to intranode excitation (i.e., H_e and C_{ep}; see 1^{st} and 2^{nd}-3^{rd} columns of Figure 3.2, respectively) showed quadratic relationships in their parameter spaces, producing curved isopleth borders separating the slow and fast oscillatory behaviours (i.e., theta and alpha, respectively). These curves represented a convex relationship between the parameters and the neural behaviour in terms of frequency, power, and firing rate. The position of their original values derived from biology (Jansen & Rit, 1995) differed with respect to the vertex of the quadratic curve: the original H_e was found at lower values than the vertex, while C_{ep} was found at higher values.

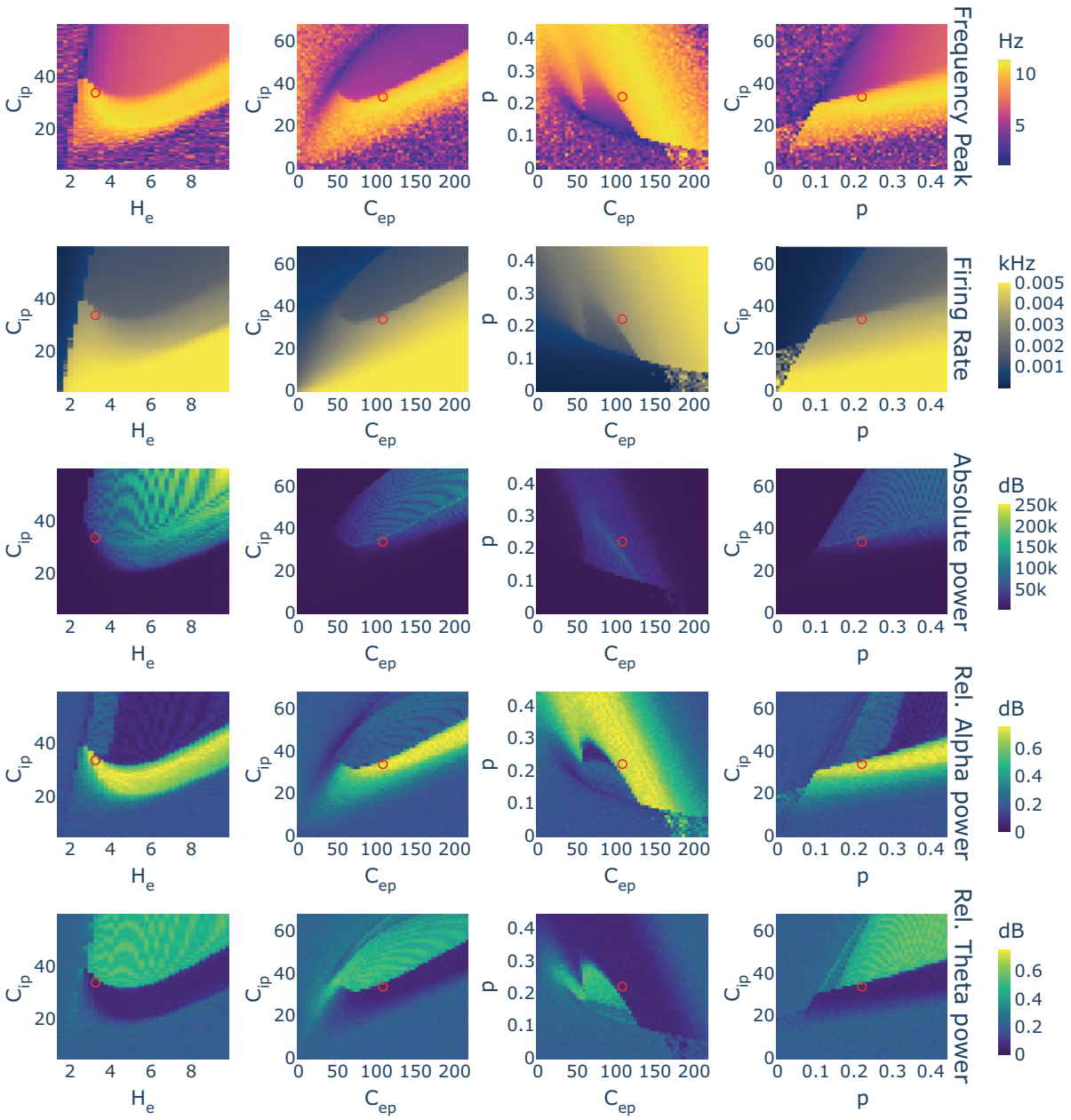


Figure 3.2: Single node in-silico experiment. The behaviour of a single neural mass model was simulated varying parameter values. Four different experiments are presented in columns exploring different combinations of parameters. In rows, measures derived from the simulations: oscillatory frequency peak of the node, mean firing rate, absolute power, and the relative power in two frequency bands: alpha and theta. The red circle points out the default parameter values. A 2D representation of each parameter change is shown in extended Figure 2-1. Sample time series for the different oscillatory regimes are shown in extended Figure 2-2.

For the other two parameters (i.e., C_{ip} and p) the observed changes inside the limit cycle regions were monotonical, and better described as logistic relationships in which the changes happen quickly at the edge between behaviours (see extended Figure 2-1). These relationships were direct in the case of p with both frequency peak and firing rate, in contrast to the inverse relationship found for C_{ip} (i.e., lower inhibition raised the firing rate and the frequency of oscillation). Note that lowering inhibition out of the limit cycle regions had two different effects on firing rate and spectra. The firing rate kept rising monotonically as inhibition lowered, while the frequency peak and power tended to be reduced getting into the noisy low amplitude and slow region commented above.

In this model, two parameters could explain the hyperactivation produced by $A\beta$: C_{ip} lowering down due to the reduction of GABAergic synapses, and H_e rising due to the disruption of glutamate reuptake. Assuming that the original values of these parameters, which were based on biological observations (Jansen & Rit, 1995), are a good approximation of the underlying ground truth, our experiment would favour a hypothesis in which the hyperactivity found in AD is explained more likely by the reduction of C_{ip} than by the increase of H_e given that the latter would induce an initial reduction of activation levels that is not expected in AD (see the effects of lowering C_{ip} and rising H_e in Figure 3.2, second row, first column).

3.3.2 Closed-loop neurotoxicity model: from proteins to neural activity

To explore the link between proteinopathy and neural activity, we extended a previously published multiscale model of AD evolution (Alexandersen et al., 2023; Thompson et al., 2020) by implementing a biologically plausible NMM (Jansen & Rit, 1995) and establishing a bidirectional interaction between neural activity (eqs. 3.1-3.6) and proteinopathy (eqs. 3.9-3.12). The proteinopathy starts from an initial distribution of toxic seeds, and during the temporal evolution of the model, the BNM integrates the effects of those proteins over neural tissue, which in turn influences the production of $A\beta$ and the propagation of hp-tau based on firing rate.

The regional evolution of the proteinopathy follows a sigmoidal shape with a final slight decay in $A\beta$ toxic concentration (see average curves in Figure 3.3A). The model captures the time delays between the rise of $A\beta$ and hp-tau reported in the literature (Therriault et al., 2022). The effect of proteinopathy on neural activity was modelled through changes in the NMM parameters mediated by a damage variable (see Figure 3.3B). These changes were monotonical and followed the sigmoidal shape of the proteinopathy and its damage. The impact of $A\beta$ over the neural tissue was modelled as a reduction of C_{ip} and an increase in H_e, while the impact of hp-tau was modelled as reductions of the local and interregional connectivity parameters explored before (C_{ip}, C_{ep}, w_{ij}) as shown in Figure 3.3C and extended Figure 3-1. The changes in parameters due to the proteinopathy generated a rise and decay in firing rate over time (see Figure 3.3D) that affected the production of $A\beta$ and the distribution of hp-tau through a hyperactivity damage variable (see Figure 3.3E).

The specific limits of change of the parameters (included in Table 3.2) were fitted by iterative explorations of the parameter spaces generated with the neurotoxicity model to achieve the reproduction of some of the main pathophysiological changes of AD evolution (Maestú et al., 2021): frequency slowing, reduction in relative alpha power, hypo-/hyperactivity, and hypo-/hypersynchrony in alpha (see Figure 3.4). We noticed that the reduction of alpha FC does not translate into an enhancement of FC in lower frequency bands (i.e., theta/delta; see extended Figure 4-1). Additionally, we could not reproduce a clear temporal distinction between antero-posterior effects of the proteinopathy on FC (i.e., posterior regions are affected first) as it has been previously proposed (see Figure 3.4A-PLV). However, we also found slight antero-posterior differences in magnitude between those regions for FC and firing rate.

3.3.3 Hyperactivity is not directly linked to hypersynchrony

The parameter space explorations that allowed us to fit the model are used in the following to establish relationships between different variables and outcomes derived from the neurotoxic model simulation. To obtain these parameter space explorations, we simulated the model with different values of the parameter candidates' limits of change.

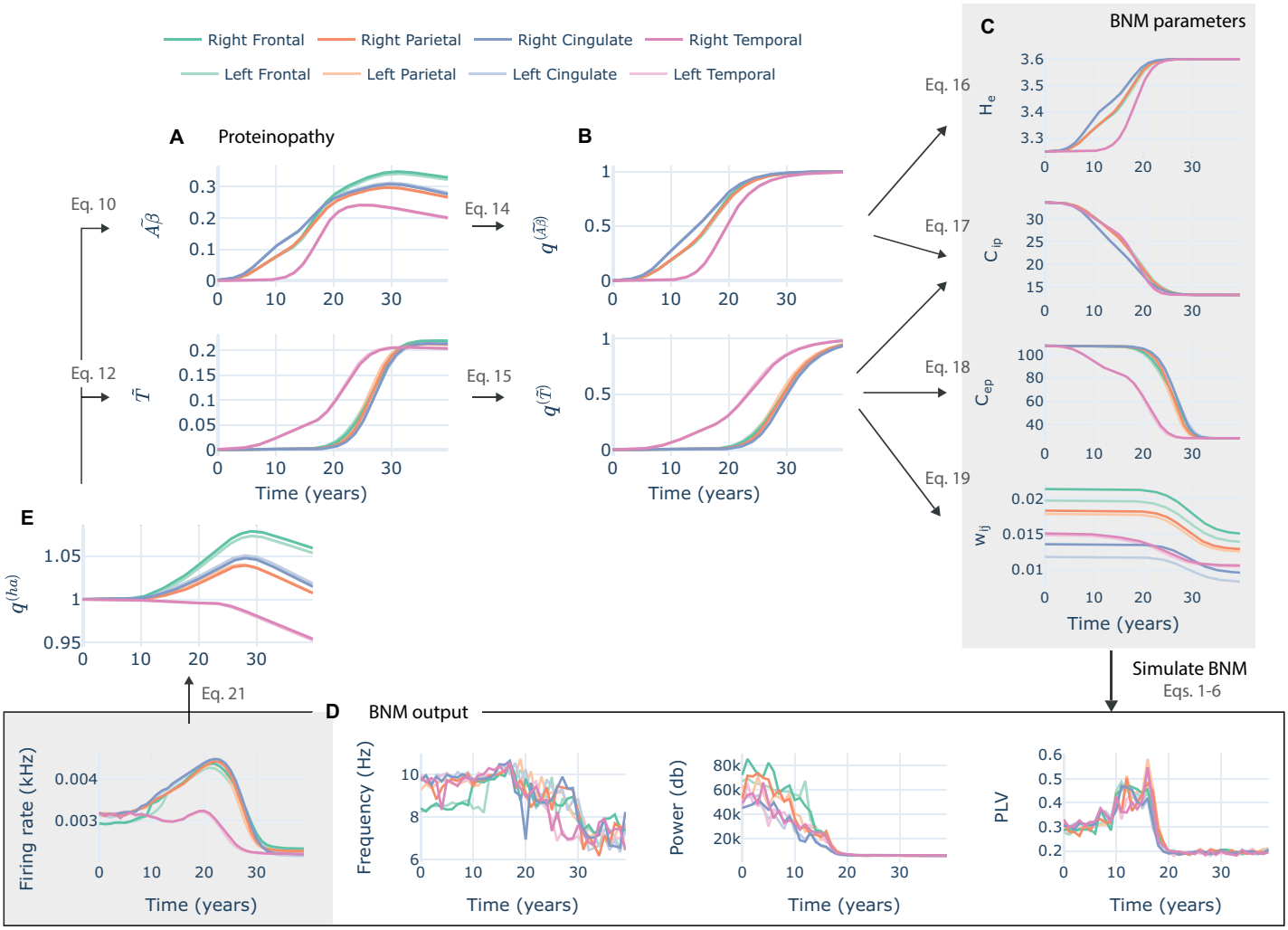


Figure 3.3: Evolution of the parameters, state variables and neural activity outputs from the closed-loop neurotoxicity model. Results are averaged over regions included in eight categories including frontal, parietal, temporal and cingulate regions. A) Concentration of toxic proteins over time during model execution. B) Damage variables that determine the impact of the proteinopathy over the neural activity (i.e., JR-BNM parameters). C) JR-BNM parameters change over time. D) Functional measures derived from the simulation of the BNM including spectral frequency peak and power, PLV and firing rate. The latter is used in the calculation of $q^{(ha)}$. E) Damage variable $q^{(ha)}$ that determines the impact of hyperactivity on the production and propagation of toxic proteins. The average of the parameter changes shown in C) are plotted over the single node experiments' heatmaps in Figure 3-1).

The model behaviour could be analyzed by dividing it into two stages: a first stage in which we find an increase in relative alpha power, firing rate, and FC; and a second stage in which all these measures decay (see Figure 3.5). These two stages are not synchronized for all measures. We observed a delayed peak in firing rate at the time interval of years 18 to 25, while all other measures peak earlier in time between years 10 and 18. From year 18 to 25, the firing rate keeps rising while power and FC have already lowered. This observation suggests a dissociation between firing rate and FC that has not been previously established.

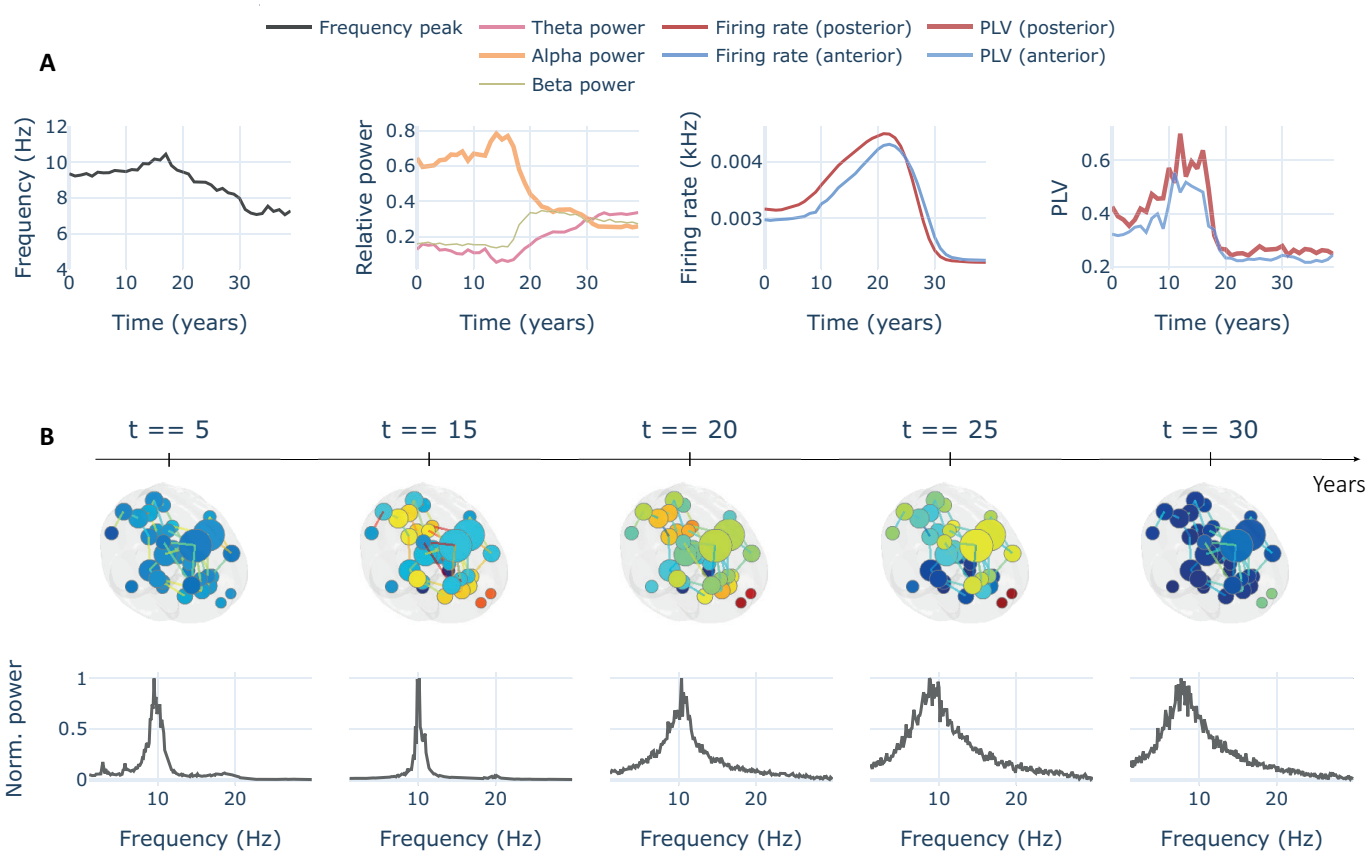


Figure 3.4: Functional measures from the closed-loop neurotoxicity model. Metrics averaged from the simulation shown in Figure 3.3. A) We extracted spectral frequency peak, relative band power, firing rate, and alpha FC from the simulation over 40 years of the neurotoxicity model. A quadratic relationship is found over time for all these metrics (i.e., measures increase early in time and decrease later). B) Temporal excerpts of the same simulation including 3D representations of the BNM with node size as degree, node colour as firing rate (orange/red is a higher rate), and edge colours as PLV. Last row shows averaged normalized spectra for all the regions included in the model. FC evolution in other frequency bands is shown in Figure 4-1). Regional spectra at several time points are shown in Figure 4-2.

3.3.4 The changes in inhibition lead the evolution of AD

Two parameter candidates could be responsible for the initial rising stage: the increase of H_e and the reduction of C_{ip}. Looking at the parameter spaces, only the changes to the C_{ip} limits showed a disruption in the rising phase when reduced less than a 20% (see Figure 3.5 second row). On the other hand, changes to the limits of H_e did not show any significant effect in this

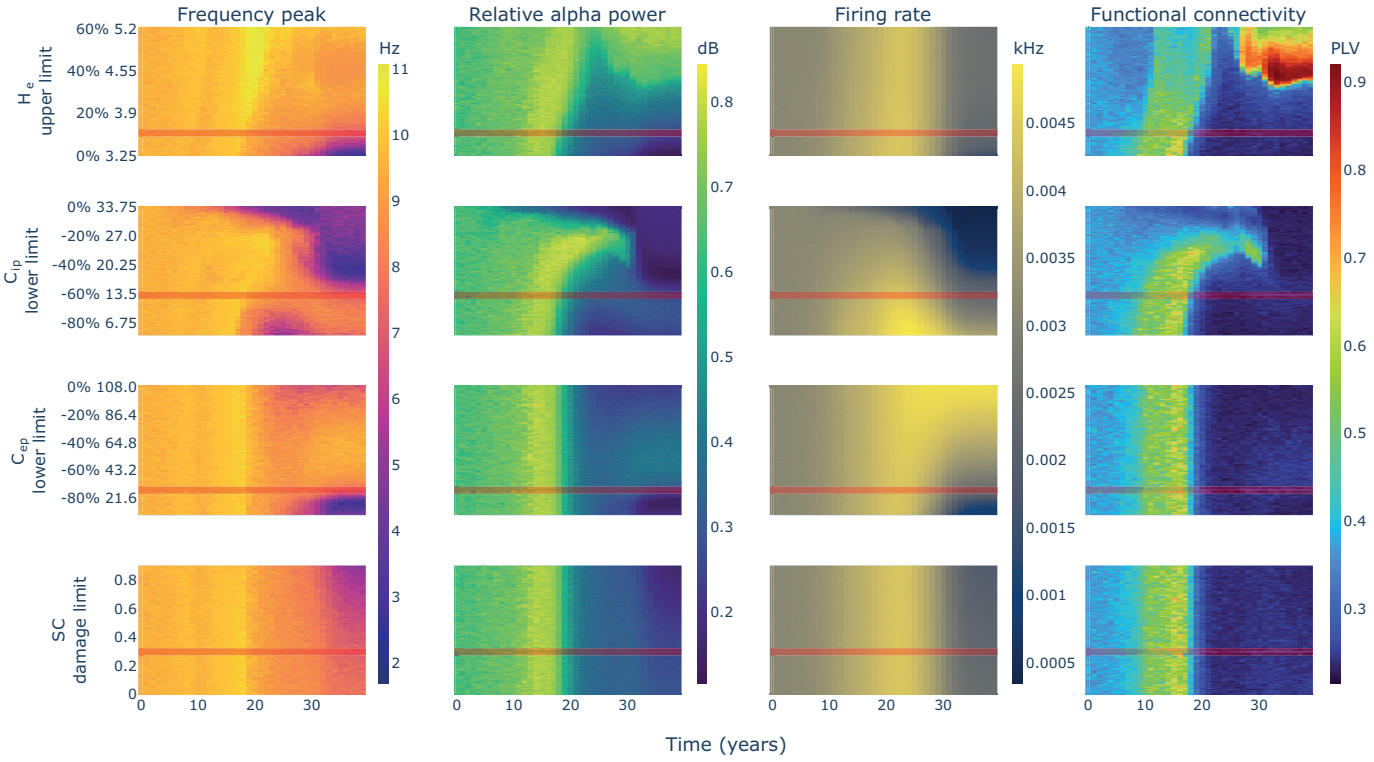


Figure 3.5: Parameter spaces for the limits of change of the JR-BNM parameter candidates. For each parameter candidate (rows) and limit value explored (heatmaps y-axis), one simulation of 40 years (heatmaps x-axis) is performed. For each simulation, four neural activity measures are extracted including averaged frequency peak, relative alpha power, firing rate, and functional connectivity (columns). When exploring a parameter candidate, all other parameters are kept fixed with their default values that are highlighted in red and included in Table 3.2. These default values were used in the simulations for Figures 3.3 and 3.4. Note how taking apart from zero the limits of change impact differently the resulting behaviour of the model. Two additional parameter spaces were computed to define values for g and s (see Figure 5-1).

stage, even using an upper limit equal to 0% (i.e., keeping the parameter fixed in time) the rise in all measures could still be observed (see Figure 3.5, first row). This would suggest that the rising stage is mainly controlled in our model by the changes in inhibition (i.e., the reduction of C_{ip} parameter) representing the $A\beta$ dependent reduction of GABAergic synapses.

The decaying stage required a more complex analysis. In the previously exposed single-node experiments, we observed that lowering inhibition showed a transition from the slow limit cycle, to the fast limit cycle, to the noisy low frequency and amplitude oscillation in which excitation-inhibition imbalance saturates the regional response and leads the JR NMMs to operate in a fixed point state (see Figure 3.2 and further explanations above). In that context, the reduction of C_{ip} itself could explain the decay stage for frequency peak and relative alpha power by entering the noisy region where lower inhibition (i.e., further imbalance of excitation-inhibition) leads to a more stable JR fixed-point state and lower spectral frequencies. Interestingly, those spectral changes were time-locked with the changes in alpha band FC (see Figure 3.4 and Figure 3.5). Despite explaining the decay stage for those three measures, the reduction of C_{ip} could not explain the decay for firing rate. Lowering inhibition produced a monotonic ascent as could be expected from Figure 3.2 even in the noisy low amplitude region of the single-node parameter spaces.

The decay of firing rate could then be explained by another two parameter candidates related to the tau-derived reduction of pyramidal dendritic spines: the reduction of C_{ep}, and the reduction of SC weights. The parameter spaces showed that only the reduction of local excitation (i.e., C_{ep}) interacted with the firing rate (see Figure 3.5, third column). Disabling the change for C_{ep} (i.e., C_{ep} change limit of 0%) showed a plateau in firing rate during the decay stage, while activating its reduction showed a progressive effect on the decay of the firing rate (see Figure 3.5 third row, compare -40%, -60%, and -80% change limits). This effect was not found for different levels of damage to the SC weights.

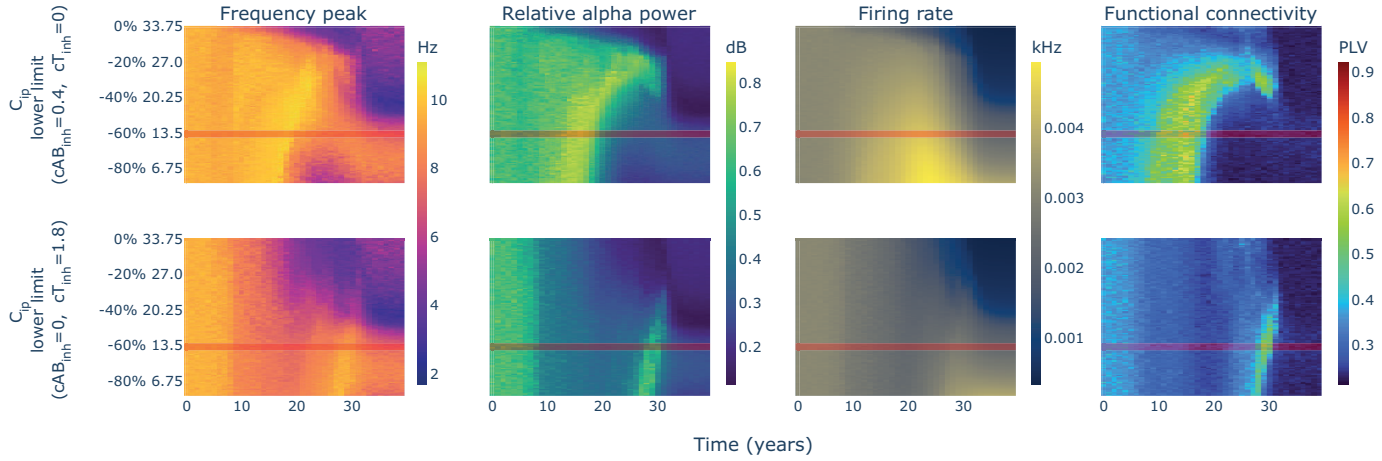


Figure 3.6: Parameter spaces for C_{ip} isolating the effects of $A\beta$ and hp-tau. First row shows the results of simulating the neurotoxicity model with different limits of change for C_{ip} isolating the effects of $A\beta$ on inhibition, while the second row shows the results of simulating the same parameter space isolating the effects of hp-tau on inhibition.

3.3.5 Amyloid-beta controls changes in inhibition

From the analysis above, we can derive that the disruption of inhibition is a relevant driver of AD progress. Given that both $A\beta$ and hp-tau contribute to the disruption of inhibition by reducing GABAergic synapses and reducing dendritic spines respectively, we wondered whether they contribute differently to the inhibitory-related effects reported above.

To disentangle their contribution, we computed an additional set of parameter spaces in which we evaluated independently the impact of the inhibitory disruption caused by each protein (Figure 3.6). We observed a clear similarity between the parameter space of $A\beta$-only effects and the previously shown in Figure 3.5 full model. The isolated effect of TAU could also generate a slight rise and decay in power, frequency and FC delayed from the $A\beta$ effect and shorter in time, with a more moderate change in firing rate. This would suggest that both proteins could produce to some extent the effects observed in AD due to the disruption of inhibition, although with different timings and hyperactivity levels.

3.3.6 Toxic seeding determines the spatiotemporal profile of the evolution

The spatiotemporal sequence of hp-tau spreading in AD has been accurately characterized through the Braak stages. We used this characteristic spatiotemporal sequence to evaluate the spatial accuracy of the tauopathy simulated in our model, and the impact of the selected toxic proteins' seeding regions on its spatial evolution. We implemented four seeding strategies including fixed seeding, $A\beta$ randomized, hp-tau randomized and both randomized. We performed 100 simulations per strategy and we measured the concentration of hp-tau in the regions of the Braak stages extracting the dominant spatial sequence of propagation per simulation.

Results showed that fixed (i.e., as usual) and $A\beta$ random seeding strategies reproduced effectively the Braak staging in 100% and 70% of the simulations, respectively (Figure 3.7A). In these simulations, just a slight temporal shift separated stages II (i.e., hippocampus) and III (i.e., parahippocampus and amygdala), and this way 30% of the simulations with $A\beta$-random seeding showed a sequence in which hp-tau reached stage III before stage II. Interestingly, randomizing tau seeding produced a variety of Braak sequences that lowered the dominance of the theoretical sequence to less than 5% of the simulations, at the same levels of randomizing both seeding locations. Examples of these sequences in time are shown in Figure 3.7B. These observations posit the importance of the localization of hp-tau seeds (i.e., early accumulations) to determine the evolution of its propagation.

In addition, we wondered to what extent the antero-posterior temporal differentiation of the neurophysiological changes observed along the AD continuum could be related to the seeding of $A\beta$ and hp-tau. We performed an additional set of simulations randomizing the seeding of $A\beta$ and hp-tau and measuring the differences in firing rate and FC between anterior and posterior regions.

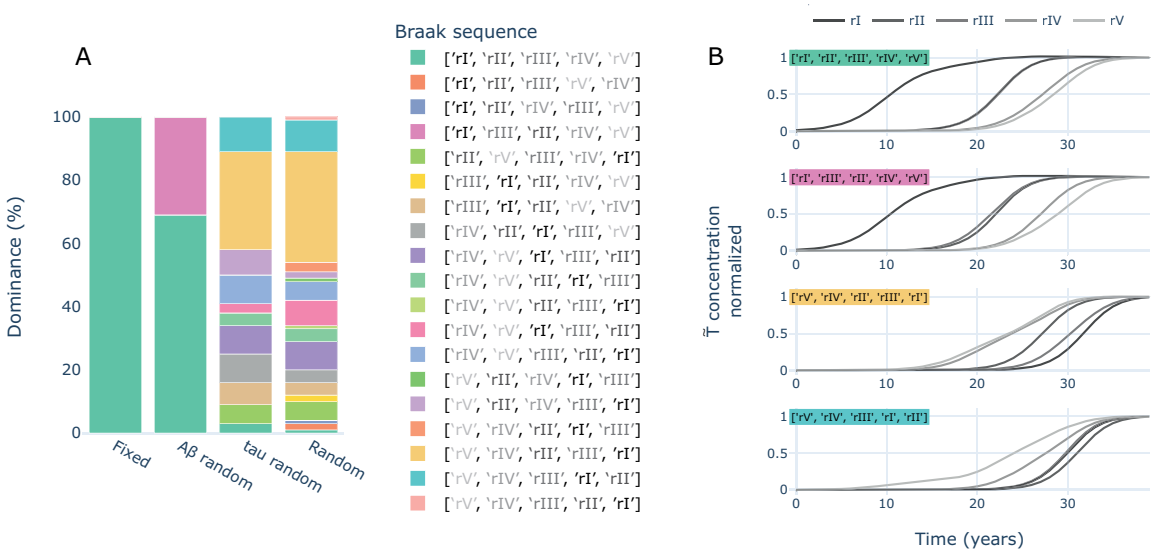


Figure 3.7: Dominance of Braak sequences per seeding strategy. A) The percentage of simulations per seeding mode in which different Braak sequences of hp-tau propagation were dominant. Fixed implied seeding a usual, $A\beta$ random implied randomizing $A\beta$ seeding and using the fixed version for hp-tau, vice versa for tau random, and Random implied randomizing both $A\beta$ and hp-tau seeding. B) Samples of the most representative Braak sequences showing the normalized concentration of $\tilde{T}$ over time.

We observed a stable precession of posterior regions in terms of firing rate for the cases of fixed seeding (i.e., following Palmqvist et al. (2017)), randomizing $A\beta$ and hp-tau in posterior regions, and randomization them over all regions (see Figure 3.8). Only in the case of anterior seeding, the model showed a slightly faster peak in anterior regions. This suggests that hyperactivity tends to appear earlier in posterior regions disregarding where $A\beta$ and hp-tau start to accumulate. Note that $A\beta$ and hp-tau seedings affected differently the levels of hyperactivity shown by the regions: non-$A\beta$-seeded and tau-seeded regions lowered their maximum firing rates as shown in extended Figure 8-1.

In contrast, the antero-posterior temporal differentiation for FC relied more on the seeding of $A\beta$. When the seeding was located in posterior regions they peaked earlier while, on the contrary, when anterior regions were seeded they tended to peak earlier. Interestingly, these two strategies generated a general delay in the time to peak both in the seeded region and in the complementary. Note that changing hp-tau seeding reduced the time to peak but did not affect the antero-posterior differentiation relative to the fixed strategy.

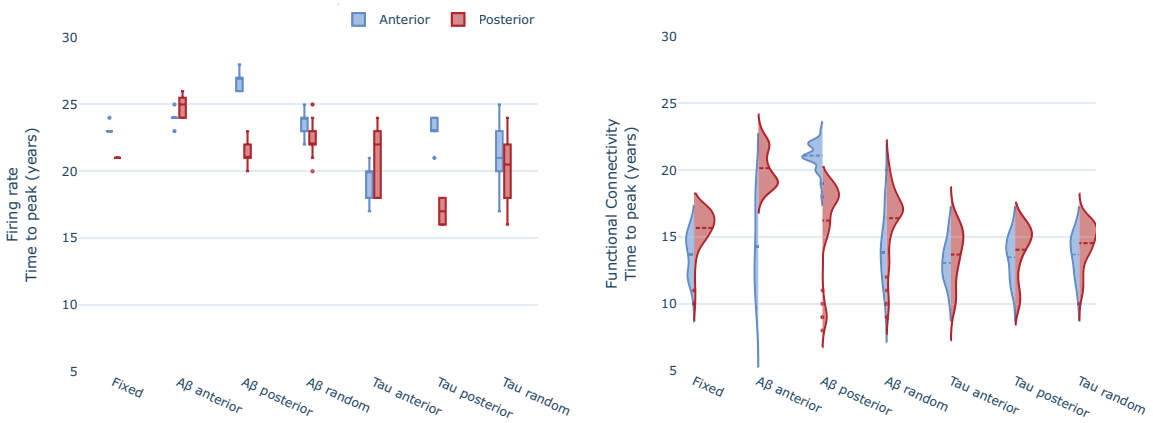


Figure 3.8: Impact of $A\beta$ and hp-tau seeding on the antero-posterior temporal differentiation for firing rate (top) and FC (PLV; bottom). The neurotoxicity model shows a rise and decay for several variables including firing rate and FC. We measured the time elapsed to that peak for anterior and posterior regions as a proxy to understand where the neurophysiological changes happened before. Samples of the temporal evolution for each seeding strategy and for both firing rate and FC are represented in Figure 8-1.

3.4 Discussion

In this study, we developed a multiscale closed-loop neurotoxicity model of AD integrating a BNM that reproduced brain activity with another modelling the production and propagation of toxic proteins in the brain, both influencing each other through biologically plausible links. Our results showed that the disruption of inhibition was favoured to explain cellular hyperactivity, and indeed that inhibition was key to explaining the AD-related changes in frequency, power and FC. These changes in inhibition were primarily attributed to $A\beta$ effects. Additionally, our results suggested a disconnection between cellular hyperactivity and interregional hypersynchrony. Finally, we observed a significant association between the spatiotemporal profile of the evolution of AD to the initial localization of the accumulation of AD proteins.

Single-node experiments favoured the lowering of inhibition (related to GABAergic synapses' disruption) over the rising of excitation (related to impaired glutamate reuptake) to explain the characteristic hyperactivity produced by toxic $A\beta$ on neural tissue. This idea is in line with previous animal studies showing a direct association between the levels of GABAergic synaptic activity and the hyperactivity found in the vicinity of amyloid plaques (M. A. Busche et al., 2008, 2015). The conclusions derived from the single-node experiments are based on the

assumption that the original definition of the JR parameters approximates well the characteristics of neural populations. Another definition of parameters could lead to different results. However, note that JR parameters were derived from empirical studies, for instance, C_{ip} and C_{ep} were suggested in light of histological research establishing proportions of synaptic connections between different cell types in several neocortical regions (Jansen & Rit, 1995). In any case, these experiments propose testable predictions regarding the extent to which these two $A\beta$-derived physiopathological phenomena may contribute to neural activation in AD.

Additionally, single-node experiments showed different effects for the changes implemented to the parameter candidates in terms of neural activity measures. Inside the limit cycle space, we observed quadratic relationships with firing rate and power for the local excitation parameters (i.e., H_e and C_{ep}), while a monotonical relationship was found for the inhibitory parameter (i.e., C_{ip}; Figure 3.2). These observations suggest two different roles for excitation and inhibition. While inhibition would predispose the system to order neural activation into synchronized oscillations, excitation is needed to trigger this mechanism.

Therefore, both increasing and decreasing excitation levels could lead to a rise in cellular firing rate: while low excitation may become ineffective to trigger inhibition, high excitation could overcome the capacity of inhibition to organize action potentials and generate oscillatory behaviour. This type of contradictory effect (i.e., rising excitation parameter could lower firing rate, and vice versa) has been reported in empirical studies under the name of inhibitory stabilization of network dynamics, in which, for instance, the stimulation of inhibitory neurons produce a counterintuitive suppression of inhibitory firing (Sadeh & Clopath, 2020; Sanzeni et al., 2020). This mechanism is characteristic of networks with strong recurrent connectivity and protects the system from unstable dynamics such as epileptic seizures.

In agreement with single-node experiments, the simulation of the multiscale neurotoxicity model gave a prominent role to inhibition leading the neural activity changes typically observed in AD. Despite both $A\beta$ and hp-tau can be associated with changes in inhibition -due to the disruption of GABAergic synapses, and to the reduction of dendritic spines that reduces the

number of inhibitory inputs to pyramidal cells, respectively-, in the model, $A\beta$ was linked to the main inhibitory changes that lead AD evolution. However, it was also shown that hp-tau alone could generate inhibitory effects in the same direction but weaker, shorter, and delayed in time.

The relationship between cellular hyperactivity and inter-regional hypersynchrony in AD has been suggested (Koelewijn et al., 2019; Maestú et al., 2021; Sepulcre et al., 2017; C. J. Stam et al., 2023) but not directly tested to our knowledge. The rationale behind this association is based on the studies linking $A\beta$ independently with both hyperactivity and hypersynchrony. On one hand, some studies report higher cellular activation, or lower firing thresholds, in regions affected by $A\beta$ (M. A. Busche et al., 2008; Palop & Mucke, 2010). On the other hand, some studies report spatial correlations between $A\beta$ accumulation (and hp-tau later) and the levels of FC, which are mainly observed within the default mode network (Mormino et al., 2011; Quevenco et al., 2020; Ranasinghe et al., 2020; Schoonhoven et al., 2023; Schultz et al., 2017). From these observations, it has been derived that $A\beta$ produces cellular hyperactivity, and that cellular hyperactivity, in turn, produces FC hypersynchrony. In our study, we show that hyperactivity and hypersynchrony might not be directly linked, as we found a reduction of FC while $A\beta$ accumulation was still enhancing cellular hyperactivity, suggesting a temporal mismatch between the two. In contrast, FC levels were strongly associated in time with changes in spectral power. We believe that this dissociation between spectral power and firing rate is essential to understand the hyperactivity/hyperconnectivity question. Whenever hyperactivity overcomes the capacity of inhibition to order neural firing into an oscillatory behaviour, the regional activity may become noisier and therefore more difficult to synchronize interregionally. However, when hyperactivity moves the excitation/inhibition ratio towards a more balanced state, larger oscillations appear that may give rise to FC changes in a network.

The simulation of the closed-loop neurotoxicity model showed a sigmoidal shape in the evolution of the concentration of toxic proteins with a final slight decay for $\tilde{A\beta}$ that is found in the empirical literature (Therriault et al., 2022). This decay is associated in our model with the reduction of hyperactivity that lowers the production of $A\beta$ and therefore, leads to the recovery

of the production-clearance balance. The impact of hyperactivity on the production of $A\beta$ has been suggested in previous studies and linked to alterations in the endocytic machinery that could increase the rate of clathrin-mediated endocytosis of the amyloid precursor protein (APP), and also enlarge APP endosomes (Stargardt et al., 2015). After releasing these APP vesicles, a molecular cascade mediated by β-secretase and γ-secretase cleaves the molecule to generate $A\beta$ (Haass & Selkoe, 2007).

In this work, we used the entorhinal cortex as the seeding region for hp-tau propagation. However, recent studies suggest that the classical Braak staging of tau pathology in AD (H. Braak & Braak, 1991a) may not offer a comprehensive view and may disregard alternative tau epicentres and propagation trajectories (Franzmeier et al., 2020; Lamontagne-Kam et al., 2023). From the epicentres, hp-tau spreads to functionally connected regions (Franzmeier et al., 2022; Schoonhoven et al., 2023) producing different network disruptions and clinical profiles. In a study by Vogel et al. (2021), they identified four distinct tau propagation patterns, each capable of explaining between 18 to 33% of the cases. We believe that our framework poses a good opportunity to advance the understanding and prediction of personalized tau propagation trajectories. Our approach considers not only structural and functional connectivity networks but also accounts for the progressive changes in neural activity due to proteinopathy.

An aspect that has not been captured by our model is the effect of chronic neuroinflammation. It may affect the normal functioning of glial cells, disrupting the clearance function of both microglia and astrocytes and, therefore, fostering protein accumulation and neuroinflammation (Heneka et al., 2015; Henstridge et al., 2019). Although it is not the only additional aspect that could be implemented in the model due to its impact on AD progression (e.g., vascular damage leading to reduced protein clearance, infections such as herpes virus, genetic factors, etc.), we expect that by including these glial effects, we could reproduce the slight decay in hp-tau concentration that is found in literature, but not reproduced in our results. Further modelling studies including additional AD-related factors are needed.

Regarding simulated neural activity, our model qualitatively reproduced some of the most relevant biomarkers along the AD continuum, including the slowing of the alpha frequency, the rise and decay of relative alpha power, firing rate, and alpha FC, and the Braak stages (Maestú et al., 2021). However, we could not directly reproduce two FC-related phenomena reported in the literature: the rise of FC for lower frequency bands (Nakamura et al., 2017; Schoonhoven et al., 2022), and the spatiotemporal dissociation in FC between posterior and anterior brain regions (López-Sanz et al., 2016b; Nakamura et al., 2017, 2018; Pusil et al., 2019). The latter was dependent on spatial seeding of $A\beta$ that, by including the orbitofrontal cortex in addition to the precuneus and posterior cingulate cortex (Palmqvist et al., 2017), balanced antero-posterior changes in time. We believe that assuming this spatial seeding to be correct, the result could be expected empirically. However, we wonder whether the technical difficulties in detecting accumulations of $A\beta$ could hinder the detection of earlier accumulations in posterior regions that could explain the electrophysiological evidence mentioned above.

Previous modelling research has explored the mechanisms underlying frequency slowing in AD, including the work by Alexandersen et al. (2023) that served as the basis for the research presented here. They found that the oscillatory changes in the AD continuum were more related to local neurodegeneration than to the disruption of interregional structural connectivity. Our results reproduced most of their observations, supporting the local neurodegeneration hypothesis. Additionally, van Nifterick et al. (2022) presented an exploration of six excitatory-inhibitory mechanisms that could lead to the slowing of AD. They found that both hyperexcitation and disinhibition (related to the $A\beta$ neurotoxic effects) could lead to oscillatory slowing. Our model integrated three of these mechanisms: rise of the excitatory postsynaptic potential (H_e), lowering of the inhibitory coupling (C_{ip}), and lowering of excitatory coupling (w_{ij}). Their results fit into the single node experiments parameter spaces presented here, which offer a comprehensive picture in which non-linear relationships between the levels of excitation-inhibition and the spectral frequency changes can be observed. Finally, other studies have previously modelled the frequency slowing observed in AD by manipulating the time constants of the NMMs. Ranasinghe et al. (2022) fitted the model parameters to

match empirical spectra from patients, finding relationships between $A\beta$ accumulation and inhibitory time constants changes, and between hp-tau accumulation and excitatory time constants. Also, Stefanovski et al. (2019) modelled the inhibitory disruption through changes in the inhibitory time constants linked to $A\beta$ accumulation. These models point to inhibitory disruptions due to $A\beta$ accumulation, in line with the results here presented. We did not include effects on time constants in our modelling approach considering that the empirical evidence for AD at the cellular level has reported more often changes in the magnitude of excitation/inhibition instead of changes in neural time constants.

This work provides a comprehensive and self-contained mechanistic explanation of how different factors contribute interactively to the course of AD and, therefore, it becomes relevant for urgent clinical needs. First, the observed hyperexcitation is the treatment target of the approved symptomatic drug Memantine (Reisberg et al., 2003, 2006) and other treatments currently under investigation such as the anti-epileptic drug Levetiracetam (Vossel et al., 2021). Several clinical trials in AD have determined that selecting the correct individuals at the correct disease stage for a particular intervention is crucial, our model aims to help in this process in the future. Further, both increased neural activity and altered synchrony can be targeted with invasive or non-invasive brain stimulation (Chang et al., 2018). Deep brain stimulation in the fornix has positively affected cognition, but mainly if the stimulation site precisely activates memory networks (Ríos et al., 2022). The promising effects of transcranial magnetic stimulation depend on a particular adaptation between the used frequencies and their effects on the excitation-inhibition balance (Weiler et al., 2019). Neuromodulation cannot only improve but also deteriorate the function of a diseased brain, and the prediction of an individual stimulation regime requires a deep understanding of the underlying mechanisms. The same applies to pharmacological treatments: while the recent success of Lecanemab in slowing down cognitive decline is promising and raises hopes for the amyloid hypothesis after decades (van Dyck et al., 2023), the observed effects are minimal, and the long-term outcome is still unclear. One avenue towards more efficient use of potentially disease-modifying treatments is, again, the choice of the correct timing for the therapy. The closed-loop-model

in this work can even explain several potential reasons that hinder an effective slowing of the neurodegenerative process: it explains how both $A\beta$ and hp-tau can drive the vicious circle independent from each other, and it formalizes how the self-sustaining process evolves even without the presence of the initiating factor. Altogether, only a holistic understanding of AD will open the possibility to once even preventing the development of dementia, and computational neuroscience can powerfully contribute to this.

PART III

Restoring healthy brain function with tACS

"Science and everyday life cannot and should not be separated"

Rosalind Franklin

The last aim of this thesis was to explore from a computational perspective the potential of tACS as an intervention for AD. We decided to focus on the anteroposterior hypersynchrony reported in early stages of the disease. We hypothesize that lowering the levels of hypersynchrony may modulate the underlying cellular hyperactivity that interacts bidirectionally with the deposition of $A\beta$.

In chapter 5, we will stimulate the virtual version of the healthy brain to explore the best approach to reduce the FC levels between anteroposterior regions. We will test two different protocols, one targeting frontal regions and another targeting posterior ones, and a wide range of stimulation frequencies. Importantly, to model the effects of the stimulation, we will use a specialized MATLAB toolbox called ROAST (Y. Huang et al., 2019) that provides a distribution of electric field vectors in the brain volume. Usually, to connect the stimulus with the BNM, an average is performed over the magnitude of the normal components of the electric field vectors per region, and this procedure might result problematic. The effective stimulation of the underlying tissue is thought to depend mostly on the orientation and morphology of the pyramidal cells in the cortex (Aberra et al., 2020; A. Liu, Vöröslakos, Kronberg, Henin, Krause, et al., 2018). Therefore, averaging the normal components, might obscure the actual distribution of cellular orientations and generate misleading results. Therefore, we will first investigate from a spiking neural network approach (chapter 4) the effects of cortical folding and pyramidal cells' orientation in relation to the stimulation's electric field over the neural activity of the regions in the BNM.

Chapter 4

Understanding the effects of cortical gyrification in tACS: insights from experiments and computational models

The alpha rhythm is often associated with relaxed wakefulness or idling and is altered by various factors. Abnormalities in the alpha rhythm have been linked to several neurological and psychiatric disorders, including Alzheimer's disease. Transcranial alternating current stimulation (tACS) has been proposed as a potential tool to restore a disrupted alpha rhythm in the brain by stimulating at the individual alpha frequency (IAF), although some research has produced contradictory results. In this study[1], we applied an IAF-tACS protocol over parieto-occipital areas to a sample of healthy subjects and measured its effects over the power spectra. Additionally, we used computational models to get a deeper understanding of the results observed in the experiment. Both experimental and numerical results showed an increase in alpha power of 8.02% with respect to the sham condition in a widespread set of regions in the cortex, excluding some expected parietal regions. This result could be partially explained by taking into account the orientation of the electric field with respect to the columnar structures of the cortex, showing that the gyrification in parietal regions could generate effects in opposite directions (hyper-/depolarization) at the same time in specific brain regions. Additionally, we used a network model of spiking neuronal populations to ex-

1. Work in this Chapter can be found in Cabrera-Álvarez J, Sánchez-Claros J, Carrasco-Gómez M, del Cerro-León A, Gómez-Ariza CJ, Maestú F, Mirasso CR and Susi G (2023) Understanding the effects of cortical gyrification in tACS: insights from experiments and computational models. Front. Neurosci. 17:1223950.

plore the effects that these opposite polarities could have on neural activity, and we found that the best predictor of alpha power was the average of the normal components of the electric field. To sum up, our study sheds light on the mechanisms underlying tACS brain activity modulation, using both empirical and computational approaches. Non-invasive brain stimulation techniques hold promise for treating brain disorders, but further research is needed to fully understand and control their effects on brain dynamics and cognition. Our findings contribute to this growing body of research and provide a foundation for future studies aimed at optimizing the use of non-invasive brain stimulation in clinical settings.

4.1 Introduction

The oscillatory behaviour of the brain is characterized by a well-defined set of rhythms that play a crucial role in cognitive processes such as attention, memory and perception, among others. Importantly, the alpha rhythm, which typically ranges between 8 and 12 Hz and is prominent in posterior regions of the brain (Britton et al., 2016), is often associated with a state of relaxed wakefulness or idling (Buzsaki, 2006) and can be altered by various factors such as sensory stimulation, mental effort, and attention (Webster & Ro, 2020). It has been suggested that the alpha rhythm reflects inhibitory processes that suppress irrelevant sensory inputs and promote the processing of internal information (Payne & Sekuler, 2014). Abnormalities in the alpha rhythm have been associated with various neurological and psychiatric disorders (see, e.g., Babiloni et al. (2020) and Ippolito et al. (2022)). For instance, in Alzheimer's disease, a reduction in alpha power relative to healthy controls has been reported along the disease progression (Babiloni et al., 2009; Lejko et al., 2020; López-Sanz et al., 2016a). These previous findings raise up the question, whether the modulation of those brain rhythms could improve cognitive functions in these clinical conditions or even in control subjects.

Transcranial alternating current stimulation (tACS) is a non-invasive brain stimulation technique that uses external electrical currents to modulate the neuronal oscillatory activity at specific frequencies. Similar to other types of brain stimulation, tACS has the potential to advance our understanding of brain function by establishing causal links between brain activity,

cognition, and behaviour (Dayan et al., 2013; Herrmann et al., 2013; Polanía et al., 2018). The mechanistic underpinnings of tACS imply weak electrical currents delivered through the skull altering the polarization of cellular membranes, and thereby modulating the thresholds of neural activation (A. Liu, Vöröslakos, Kronberg, Henin, Krause, et al., 2018; Reato et al., 2013). This effect can enhance neural synchronization by biasing the timings of neural activation with the rhythm of the stimulation (Helfrich et al., 2014; A. Liu, Vöröslakos, Kronberg, Henin, Krause, et al., 2018; Vogeti et al., 2022). Additionally, some recent reports point out that tACS may also modulate neural plasticity, inducing long-term potentiation and depression (Jeong et al., 2021; Schwab et al., 2021).

tACS has emerged as a promising technique for modulating brain activity and has shown promise in reversing the reduction of alpha power observed in several disorders. Some studies have already explored the use of a specific application of tACS at the individual alpha frequency (IAF) to enhance the power of alpha oscillations (Helfrich et al., 2014; Kasten et al., 2019; Zaehle et al., 2010; Zarubin et al., 2020). In this type of experiments, the IAF-tACS stimulation is delivered at parieto-occipital regions to generate an entrainment with the predominant posterior alpha rhythm. The results of these experiments are contradictory, both in terms of the effective results of stimulation, and the locations where the effects are found. tACS can be influenced by several factors, including the selection of electrode montages, current dosage, targeted regions, skull conductivity, head positioning, cortex morphology, and cells' orientation (Datta et al., 2012; Guerra et al., 2020; Y. Huang et al., 2019; Kasten et al., 2019).

One of the issues being discussed is how the orientation of the cellular body axis influences the effects of electric field stimulation. Pyramidal neurons are arranged in the form of a palisade, with their main axes parallel to each other and perpendicular to the cortical surface (da Silva, 2022; Hansen et al., 2010; Susi et al., 2019). Their elongated morphology makes them responsive to the application of external electromagnetic fields (Aberra et al., 2020; A. Liu, Vöröslakos, Kronberg, Henin, Krause, et al., 2018), and previous research has demonstrated that the impact of the electric fields depends on its relative orientation with respect to the

axodendritic direction of the pyramidal cells' bodies (Aberra et al., 2020; Dmochowski et al., 2012; Radman et al., 2009). However, more research is needed to optimize tACS and better understand the variables that affect its mechanisms. This will pave the way for efficient and controlled tACS application, leading to better outcomes for patients.

Computational modelling has emerged as a valuable tool for investigating the mechanistic effects of electrical stimulation on the brain. Within this field of research, two types of models have become particularly prominent: current propagation models and neural activation models. Current propagation models are designed to analyse, predict, and regulate the electric fields produced in the brain by the applied stimulation. These models consider the impact of different head tissues, their shape, and the specific montages used for stimulation (Forssell et al., 2021; Holdefer et al., 2006; Y. Huang et al., 2017; Miranda et al., 2006; Russell et al., 2014). Neural activation models provide a detailed understanding of how electric fields generated by stimulation impact the activation of neural tissue at different levels of analysis, ranging from individual cells to the entire brain (Aberra et al., 2020; Deco et al., 2019; Meier et al., 2022b; Merlet et al., 2013; Tran et al., 2022; B. Wang et al., 2023). These models offer a more comprehensive explanation of the effects of stimulation. Neural activation models can be integrated into a network of brain regions (i.e.,*brain network model*, and stimulated in-silico (Merlet et al., 2013). To ensure the accuracy of the models, they are usually calibrated using empirical data to replicate the phenomenon being studied as closely as possible. By combining empirical and computational methodologies, researchers can strengthen their understanding of the mechanisms underlying electrical stimulation and the effects on brain function.

Our study utilized a bipolar electrode montage to deliver alternating currents to the posterior regions of the brain to modulate alpha power through an IAF-tACS stimulation protocol. Given the literature mentioned before, we hypothesized to achieve an increase in alpha power over parieto-occipital areas. To gain a deeper understanding of the results and explain any vari-

ability observed in them, we constructed and analysed a spiking neural network (SNN) model comprising neural populations distributed throughout large brain networks, hypothesizing that cortical gyrification can be used to explain the effects of neurostimulation. Our findings provide insights that could facilitate more precise and effective application of tACS in the future.

4.2 Methods

4.2.1 Empirical methods

Study design

The study consisted of one tACS session and three magnetoencephalography (MEG) scans, two before (i.e., *pre1* and *pre2* sessions) and one after the stimulation (*post* session). We initially captured the neurophysiological activity of each participant through two successive 5-minute eyes-closed resting state MEG recordings, with a 10-minute interval between sessions. The reason to include two MEG recordings before the stimulation was to account for any possible variability in the individual alpha-peak frequency (IAF) of the participants. The IAF was derived from each recording using a fast preprocessing algorithm that we describe in a later section, and then averaged. Participants were then randomly assigned to either the *verum* or *sham* group, and received 20 minutes of stimulation at their own IAF with their eyes closed. Immediately after the stimulation, we performed a third MEG recording to measure its effects on the participants. We decided to use a resting-state eyes-closed paradigm given its prominent alpha activity, and previous work on the same kind of stimulation (Y. Wang et al., 2022; Zarubin et al., 2020).

Empirical dataset

11 female and 16 male healthy participants, with ages ranging from 22 to 55 years (32.80 ± 8.52 and 32.00 ± 8.98 , respectively) were recruited at the Center for Cognitive and Computational Neuroscience (C3N) associated with the Complutense University of Madrid (UCM) for the neurostimulation study. Our study included only right-handed, native Spanish-speaking

participants without any previous neuropsychiatric history or metallic prostheses that could interfere with neuroimaging and neuromodulation. Participants with undistinguishable IAF were also excluded. We followed current guidelines and safety regulations throughout the research, and obtained informed consent from every participant before their participation.

MEG signals were acquired during five minutes of eyes-closed resting state at 1 kHz sampling rate, using 306 channels (102 magnetometers and 204 gradiometers) whole-head Elekta Neuromag system (Elekta AB, Stockholm, Sweden) located in a magnetically isolated room (VacuumSchmelze GmbH, Hanau, Germany). Using a Fastrak 3D digitizer (Polhemus, Colchester, Vermont), the positions of four head position indicator (HPI) coils attached to the scalp were defined and the shape of each participant's head relative to three anatomical locations (nasion and both preauricular points) was modelled. An online anti-aliasing filter ([0.1-330] Hz) was applied during the whole session.

Raw data was pre-processed by the Maxfilter software (v.2.2, correlation threshold = 0.9, time window = 10 s) to remove the environmental noise using the temporal extension of the signal space separation (tSSS) method with movement compensation (Taulu & Simola, 2006). Given the elevated redundancy of gradiometer data after applying the tSSS (Garcés et al., 2017) only data from magnetometers were considered for subsequent analyses. Eye, muscle, and jump artefacts were automatically located using Fieldtrip software (Oostenveld et al., 2011) and reviewed by MEG signal experts. Finally, the noise-free signal was divided into 4-second segments and an independent component analysis (ICA) based on SOBI (Belouchrani et al., 1997) was used to remove eye-blink and cardiac magnetic field artefacts. After applying ICA, we eliminated all segments that still contained any eye-blink or muscle artifacts. Preprocessed MEG data was then used to carry out source localization using a Linearly Constrained Minimum Variance (LCMV) beam former (Van Veen & Buckley, 1988). Because we did not have a T1 MRI for all subjects, a 1 mm resolution template of healthy adults normalized to the Montreal Neurological Institute (MNI) 1 mm voxel size template was used to place the sources inside the brain in a homogeneous grid of 1 cm. Then both the template and grid were linearly transformed to fit the head shape of each subject. The lead fields were defined

using a local spheres approach to fit the head shape of each subject in the vicinity of each sensor. Spatial filter coefficients were estimated for each subject using the computed lead field and an average of the covariance matrix for all the segments. Thereafter, this filter was used to compute the source time series separately for each segment and source location. Sources were grouped according to the Automated Anatomical Labeling (AAL) atlas cortical map (Tzourio-Mazoyer et al., 2002). From the original 4560 source locations, only those 2459 labelled as belonging to an area defined in the atlas were considered in the following steps. The other sources were placed in areas not defined in the atlas (i.e., white matter, CSF, or subcortical regions) and therefore cannot be source generators of MEG signals (M. Hämäläinen et al., 1993). From the reconstructed activity, the power spectrum for each cortical source was calculated by applying a multi-tapering method of Slepian sequences (DPSS) (McCoy et al., 1998; Slepian, 1978) between 2 and 45 Hz, then normalizing by dividing the spectra by the power between 2 and 45 Hz. The individual alpha frequency (IAF) was determined using a fast-processing algorithm on the *pre1* and *pre2* session scans, immediately after their recording. The data was processed using the same pipeline as described in the previous paragraph, but some steps were omitted to obtain a quick result, as the resulting frequency was needed for subsequent stimulation of the participant. Specifically, no tSSS or movement compensation method was applied, and manual revision of artefacts was skipped as well. Independent component analysis (ICA) was used to remove eye-blink and cardiac activity, while the remaining contaminated segments were removed manually. The power spectrum for each magnetometer was calculated using DPSS, and then averaged. The resulting spectra were visually inspected, and the frequency of the power peak in the alpha band (8 - 12 Hz) was defined as the IAF. The IAFs from sessions *pre1* and *pre2* were averaged to determine the final frequency for the neurostimulation procedure.

Neurostimulation

The neurostimulation sessions were carried out using a bipolar tACS stimulation with two conductive rubber electrodes (7x5 cm) located at Cz and Oz (midline central and midline occipital, respectively) using a microprocessor-controlled current source *NeuroConn DC-StimulatorPlus* (Neurocare, Ilmenau, Germany). The electrodes were covered by sponges and wet with saline solution. Verum stimulation was performed at the IAF during a 20-minute session with a current intensity of 3 mA peak-to-peak, while those undergoing sham stimulation only received stimulation during the fade-in and fade-out periods (30 seconds each).

Statistical analysis

To assess the effect of stimulation in areas with maximal current density, an independent sample t-test was conducted to compare the pre2-post rate of change in the power of the IAF (± 2 Hz bandwidth) between the *verum* and *sham* groups. The statistical analysis focused on the parieto-occipital regions of the AAL atlas, including the Calcarine fissure, Cuneus, Occipital lobe, Parietal gyrus, Angular gyrus, Precuneus, and Paracentral lobule. The statistical test was right-tailed since we hypothesized that the *verum* group would experience an increase in power due to the neurostimulation session. We chose to use the *pre2* MEG recording as a baseline because it was the closest to the neurostimulation session, and all patients had experienced a similar situation until that point. Furthermore, we utilized a non-parametric cluster-based permutation (CBPT) test (Bullmore et al., 1999) to investigate the *pre2-post* changes in power. This analysis enabled us to identify significant differences at the source level without the need for atlases and frequency bands and accounted for the problem of multiple comparisons. To align the IAFs of each participant, we shifted the spectra of each individual. An analysis of variance (ANCOVA) was conducted at each node, including age and sex as covariates, and the source-level significance threshold and cluster-level significance

threshold were set at 0.05. Finally, we performed a Levene test, again on the parieto-occipital regions in the AAL atlas, averaging the power over the frequencies in which the previous CBPT analysis revealed significant changes. This analysis aimed to examine the variability of the effects of tACS.

4.2.2 Computational methods

Data for simulations

For the computational modelling, different set of data was needed, as MRI-T1 or dw-MRI recordings from the participants in the empirical dataset were not available. We used a dataset owned by the C3N consisting of 10 healthy subjects (7 females; age 69 ± 4.16) with resting-state eyes-closed MEG, MRI-T1 and dw-MRI recordings. MEG acquisition and preprocessing were performed following the description in the previous section. T1-MRIs were recorded using a General Electric 1.5 Tesla magnetic resonance scanner, using a high-resolution antenna and a homogenization PURE filter (fast spoiled gradient echo sequence, with parameters: repetition time/echo time/inversion time = 11.2/4.2/450 ms; flip angle=12º; slice thickness=1mm, 256x256 matrix, and field of view = 256 mm). dw-MRIs were acquired with a single-shot echo-planar imaging sequence with the parameters: echo time/repetition time=96.1/12,000 ms; NEX 3 for increasing the SNR; slice thickness=2.4 mm, 128x128 matrix, and field of view=30.7 cm yielding an isotropic voxel of 2.4 mm; 1 image with no diffusion sensitization (i.e. T2-weighted b0 images) and 25 dw-MRI (b=900s/mm2).

To obtain the functional connectivity (FC) matrices, source reconstruction was performed using the minimum norm estimates method (M. S. Hämäläinen & Ilmoniemi, 1994), with the *constrained dipoles* variant, by which the current dipoles are oriented perpendicular to the cortical surface, to model the orientation of the macrocolumns of pyramidal neurons (Tadel et al., 2019). Source-space signals were then filtered in the alpha (8–12 Hz) band to calculate

functional connectivity between sources using the Phase Locking Value (PLV, (Lachaux et al., 1999)). For the calculation of PLV, the instantaneous phase of each time-series is given by the Hilbert transform at time points t in every segment n, and then the following equation is applied:

$$PLV = \frac{1}{N}\left|\sum_{n=1}^{N} exp(j\theta(t,n))\right| \tag{4.1}$$

Where θ(t, n) is the phase difference of the two time series at time t and trial n. The resulting source matrices were averaged into AAL parcellation scheme.

The constrained dipoles method allowed us to obtain the source space signal at one point, taking into account the real orientation of the subtended cortical column, an aspect that is crucial to avoid sign/phase errors on the reconstructed time series. This is useful for computational purposes but recommended only when the T1-MRI of the participant is available.

To obtain structural connectivity (SC) matrices, a deterministic fibre tracking algorithm (F.-C. Yeh et al., 2013) was used with augmented tracking strategies (C.-H. Yeh et al., 2020) to improve reproducibility using DSI studio (http://dsi-studio.labsolver.org). The angular threshold was randomly selected from 15 degrees to 90 degrees. Tracks with lengths shorter than 15 or longer than 180 mm were discarded. A total of 5 million seeds were placed in the whole brain volume. AAL atlas was used as the brain parcellation and the connectivity matrix was calculated by counting the number of connecting tracks passing through each pair of regions. Additionally, we extracted a mean track length for each pair of regions.

Spiking population model

We built a spiking neural network with 22 regions extracted from the AAL atlas reproducing the cingulum bundle of the brain (Bubb et al., 2018a), one of the most prominent white matter structures interconnecting frontal, parietal, and temporal lobes (Bubb et al., 2018a). Each region was modelled as a balanced fully-connected network with 80 excitatory and 20 inhibitory neurons. The dynamics of the membrane potential of each neuron was described by the

adaptive exponential integrate-and-fire (*aeif*) model (Naud et al., 2008), while the dynamics of the synapses was described by the alpha function. Both dynamics were implemented together in the *aeif_cond_alpha_multisynapse* class in the NEST environment package (Eppler et al., 2008; Gewaltig & Diesmann, 2007). Mathematically, the dynamics of the neuron i in the population k was described as follows:

$$\begin{aligned} C_i \frac{dv_i^k}{dt} &= -g_{\mathrm{L},i}(v_i^k - E_{\mathrm{L},i}) + g_{\mathrm{L},i}\Delta_{T,i}\exp\left(\frac{v_i^k - v_{\mathrm{th},i}}{\Delta_{T,i}}\right) \\ &\quad - w_i^k + I_i^k + I_{\mathrm{noise},i}^k - I_{\mathrm{syn,i}}^k + I_{\mathrm{ext},i}^k, \\ \tau_{w,i}\frac{dw_i^k}{dt} &= a_i(v_i^k - E_{\mathrm{L},i}) - w_i^k, \\ \text{if } v_i^k > v_{\mathrm{vpeak}} &\begin{cases} v_i^k & \to v_{\mathrm{reset},i} \\ w_i^k & \to w_{\mathrm{reset},i}^k = w_i^k + b_i \end{cases} \end{aligned} \tag{4.2}$$

where I_i^k is an external bias current. $I_{noise,i}^k$ is a current generated by a Poissonian spike train with a rate of 2.4 kHz that accounted for the activity received from neurons that were not included in the population. $I_{syn,i}^k$ is the sum of all synaptic currents, and $I_{ext,i}^k$ is the current produced by an external sinusoidal stimulation. Parameters without superindex k mean that their values only depend on whether the neuron is excitatory ($i \in [1, 80]$) or inhibitory ($i \in [81, 100]$). The values of the whole set of parameters and their description can be found in Table 1. These values were selected to replicate the somatic dynamics of the regular spiking pattern of pyramidal cells and the fast-spiking pattern of interneurons in the cortex for the excitatory and inhibitory neurons in the model, respectively (Naud et al., 2008).

The synaptic current was expressed as the sum of the synapses within each population (intra-connectivity) and the synapses between different populations (inter-connectivity). While intra-synapses could be both excitatory (AMPA) and inhibitory (GABA_A), external long-range synaptic projections were assumed only excitatory (AMPA):

$$
\begin{aligned}
I^k_{\text{syn,i}} &= I^k_{\text{intra},i} + I^k_{\text{inter},j}, \\
I^k_{\text{intra,i}} &= \sum_{j=1}^{n_e} A^{kk}_{ij} g^{kk}_{ij,\text{AMPA}}(t-\delta^{kk}_{ij})(v^k_i - E_{\text{AMPA}}) \\
&\quad + \sum_{j=n_e+1}^{n_e+n_i} B^{kk}_{ij} g^{kk}_{ij,\text{GABA}}(t-\delta^{kk}_{ij})(v^k_i - E_{\text{GABA}}), \\
I^k_{\text{inter,i}} &= \omega \sum_{\substack{k'=1 \\ k'\neq k}}^{N} \sum_{j=1}^{n_e} A^{kk'}_{ij} g^{kk'}_{ij\text{AMPA}}(t-\delta^{kk'}_{ij})(v^k_i - E_{\text{AMPA}}), \\
g^{kk'}_{ij,\text{syn}}(t) &= \bar{g}^{kk'}_{ij,\text{syn}} \left(\frac{t-t^{k'*}_j}{\tau_{\text{syn}}}\right) \exp\left(\frac{t-t^{k'*}_j-\tau_{\text{syn}}}{\tau_{\text{syn}}}\right)
\end{aligned}
\tag{4.3}
$$

where A and B are the connectivity matrices for excitatory and inhibitory projections, δ is the matrix representing the delays in the synaptic connections, ω is the coupling factor, $\bar{g}^{kk'}_{ij,\text{syn}}$ is the maximum strength of the synapse between presynaptic neuron j from population k' and postsynaptic neuron i from population k, and $t^{k'*}_j$ is the time when the presynaptic neuron j in population k' spiked.

The local field potential (LFP) in each node was computed as the sum of all synaptic currents in that node.

The development of the SNN models was carried out in Python, and all scritps are available in the following github: https://github.com/LCCN/Frontiers2023.

Working point **simulations**

A common protocol to adjust the model to empirical observations consists in determining the optimal coupling factor for which the similarity between the experimental functional connectivity (eFC) and the functional connectivity resulting from the simulation (sFC) is maximized. The degree of similarity is typically determined by the Pearson correlation between the vectorized upper triangular matrices, and therefore, the best fit is the one that maximizes this correlation (Cabral et al., 2014; Nakagawa et al., 2014). However, we considered two additional conditions: on one hand, to avoid highly synchronized states in the SNN model, we discarded unrealistically high mean PLV values as a criterion to select the working point. To enable the

Table 4.1: SNN parameters used in simulations.

	Value			
Parameter	exc	inh	Unit	Description
C	104	59	pF	Capacity of the membrane
v_{reset}	-53.0	-54.0	mV	Reset value for v_m after a spike
E_{L}	-65.0	-62.0	mV	Leak reversal potential
g_{L}	4.3	2.9	nS	Leak conductance
a	-0.8	1.8	ns	Subthreshold adaptation
b	65.0	61.0	pA	Spike-triggered adaptation
ΔT	0.8	3.0	mV	Slope factor
τ_w	88.0	16.0	ms	Adaptation time constant
v_{th}	-52.0	-42.0	mV	Spike initiation threshold
v_{vpeak}	0.0		mV	Spike detection threshold
t_{ref}	2.0		ms	Duration of the refractory period
I	variable		pA	Constant external input current
$\bar{g}_{\text{AMPA}}$	variable		nS	Maximum conductance of the excitatory synapses
$\bar{g}_{\text{GABA}}$	variable		nS	Maximum conductance of the inhibitory synapses
$\bar{g}_{\text{noise}}$	variable		nS	Maximum conductance of background activity synapses (AMPA)
E_{AMPA}	0.0		mV	AMPA Excitatory reversal potential
E_{GABA}	-85.0		mV	GABA Inhibitory reversal potential
$\tau_{\text{syn,AMPA}}$	3.0		ms	Rise time of AMPA excitatory synaptic conductance
$\tau_{\text{syn,GABA}}$	3.2		ms	Rise time of GABA inhibitory synaptic conductance
δ^{kk}	1.0		ms	Intra-synaptic delay due to axon length
$\delta^{kk'}$	range		ms	Inter-synaptic ($k \neq k'$) delay due to axon length

exploration of alpha frequency bands relevant to our study, we selected working points where the main oscillatory frequency of the nodes fell within the alpha range (see supplementary Fig. 2). These simulations were performed three times during 25s, removing the initial 4s to avoid transients.

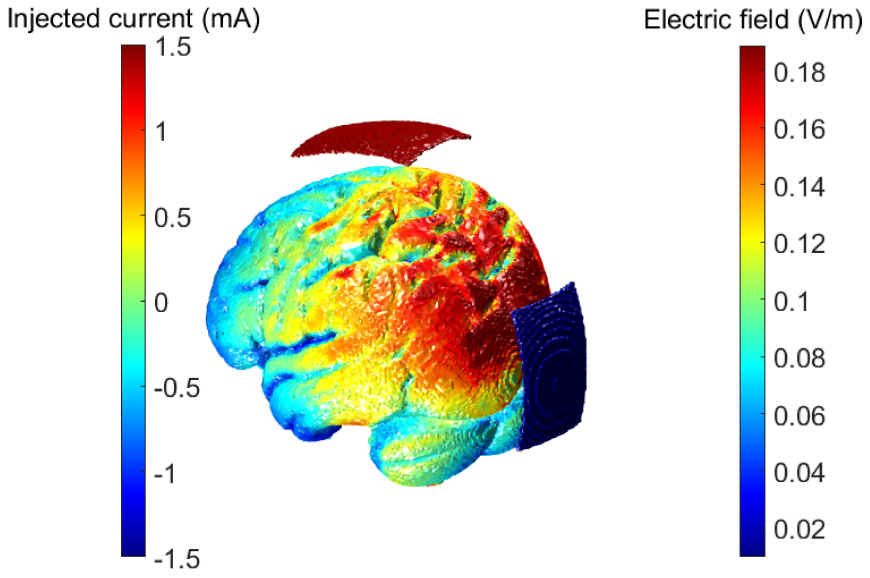


Figure 4.1: Electric field magnitudes computed with ROAST. The protocol used was the same as in the empirical experiment: Oz-Cz protocol. Left side colorbar referring to the injected current at the electrodes. Right side colorbar referring to the resulting electric field magnitude calculated for each cortical voxel.

From the current propagation model to the stimulation of the SNN

We estimated the electric field generated in the brain with an Oz-Cz stimulation protocol (in line with the empirical experiment) using ROAST software (Y. Huang et al., 2019). ROAST uses each of the participant's MRI-T1 images to segment brain tissues and generate a personalized FEM volumetric mesh. By assigning each tissue default values for conductivity and solving the underlying Laplace's equation, the software estimates the electric field propagation through the brain under DC stimulation (Y. Huang et al., 2013, 2019). An electric field vector (in V/m) per MRI voxel is the main output of the model (see Fig. 4.1).

Additionally, we took into account the orientation of the pyramidal cells' body axis by using an isometric triangular mesh of the boundary surface between white and gray matter. In this way, the value of the projections of the electric field to the normal direction referred to each surface triangle t (i.e., the normal component of $\vec{E}$ with respect to the triangle t, $E_{t\perp}$) were computed through the scalar product:

$$E_{t\perp} = \vec{E}_t \cdot \hat{n}_t = |E_t| \cos\theta_t \tag{4.4}$$

where $\hat{n}_t$ is the unit vector perpendicular to triangle t (see Fig. 4.2) pointing towards the white matter volume. In this way, fields aligned with the orthodromic direction (dendritic tuft to axon) will result in positive values, as opposed to those aligned with the antidromic direction (Bikson et al., 2004; Merlet et al., 2013). For each subject, the projections of the electric fields were grouped for each region k of the AAL, to generate a set of distributions $\underline{E_{k\perp}}$ (see supplementary Fig. 1).

Finally, to implement the tACS within the SNN model, each region-specific distribution was used to generate a set of sinusoidal currents with heterogeneous amplitudes and fixed frequency. Defining a global calibration constant Λ for scaling the stimulation intensity, the current input for neuron i belonging to node k is:

$$I^k_{ext,i}(t) = A^k_i \Lambda \sin(2\pi f t) \tag{4.5}$$

where A^k_i is a random value obtained from the distribution related to k.

tACS simulations

Two types of tACS simulations were carried out in this study with SNNs. First, we performed single-node simulations to test the effects of different hypothetical shapes on the distribution of normal components in the underlying neural activity. We explored the effect of the stimulation frequency (from 4 Hz to 18 Hz), and amplitude (from 0 to 200 pA) over the underlying nodes' dynamics. To characterize the impact of the stimulation, we computed the power spectral density (PSD) of the simulated population extracting information regarding the frequency peak of the nodes, and the value of power at both the peak and the stimulation frequency. Second, we performed a calibration procedure to find the scaling factor Λ that maximizes the matching

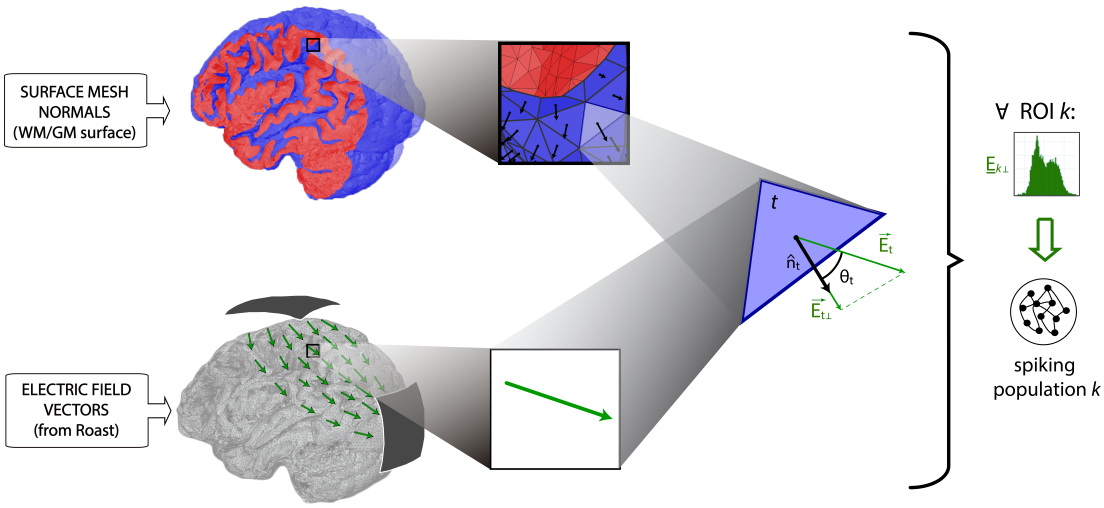


Figure 4.2: Estimation of the normal component of the electric field on the white matter surface. The estimation is calculated for each triangle t of the white matter surface ($E_{t\perp}$), as the dot product between the electric field in this point (i.e., $\vec{E}_t$, computed by Roast), and the normal vector to the surface t (i.e., $\hat{n}_t$, obtained from the triangular mesh). Note that $\hat{n}_t$ represents the direction of the cortical columns subtended to the cortex. Red colour indicates a sagittal section of the gray matter, where blue colour indicates its inner and outer surfaces. ROI-specific distributions of the normal components of E (i.e., $E_{k\perp}$) are finally used for the stimulation of spiking populations.

with the empirical observations. These simulations were performed considering the cingulum bundle networks (see *Spiking population model* section) of the ten subjects included in the computational dataset. Both types of simulations were performed 3 times for 50 seconds duration, removing the initial 4 seconds of potential transients.

Statistics

We checked for statistically significant differences between the baseline simulations and the fitted using Wilcoxon's ranked comparisons (Wilcoxon, 1945) due to the small sample size, and correcting significance with a step-down method using Bonferroni adjustments (Holm, 1979).

To evaluate the impact of different variables on the increase of alpha power, we performed a stepwise multiple linear regression. We considered 7 candidate variables per region: i) the electric field modelled through the distributions of normal components; ii) the squared value of the mean (as the effect is expected to be equivalent for negative and positive values and

Table 4.2: Demographics table for the empirical data.

	Verum	Sham	p-value
N	11	10	-
Age	35 ± 8.44	32.1 ± 9.37	0.273
Sex	8(M) / 3(F)	5(M) / 5(F)	0.387
IAF (Hz)	10.34 ± 1.09	10.23 ± 1.16	1

to linearize the data); $iii)$ the *skewness*, $iv)$ the *kurtosis*, and $v)$ the number of *modes*; $vi)$ the structural connectivity, with the logarithm of the nodes' *connectivity strength* to linearize the exponential shape observed in the structural connectivity data; and $vii)$ the network function before stimulation, using the average PLV value, and the frequency difference between the stimulation and the node's baseline oscillation. Two variables were transformed to get a better fit for the data. We used the square of the mean of the normal components of the electric field with the purpose of obtaining. Additionally, we used the base 2 logarithm of the node strength to get a better fit to the structural connectivity data.

The values of these variables were normalized in order to get a meaningful comparison of the resulting coefficients. Due to the violation of residuals' normality, we used an iteratively reweighted least squares algorithm as a robust version of the multiple linear regression. The weighted function for residuals was a Huber's T.

4.3 Results

4.3.1 Empirical results

Participant demographics

From the 27 participants, 6 participants were discarded (3 *verum* and 3 *sham*), due to the impossibility to achieve a proper impedance value for the neurostimulation session (n=2), an increased wait time between the end of the stimulation and the beginning of the post recording (n=2), or the impossibility to identify the participants' IAF (n=2). The demographics of the participants meeting all the inclusion criteria can be found in table 2.

IAF-tACS did not modulate occipito-parietal activity

While we expected an increase in power over the parieto-occipital areas after the stimulation, no significant differences were observed when comparing the rate of change in power between the *verum* and *sham* groups ($p = 0.1216$).

The stimulation sustained the decay of alpha power in time

After performing CBPT analysis, it was found in the *verum* group a higher rate of change in power for frequencies between IAF - 2.5 Hz and IAF + 5 Hz, with an increase in the power ratio of 8.02% in the *verum* group, in a cluster comprised of bilateral frontal, temporal and occipital cortical sources ($p<0.01$; Fig. 4.3). At low frequencies, the cluster is located in the inferior frontal gyrus and left temporal pole, spreading to fronto-orbital and temporo-occipital regions as the frequency increases. Although there was a significant increase in power observed in the *verum* group compared to the sham group, Figure 4.3 reveals that the stimulation prevented the decrease in power seen in the sham group. It is noteworthy that even though the stimulation targeted the IAF, the significant effects of the stimulation were observed across a broader frequency band, with the maximum number of significant nodes detected at IAF + 1 Hz.

Neurostimulation effects are highly variable

A post hoc Levene test was conducted in the frequency band where the CBPT was found significant in the previous section (IAF - 2.5 Hz, IAF + 5 Hz). The average power ratio in the parieto-occipital nodes of the brain was used, based on the AAL atlas (Fig. 4.4B), where no significant changes in power were initially observed. The *verum* group showed a significantly larger variance ($p = 0.0388$) compared to the *sham* group, as shown in Fig. 4.4B. Interestingly, there was no significant increase in the power ratio in this same region and frequency band ($p = 0.1956$). Fig. 4.4A displays the individual spectra of all participants and the mean spectra of

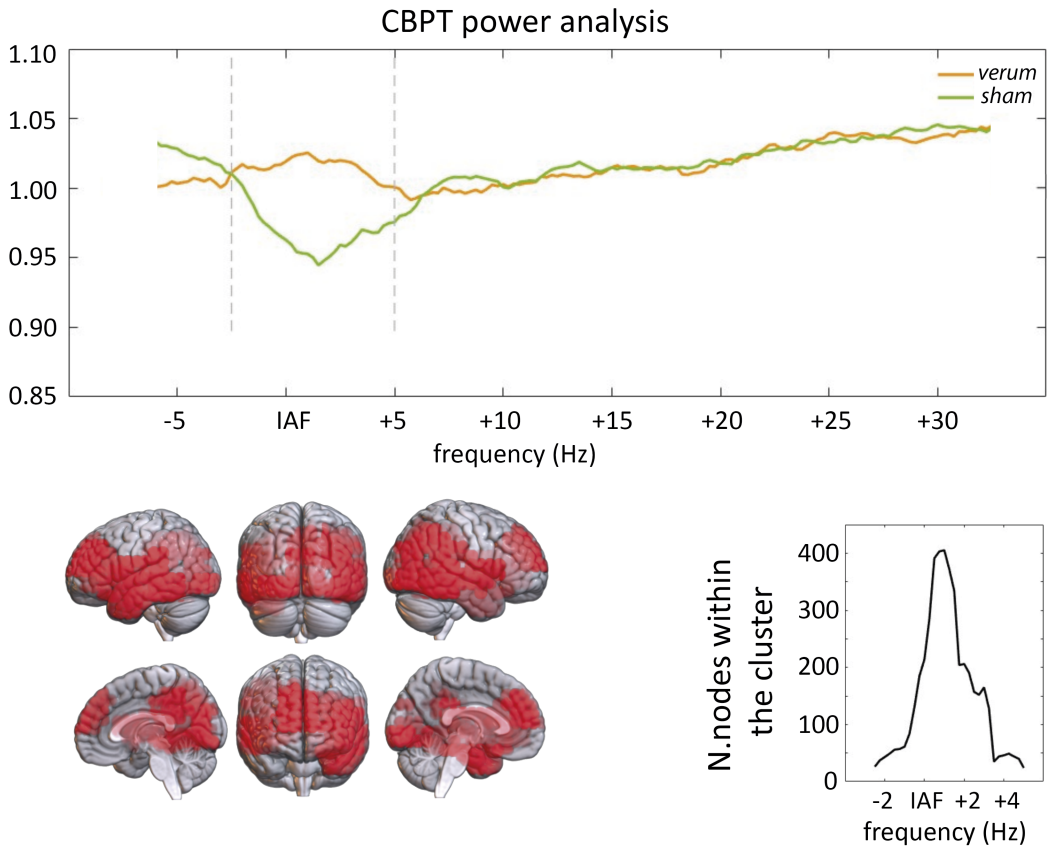


Figure 4.3: Power ratio comparison results through CBPT. Upper graph shows the power ratio (Power from the post session divided by that of the pre2 session) over the whole spectrum. Vertical lines delimit the frequency range where the significant cluster was found (IAF - 2.5 Hz, IAF + 5 Hz). The lower part of the figure shows the distribution of the significant cluster over the brain, and the number of nodes included in the cluster over its different frequencies.

the *verum* and *sham* groups in the *pre2* and *post* sessions. These spectra were obtained in the previously described CBPT cluster. The graph shows the power depression in the sham group and the inconsistency of the effect of tACS in the *verum* group, with individual spectra showing both increases and decreases in the power rate.

4.3.2 Simulation results

Cortical Gyrification Modulates the Effects of tACS: Evidence of Contradictory Outcomes

In order to perform the simulations, we calculated the electric field generated by the Oz-Cz stimulation protocol over the ten subjects in the computational sample. Given that the impact of tACS currents is primarily on pyramidal cells, and that the relative mismatch between the electric field direction and cell body axis can influence the efficacy of the stimulation, we computed the normal component of the electric field in relation to the white matter surface (see *Methods*). We grouped the components into regions of the AAL and then analysed the results for the regions of the cingulum bundle.

The Oz-Cz stimulation protocol induced currents flowing in the direction of the anterior-posterior brain axes (see Fig 1 in Methods). The evaluation of the direction of $\vec{E}$ with respect to the normal vectors of the triangulated surface between white and grey matter, interestingly showed two types of distributions (Fig. 4.5): unimodal and bimodal distributions, according to the position and shape of different brain regions. All regions showed positive (i.e., oriented towards white matter) and negative values of $E_{t\perp}$, meaning that all regions had at least some pyramidal cells oriented parallel and some oriented antiparallel to the electric field.

Regions situated along the antero-posterior axis, which are aligned with the orientation of the electric field such as the cingulate cortex, insula, and middle frontal gyrus, showed distributions that tended to be unimodal with a slight skewness, shifting the mean towards either positive or negative values. We found that the level of gyrification was related to the strength of the bimodality observed. For instance, the cingulate cortex, which is defined in the interhemispheric face of the brain, displayed less bimodality than the middle frontal gyrus which

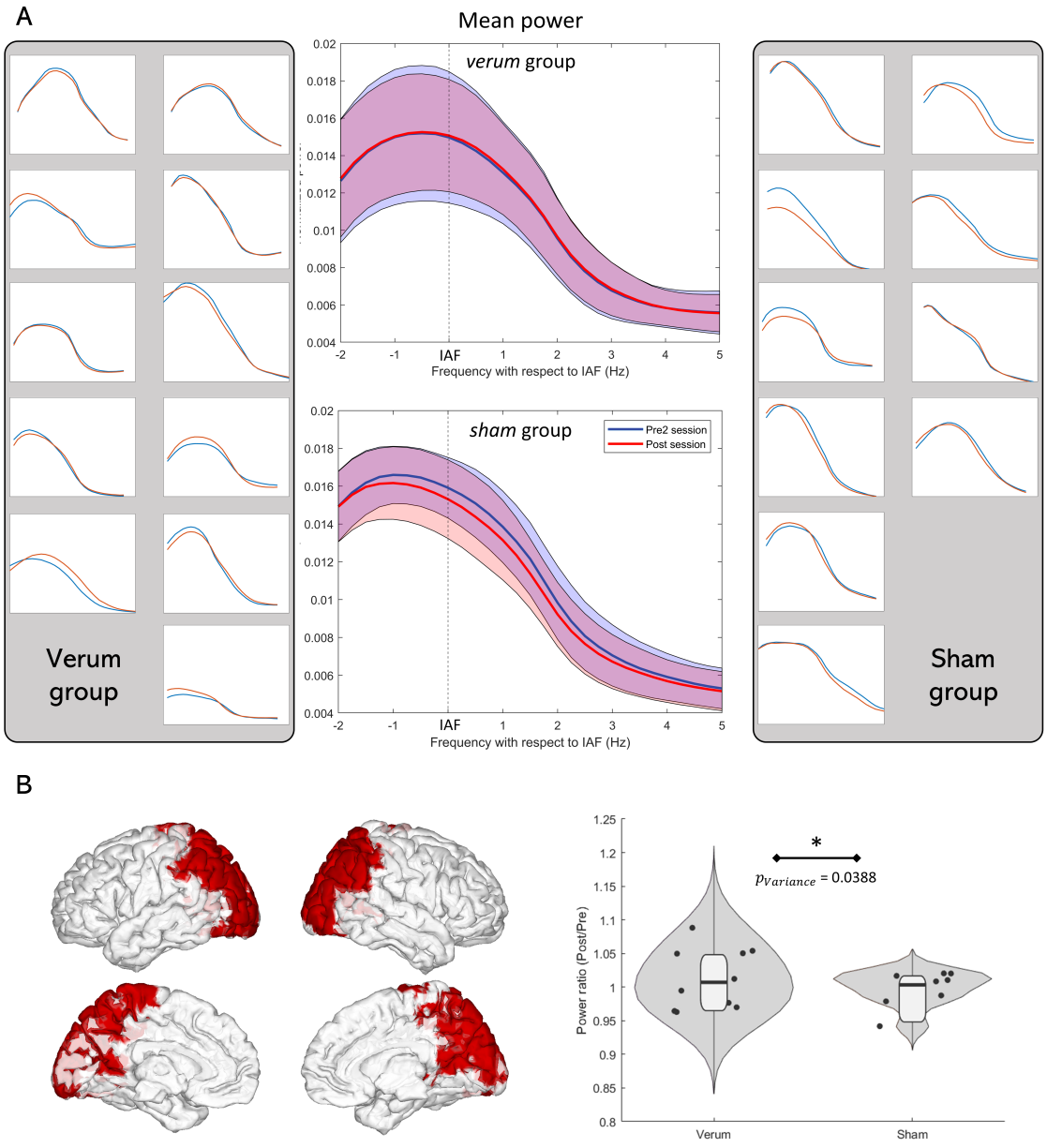


Figure 4.4: Power spectra empirical experiment results. A. Power spectra in the pre2 (curves in blue) and post (curves in red) sessions of all participants in the significant cluster presented in Fig. 4.3A. Verum participants are shown on the left and sham participants on the right. Mean power spectra of each group is shown in the middle. All graphs have the same axis scale. B. Parieto-occipital regions of the AAL atlas where the variance in the verum group was significantly higher as well as the violin plots of the average power ratio in the same regions, both in the verum and sham groups. The violin plots were created using the RST toolbox for MATLAB (Pernet et al., 2013). Levene test showed that the verum group had a significantly larger variance than that of the sham group (p = 0.0388).

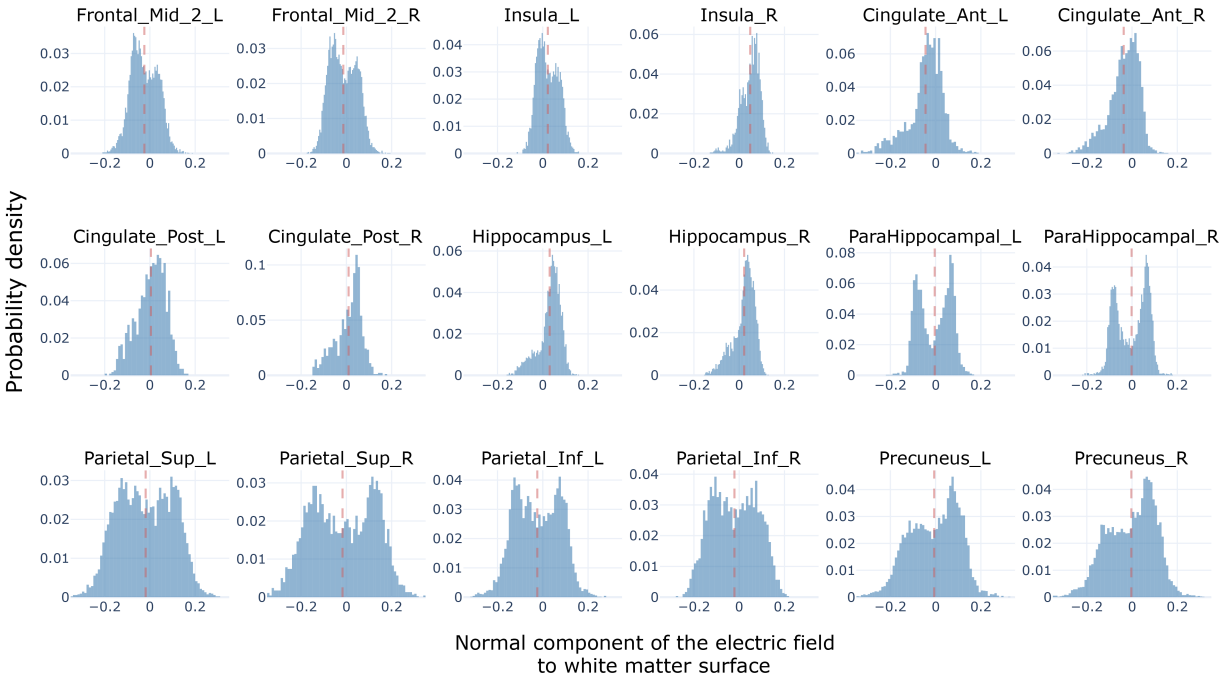


Figure 4.5: Normal component distributions (i.e., $\underline{E}_{k\perp}$). Histograms showing the accumulated (across subjects) distribution of normal components -to the white matter surface- of the electric field generated by the Oz-Cz stimulation protocol over the regions of the cingulum bundle, and including all subjects in the computational sample. Electric field distributions of subcortical regions are not included in the figure.

tends to have a more intricate shape. Interestingly, all these regions exhibited a bias towards the same value in both hemispheres. For instance, both left and right insulas were positively skewed, anterior cingulate cortices were negatively skewed, and both middle frontal gyri were negatively skewed.

Bimodal distributions were observed in posterior regions such as the parietal cortices and the precuneus, where the intricacy of the gyrification is maximized. These parietal regions have highly symmetric distributions around zero with two strong peaks, one positive and another negative. This implies that the gyri of these regions are mostly defined perpendicular to the orientation of the electric field. Therefore, it could be expected that by stimulating with the Oz-

Cz protocol, certain cells in these regions get hyperpolarized, while others get depolarized. Although some studies (Aberra et al., 2020) have started to unravel the contradictory effects that an electric field might deliver to the pyramidal cells into a gyrus, it is yet unknown how these regions would interact with others inside a network.

The distribution of normal field components modulates the effects of the stimulation

We utilized spiking neural models to gain insights into the dynamics of a single population of neurons when exposed to two sets of anti-phase sinusoidal signals with varying amplitude values, as derived from the histograms presented earlier. To accomplish this, we defined a set of distributions that could illustrate the typical shapes observed in the regions of the cingulum bundle. We defined three pairs of distributions with different shapes: bimodal symmetric, bimodal asymmetric, and Gaussian. We centred one version of these prototypical distributions at mean 0, and another version at mean 0.05 (see Fig. 4.6, centre column). By treating those distributions as probability densities, we assigned an electric field component to each neuron in the network. Then, we simulated the activity of a node being stimulated with the assigned electric field components, for a defined range of frequencies and stimulation intensities (the *space parameter*).

In general terms, the results revealed that the mean of the distribution was not enough to capture the effects of the stimulation at the target node. For the distributions with zero mean, we observed that whenever entrainment was reached (1:1 synchronization state), the resulting oscillatory frequency of the node raised above the frequency of stimulation (Fig. 4.6, right columns). Two levels of this behaviour were found in the parameter space. With enough stimulation intensity, and frequencies close to the node's natural frequency of oscillation, we found a region in which the stimulation produced an oscillatory dynamic at twice the stimulation frequency (2:1 synchronization state). This region was wider for the symmetric bimodal distribution than for the other two (Fig. 4.6, top left). Indeed, for the asymmetric bimodal and the Gaussian (Fig. 4.6, centre and bottom left, respectively), the 2:1 synchronization effect was found just for stimulation frequencies lower than the node's own oscillatory dynamic. This 2:1

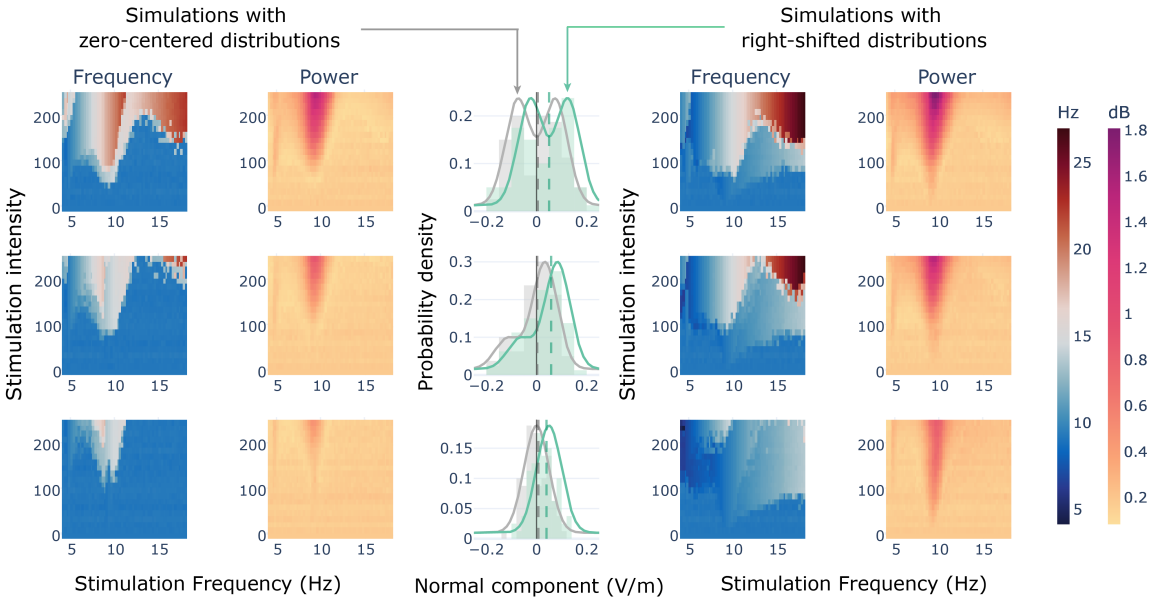


Figure 4.6: Stimulation of a single node with theoretical distributions. Central column showing the probability density distributions (i.e., curves) and the actual values extracted for the simulations (i.e., histograms). Vertical dashed lines showing the means of the values extracted for the simulations. In gray, the distributions with a theoretical mean centred at 0; in green, the right shifted distributions with a theoretical mean at 0.05. Lateral heat maps showing the results of simulating a single spiking node with the values extracted from the theoretical distributions within a range of frequencies and stimulation intensities.

response is due to the opposite and alternating polarizing effects that the stimulation exerts over the neurons, some of them were receiving a depolarizing current, while others were receiving a hyperpolarizing current. Therefore, in one period of the tACS wave two different sets of neurons become depolarized, generating neuronal discharges at a doubled oscillatory frequency. Surrounding this 2:1 response, we found a region of the parameter space in which the induced dynamics were approximately 50% faster than the stimulation. In terms of power, the highest increases were found at the natural frequency of the node. Additionally, a slight decrease could be observed at the borders of the doubled-frequency Arnold's tongue.

For the positively shifted distributions (Fig. 4.6, right columns), we found the emergence of the classical Arnold's tongues, in which the frequency of stimulation equals the frequency of the node for enough stimulation intensity (1:1 synchronization states). Also, the 2:1 synchronization state region of the parameter space mentioned previously was found for these distributions, as well as an additional region with an approximately 20% slower dynamic than the stimulation frequency, that expands from the nodes' frequency to higher frequencies with lower stimulation intensity threshold.

After comparing the three pairs of distributions, we have reached a conclusion that although they had the same mean, the bimodal symmetric distribution had more intense entrainment and increase in power than the bimodal asymmetric and Gaussian distributions. Hence, the probability distribution shape, in addition to the external frequency and stimulation intensity, plays an essential role in the emergence of different dynamical states discussed earlier.

The mean of the distribution is the main predictor of alpha power rise

To investigate the sources of variability observed in the empirical results, we constructed a spiking neural network model consisting of 22 regions of interest using the data from our computational dataset. We then implemented a tACS stimulation protocol using Oz-Cz pad electrodes. We calculated the distributions of normal components per subject and used them as probability density distributions to assign a component to each neuron. In this section, we calibrated the impact of tACS currents over the regional dynamics of our models (i.e., stimulation intensity) by fitting the calibration constant Λ to a value in which a group-averaged rise of 8.02% in alpha power is found in the same cluster of regions that emerged from the empirical experiment. Once calibrated, we used a robust multiple linear regression model to evaluate the impact of different variables in the power rise.

The calibration process, similar to empirical results, revealed a variable effect of the stimulation on the subjects included in the computational sample (Fig. 4.7). We found a fit for $\Lambda = 35$ (see supplementary Fig. 3 to observe the detailed effect on each region, Fig. 4 for the simulated LFPs during baseline and stimulation stages, and Fig. 5 for single node dynamics). At this level

of intensity, three subjects increased significantly their alpha power from baseline [$\sim 40\%$ rise; W=0, p$<$0.05, RBC=1, CLES=0.85], while the rest of the sample did not exhibit statistically significant changes (i.e., alpha power fluctuated around zero). However, moderate reductions in alpha power were observed among these subjects ($\sim 10-25\%$ decrease).

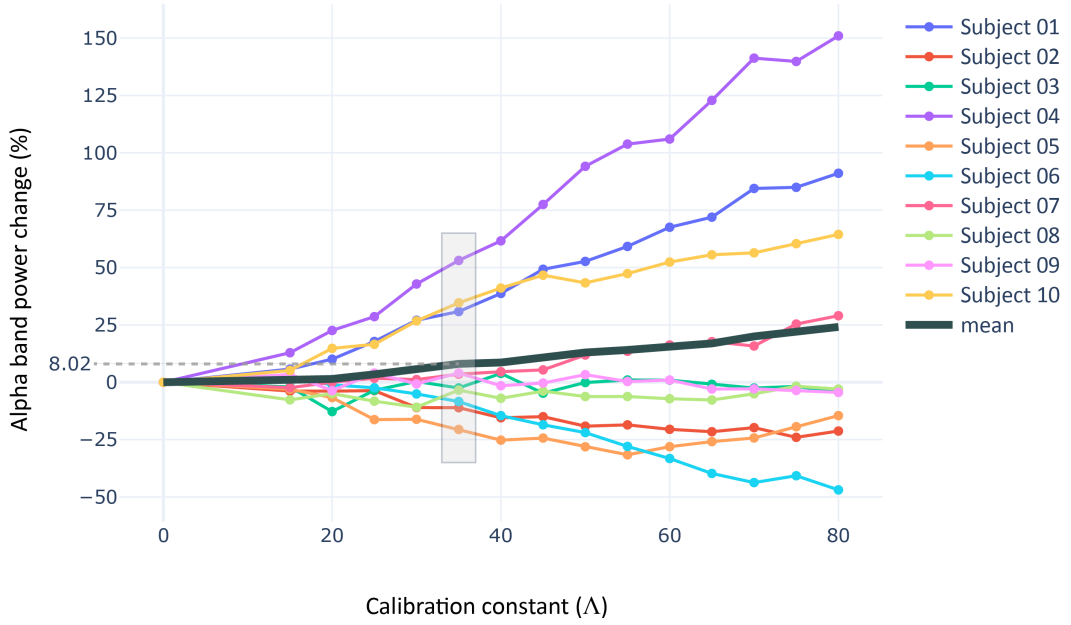


Figure 4.7: Stimulation intensity fitting. Procedure used to fit the intensity of stimulation to the results of the empirical experiment. The scatter shows the percentage of alpha band power rise for thirty simulations per intensity value and subject in the computational sample. The alpha band power rise is measured in the regions of the CBPT cluster described in the empirical section, and considering a frequency band (+/- 0.5 Hz) around the trial-specific IAF measured in our models.

With the calibrated computational model, we performed a stepwise multiple linear regression (MLR) to evaluate the impact of different variables in the increase of alpha power for the regions included in the model. We considered 7 candidate variables regarding structural connectivity, electric field modelling, and network function before stimulation (see Fig. 4.8). The values of these variables were standardized in order to get a meaningful comparison of the resulting coefficients. One variable was discarded during the stepwise process due to non-significance: the difference between the stimulation frequency and the baseline frequency of the node (coefficient=0.043, SE=0.037, p=0.236). The rest of the variables showed

statistically significant coefficients. The most relevant coefficient was related to the mean of the distribution of the electric field's normal component that was directly related to the change in alpha power (coefficient=0.44, SE=0.039, $p<0.0001$). Other measures describing the distribution had also statistically significant coefficients, including the skewness (coefficient=-0.256, SE=0.049, $p<0.0001$), kurtosis (coefficient=-0.137, SE=0.053, p=0.009), and the number of modes (coefficient=-0.0687, SE=0.029, p=0.017). Additionally, regarding connectivity variables the functional connectivity of a region previously to the stimulation was a better predictor of alpha rise (coefficient=-0.2, SE=0.034, $p<0.0001$) than the structural connectivity (coefficient=-0.1, SE=0.037, p=0.008).

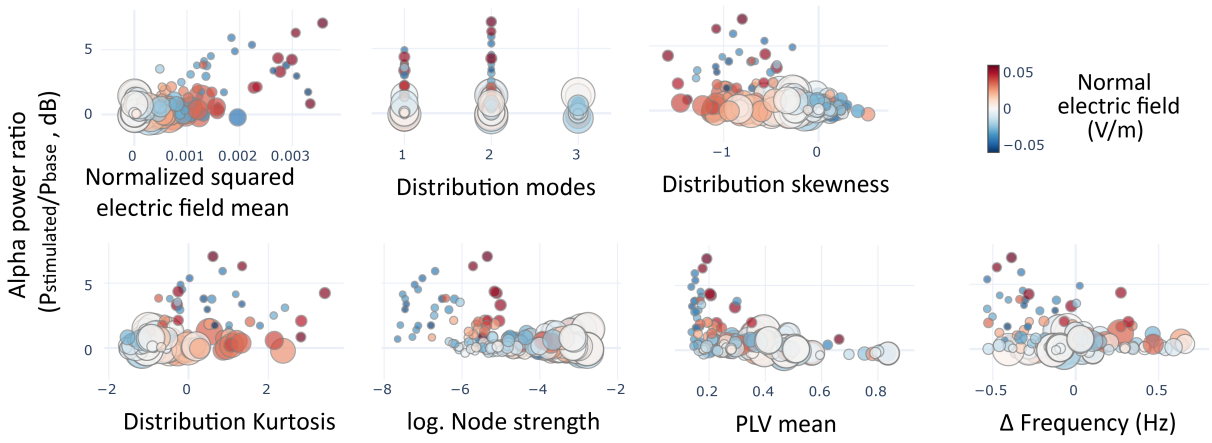


Figure 4.8: Predictors of alpha rise. Scatter plots showing the average alpha power variation in the simulated regions (circles) as a function of the variables included in the multiple linear regression model. In size, the mean node strength of the region, and in colour the average of normal components of the electric fields pertaining to each region.

From the model coefficients, it could be derived that all the significant variables, except the squared mean of the distribution, could be responsible for the slight lowering of alpha power in certain simulated subjects (e.g., subjects 5 to 7) as negative coefficients. Given the relatively small magnitude of alpha lowering with respect to the rise, we wanted to discern more clearly whether those variables were directly related to a reduction in power or whether they were involved in softening a rising effect. To do this, we performed an additional MLR model using just the data from regions whose power lowered with the stimulation (see supplementary Fig.

6). This model showed that only the functional connectivity (coefficient=-0.0423, SE=0.007, $p<0.0001$) could predict the lowering in power, with the protective effect of structural connectivity (coefficient=0.024, SE=0.01, p=0.015). All other candidate variables did not reach significance.

4.4 Discussion

Non-invasive brain stimulation has been proposed as a candidate tool for the treatment of brain disorders, and specifically, tACS has shown the potential to interact and modulate endogenous rhythms shaping brain dynamics and cognition. However, the mechanisms underlying the effects of this technique remain elusive. In this study, we replicated an IAF-tACS stimulation protocol with square patches at Oz-Cz positions, intending to rise alpha power in occipito-parietal regions. Additionally, we used computational modelling to dig into the mechanisms that might be mediating the effectiveness of its application. We calculated a current propagation model through head tissues into the brain and extracted the components of the electric field that are orthogonal to the white matter surface (i.e., the normal component of the electric field) to take into account the effect of the electric field orientation. Finally, we used this information to build an SNN model in which we could systematically test different aspects of brain activity under stimulation. This study provides a deeper understanding of the variables affecting brain dynamics under stimulation.

Our empirical results were in line with previous research findings showing an increase in power that involved many brain regions, with the exception of some occipito-parietal ones Kasten et al. (2019). This is an unexpected finding, opposite to what we hypothesized, as the stimulation was delivered over occipito-parietal regions, where the alpha power tends to be more prominent and the induced current density is maximized. At the same time, we observed an increased variability of the power change over the same areas in the verum group. Based on the results of our computational model, these unexpected findings could be related to the distributions of normal components of the electric field found in our study for parietal regions, as we hypothesized. In these cases, the reduced effect found in certain areas could potentially

be explained by a bimodal distribution of the electric field with respect to the pyramidal neurons' body axis. This would result in a mean of $E_{t\perp}$ close to zero, which our simulations showed to be the best predictor of power increase. These distributions might be particularly important to consider when translating tACS application results across different species (Beliaeva et al., 2021), as significant differences in cortical gyrification between species may confound the results. Other studies that have focused on analysing occipito-parietal regions have reported contradictory results (Zaehle et al., 2010; Zarubin et al., 2020), with some reporting increases in alpha power after tACS stimulation, while others report decreases.

Brain stimulation studies have revealed significant intersubject variability in the effects of applied protocols (Kasten et al., 2019; B. Krause & Cohen Kadosh, 2014; Wischnewski et al., 2023). This variability was also observed in both our empirical study and simulations. In the empirical study, we found subjects in the stimulation group that responded in three different ways: rising alpha power, getting the same power, and lowering it. Interestingly, a similar result was found in the simulations, in which three subjects raised significantly their alpha power while others kept the same value or lowered it. The MLR model, in combination with the distributions of normal components, could explain why some subjects exhibited enhancements in power while others did not. For instance, high functional or structural connectivity protects a region from entraining with the stimulation.

To explain why some subjects reduced alpha power, we performed a second MLR model focusing on lowering alpha-power values, and the best predictor was found to be the mean functional connectivity of a region: higher values of PLV predicted larger reductions. This is in line with previous research suggesting that the stimulation entrainment competes with the internal entrainment of the network between neighbours (M. R. Krause et al., 2022). Therefore, the stimulation could reduce the internal entrainment of the network, by modulating the regional oscillatory activity, and leading to a reduction in power.

An additional factor, not captured by the MLR models, may influence the rise/decay of the alpha power: the inter-regional communication through synaptic coupling. Previous research on information transmission in neural networks have suggested that communication between regions, in addition to the degree of coherence (PLV), depends on the conduction delay, determined by axon length, and the frequency mismatch between them Pariz et al. (2021) and Sánchez-Claros et al. (2021). The interplay of these two factors may enable or disable communication pathways trough regions. In a favorable scenario of effective communication, the power rise could be transmitted inter-regionally, and contribute to the power increase of connected regions (see supplementary Fig. 7). Consequently, it is reasonable to infer that from our neural network models may emerge subnetworks with optimized inter-regional communication that would benefit alpha band power rise. Nevertheless, a more comprehensive analysis is needed to investigate this possibility, thus paving the way for further research.

Optimizing the dosage and montages in brain stimulation is a current challenge that must be faced to achieve the desired effects from the intervention (Wischnewski et al., 2023). The complexity of this process is importantly limited by the stimulation hardware at use and implies the availability of structural images of the brains to be stimulated. However, in the process of optimization, it is often disregarded the orientation of the electric field with respect to brain tissue to focus on the maximization of the delivered field module and the spatial accuracy, despite the empirical and computational evidence that is raising awareness regarding the importance of this concept (Aberra et al., 2020; Kabakov et al., 2012; Modolo et al., 2018; B. Wang et al., 2023). In this study, we presented a simple way of employing the distributions of normal components, which could be integrated into the optimization protocols to take into consideration the orientation of the pyramidal cells' body axis in tACS.

The SNN simulations of theoretical distributions showed differential effects depending on the shape of the distributions of EF normal components while sharing approximately the same mean. In contrast, further regression analysis showed that although it does not explain the whole variance, the absolute mean of the distribution was the best predictor for alpha rise in a region. It should be noticed that the fitted value to empirical data of stimulation

intensity used for regression was in the lower range of the theoretical experiments, in which the different results for distribution shapes were less prominent. This could suggest that using the mean of the distribution as in previous studies (Merlet et al., 2013) could be an acceptable approximation to model the effects on power, although missing a certain level of accuracy. Importantly, we assumed spatial homogeneity in the distribution of excitatory and inhibitory neurons in our SNN models, being this common practice in whole-brain modelling (Deco & Jirsa, 2012; Kazemi & Jamali, 2022; Nakagawa et al., 2014; Stefanovski et al., 2019). However, future studies should consider spatial inhomogeneity in their methodology to capture a higher degree of diversity in regional dynamics.

In conclusion, this study contributes to the understanding of the tACS mechanisms that modulate brain activity by combining empirical and computational approaches. We investigated the variables affecting brain dynamics under stimulation revealing unexpected findings. Additionally, the orientation of the electric field with respect to brain tissue was identified as a crucial factor in optimizing the dosage and montages for brain stimulation. This study rises awareness on the relevance of acquiring MRI data from the participants to effectively design the stimulation protocols. Furthermore, clinical trials involving this kind of technology as a treatment, such as those developed for depression, anxiety disorders or schizophrenia among others, could benefit from taking into account the direction of the elicited electric fields in the brain in order to increase the likelihood of success of their neuromodulatory approaches. One limitation of our study is the fact that the empirical and computational datasets are different, as we did not have MRI scans of the participants that underwent neuromodulation. Thus, a further study combining empirical and computational approaches on the same sample of subjects would be of interest to confirm the observations made in this research. Non-invasive brain stimulation, and specifically tACS, are potential tools for the treatment of brain disorders, however further research is necessary to fully understand and control the effects of these techniques on brain dynamics and cognition. Computational models would help in shaping stimulation protocols, providing a model driven approach for the application of tACS achieving more specific targets of brain signals and potentially improving results of neuromodulation.

Chapter 5

Reducing fronto-parietal synchrony with tACS: a modelling study

Rhythms are key for information processing and communication within the brain. However, the neuronal synchronization that underlies those rhythms may become problematic. In Alzheimer's disease, abnormal levels of hypersynchrony between fronto-parietal areas appear in early stages of the disease, and it is thought to contribute to the production and accumulation of toxic protein in the brain, and hence, to the evolution of the disease. In this work, we use computational modelling to test the potential of transcranial alternating current stimulation (tACS) as an intervention to modulate the hypersynchrony between fronto-parietal regions in AD. We applied different virtual stimulation protocols to our brain network models to test their ability for reducing hypersynchrony. Results showed that the desynchronization between fronto-parietal regions is theoretically plausible through the differential entrainment of the targeted regions. We also demonstrate that the centrality of a node in the brain network determines its vulnerability to the stimulation: the more central the node, the more difficult it becomes to modulate its activity. Moreover, our experiments show that the structural connectivity has a larger impact than the actual electric field reaching the region. In conclusion, this study proposes a new tACS approach to tackle Alzheimer's disease in its early stages, opening the opportunity to slow or halt down its progression.

5.1 Introduction

Synchrony is a key phenomenon in neuroscience which occurs at different levels of analysis from cells to networks to the brain. At the cellular level, the interaction between inhibitory and excitatory neurons generates rhythmic activity that is usually studied into frequency bands (delta, theta, alpha, beta, gamma) and correlates with physiological and cognitive phenomena (Buzsaki, 2006). From a coarser scale, brain synchrony is understood as the statistical relationship between activation patterns of different regions in time. This phenomenon is captured by the concept of functional connectivity (FC) (K. J. Friston, 1994). It is assumed that the regions that are functionally connected are interacting to carry out specific tasks (Bullmore & Sporns, 2009; Power et al., 2011).

Abnormal levels of interregional synchrony have been reported as an early biomarker in Alzheimer's disease (AD). In AD, the abnormal accumulation of amyloid-beta ($A\beta$) protein in the extracellular space alter the excitation-inhibition balance, leading to cellular hyperactivity (M. Busche & Konnerth, 2016; Kazim et al., 2021). It is thought that this hyperactivity could be generating the fronto-parietal hyper-synchronization observed in early stages of AD: from cognitively intact AD relatives (Ramirez-Toraño et al., 2020), to individuals with subjective cognitive decline (Hafkemeijer et al., 2013; López-Sanz et al., 2017), to patients in early stages of mild cognitive impairment (MCI) (López et al., 2014). Additionally, this hyperactivity accelerates the spreading of another toxic protein called hyperphosphorylated tau (hp-tau) from the hippocampal formation, where it first appears, towards cortical hubs (Therriault et al., 2022), accumulating inside cellular bodies and disrupting the synaptic connectivity of the neurons affected (Merino-Serrais et al., 2013). It is believed that the neurodegeneration produced by hp-tau is linked to the cognitive symptomatology and to the reduction of FC observed in later stages of AD (Maestú et al., 2021; Pusil et al., 2019). Therefore, reducing the hypersynchrony/hyperexcitation in the early stages of AD could be a therapeutical target to slow down the evolution of the disease.

Transcranial alternating current stimulation (tACS) represents a promising non-invasive tool for modulating brain oscillations. The application of sinusoidal electrical currents over the scalp influences the excitability of targeted neuronal groups (Radman et al., 2009; Ridder et al., 2017), entrains neural activity at certain frequency bands (Antal et al., 2008) and influences brain function effectively (Moliadze et al., 2010). Importantly, empirical studies have shown the potential long-term effects of neurostimulation with effects in different protocols lasting even longer than an hour (Kasten & Herrmann, 2022; Kasten et al., 2016; Moliadze et al., 2010; Neuling et al., 2013; Vossen et al., 2015; Zaehle et al., 2010). These effects have been supported by computational studies showing how the stimulation may modulate brain plasticity and synaptic coupling (Butz & van, 2013; Giannakakis et al., 2020; Manos et al., 2021; Markram et al., 1997).

The efficacy of tACS is still a matter of debate (Polanía et al., 2018) given the variability of results reported in literature, and the remaining knowledge gaps regarding its underlying mechanisms (A. Liu, Vöröslakos, Kronberg, Henin, Krause, et al., 2018). Here, we use computational modelling to guide the experimental design and the definition of stimulation protocols. We integrated two types of personalized computational models, including current propagation models, that calculate the electric field generated by stimulation electrodes (Y. Huang et al., 2018), and brain network models (BNM) that simulate brain activity (Sanz-Leon et al., 2015; Schirner et al., 2015). By integrating these two models, we could test different target locations and stimulation parameters (i.e., frequency and amplitude) aiming at generating a functional desynchronization between brain regions.

This study is composed of two complementary phases. First, we adjusted the stimulation strength of the model to empirical data presented in a previous study from our group (Cabrera-Álvarez et al., 2023), in which a tACS at the individual alpha frequency (IAF) over pareto-occipital showed an increase in power of 8.02% from baseline. With this data, we fitted the integration between the current propagation model and the BNM, following the approach proposed by Merlet et al. (2013). Second, we used the already fitted model to simulate the effect of two different stimulation protocols, exploring whether - and how - we could generate

functional desynchronization between fronto-parietal areas. We hypothesized that modulating the oscillatory behaviour of a region far from the IAF may generate a desynchronization with the rest of the brain. A priori, we do not expect differences between targeting anterior or posterior regions.

5.2 Methods

5.2.1 Dataset

We used a complete set of MEG recordings, T1- and diffusion-weighted MRI images from 10 healthy subjects (7 females; age mean=69 and sd=4.16) from the database of the Center for Cognitive and Computational Neuroscience (C3N) at the Complutense University of Madrid (UCM), gathered in the context of a national research project [ID: PSI2009-14415-C03-01].

MEG signals were acquired during five minutes of eyes-closed resting state at 1 kHz sampling rate, using 306 channels (102 magnetometers and 204 gradiometers) whole-head Elekta Neuromag system (Elekta AB, Stockholm, Sweden) located in a magnetically isolated room (VacuumSchmelze GmbH, Hanau, Germany). Using a Fastrak 3D digitizer (Polhemus, Colchester, Vermont), the positions of four head position indicator (HPI) coils attached to the scalp were defined and the shape of each participant's head relative to three anatomical locations (nasion and both preauricular points) was modelled. An online anti-aliasing filter ([0.1-330] Hz) was applied during the whole session. Raw data was pre-processed by the Maxfilter software (v.2.2, correlation threshold=0.9, time window=10 s) to remove the environmental noise using the temporal extension of the signal space separation (tSSS) method with movement compensation (Taulu & Simola, 2006). Given the elevated redundancy of gradiometer data after applying the tSSS (Garcés et al., 2017) only data from magnetometers were considered for subsequent analyses. Eye, muscle, and jump artefacts were automatically located using Fieldtrip software (Oostenveld et al., 2011) and reviewed by MEG signal experts.

T1-MRIs were recorded using a General Electric 1.5 Tesla magnetic resonance scanner, using a high-resolution antenna and a homogenization PURE filter (fast spoiled gradient echo sequence, with parameters: repetition time/echo time/inversion time=11.2/4.2/450 ms; flip angle=12°; slice thickness=1 mm, 256×256 matrix, and field of view=256 mm). Diffusion-weighted images (dw-MRI) were acquired with a single-shot echo-planar imaging sequence with the parameters: echo time/repetition time=96.1/12,000 ms; NEX 3 for increasing the SNR; slice thickness=2.4 mm, 128×128 matrix, and field of view=30.7 cm yielding an isotropic voxel of 2.4 mm; 1 image with no diffusion sensitization (i.e., T2-weighted b0 images) and 25 dw-MRI (b=900 s/mm2).

5.2.2 Functional Connectivity

The preprocessed MEG data were imported in *Brainstorm* (Tadel et al., 2011) and the MRI-T1 images of the real subjects were used for the co-registration with MEG recordings using digitalized head points and fiducials. We used CAT12 tissue segmentation algorithm to extract a cortical surface mesh of 5000 vertices. We transformed T1 images into MNI space using an affine linear normalization, and we matched each cortical vertex to a ROI in the AAL2 (Rolls et al., 2015) atlas template. The forward model was solved using the overlapping spheres method (M. Huang et al., 1999) and subsequently, we calculated source-space signals using the Minimum Norm Estimate (MNE) technique (Baillet et al., 2001) with constrained dipoles normal to the cortical surface.

Finally, static FC in the alpha band (8-12 Hz) was estimated for each subject using Phase Locking Value (PLV) (Bruña et al., 2018; Lachaux et al., 1999), between each pair of source-reconstructed signals:

$$PLV_{jk} = \frac{1}{T}\left|\sum_{t=1}^{T} e^{i(\phi_j(t)-\phi_k(t))}\right| \tag{5.1}$$

Where ϕ stands for the instantaneous phase of the signals via the Hilbert transform and i for the imaginary unit. Finally, regional values were averaged following the AAL2 brain parcellation (Rolls et al., 2015).

5.2.3 Structural Connectivity

Diffusion-weighted images were processed using DSI Studio (http://dsi-studio.labsolver.org). The quality of the images was checked before fibre tracking and corrected for motion artefacts, eddy currents, and phase distortions. Then, tensor metrics were calculated. To improve reproducibility, we used a deterministic fibre tracking algorithm with augmented tracking strategies (F.-C. Yeh, 2020; F.-C. Yeh et al., 2013; F. Yeh et al., 2010). The whole brain volume was used as a seeding region. Both the anisotropy and angular thresholds were randomly selected (the latter, from 15 degrees to 90 degrees). The step size was randomly selected from 0.5 voxels to 1.5 voxels. A total of 5 million seeds were placed and tracks with lengths shorter than 15 or longer than 180 mm were discarded. To obtain structural connectivity (SC) matrices, we performed a connectivity analysis using AAL2 atlas with parameters 'pass-through' region (i.e. tracts count take into account all streamlines passing through a ROI) and threshold=0.0001 (i.e. only tracts with 0.0001 times the number of the maximum number of connecting tracks will be considered). We extracted two SC matrices: the weights' matrix, containing the number of streamlines connecting each pair of ROIs and the tract lengths matrix, containing the average tract lengths between each pair of ROIs.

5.2.4 Current propagation model

We used the ROAST toolbox (Y. Huang et al., 2019) to calculate electric current propagation through the brain given a stimulation setup. First, it segments the MRI-T1 images into its different tissues: scalp, skull, CSF, gray matter and white matter. Then, a FEM tetrahedral mesh of the head is constructed and electrodes are placed over the scalp. Defining electrode position, orientation, shape, size, and input current is possible within ROAST. Finally, the Laplace equation is solved to estimate how electric current spreads over the brain, resulting in an electric field vector (in V/m) per voxel in the brain volume.

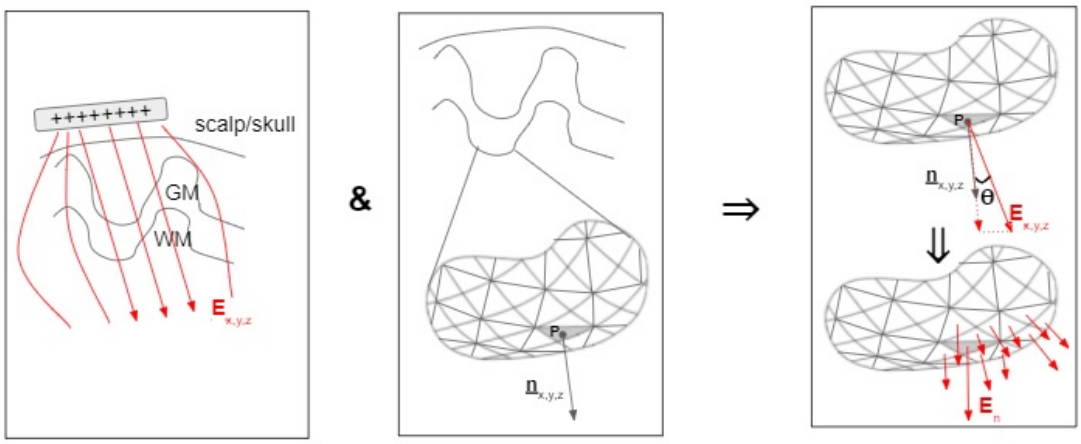


Figure 5.1: Scheme of the method adopted to estimate the orthogonal component to the white matter surface $|E_{\perp}|$, as the dot product between the vector normal to the surface ($\vec{n}$) and the electric field vector assigned to that mesh triangle ($\vec{E}$).

It has been proposed that the effects of electric fields over cortical activity depend on its orientation, related to the axo-dendritic direction of pyramidal cells (Dmochowski et al., 2012; Radman et al., 2009). As pyramidal cells tend to be aligned perpendicular to the white matter surface, we extracted the orthogonal component of each electric field vector ($\vec{E_{\perp}}$) related to the white matter surface (Merlet et al., 2013) (see fig. 5.1). Then, the magnitude of that orthogonal component ($|E_{\perp}|$) was averaged per ROI using the AAL2 atlas.

For the purposes of this study, we explored the effect of three different stimulation setups personalized per subject (Fig. 5.2). First, the Oz-Cz protocol, designed in order to replicate the experimental setup used in Cabrera-Álvarez et al. (2023) and to fit the brain model to empirical observations. It consisted of two pad electrodes (70, 50, 3 mm) placed over Oz-Cz positions with 3 mA peak to peak, oriented in the superior-inferior and anterior-posterior directions, respectively.

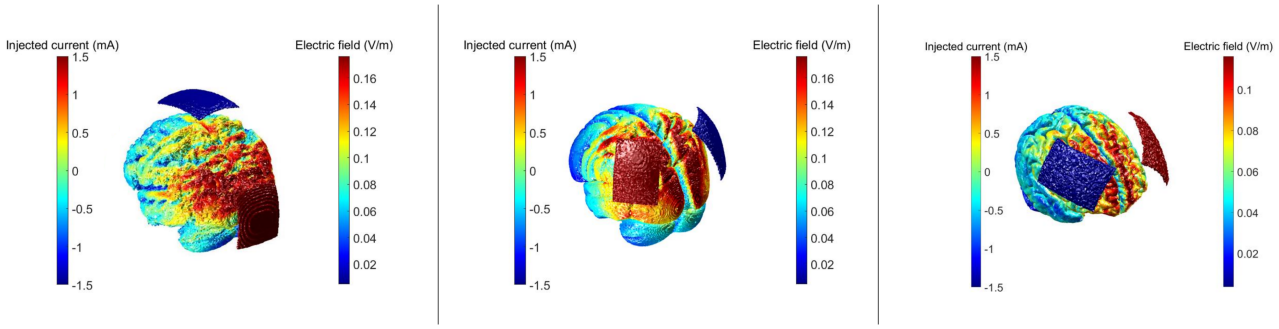


Figure 5.2: Stimulation setups. Left, pareto-occipital stimulation setup for alpha increase with electrodes over Oz-Cz. Centre, Precuneus stimulation for desynchronization with electrodes over P3-P4. Right, optimized stimulation setup for desynchronization targetting ACC. Injected current colorbar refers to electrodes.

The next two models were designed to explore the desynchronization hypothesis held in this study. P3-P4 protocol consisted in two pad electrodes (70, 50, 3 mm) placed over P3-P4 positions with 3 mA peak to peak, both oriented in the superior-inferior direction. This protocol was design to target parietal areas, and more specifically Precuneus. F3-F4 protocol consisted in two pad electrodes (70, 50, 3 mm) placed over F3-F4 positions with 3 mA peak to peak, both oriented in the anterior-posterior direction. This protocol was design to target anterior areas, and more specifically, the Anterior Cingulate Cortex (ACC).

5.2.5 Brain network model

To reproduce the electrophysiological dynamics and obtain the FC matrices, we used The Virtual Brain package (Sanz-Leon et al., 2013) in Python 3.9, which allows the user to model the neural population dynamics starting from their personalized SC and using a neural mass model approach.

The Jansen-Rit model (Jansen & Rit, 1995) has been employed to reproduce the electrophysiological dynamics of our system. This model is a biologically informed abstraction of a cortical column capable of reproducing the typical alpha activity. It includes three types of neurons: pyramidal, excitatory and inhibitory interneurons. These three subpopulations are connected

and interact with each other, and a set of coupled differential equations deploy their dynamics. The activity of pyramidal neurons is the main output of the model, as they are thought to be responsible for the signals recorded with M/EEG given their electrophysiological properties and their shape and orientation.

$$\dot{y}_{0_i}(t) = y_{3_i}(t) \tag{5.2}$$

$$\dot{y}_{1_i}(t) = y_{4_i}(t) \tag{5.3}$$

$$\dot{y}_{2_i}(t) = y_{5_i}(t) \tag{5.4}$$

$$\dot{y}_{3_i}(t) = AaS[y_{1_i}(t) - y_{2_i}(t)] - 2ay_{3_i}(t) - a^2 y_{0_i}(t) \tag{5.5}$$

$$\dot{y}_{4_i}(t) = Aa(p(t) + lrc + stim(t) + C_2 S[C_1 y_{0_i}(t)]) - 2ay_{4_i}(t) - a^2 y_{1_i}(t) \tag{5.6}$$

$$\dot{y}_{5_i}(t) = Bb(C_4 S[C_3 y_{0_i}(t)]) - 2by_{5_i}(t) - b^2 y_{2_i}(t) \tag{5.7}$$

Where:

$$S[v] = \frac{(2v_{max}}{1 + \exp^{r(v_0 - v)}} \tag{5.8}$$

$$lrc(i,t) = \sum_{j=1}^{N} y_{0_j}(t - \tau_{ji}) w_{ji} \tag{5.9}$$

$$stim(i,t) = k * E_{\perp_i} * sin(2\pi f t) \tag{5.10}$$

lrc stands for long range coupling - the incoming input from other regions - and w_{ji} for the connection weights from region j to i. y_0 represents the output of each region and, therefore, the inputs to neighbour regions. τ_{ji} represents the delay between regions based on SC tract lengths and conduction speed. $E_{\perp_i}$ refers to the stimulation intensity per region given the current propagation modelling performed with ROAST. k stands for a constant calibration term (see *Stimulation integration* below). Our model follows parameter definition in (Stefanovski et al., 2019):

Table 5.1: JR parameters used in simulations.

Parameter	Value	Unit	Description
A	3.25	mV	Maximum amplitude of the excitatory PSP
B	22	mV	Maximum amplitude of the inhibitory PSP
a	0.1	ms^{-1}	Time Constant of excitatory PSP
b	0.06	ms^{-1}	Time Constant of inhibitory PSP
C1	135		Average synaptic contacts: pyramidals to excitatory interneurons
C2	108		Average synaptic contacts: excitatory interneurons to pyramidals
C3	33.75		Average synaptic contacts: pyramidals to inhibitory interneurons
C4	33.75		Average synaptic contacts: inhibitory interneurons to pyramidals
v_{max}	0.0025	ms^{-1}	Half the maximum firing rate
r	0.56	mV^{-1}	Slope of the presynaptic function at v_0
v_0	6	mV	Potential when half the maximum firing rate is achieved
p	0.1085	ms^{-1}	Mean of random Gaussian intrinsic input
η	0	ms^{-1}	Standard deviation of random Gaussian intrinsic input (noise)
g	variable		Coupling factor for inter-regional communication -multiplier of weights-
s	variable	mm/ms	Conduction speed for inter-regional communication

The coupling factor (g) and conduction speed (s) have been considered free parameters of this model, and adjusted to empirical data per subject through the correlation between empirical and simulated FC. This fit is known as the working point in the parameter space. One subject showed an outlier working point outside the limit cycle range of the JR model. To maintain the same model behaviour across models, we constrained the coupling factor of this subject to fall within the range of the limit cycle regime.

5.2.6 Stimulus integration and calibration

To simulate the perturbation arising from the virtual stimulation, we implemented sinusoidal signals at several frequencies and weighted in amplitude by the averaged orthogonal component of the electric field. These signals were inputted to the excitatory interneurons of the JR column, as expressed in Eq. 5.10.

To calibrate the impact of the stimulation in the model, we fitted a calibration constant k such that the stimulation in occipito-parietal areas (Oz-Cz model) generates an average power rise that matches the 8.02% reported in our previous study (Cabrera-Álvarez et al., 2023). Simulated alpha peak rise was measured as follows:

$$rise = \frac{\int_{IAF-2}^{IAF+2} stimulated\ spectra}{\int_{IAF-2}^{IAF+2} baseline\ spectra} * 100 \tag{5.11}$$

In addition to the sinusoidal stimulation, we also tested the effect of random noise stimulation (tRNS) to reduce the synchronization between fronto-parietal regions.

5.2.7 Statistics

We performed a two-way repeated measures ANOVA on the results of stimulating 10 healthy brains with several stimulation frequencies and two electrode montages. The increase in FC between ACC and precuneus was considered as dependent variable. Then, to test what stimulation frequencies generated statistically significant changes in FC, we averaged the effects of both montages, and we tested the differences in FC after stimulation against baseline with the Student's t-test. Correction for multiple comparisons was performed with Bonferroni's method.

Additionally, a robust multiple linear regression model was used to test the influence of node strength and the averaged orthogonal component of the electric field over the change in oscillatory frequency per node:

$$\Delta f_{peak_i} = log(strength_i) + abs(E_{\perp_i}) + C \tag{5.12}$$

We used the absolute of the $E_\perp$ value as we are implementing oscillatory stimulations and the sign of the signal gets inverted periodically. All the statistical analysis were performed with the pingouin statistical toolbox (Vallat, 2018) in Python 3.9.

5.2.8 Network analysis

Network analysis was carried out with Networkx package in Python 3.9. We computed node strength, betweenness and shortest path length as measures of centrality in the averaged (over the 10 subjects) SC network. Node strength was calculated as the degree of the weighted SC matrix and was normalized by the maximum value of strength. Betweenness and shortest path lengths were calculated on the binary SC matrix.

5.3 Results

5.3.1 Interindividual variability in response to stimulation during model calibration

In order to adjust the stimulation model, we fitted the calibration constant (k) that scales globally the $E_{\perp}$ values such that the stimulation generates a rise in IAF band power (IAF +/- 2Hz) of 8.02% as reported in Cabrera-Álvarez et al. (2023). For that purpose, we applied tACS stimulation to our computational brain model with the Oz-Cz protocol and increasing values of the calibration constant k. Figure 5.3 shows the percentage of alpha rise per k value during the calibration process. The general trend was an initial decrease in IAF band power, followed by a generalized rise for all subjects. Some interindividual variability was found in this trend. Some subjects did not show the initial decrease, and we observed one outlier whose alpha power rose faster. We selected k=0.29 with a mean power rise of 8.49% being the first k value to overcome the empirical measure of 8.02%.

Once the model's stimulation was calibrated, we proceeded to explore whether we could desynchronize fronto-parietal areas in our brain models with tACS stimulation.

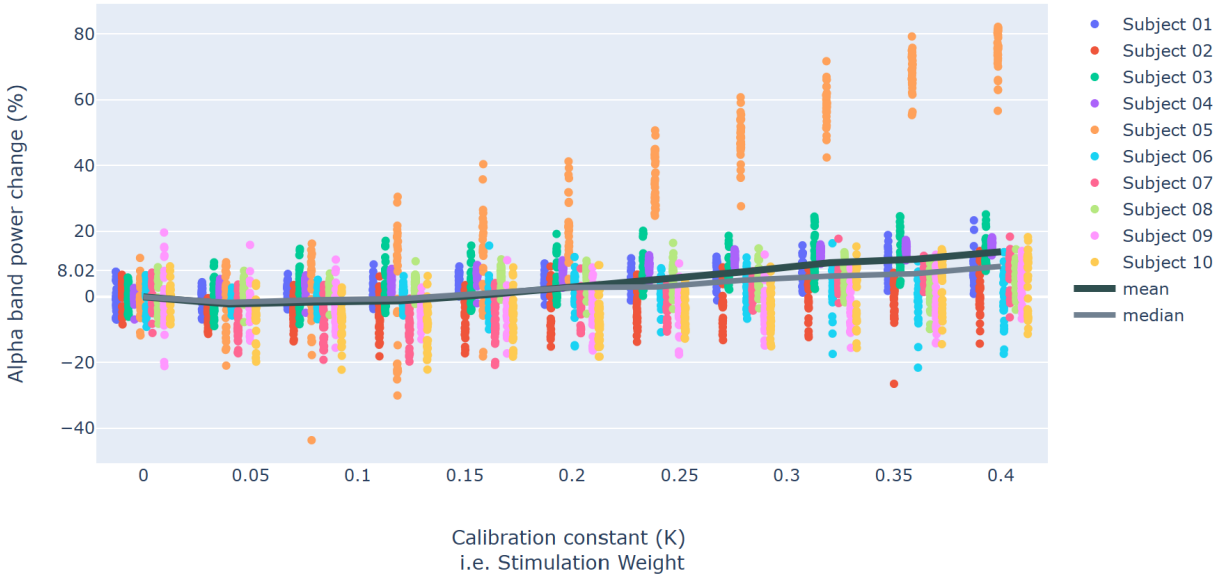


Figure 5.3: Simulations for model calibration. Percentage of alpha-band power rise by subject varying the stimulation calibration constant (k). Scatter showing results for 20 simulations.

5.3.2 tACS desynchronization is theoretically feasible

We explored two different stimulation protocols to test for functional desynchronization between Anterior Cingulate Cortex (ACC) and Precuneus. The P3-P4 protocol (over parietal regions) was designed to target Precuneus while the F3-F4 protocol (over frontal regions) was designed to target ACC. Our results showed that we could generate a desynchronizing effect at a certain frequency range but, surprisingly, the effect was mediated by the entrainment of ACC in both protocols (see figure 5.4 lower plots). This was not expected for P3P4 protocol. More expected was that the range of entrainment for ACC was larger using the F3F4 protocol than using the P3P4, and vice versa for Precuneus.

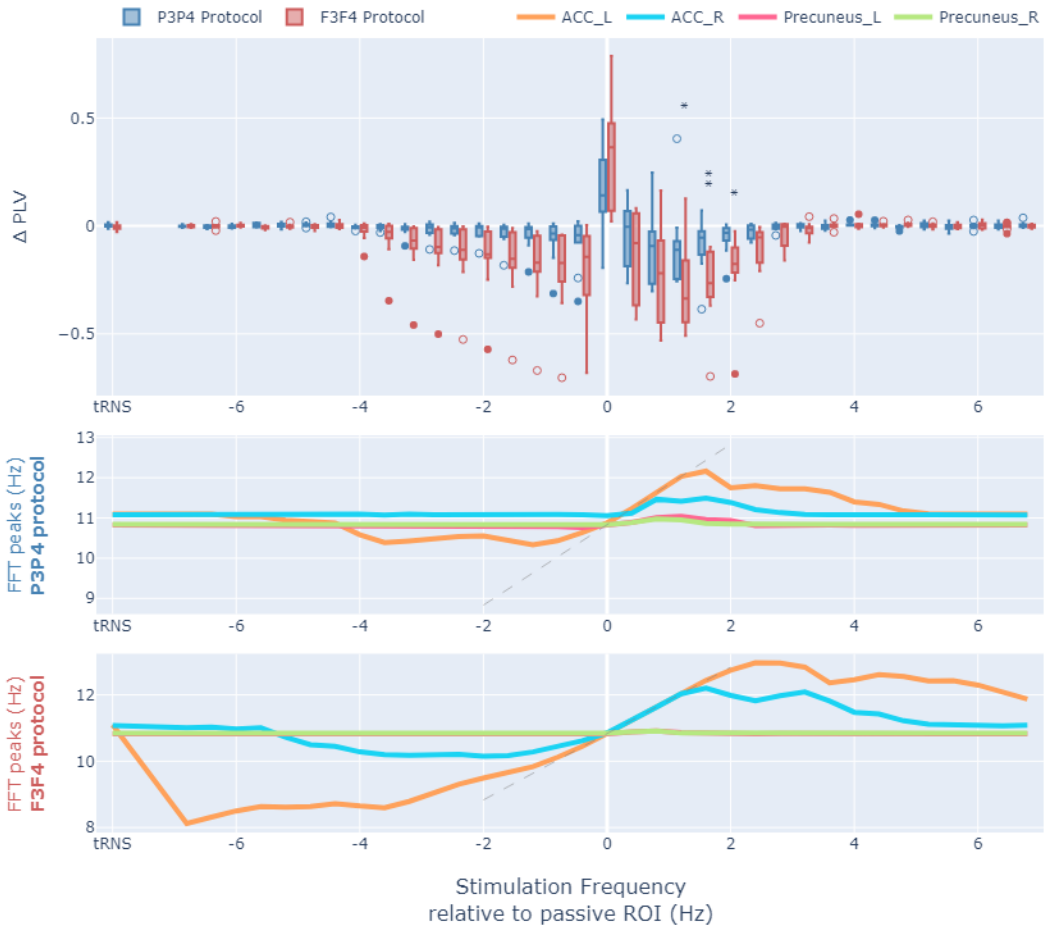


Figure 5.4: Effects of stimulation in the computational model. A range of 6 Hz around the oscillatory frequency of the passive ROI (i.e. Precuneus) was tested. First row shows the effects on FC between ACC and Precuneus. Lower two plots showing the spectral peak of each node implicated in the effect: in the middle, P3P4 protocol, in the lower, F3F4 protocol.

We also noticed that the desynchronization effect was centred around the oscillation frequency of the Precuneus at baseline instead of the general IAF. This is reasonable as we are specifically evaluating the FC between Precuneus and ACC. We expect one region to have a 'passive' role keeping its oscillatory behaviour unchanged, while the other has an 'active' role getting modulated. The generated dynamical mismatch would be the cause of the reduction in FC. Therefore, and for the sake of clarity, we defined the stimulation frequency in figure 5.4 relative to the averaged (i.e., left and right) frequency of Precuenus.

We performed a two-way repeated measures ANOVA for the change of FC between ACC and Precuneus using stimulation frequency and electrode montage (i.e., F3F4 and P3P4 protocols) as independent variables. Results showed that both the stimulation frequency [F=8.4, p<0.005, η_p^2=0.385] and electrode montage [F=12.51, p<0.01, η_p^2=0.061] had a significant effect modifying FC. The impact was more pronounced for the F3F4 protocol, as it can be observed in figure 5.4. The interaction between both factors was also statistically significant.

To test what stimulation frequencies generated the greatest desynchronization effect, we compared the increase in PLV (averaged for both protocols) for each stimulation frequency against baseline. Stimulation frequencies were considered in relation to the oscillatory frequency of the passive ROI (i.e. the Precuneus). After correcting for multiple comparisons, three stimulation frequencies showed statistically significant desynchronization: +1.2 Hz [T=-3.84, Cohen's d=0.858, p=0.040], +1.6 Hz [T=-4.46, Cohen's d=0.997, p=0.009], and +2 Hz [T=-3.75, Cohen's d=0.837, p=0.049]. Some level of desynchronization was also be found for slowing stimulation (i.e., $f_{stim} < f_{passive}$) although not reaching statistically significance. In general, accelerating stimulation (i.e., $f_{stim} > f_{passive}$) was more effective than slowing stimulation. No significant effect was found for tRNS [T=-1.033, Cohen's d=0.23, p>0.05].

5.3.3 High network centrality reduces the impact of stimulation

SC is one of the two main components of our BNMs. We wondered whether network topology could be related to the differences in entrainment shown above for ACC and Precuneus. For this purpose, we averaged the SC matrices of our ten subjects and we performed a graph theory analysis. The network showed a typical small-world structure with high clustering coefficient (mean=0.89, sd=0.03) and low path length between nodes (mean=1.149, sd=0.118). This architecture allows the network to share information efficiently, enhance synchronization and create a wide range of functional patterns (Sporns, 2010; Watts & Strogatz, 1998).

Within this big picture, Precuneus showed hub features with high centrality (normalized strength=0.53), under-average path length (path length=1.07), and over-average betweenness (betweenness=0.002; see Fig. 5.5). This is consistent with previous studies analysing the topology of brain networks (Iturria-Medina et al., 2007; van den Heuvel & Sporns, 2013). On the other hand, a less central status was found for ACC that was relatively disconnected with a lower degree (normalized strength=0.15), over-average path length (path length=1.18) and under-average betweenness (betweenness=0.0007).

Therefore, if Precuneus is more densely connected than ACC, could it be that the higher the centrality of a node, the less vulnerable it becomes to stimulation? To explore this hypothesis, we ran a set of simulations varying the degree of both nodes by randomly deleting their connections. The number of deleted connections ranged between 1-85% of each node's connections. With the resulting modified SCs, we simulated one of the tACS stimulation protocols shown above (P3P4 protocol) for frequencies between 4 and 18 Hz, enabling us to measure a range of entrainment as a function of node degree. We considered that a node was experiencing entrainment when its oscillatory frequency was closer to stimulation than to its baseline oscillatory rhythm measured without stimulation (i.e., $f_{entr} = \{x \mid f_x - f_{base} > f_x - f_{stim}\}$). Thus, the entertainment range can be defined as:

$$R_{entr} = \max(f_{entr}) - \min(f_{entr}) \tag{5.13}$$

Results showed that R_{entr} was strongly dependent on nodes' degree (Fig 5.6). We could observe that removing connections from Precuneus leads to a similar entrainment range as the one of ACC. Thus, we conclude that although our protocol was intended to target Precuneus by positioning electrodes in P3-P4, its high centrality protected it from the modulation. Additionally, as the stimulation setup was not focal, ACC was also receiving input within the P3P3 protocol and could be entrained more readily due to its lower centrality.

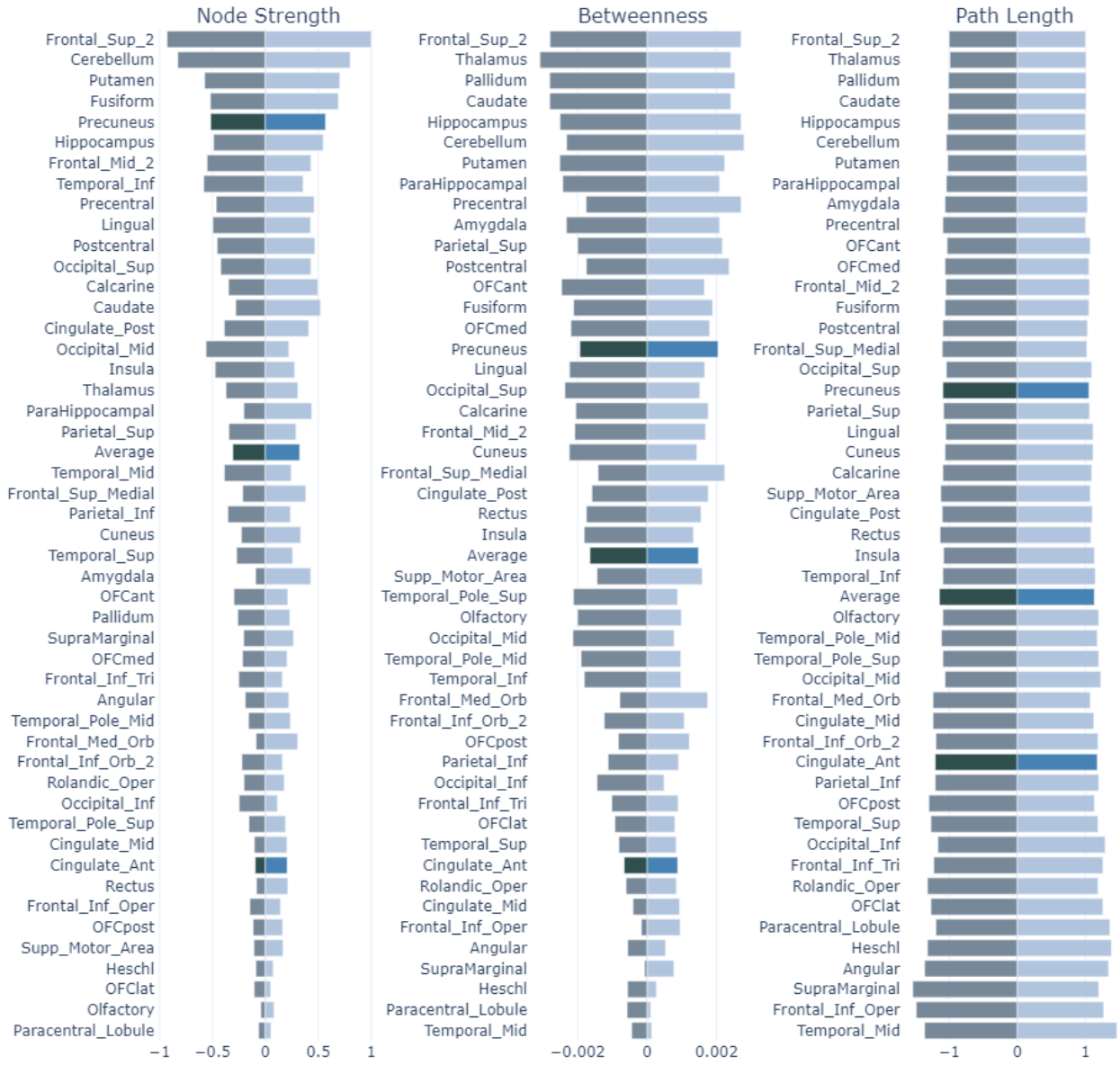


Figure 5.5: Network analysis showing normalized node strength, betweenness, and path length for the average SC of the ten subjects. Negative values represent left hemisphere regions. Highlighted rows for the network's average, the Precuneus and the ACC rois.

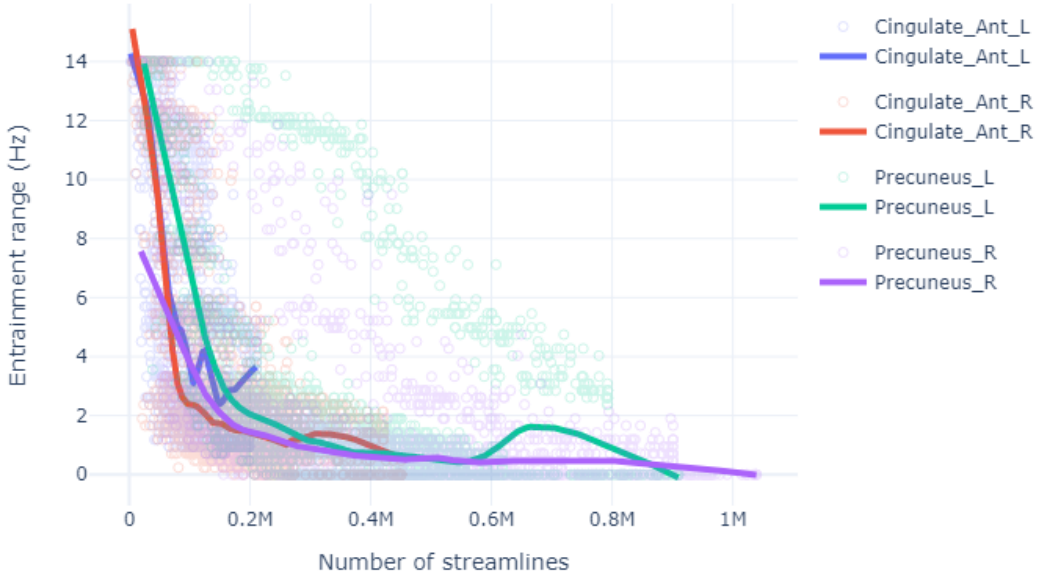


Figure 5.6: Disconnection experiment showing the simulated entrainment range for each ROI (in colour) by the number of streamlines left in that region. The number of streamlines varied due to the random deletion of connections from the SC matrix. Independent experiments were performed per region (left and right ACC and Precuneus) in which every other node's SC including ACC and precuneus remained unchanged. Lines smoothing scatter plot with the locally weighted scatterplot smoothing method (LOWESS).

5.3.4 Stimulation effects over the whole network

Previous sections focused on modelling the desynchronization between two specific fronto-parietal regions with tACS. Now, we wanted to expand our analysis by exploring the effects on the rest of the brain. We simulated 20 seconds of brain activity for each subject with and without stimulation. We used the F3F4 protocol at +1.6 Hz over the Precuneus' baseline frequency. We calculated FC in alpha band, and we recorded the frequency peak for every region.

Results showed that during stimulation many regions get desynchronized and lower their FC levels (Fig 5.7 upper). Focusing on the connectivity with ACC, the regions that suffered most intensely the lower of FC were the ones that did not change their oscillatory pattern due to the stimulation (Fig 5.7 lower). Other regions that responded more readily to stimulation showed less desynchronization with the ACC.

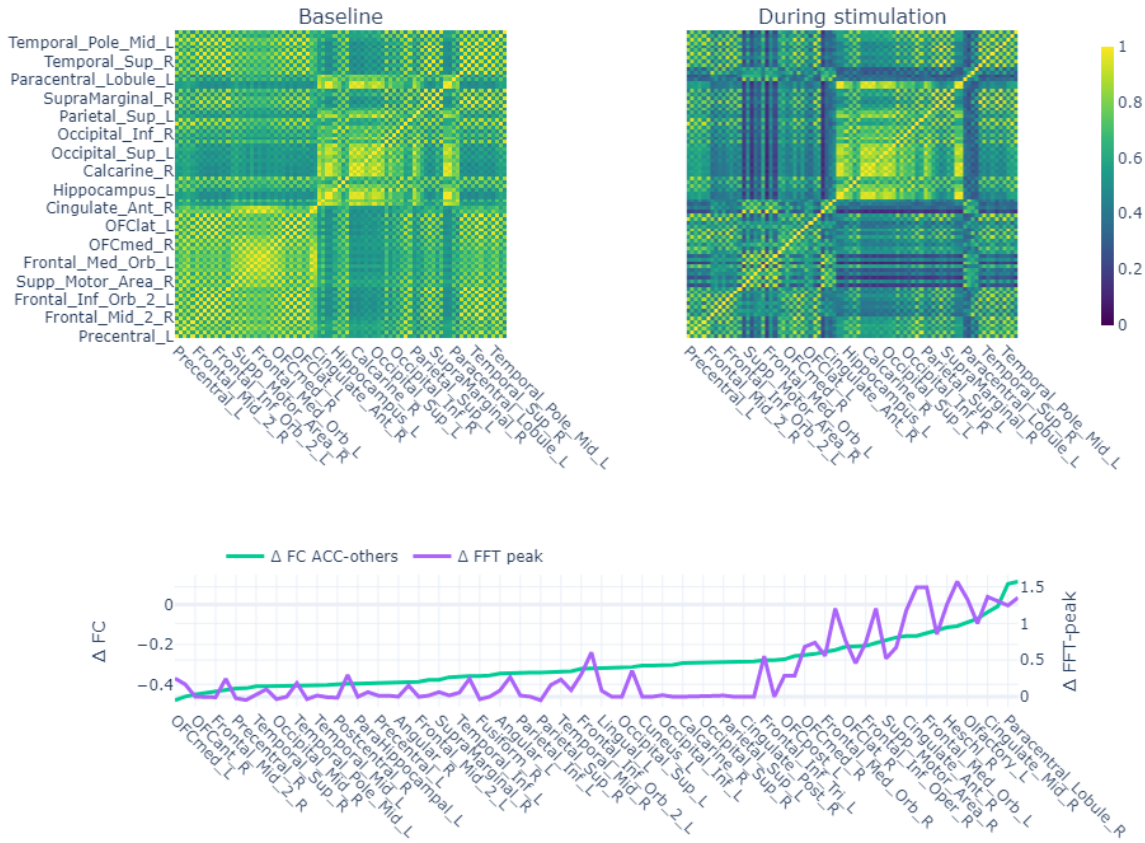


Figure 5.7: Baseline vs stimulation metrics. Upper plots show the PLV matrices without stimulation (left) and during stimulation (right). Lower plot shows the increment -from baseline to stimulation- in FC between ACC and other nodes (green), and the increment in oscillation frequency (violet) for every region. The simulation was performed with the F3F4 protocol over the average brain of our virtual sample (10 subjects).

Finally, we wondered to what extent nodes' strength and $E_{\perp}$ were driving/mediating the changes observed during stimulation. We used a multiple linear regression model to test the influence of these factors in changing regional dynamics. Results showed an inverse and strong relationship for node strength [coefficient=-0.49, z=-22.15, p<0.0001] and a direct and relatively less intense relationship for the absolute value of the $E_{\perp}$ [coefficient=0.45, z=20.4, p<0.0001]. In figure 5.8, we can observe that nodes with higher node strength are less likely to get entrained by stimulation.

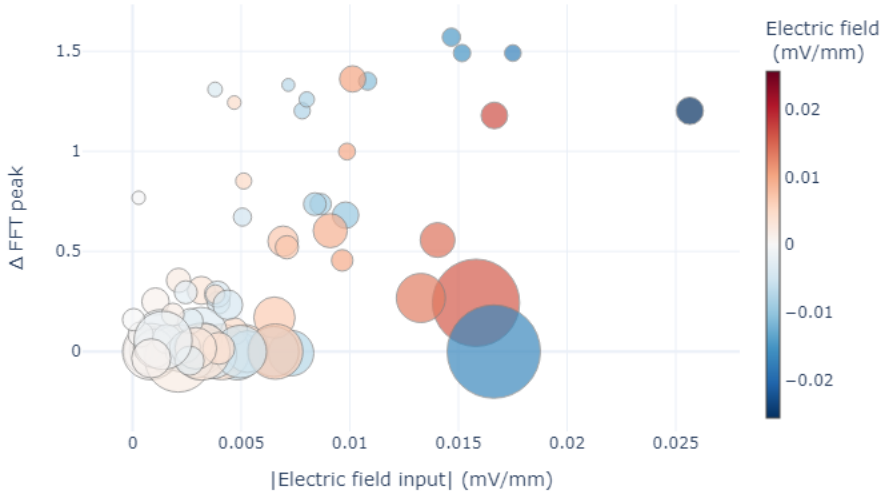


Figure 5.8: Impact of electric field $E_{\perp}$ and node strength over nodes' spectral frequency peak. Size representing node strength, colour showing the phase and magnitude of $E_{\perp}$.

5.4 Discussion

Desynchronizing fronto-parietal regions with tACS may help AD patients by slowing down disease progression. Reducing the hypersynchronization found in early stages of the disease (Ramirez-Toraño et al., 2020), may in turn help to control the vicious cycle between excitation and $A\beta$ deposition (M. A. Busche & Hyman, 2020; Zott et al., 2019). In this study, we computationally explored the use of tACS as an intervention in early stages of AD to

reduce the hypersynchrony between fronto-parietal regions. We virtually stimulated BNMs to demonstrate the theoretical plausibility of a desynchronization between ACC and Precuneus. We tested two complementary protocols, one targeting frontal areas (F3F4) and another targeting parietal regions(P3P4), that resulted in a reduction of synchrony between the regions under study that was more intense when stimulating at +1.6 Hz from IAF. surprisingly, this effect could be attributed to the entrainment of the ACC with the stimulation in both protocols. We further explored these results by linking the effects of stimulation to the individual SC of the subjects. We found that the Precuneus had a denser connectivity in average than the ACC, and also that the centrality of a region and its vulnerability to stimulation are inversely related. Furthermore, we showed that the SC strength of a region was more determinant to the impact of stimulation than the magnitude of the electric field reaching that region. Finally, we explored the effects over the whole network, observing a general reduction of FC due to the differential modulation of oscillatory frequencies.

To our knowledge, no previous experiments have tested this tACS approach for AD, however, other NIBS protocols have been tested with several stimulation techniques, sites, frequencies, and mechanisms targeted. For instance, transcranial magnetic stimulation (TMS), that involves the non-invasive application of magnetic fields to the brain, has been applied in the AD continuum targeting the DLPFC with pulses at 10/20 Hz (Menardi et al., 2022) showing significant improvements in general cognitive scales such as MMSE, MOCA and the AD specific ADAG-Cog after 2 to 6 weeks of stimulation with 5 sessions per week (X. Li et al., 2021; Rutherford et al., 2015). Other TMS studies have also showed positive results in the ADA-Cog test in mild to moderate patients of AD by targeting more spatially distributed set of regions including the inferior frontal gyrus, inferior parietal lobule, superior temporal gyrus, and language-associated regions as Broca's and Wernicke's (Brem et al., 2020; J. Lee et al., 2016; Sabbagh et al., 2020). Transcranial direct current stimulation (tDCS), that involves delivering continuous electrical currents to modulate neuronal excitability, has also been applied targeting the DLPFC for about 25 minutes in 10 sessions distributed in 2 weeks, showing cognitive improvements after the stimulation (Boggio et al., 2008; Cotelli et al., 2014;

Khedr et al., 2014). Other tDCS studies have also targeted temporal areas implicated in memory and attention using the T3/T4 electrode positions as anode for 5/6 sessions of 30 minutes distributed in 5/10 days showing mixed results (Boggio et al., 2012; Bystad et al., 2016; Chang et al., 2018; Ferrucci et al., 2008). tACS has received less attention. Some studies have been performed with stimulation frequencies in the gamma (30-80 Hz) and theta (4-7 Hz) bands, targeting the prefrontal cortex (PFC), temporal cortex, and default mode network (DMN) (Bréchet et al., 2021). The evidence in animal models of gamma frequency light-stimulation producing a reduction of $A\beta$ burden and an increased in microglial activation (Iaccarino et al., 2016) led to the experimentation with gamma tACS in humans. Results showed a positive impact on memory performance in AD with 3/4 weeks of 30 minutes daily stimulations over the DLPFC (Kehler et al., 2020). In young subjects, Nomura et al. (2019) have shown an improvement of memory performance by applying gamma tACS stimulation to the PFC during learning tasks. Theta stimulation has been applied to healthy and elderly subjects on the fusiform gyrus (Lang et al., 2019) and the PFC (Klink et al., 2020) during task performance, reporting mixed effects. The variety of protocols, experiments, scales and samples used in these studies have made it difficult to reach consistent conclusions on the effects of NIBS protocols for AD. Among those protocols, our approach resembles unexplored but potentially effective to deliver long-term effects on brain function and cognition.

Our findings underscore the critical influence of the SC of the targeted region to determine the level of modulation produced in that region. The impact of the SC was found to be even superior to the intensity of the electric field reaching that area. These results are contingent to the calibration process and the empirical data used. The precise intensity of the stimulation applied in that empirical context determines the impact of the virtual stimulation over the simulated brain activity. Hence, the more intense the empirical stimulation, the larger the impact of stimulation in the model. In our case, the empirical study used a 3 mA peak to peak stimulation intensity (Cabrera-Álvarez et al., 2023) which is close below to the limits of the safety recommendations for tES, approximately 4 mA peak to peak (Antal et al., 2017). This observation posits a testable prediction for future empirical studies on tACS. To our

knowledge, no previous research has approached the relationship between stimulation and SC from this perspective, but it has been explored from the angle of stimulation spread. They focus on how the integrity of the white matter tracts within the networks relevant for the stimulation effects determine the effectiveness of the protocols applied (Johnson et al., 2020; Lin et al., 2017; Momi et al., 2021). Therefore, an open question remains open regarding the mechanisms that would make a central node less vulnerable to stimulation. We believe that the number and strength of the functional interactions supported by the SC gives stability to a node's behaviour, similar to social environments in which an isolated individual may become more vulnerable to external influences than people with wider social networks and more connected. Further research is needed to confirm and explain these results.

Our results refer to the immediate effects during stimulation, however, the desired impact of stimulation would be to generate a long-lasting reduction of hypersynchrony between those regions to help slow down the deposition of $A\beta$. Empirical studies, both in vitro and in vivo, have shown that the stimulation may activate plasticity mechanisms generating long-lasting effects after the intervention (Antonenko et al., 2023; Chan et al., 2021; Kronberg et al., 2020; Ridding & Ziemann, 2010). We believe that the protocols proposed here, if administered appropriately, could generate the anatomical changes necessary to diminish FC levels post-intervention. Moreover, future research should work on the integration of plasticity mechanisms into the proposed modelling framework to enhance the insights over long-term effects of stimulation.

Although this is not the first study using JR NMMs to investigate brain stimulation, a comment regarding its appropriateness and caveats must be delivered. The JR is a biologically plausible model of a cortical column, generally used to reproduce neural activity in the form of waxing and waning alpha oscillations (Jansen & Rit, 1995). The model has other possible behaviours, including a slow limit cycle of delta/theta frequency band and fixed points, depending on its parametrization (Grimbert & Faugeras, 2006; Spiegler et al., 2010). In this work, we have used the JR model parameterized to operate in the alpha limit cycle, which generates a continuous alpha activity expressed in the frequency domain as a high and thin peak in the alpha band. This type of activity is implemented for each region of the brain disregarding

two relevant aspects of real brain activity: 1) not every region in the brain shows alpha activity with the same intensity (Capilla et al., 2022); 2) alpha activity is not continuous, even in resting state with eyes closed time-frequency analysis show that alpha stretches and shrinks in an apparently random manner (S. R. Jones, 2016). These two limitations are relevant for our modelling approach as the continuous alpha signal may be more easily synchronized between regions generating a high baseline FC values that would, in turn, affect the measures of desynchronization obtained. Moreover, the desynchronization produced by entraining one region might become more pronounced due to the highly deterministic alpha rhythms, once the spectral peaks differ in frequency, FC lowers. That said, we believe that in empirical settings, the effects might become more subtle and difficult to generate due to the lower baseline FC levels and the wider and richer underlying regional spectra. Advancing the biological plausibility of whole brain models of neural activity will be key to bring forward the application of models to applied contexts.

In conclusion, our study presents a novel approach utilizing tACS as a potential intervention for Alzheimer's disease in its early stages. By targeting the abnormal hypersynchrony between fronto-parietal regions, our computational modelling experiments demonstrate the theoretical feasibility of desynchronization through differential entrainment with the targeted regions. These results offer promising insights into the potential of tACS as a therapeutic tool for AD. Moving forward, further research and clinical trials are needed to validate and optimize this approach, paving the way for novel interventions in the fight against Alzheimer's disease.

Conclusions

Chapter 6

General discussion

This thesis aimed at building a computational framework to understand the FC changes observed in AD. We divided this main objective into three complementary parts: first, to construct and simulate a model of healthy brain resting state activity, aiming to reproduce network dynamics associated with episodic memory; second, to assess the effects of AD-related neurobiological alterations on neural activity and network integrity; and last, to investigate from a computational perspective the therapeutic potential of a tACS protocol to recover the healthy brain functioning altered in AD. In this general discussion, I summarize the key findings of this thesis and put them into a broader context, building a complete computational journey from the basic mechanisms of FC to alterations in AD to potential interventions.

In our first research study (chapter 2), we built ten personalized models of healthy brain activity to explore the role of the thalamus, as a deep central structure, in shaping rsFC. We tested two key features of thalamocortical networks: the presence of thalamic *afferences* related to the RAS and first-order sensory relays, and the *structure* of thalamus - parcelled thalamus, single node thalamus, and without thalamus. The inclusion of thalamus in the simulations only affected the dynamics when implemented along with noisy thalamic afferences. The effects were not linked to the specific SC pattern of the thalamus, given that similar effects could be reproduced with the SC of the cerebellum. We concluded that a limited set of driving nodes were likely to underlie the dynamics of rsFC, supporting the view of the thalamus as a driver

of cortical dynamics suggested in previous research (Alonso & Swadlow, 2015; Logiaco et al., 2021; Mofakham et al., 2021; Schmitt et al., 2017; S. Sherman, 2016). These findings contributed to a better understanding of the role of subcortical areas in rsFC but shifted our focus towards a more distributed approach to AD alterations.

In our second study (chapter 3), we developed a multiscale closed-loop neurotoxicity model of AD progression by integrating a BNM, reproducing neural activity, and a model for the prionic-propagation and accumulation of toxic proteins in the brain. The integration was performed through biologically plausible links between both models. This integration allowed us to better understand the interactions between the different levels of analysis from which AD can be framed (i.e., molecular, cellular, and interregional) over the course of the disease. Our results showed that the disruption of inhibition could explain better the cellular hyperactivity resulting from $A\beta$ accumulation, and similarly, that the progressive changes in inhibitory levels were key to explaining the AD-related electrophysiological changes in frequency, power and FC during disease evolution. Additionally, our results suggested that cellular hyperactivity and interregional hypersynchrony are not directly linked, in contrast to what has been previously thought (Maestú et al., 2021; Sepulcre et al., 2017; C. J. Stam et al., 2023), but mediated by changes in spectral power. Finally, we observed a significant association between the spatio-temporal profile of the electrophysiological changes along AD evolution and the initial distribution of AD toxic proteins, suggesting that the spatial onset of the disease exerts an influence over its progression.

In the last part (chapters 4 and 5), we explored from a computational perspective the potential of tACS as a intervention for AD in two complementary chapters. In chapter 4, we deepen the neural mechanisms underlying the effects of an IAF-tACS protocol in order to enhance the effectiveness of stimulation. Results highlighted the importance of the relative orientation of pyramidal cells with respect to the electric field applied that might exert differential and even opposed effects over the underlying cells included in a region. These differential effects generate a regional distribution of effects, and we further showed using a spiking neural network model that the mean of those distributions were a good proxy for the global influence

of stimulation over a region, as previously implemented in BNMs experiments. Finally, in chapter 5, we investigated the potential use of tACS as an intervention for AD targetting the reduction of front-parietal synchrony that is exacerbated in early stages of the disease (Ramirez-Toraño et al., 2020). We tested two different tACS montages, one targeting the ACC and another targeting the Precuneus, along with a wide range of stimulation frequencies. Simulations showed that both protocols could theoretically reduce the synchrony between ACC and Precuneus when stimulating at +1.6 Hz from baseline frequency. Strikingly, the effect of both protocols was attributed to the entrainment of the ACC with the stimulation. This was further explained by the protective effect of regional high centrality in the brain network that was found to be inversely related to the vulnerability of that region to stimulation.

In the upcoming section, I will examine and discuss these discoveries within the context of the existing scientific literature.

6.1 Is the thalamus key to explain FC disruptions in AD?

In the proposal of this thesis, we planned to explore whether subcortical areas, and more specially the thalamus, could contribute to the FC disruptions observed in AD. In consequence, our first study explored the role of thalamus in shaping healthy rsFC. Our results suggested that the thalamus modulates FC through its involvement in the RAS system and as a sensory relay node. Both brain aspects are disrupted in AD due to the tau-related synaptic dysfunction and neuronal loss.

Multiple structures involved in the RAS system have been shown to become altered during disease progression, (Mesulam, 2013; Parvizi et al., 2001) including the noradrenergic locus coeruleus (Kelly et al., 2017; Matchett et al., 2021; Weinshenker, 2008), the serotoninergic raphe nuclei (Aletrino et al., 1992; Rüb et al., 2000; T. Yamamoto & Hirano, 1985) and the dopaminergic tegmental area (D'Amelio et al., 2018; De Marco & Venneri, 2018) among

others. Dysfunction in the RAS may result in reduced alertness, impaired attention, and disrupted sleep-wake cycles, all of which are common symptoms experienced by individuals with AD (Irwin & Vitiello, 2019; Malhotra, 2019; McGuinness et al., 2010; Van Erum et al., 2019).

Also, impairments in sensory processing affecting various modalities become increasingly apparent since early stages of the disease, (Golob et al., 2001; Murphy, 2018; N. K. Zhang et al., 2023) including vision (Festa et al., 2005; López-Cuenca et al., 2023; Salobrar-García et al., 2019), olfaction (Murphy, 2018; Talamo et al., 1989) and hearing (O'Mahony et al., 1994; Pekkonen et al., 2001). These disruptions not only impair the individual's ability to perceive and interpret sensory information but also contribute to social isolation, communication difficulties, and challenges in daily functioning.

These alterations suggest the involvement of the thalamus as an AD-related physiological alterations, but they do not directly explain the cortical FC changes observed during disease progression. To our knowledge, there are no studies exploring directly this mediation. In contrast, reductions in FC *between* thalamic nodes -including the intralaminar nuclei and medial thalamus- and other brain regions including the precuneus, posterior cingulate cortex and the frontal gyrus have been shown in clinical stage of Alzheimer's (Ng et al., 2021; Wu et al., 2022; Zhou et al., 2013).

Other studies have linked the thalamus to the disease without considering FC effects. Specifically, early disruptions to the anterior thalamus, involved in the Papez circuit of the limbic system, has been associated to the episodic memory loss in AD (Aggleton et al., 2016; H. Braak & Braak, 1991b). Additionally, a thalamic atrophy in prodromal and clinical stages of AD has been observed including the shrinkage of mediodorsal, pulvinar, medial, and geniculate nuclei of the thalamus showing significant changes from HC to MCI to AD (Bernstein et al., 2021; de Jong et al., 2008; Forno et al., 2023; Novellino et al., 2019).

All the disruptions outlined above are intricately linked to the underlying molecular pathology in AD. They are manifestations of a broader anatomical disconnection occurring at the cellular level, attributable to the effects of $A\beta$ and hp-tau. Therefore, while the thalamus is indeed pertinent for understanding alterations FC alterations in AD, its significance lies within a larger framework of systemic changes affecting neural connectivity throughout the brain. In this line, we decided to adhere the second study of this thesis (chapter 3) to a more widespread approach to AD integrating distributed molecular toxic effects into our modelling framework.

6.2 The asymmetric relationship between hyperactivity, hypersynchrony and spectral power

In AD, a direct relationship between $A\beta$-related cellular hyperactivity and FC hypersynchrony has been suggested due to their spatial correlation along disease progression (Koelewijn et al., 2019; Maestú et al., 2021; Sepulcre et al., 2017; C. J. Stam et al., 2023). To our knowledge, there are no empirical data supporting this direct association. In chapter 3, we proposed that this relationship is mediated by relative power. Hyperactivity implies an increase in firing rate, but it may (or may not) develop into organized oscillatory activity. See as an example the characteristic low-amplitude fast activity observed in epilepsy, periods of desynchronized hyperactivity that precede the neural synchronization and high amplitude oscillations of the seizure (Jiruska et al., 2013; Netoff & Schiff, 2002; Wendling et al., 2002). In our studies, the rise in FC was only observed when the increase in cellular hyperactivity was transformed into meaningful oscillations and rose relative power.

We hypothesize that the ability of a neural network to re-organize its hyperactivity into meaningful oscillations depend on the power of inhibitory mechanisms that set the excitation/inhibition balance. Considering a state of high neuronal activity, a continuum of effects can be expected for different levels of inhibition: 1) low inhibition would result in a state of desynchronized low amplitude hyperactivity; 2) high inhibition would result in a reduction and silencing of neuronal activity; and 3) between these extremes there will be an intermediate range of states

in which inhibition enables activation but bias the spikes timing, hence, organizing activity into oscillatory patterns. At this intermediate range of states, rising inhibition may become paradoxically excitatory, as the temporal sorting of spikes concentrates activation power and is able to recruit further neuronal activity. This paradoxical effect of inhibition has also been experimentally tested in the context of epilepsy (Cope et al., 2009; Kaila et al., 2014; Knoflach et al., 2016) demonstrating that inhibitory mechanisms not only serve to control excessive excitation, but they can even initiate and foster the propagation of a seizure contributing to recruit neural activity from other regions and enhancing activation (Alfonsa et al., 2015; Cossart et al., 2005; Trevelyan, 2016).

In this scenario, how does the proposed tACS desynchronizing protocol (chapter 5) fit? How are hyperactivity and hypersynchrony related in the inverse direction? Can we modulate cellular hyperactivity by lowering interregional synchrony? To our knowledge, there is no previous research answering these questions. However, if we consider the process of seizure propagation, in which a progressive recruitment and synchronization of further regions add power to the epileptic activation pattern (Trevelyan et al., 2006, 2007), we could hypothesize that breaking that synchronization into smaller patterns may, in turn, reduce their power to recruit further cellular activation. Moreover, generating a frequency mismatch between a pair of functionally connected nodes lowers their chances to integrate their bidirectional afferences contributing to reduce the power to recruit activation (Pariz et al., 2021). In conclusion, we believe that using tACS to control hypersynchrony, and potentially cellular hyperactivity, in early stages of AD is a promising approach that might impact the accumulation of toxic proteins in the brain and should be further explored within experimental contexts.

6.3 The disconnection hypothesis explains AD symptoms

While a rise in FC is found in early stages of the disease, a disconnection process at several scales leads to the appearance of AD symptomatology in later stages. At the cellular level, the disconnection derives from the intracellular accumulation of hp-tau and NFTs that reduce the number of dendritic spines in pyramidal cells, shrinking the intra- and inter-regional anatomical

connectivity (Merino-Serrais et al., 2013; Mijalkov et al., 2021). Indeed, this accumulation starts in the entorhinal cortex, a key brain region for memory processes that functions as a gateway between the neocortex and the hippocampal formation (H. Braak et al., 2011; Therriault et al., 2022; van Hoesen et al., 1991). Importantly, the uptake of this biomarker in PET recordings correlates with the severity of cognitive decline in AD (Bejanin et al., 2017; Dang et al., 2022; Ossenkoppele et al., 2019).

This anatomical disconnection affects the functional interactions between brain regions that become abnormally desynchronized in moderate to advanced stages of AD (Maestú et al., 2021; Pusil et al., 2019). As observed in resting-state studies, the desynchronization begins in posterior areas of the brain and follows to anterior ones (Damoiseaux, 2012; López-Sanz et al., 2017), generating topological changes in the network such as increasing the characteristic path length in Alzheimer's patients (C. Stam et al., 2006). The rate of these changes in FC have also been correlated with the rate of cognitive impairment (D. Jones et al., 2011; Y. Liu et al., 2013; Malotaux et al., 2023). In chapter 3, we suggested that these reductions in FC may stem from local -rather than interregional- synaptic disruptions attributable to the proteinopathy, and this result is aligned with previous modelling research (Alexandersen et al., 2023).

In conclusion, AD involves a widespread synaptic dysfunction and reductions in FC throughout the brain that resembles a disconnection syndrome in which the disruption of neural networks ultimately leads to the cognitive deficits and functional impairments (Brier et al., 2014; Delbeuck, 2003).

6.4 Computational neuroscience and its transference

The proliferation of publicly accessible datasets (Ascoli et al., 2017; Eke et al., 2022; Martone, 2024), the exponential increase in computational power (Lundstrom & Alam, 2022; Mack, 2011) and the refinement of simulation tools (Fan & Markram, 2019; McDougal et al., 2016) have allowed computational neuroscience to flourish in the last decades (D'Angelo &

Jirsa, 2022). The process has been supported by a myriad of international and collaborative research projects launched to understand the brain structure and function, some of which have explicitly included computational goals (Adams et al., 2020; Amunts et al., 2016; Insel et al., 2013; Poo et al., 2016; Yuste & Bargmann, 2017). In this context, the amount of published research in the field of computational neuroscience has grown intensely since the 90s, along with the global interest in neuroscience (see Fig 6.1). A richful dialogue between empirical research and computational modelling have emerged, fostering theoretical insights, experimental designs, and practical applications in cognitive neuroscience (Kriegeskorte & Douglas, 2018).

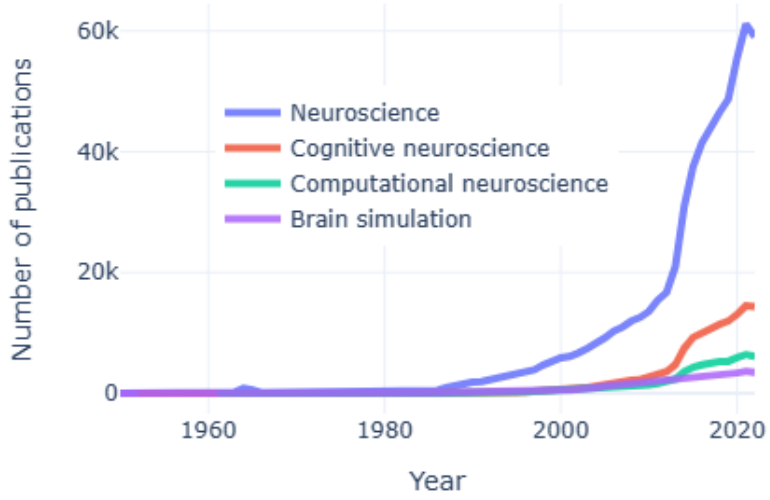


Figure 6.1: Publication rates in computational neuroscience. Number of publications per year since 1950 including the terms "Neuroscience", "Cognitive AND Neuroscience", "Computational AND Neuroscience" and "Brain AND Simulation" indexed in Pubmed.

This thesis is one among the many computational endeavours being developed nowadays to understand brain function in health and disease. By integrating empirical data and cutting-edge computing infrastructure, we could pave a way from basic neuroscience to practical applications. This trajectory mirrors other successful research endeavours as, for example,

the work done in the context of epilepsy, where a continuum of research has progressed from deciphering the local mechanisms of neural dynamics (El Houssaini et al., 2020; Wendling et al., 2002), to understanding its propagation throughout the brain (Proix et al., 2018; Proix et al., 2017), and to the use of personalized models of epileptic patients to guide surgical interventions (V. Jirsa et al., 2023; V. Jirsa et al., 2017). Likewise, progress is being made in stroke (Adhikari et al., 2015; Falcon et al., 2015, 2016), tumour (Aerts et al., 2020; Aerts et al., 2018), schizophrenia (Costa-Klein et al., 2020), and AD (Alexandersen et al., 2023; Stefanovski et al., 2019; Zimmermann et al., 2018) to mention a few.

In conclusion, computational modelling offers powerful tools to develop basic science and to transform it into applications. It allows the integration of multiscale phenomena and different data types into unified mechanistic models that aim to understand human brain, cognition and behaviour. The knowledge derived from these modelling endeavours can contribute to advance diagnostic tools and to develop new interventions for mental health issues.

6.5 The quest to understand and treat Alzeimer's

AD remains one of the most pressing challenges in modern medicine. Its intricate web of causes and effects has confounded researchers for decades. However, with advancements in technology and a deeper understanding of the brain, the quest to comprehend AD has taken a new vigor, offering hope for potential breakthroughs in the future.

Once symptoms appear in AD, an extensive neurodegeneration has taken place in the brain (Briggs et al., 2016; Holtzman et al., 2011). Therefore, a trend towards preclinical detection and treatment have emerged to intervene as early as possible in the pathological process (Briggs et al., 2016; Gregory et al., 2022; Jeremic et al., 2021; Langbaum et al., 2013; R. A. Sperling et al., 2012; van Bokhoven et al., 2021). This thesis can be framed within the research lines targetting these early stages of the disease, focusing on the mechanisms underlying the FC changes observed in preclinical AD considered as an early biomarker of the disease (Damoiseaux, 2012; R. Sperling, 2011).

Despite the extensive research and investment in AD treatments for the last 50 years, only recently a disease-modifying pharmacological therapy has been shown to slow down the progression of the disease, being approved by the FDA for commercialization (Perneczky et al., 2023). The drug agent, known as Lecanemab, is an immunotherapy that reduces the deposition of $A\beta$ with antibodies, and it has been shown to slow down cognitive decline after 18 months of administration (van Dyck et al., 2023). While promising, it comes with adverse effects and the long-term consequences of drug administration are not yet determined. Furthermore, the treatment does not halt or revert the pathological process, but it slows down its progression. Additionally, it only targets one biomarker of the disease ($A\beta$) and several authors highlight the necessity for integrative multi-target approaches to effectively address AD (Gong et al., 2022; Jeremic et al., 2021).

Besides the lines focused on the proteinopathy to understand and treat AD, a new perspective is gathering attention these days: the neuroinflammation hypothesis. While inflammation has been considered for long time a mere bystander of the neurodegenerative process, now it is thought to actively contribute to the pathogenesis of the disease and to be implicated in neuronal damage and cognitive decline (Heneka et al., 2015). The hypothesis suggests that an intricate reaction of microglia and astrocytes generate an altered neuroinflammatory response leading to disrupted $A\beta$ phagocytosis, oligodendroglia death, disrupted synapses, network dysfunction, and neuronal death (Arranz & De Strooper, 2019; Lananna et al., 2020; Leng & Edison, 2020). Understanding how these cells and the neuroinflammatory process interact to influence disease progression could unlock novel therapeutic avenues.

Looking ahead, interdisciplinary collaborations and innovative technologies will be instrumental in advancing our understanding of AD. Integrating data from different aspects of AD pathology and leveraging artificial intelligence and machine learning algorithms holds the promise of identifying new biomarkers for early detection and monitoring disease progression.

6.6 Where is episodic memory in this thesis?

In this thesis, we have simulated resting-state brain activity, a state in which the default mode network (DMN) activates prominently, being anticorrelated with task situations (Raichle, 2015; Raichle et al., 2001). The brain is far from quiet during these resting periods, our minds wander and previous experiences are spontaneously replayed (Albert et al., 2009; Kaefer et al., 2022). This cognitive process and the underlying activation of the DMN are strongly associated with episodic memory and memory consolidation (Kaefer et al., 2022; Wamsley, 2022). For instance, Kukolja et al. (2016) used a visual spatial contextual memory task along with fMRI recordings to study early memory consolidation in postencoding resting. They showed an increased connectivity in temporobasal and temporo-occipital networks, partially overlapping with the regions active during task encoding, and more importantly, that a reduced activation of the DMN in elderly subjects correlated with memory deficits. In a different modality, Huo et al. (2018) found significant correlations between the DMN FC and the performance in the Auditory Verbal Learning Test for delayed recall. Also, it has been shown that resting for 10 to 15 minutes after listening a short story leads to significant improvements in recall after 15 to 30 minutes, and even after a week (Brokaw et al., 2016; Dewar et al., 2012). Finally, Humiston et al. (2019) performed a meta-analysis including 10 similar studies on verbal memory tasks showing a significant benefit on recall of a waking rest after the tasks ($d=0.38$, $p<0.001$). These findings collectively highlight the importance of resting states and the DMN activation in facilitating episodic memory and consolidation processes.

Further, Ferguson et al. (2019) strengthened this association between the DMN and episodic memory based on lesion studies reported after stroke. They evaluated whether lesions causing amnesia were affecting parts of a network different from those affected by lesions not causing amnesia. They found that over 95% of amnesic lesions were related to a memory network, including the Papez circuit and the DMN. In AD, an association between the disruption of the DMN and cognitive decline has been established (Dillen et al., 2017; Greicius et al., 2004; Grieder et al., 2018). Finally, also from a theoretical perspective a unifying framework to understand large-scale brain networks, the triple network model proposed by Menon (2011),

supports the relevance of the DMN for memory processes. In this framework, while the salience network is in charge of detecting and filtering relevant information for the system, and the executive network is crucial for maintaining and manipulating information in the working memory and making decisions, the DMN is associated to self-referential processes including memory retrieval, autobiographical memory, and internal though.

In conclusion, although none of the articles in this thesis have made explicit mention of episodic memory, all of them have modelled its underlying neuronal correlates through the simulation of resting-state activity and the emergence of the DMN.

6.7 Limitations and future directions

6.7.1 Models usefulness

Computational models of brain activity have become indispensable tools in the study of the brain, however, they also come with inherent limitations that must be carefully considered in their application and interpretation. One significant limitation is the challenge of accurately capturing the complexity of the brain. When considered at the macro-scale level, the brain is composed of a set of highly interconnected regions, each of whose can be structurally and functionally different in terms of cytoarchitecture, electrophysiological properties, local and global connectivity, and rhythmic patterns (Glasser et al., 2016). Constructing models that faithfully replicate this intricate architecture while remaining computationally tractable is a daunting task. While simplifications and abstractions are often desirable to enhance interpretability and facilitate understanding, sometimes models may overlook important details or fail to capture the full richness of brain dynamics (Almog & Korngreen, 2016). In this thesis, we have included regional heterogeneity through SC matrices and adjusted global parameters to empirical data. However, we have not included other elements of complexity, for instance, the same NMMs and local parameterizations have been used all over the brain in chapters 2, 3 and 5. While this parameterization reproduces essential features of the electrophysiological

resting state dynamics, it may disregard important structural and functional features that differentiate brain regions, potentially overlooking aspects of brain activity such as cross-frequency coupling and spectral richness. Modelling abstractions may lead to potential gaps between model predictions and real-world observations.

A specific aspect of models' parametrization that has been openly discussed in the field is the use of criticality to adjust the models' behaviour. Criticality in non-linear systems (e.g., a NMM) refers to a state where small changes in a control parameter can lead to significant shifts in the system's behaviour, often manifesting in transitions between stable fixed points and limit cycles (Deco & Jirsa, 2012). This concept has also been applied to the study of electrophysiological signals in which phase transitions between stable and chaotic regimes (i.e., the edge of chaos) and power laws regarding propagating and fading activity (i.e., avalanche criticality) have been characterized (O'Byrne & Jerbi, 2022). The criticality of electrophysiological recordings have been proposed to enable efficient information processing and to enhance neural adaptability. While both types of criticality involve the sensitivity of the system to perturbations, we believe that the assimilation of the non-linear systems' criticality to the brain signals' one is far from straightforward. It is often assumed that spontaneous fluctuations around the critical point of a NMM (i.e., its bifurcation) represents the electrophysiological criticality of the brain and, in certain cases, it has shown better fits to empirical data (Deco & Jirsa, 2012; Deco et al., 2017), implicitly suggesting the parameterization of NMMs at the edge of criticality. Nevertheless, in chapter 2, we showed an enhancement in the fit to empirical data covering the whole pre-bifurcation range and not just the critical point, implying that the previously mentioned fit enhancement may not be directly related to criticality. Therefore, we believe that further research is needed to consolidate this relationship and describe to what extent both criticalities are similar and to what extent they differ: does NMMs criticality follow a power law? Are the dynamics of the NMMs chaotic? As these questions are not answered yet, in chapters 3 and 5 we decided to followed previous research parameterizations of the NMMs to operate within their own limit cycles (Alexandersen et al., 2023; de Haan et al., 2012; Merlet et al., 2013; Stefanovski et al., 2019; van Nifterick et al., 2022).

In conclusion, while computational models offer powerful tools for studying the brain, the choice of model architecture and parametrization can influence the results obtained, raising concerns about the generalizability of findings. Researchers must carefully consider the assumptions, parameters, and constraints of their models, as well as the potential sources of error and uncertainty inherent in computational modelling.

6.7.2 Technical limitations

MEG and dwMRI are two powerful techniques used within this thesis that offer insights into the structure and function of the brain. MEG measures the magnetic fields generated by the electrical activity of neurons, providing a high temporal resolution with millisecond precision (M. Hämäläinen et al., 1993). However, it suffers from low spatial resolution and low signal-to-noise ratio compared to fMRI (Colclough et al., 2016), and also from source leakage that leads to the sharing of source contributions by different recorded signals and, subsequently, to the overestimation of FC (Brookes et al., 2012). These limitations may have affected the accuracy of the spectral data and FC matrices used in chapters 2, 4 and 5 to fit the models. Even with limitations, MEG remained an appropriate tool in the context of this thesis as brain rhythms were key to all the studies presented.

On the other hand, dwMRI is a technique that measures the diffusion of water molecules in the brain, providing information about the location, orientation, and size of neural pathways. By tracking the movement of water molecules along white matter tracts, dwMRI can reconstruct SC networks in the brain. However, the analysis of dwMRI faces technical challenges such as dealing with crossing fibres locations in the brain, where multiple fibre bundles intersect within a single imaging voxel, leading to potential inaccuracies in the posterior tracking procedure (K. Schilling et al., 2017; K. G. Schilling et al., 2019). Also, mapping subcortical and small brain regions becomes difficult due to signal-to-noise ratio limitations for regions deep within the brain (Grier et al., 2020). We tried to reduce the impact of these limitations by using the

generalized q-sampling imaging method that allows for multiple fibre orientations, enhancing the flexibility of the algorithm, over DTI methodology, to adapt for different tracts directions in a voxel (F. Yeh et al., 2010). These limitations may have exerted special impact over the results showed in chapter 2, where the SC of the thalamus was mapped and simulated.

6.7.3 Future directions

Learning from the strengths and limitations of this thesis, new avenues are open to further advance basic brain modelling. There is a need for enhancing the underlying models of brain activity, on top of which we develop specific applications such as AD study or the tACS applications presented here. Introducing further regional heterogeneity, different models of neural activity, and exploring new ways of establishing the interactions between them open the horizon to embrace the dynamic complexity of brain activity that is now abstracted away. Moreover, incorporating factors such as synaptic plasticity and neurotransmission can yield more accurate simulations of resting-state dynamics. This endeavour requires a bidirectional interaction with empirical research to inform parameterizations and to improve experimental designs fostering the mechanistic knowledge of brain behaviour.

Additionally, including the lateral propagation of activity over the cortical surface of the brain holds promise for improving the fidelity and relevance of resting state models and, especially, the models of transcranial stimulation in which the shape of the cortical sheet is key to inform the orientation of pyramidal cells - usually perpendicular to cortical surface - that determine the effects of the applied magnetic fields as shown in chapter 4. Moreover, surface-based modelling leverages the possibility to model at a smaller scale than the region level, allowing to increase the resolution up to the computational resources available. Along with further advances in neuroimaging, that could eventually provide accurate connectomes with precision under the regional scale, it may open the way to a new generation of brain models that consider the cortical column as the elementary processing unit of the brain.

Finally, in chapter 3 we presented a mechanistic model for the progression of AD to understand FC alterations. This endeavour represented a qualitative approximation to empirical data, and therefore, we consider the next step in this line to fit the model quantitatively to empirical PET and MEG data, bridging the gap between theoretical predictions and experimental findings. From this calibration, new insights may emerge on the mechanisms underlying AD and potential new ways of predicting its evolution. Additionally, this data-driven approach will enable an iterative refinement of the model that fosters the interaction between computational and experimental neuroscience.

6.8 Concluding remarks

In the outline of this thesis, we planned to explore the disconnection hypothesis in AD from a computational perspective and to study potential interventions. We have developed a research pathway from basic science to applications transitioning from the underlying mechanisms of brain FC, to the explanation of FC alterations happening in AD, to the potential of tACS interventions to recover healthy brain dynamics. The methodological core of this work were the BNMs based on empirical data that have been used to simulate brain activity in different situations, such as under the effects of AD proteinopathy or under the influence of transcranial electrical stimulation. The results presented here suggested that, in Alzheimer's, the distributed influence of $A\beta$ and hp-tau proteinopathy can explain the alterations found in FC along AD progression, including the early increase (and later decrease) of FC following a posterior-anterior spatio-temporal sequence. Changes in inhibition due to $A\beta$ accumulation were found more likely to generate the cellular hyperactivity, transformed into hypersynchrony in early stages of the disease, but also inhibitory changes were suggested to drive the progress in further stages, when the disease resembles a disconnection syndrome. To potentially intervene early in AD, we proposed to use tACS to counteract hypersynchrony. Therefore,

we modelled the effects tACS to reduce a high front-parietal FC with the aim of slowing down the accumulation of $A\beta$ protein in the brain. The idea resulted theoretically plausible with a stimulation at +1.6 Hz over the IAF that would entrain the less structurally connected node among the ones targeted.

Overall, this thesis has been one of the many paths that could have emerged from the exploration of FC in AD from a computational perspective, and it provided a nuanced understanding of the condition's complex neurobiological underpinnings. Through simulation techniques, this thesis has contributed to enhance the comprehension of the disease's progression, offering potential avenues for new interventions in the ongoing battle against Alzheimer's.

Bibliography

Aberra, A. S., Wang, B., Grill, W. M., & Peterchev, A. V. (2020). Simulation of transcranial magnetic stimulation in head model with morphologically-realistic cortical neurons. *Brain Stimul.*, *13*(1), 175–189.

Adam, S., Van der Linden, M., Collette, F., Lemauvais, L., & Salmon, E. (2005). Further exploration of controlled and automatic memory processes in early alzheimer's disease. *Neuropsychology*, *19*(4), 420–427. https://doi.org/10.1037/0894-4105.19.4.420

Adams, A., Albin, S., Amunts, K., Asakawa, T., Bernard, A., Bjaalie, J. G., Chakli, K., Deshler, J. O., De Koninck, Y., Ebell, C. J., Egan, G., Hale, M. E., Häusser, M., Jeong, S.-J., Illes, J., Lanyon, L., Li, P., Li, Y., Magistretti, P., ... Zheng, J. (2020). International brain initiative: An innovative framework for coordinated global brain research efforts. *Neuron*, *105*(2), 212–216. https://doi.org/10.1016/j.neuron.2020.01.002

Adhikari, M. H., Raja Beharelle, A., Griffa, A., Hagmann, P., Solodkin, A., McIntosh, A. R., Small, S. L., & Deco, G. (2015). Computational modeling of resting-state activity demonstrates markers of normalcy in children with prenatal or perinatal stroke. *Journal of Neuroscience*, *35*(23), 8914–8924. https://doi.org/10.1523/jneurosci.4560-14.2015

Aerts, H., Schirner, M., Dhollander, T., Jeurissen, B., Achten, E., Van, R. D., Ritter, P., & Marinazzo, D. (2020). Modeling brain dynamics after tumor resection using The Virtual Brain. *Neuroimage*, *213*, 116738.

Aerts, H., Schirner, M., Jeurissen, B., Van Roost, D., Achten, E., Ritter, P., & Marinazzo, D. (2018). Modeling brain dynamics in brain tumor patients using the virtual brain. *eneuro*, *5*(3), ENEURO.0083–18.2018. https://doi.org/10.1523/eneuro.0083-18.2018

Aggleton, J., Pralus, A., Nelson, A., & Hornberger, M. (2016). Thalamic pathology and memory loss in early Alzheimer's disease: moving the focus from the medial temporal lobe to Papez circuit. *Brain*, *139*, 1877–90.

Ahnaou, A., Moechars, D., Raeymaekers, L., Biermans, R., Manyakov, N. V., Bottelbergs, A., Wintmolders, C., Kolen, K. V., Casteele, T. V. D., Kemp, J. A., & Drinkenburg, W. H. (2017). Emergence of early alterations in network oscillations and functional connectivity in a tau seeding mouse model of alzheimer's disease pathology. *Scientific Reports*, *7*(1). https://doi.org/10.1038/s41598-017-13839-6

Ajenikoko, M. K., Ajagbe, A. O., Onigbinde, O. A., Okesina, A. A., & Tijani, A. A. (2023). Review of alzheimer's disease drugs and their relationship with neuron-glia interaction. *IBRO Neuroscience Reports*, *14*, 64–76. https://doi.org/10.1016/j.ibneur.2022.11.005

Albert, N. B., Robertson, E. M., Mehta, P., & Miall, R. C. (2009). Resting state networks and memory consolidation. *Communicative & Integrative Biology*, *2*(6), 530–532. https://doi.org/10.4161/cib.2.6.9612

Aletrino, M., Vogels, O., Van Domburg, P., & Ten Donkelaar, H. (1992). Cell loss in the nucleus raphes dorsalis in alzheimer's disease. *Neurobiology of Aging*, *13*(4), 461–468. https://doi.org/10.1016/0197-4580(92)90073-7

Alexandersen, C. G., de Haan, W., Bick, C., & Goriely, A. (2023). A multi-scale model explains oscillatory slowing and neuronal hyperactivity in Alzheimer's disease. *Journal of The Royal Society Interface*, *20*(198). https://doi.org/10.1098/rsif.2022.0607

Alfonsa, H., Merricks, E. M., Codadu, N. K., Cunningham, M. O., Deisseroth, K., Racca, C., & Trevelyan, A. J. (2015). The contribution of raised intraneuronal chloride to epileptic network activity. *The Journal of Neuroscience*, *35*(20), 7715–7726. https://doi.org/10.1523/jneurosci.4105-14.2015

Alkire, M. T., Hudetz, A. G., & Tononi, G. (2008). Consciousness and Anesthesia. *Science*, *322*(5903), 876–880. https://doi.org/10.1126/science.1149213

Almog, M., & Korngreen, A. (2016). Is realistic neuronal modeling realistic? *Journal of Neurophysiology*, *116*(5), 2180–2209. https://doi.org/10.1152/jn.00360.2016

Alonso, J., & Swadlow, H. (2015). Thalamus controls recurrent cortical dynamics. *Nat Neurosci*, *18*, 1703–4.

Alves, P. N., Foulon, C., Karolis, V., Bzdok, D., Margulies, D. S., Volle, E., & Thiebaut de Schotten, M. (2019). An improved neuroanatomical model of the default-mode network reconciles previous neuroimaging and neuropathological findings. *Communications Biology*, *2*(1). https://doi.org/10.1038/s42003-019-0611-3

Alzheimer's Association. (2019). Causes and Risk Factors for Alzheimer's Disease — alz.org [[Accessed 10-01-2024]].

Amieva, H., Le Goff, M., Millet, X., Orgogozo, J. M., Pérès, K., Barberger-Gateau, P., Jacqmin-Gadda, H., & Dartigues, J. F. (2008). Prodromal alzheimer's disease: Successive emergence of the clinical symptoms. *Annals of Neurology*, *64*(5), 492–498. https://doi.org/10.1002/ana.21509

Amunts, K., Ebell, C., Muller, J., Telefont, M., Knoll, A., & Lippert, T. (2016). The Human Brain Project: Creating a European Research Infrastructure to Decode the Human Brain. *Neuron*, *92*, 574–581.

Amunts, K., Lepage, C., Borgeat, L., Mohlberg, H., Dickscheid, T., Rousseau, M.-É., Bludau, S., Bazin, P.-L., Lewis, L. B., Oros-Peusquens, A.-M., Shah, N. J., Lippert, T., Zilles, K., & Evans, A. C. (2013). BigBrain: An ultrahigh-resolution 3d human brain model. *Science*, *340*(6139), 1472–1475. https://doi.org/10.1126/science.1235381

Antal, A., Alekseichuk, I., Bikson, M., Brockmöller, J., Brunoni, A., Chen, R., Cohen, L., Dowthwaite, G., Ellrich, J., Flöel, A., Fregni, F., George, M., Hamilton, R., Haueisen, J., Herrmann, C., Hummel, F., Lefaucheur, J., Liebetanz, D., Loo, C., ... Paulus, W. (2017). Low intensity transcranial electric stimulation: Safety, ethical, legal regulatory and application guidelines. *Clinical Neurophysiology*, *128*(9), 1774–1809. https://doi.org/10.1016/j.clinph.2017.06.001

Antal, A., Boros, K., Poreisz, C., Chaieb, L., Terney, D., & Paulus, W. (2008). Comparatively weak after-effects of transcranial alternating current stimulation (tACS) on cortical excitability in humans. *Brain Stimul*, *1*, 97–105.

Antonenko, D., Fromm, A. E., Thams, F., Grittner, U., Meinzer, M., & Flöel, A. (2023). Microstructural and functional plasticity following repeated brain stimulation during cognitive training in older adults. *Nature Communications*, *14*(1). https://doi.org/10.1038/s41467-023-38910-x

Arranz, A. M., & De Strooper, B. (2019). The role of astroglia in alzheimer's disease: Pathophysiology and clinical implications. *The Lancet Neurology*, *18*(4), 406–414. https://doi.org/10.1016/s1474-4422(18)30490-3

Ascoli, G. A., Maraver, P., Nanda, S., Polavaram, S., & Armañanzas, R. (2017). Win–win data sharing in neuroscience. *Nature Methods*, *14*(2), 112–116. https://doi.org/10.1038/nmeth.4152

Babiloni, C., Frisoni, G. B., Pievani, M., Vecchio, F., Lizio, R., Buttiglione, M., Geroldi, C., Fracassi, C., Eusebi, F., Ferri, R., & Rossini, P. M. (2009). Hippocampal volume and cortical sources of EEG alpha rhythms in mild cognitive impairment and alzheimer disease. *Neuroimage*, *44*(1), 123–135.

Babiloni, C., Lopez, S., Del Percio, C., Noce, G., Pascarelli, M. T., Lizio, R., Teipel, S. J., González-Escamilla, G., Bakardjian, H., George, N., Cavedo, E., Lista, S., Chiesa, P. A., Vergallo, A., Lemercier, P., Spinelli, G., Grothe, M. J., Potier, M.-C., Stocchi, F., ... Hampel, H. (2020). Resting-state posterior alpha rhythms are abnormal in subjective memory complaint seniors with preclinical alzheimer's neuropathology and high education level: The INSIGHT-preAD study. *Neurobiol. Aging*, *90*, 43–59.

Baddeley, A., Logie, R., Bressi, S., Sala, S. D., & Spinnler, H. (1986). Dementia and working memory. *The Quarterly Journal of Experimental Psychology Section A*, *38*(4), 603–618. https://doi.org/10.1080/14640748608401616

Baddeley, A. (2000). The episodic buffer: A new component of working memory? *Trends in Cognitive Sciences*, *4*(11), 417–423. https://doi.org/10.1016/s1364-6613(00)01538-2

Baddeley, A., Sala, S. D., & Spinnler, H. (1991). The two-component hypothesis of memory deficit in alzheimer's disease. *Journal of Clinical and Experimental Neuropsychology*, *13*(2), 372–380. https://doi.org/10.1080/01688639108401051

Baddeley, A. D., & Hitch, G. (1974). Working memory. In *Psychology of learning and motivation* (pp. 47–89). Elsevier. https://doi.org/10.1016/s0079-7421(08)60452-1

Baillet, S., Mosher, J., & Leahy, R. (2001). Electromagnetic brain mapping. *IEEE Signal Processing Magazine*, *18*(6), 14–30. https://doi.org/10.1109/79.962275

Baillet, S. (2017). Magnetoencephalography for brain electrophysiology and imaging. *Nature Neuroscience*, *20*(3), 327–339. https://doi.org/10.1038/nn.4504

Ballard, C., Gauthier, S., Corbett, A., Brayne, C., Aarsland, D., & Jones, E. (2011). Alzheimer's disease. *The Lancet*, *377*(9770), 1019–1031. https://doi.org/10.1016/s0140-6736(10)61349-9

Ballesteros Jiménez, S. (2017, June). *Psicología de la memoria humana*.

Barendregt, M., & van Rappard, J. F. H. (2004). Reductionism revisited: On the role of reduction in psychology. *Theory & Psychology*, *14*(4), 453–474. https://doi.org/10.1177/0959354304044920

Barson, J. R., Mack, N. R., & Gao, W.-J. (2020). The Paraventricular Nucleus of the Thalamus Is an Important Node in the Emotional Processing Network. *Frontiers in Behavioral Neuroscience*, *14*. https://doi.org/10.3389/fnbeh.2020.598469

Battaglia, D., Boudou, T., Hansen, E. C., Lombardo, D., Chettouf, S., Daffertshofer, A., McIntosh, A. R., Zimmermann, J., Ritter, P., & Jirsa, V. (2020). Dynamic functional connectivity between order and randomness and its evolution across the human adult lifespan. *NeuroImage*, *222*, 117156. https://doi.org/10.1016/j.neuroimage.2020.117156

Beaulieu, C. (2002). The basis of anisotropic water diffusion in the nervous system - a technical review. *NMR Biomed.*, *15*(7-8), 435–455.

Becker, J. T. (1988). Working memory and secondary memory deficits in alzheimer's disease. *Journal of Clinical and Experimental Neuropsychology*, *10*(6), 739–753. https://doi.org/10.1080/01688638808402811

Behrens, T., Johansen-Berg, H., Woolrich, M., Smith, S., Wheeler-Kingshott, C., Boulby, P., Barker, G., Sillery, E., Sheehan, K., Ciccarelli, O., Thompson, A., Brady, J., & Matthews, P. (2003). Non-invasive mapping of connections between human thalamus and cortex using diffusion imaging. *Nat Neurosci*, *6*, 750–7.

Bejanin, A., Schonhaut, D. R., La Joie, R., Kramer, J. H., Baker, S. L., Sosa, N., Ayakta, N., Cantwell, A., Janabi, M., Lauriola, M., O'Neil, J. P., Gorno-Tempini, M. L., Miller, Z. A., Rosen, H. J., Miller, B. L., Jagust, W. J., & Rabinovici, G. D. (2017). Tau pathology and neurodegeneration contribute to cognitive impairment in alzheimer's disease. *Brain*, *140*(12), 3286–3300. https://doi.org/10.1093/brain/awx243

Bekinschtein, P., Cammarota, M., Igaz, L. M., Bevilaqua, L. R., Izquierdo, I., & Medina, J. H. (2007). Persistence of long-term memory storage requires a late protein synthesis- and bdnf- dependent phase in the hippocampus. *Neuron*, *53*(2), 261–277. https://doi.org/10.1016/j.neuron.2006.11.025

Beliaeva, V., Savvateev, I., Zerbi, V., & Polania, R. (2021). Toward integrative approaches to study the causal role of neural oscillations via transcranial electrical stimulation. *Nat. Commun.*, *12*(1), 2243.

Belouchrani, A., Abed-Meraim, K., Cardoso, J.-F., & Moulines, E. (1997). A blind source separation technique using second-order statistics. *IEEE Transactions on Signal Processing*, *45*(2), 434–444. https://doi.org/10.1109/78.554307

Bénar, C.-G., Velmurugan, J., López-Madrona, V. J., Pizzo, F., & Badier, J.-M. (2021). Detection and localization of deep sources in magnetoencephalography: A review. *Current Opinion in Biomedical Engineering*, *18*, 100285. https://doi.org/10.1016/j.cobme.2021.100285

Berger, H. (1929). Über das elektroenkephalogramm des menschen. *Archiv für psychiatrie und nervenkrankheiten*, *87*(1), 527–570.

Bernstein, A. S., Rapcsak, S. Z., Hornberger, M., & Saranathan, M. (2021). Structural changes in thalamic nuclei across prodromal and clinical alzheimer's disease. *Journal of Alzheimer's Disease*, *82*(1), 361–371. https://doi.org/10.3233/jad-201583

Betzel, R. F., & Bassett, D. S. (2017). Multi-scale brain networks. *NeuroImage*, *160*, 73–83. https://doi.org/10.1016/j.neuroimage.2016.11.006

Betzel, R. F., Byrge, L., He, Y., Goñi, J., Zuo, X.-N., & Sporns, O. (2014). Changes in structural and functional connectivity among resting-state networks across the human lifespan. *NeuroImage*, *102*, 345–357. https://doi.org/10.1016/j.neuroimage.2014.07.067

Bi, G.-q., & Poo, M.-m. (2001). Synaptic modification by correlated activity: Hebb's postulate revisited. *Annual Review of Neuroscience*, *24*(1), 139–166. https://doi.org/10.1146/annurev.neuro.24.1.139

Bikson, M., Inoue, M., Akiyama, H., Deans, j., E Fox, J., Miyakawa, H., & JGR, J. (2004). Effects of uniform extracellular dc electric fields on excitability in rat hippocampal slices in vitro. *J Physiol*, (557), 175–190.

Bliss, T. V. P., & Collingridge, G. L. (1993). A synaptic model of memory: Long-term potentiation in the hippocampus. *Nature*, *361*(6407), 31–39. https://doi.org/10.1038/361031a0

Boccalini, C., Ribaldi, F., Hristovska, I., Arnone, A., Peretti, D. E., Mu, L., Scheffler, M., Perani, D., Frisoni, G. B., & Garibotto, V. (2023). The impact of tau deposition and hypometabolism on cognitive impairment and longitudinal cognitive decline. *Alzheimer's & Dementia*, *20*(1), 221–233. https://doi.org/10.1002/alz.13355

Boggio, P. S., Khoury, L. P., Martins, D. C. S., Martins, O. E. M. S., de Macedo, E. C., & Fregni, F. (2008). Temporal cortex direct current stimulation enhances performance on a visual recognition memory task in alzheimer disease. *Journal of Neurology, Neurosurgery & Psychiatry*, *80*(4), 444–447. https://doi.org/10.1136/jnnp.2007.141853

Boggio, P. S., Ferrucci, R., Mameli, F., Martins, D., Martins, O., Vergari, M., Tadini, L., Scarpini, E., Fregni, F., & Priori, A. (2012). Prolonged visual memory enhancement after direct current stimulation in alzheimer's disease. *Brain Stimulation*, *5*(3), 223–230. https://doi.org/10.1016/j.brs.2011.06.006

Braak, H., & Braak, E. (1991a). Neuropathological stageing of Alzheimer-related changes. *Acta Neuropathol*, *82*, 239–59.

Braak, H., & Braak, E. (1991b). Alzheimer's disease affects limbic nuclei of the thalamus. *Acta Neuropathologica*, *81*(3), 261–268. https://doi.org/10.1007/bf00305867

Braak, H., Thal, D. R., Ghebremedhin, E., & Tredici, K. D. (2011). Stages of the Pathologic Process in Alzheimer Disease: Age Categories From 1 to 100 Years. *Journal of Neuropathology & Experimental Neurology*, *70*(11), 960–969. https://doi.org/10.1097/nen.0b013e318232a379

Breakspear, M., Roberts, J. A., Terry, J. R., Rodrigues, S., Mahant, N., & Robinson, P. A. (2005). A unifying explanation of primary generalized seizures through nonlinear brain modeling and bifurcation analysis. *Cerebral Cortex*, *16*(9), 1296–1313. https://doi.org/10.1093/cercor/bhj072

Bréchet, L., Michel, C. M., Schacter, D. L., & Pascual-Leone, A. (2021). Improving autobiographical memory in alzheimer's disease by transcranial alternating current stimulation. *Current Opinion in Behavioral Sciences*, *40*, 64–71. https://doi.org/10.1016/j.cobeha.2021.01.003

Breijyeh, Z., & Karaman, R. (2020). Comprehensive Review on Alzheimer's Disease: Causes and Treatment. *Molecules*, *25*(24), 5789. https://doi.org/10.3390/molecules25245789

Brem, A.-K., Di Iorio, R., Fried, P. J., Oliveira-Maia, A. J., Marra, C., Profice, P., Quaranta, D., Schilberg, L., Atkinson, N. J., Seligson, E. E., Rossini, P. M., & Pascual-Leone, A. (2020). Corticomotor plasticity predicts clinical efficacy of combined neuromodulation and cognitive training in alzheimer's disease. *Frontiers in Aging Neuroscience*, *12*. https://doi.org/10.3389/fnagi.2020.00200

Brier, M. R., Thomas, J. B., & Ances, B. M. (2014). Network dysfunction in alzheimer's disease: Refining the disconnection hypothesis. *Brain Connectivity*, *4*(5), 299–311. https://doi.org/10.1089/brain.2014.0236

Brigandt, I., & Love, A. (2023). Reductionism in Biology. In E. N. Zalta & U. Nodelman (Eds.), *The Stanford encyclopedia of philosophy* (Summer 2023). Metaphysics Research Lab, Stanford University.

Briggs, R., Kennelly, S. P., & O'Neill, D. (2016). Drug treatments in alzheimer's disease. *Clinical Medicine*, *16*(3), 247–253. https://doi.org/10.7861/clinmedicine.16-3-247

Britton, J., Frey, L., Hopp, L., Korb, P., Koubeissi, M., Lievens, W., Pestana-Knight, E., & EK, S. L. (2016). *Electroencephalography (EEG): An introductory text and atlas of normal and abnormal findings in adults, children, and infants*. American Epilepsy Society.

Broadbent, D. E. (1958). *Perception and communication.* Pergamon Press. https://doi.org/10.1037/10037-000

Brokaw, K., Tishler, W., Manceor, S., Hamilton, K., Gaulden, A., Parr, E., & Wamsley, E. J. (2016). Resting state eeg correlates of memory consolidation. *Neurobiology of Learning and Memory*, *130*, 17–25. https://doi.org/10.1016/j.nlm.2016.01.008

Brookes, M., Woolrich, M., & Barnes, G. (2012). Measuring functional connectivity in meg: A multivariate approach insensitive to linear source leakage. *NeuroImage*, *63*(2), 910–920. https://doi.org/10.1016/j.neuroimage.2012.03.048

Bruña, R., Maestú, F., & Pereda, E. (2018). Phase locking value revisited: Teaching new tricks to an old dog. *J. Neural Eng.*, *15*(5), 056011.

Bubb, E. J., Metzler-Baddeley, C., & Aggleton, J. P. (2018a). The cingulum bundle: Anatomy, function, and dysfunction. *Neurosci. Biobehav. Rev.*, *92*, 104–127.

Bubb, E. J., Metzler-Baddeley, C., & Aggleton, J. P. (2018b). The cingulum bundle: Anatomy function, and dysfunction. *Neuroscience & Biobehavioral Reviews*, *92*, 104–127. https://doi.org/10.1016/j.neubiorev.2018.05.008

Buckner, R. L., Snyder, A. Z., Shannon, B. J., LaRossa, G., Sachs, R., Fotenos, A. F., Sheline, Y. I., Klunk, W. E., Mathis, C. A., Morris, J. C., & Mintun, M. A. (2005). Molecular, structural, and functional characterization of alzheimer's disease: Evidence for a relationship between default activity, amyloid, and memory. *The Journal of Neuroscience*, *25*(34), 7709–7717. https://doi.org/10.1523/jneurosci.2177-05.2005

Bullmore, E., & Sporns, O. (2009). Complex brain networks: Graph theoretical analysis of structural and functional systems. *Nature Reviews Neuroscience*, *10*(3), 186–198. https://doi.org/10.1038/nrn2575

Bullmore, E., Suckling, J., Overmeyer, S., Rabe-Hesketh, S., Taylor, E., & Brammer, M. (1999). Global, voxel, and cluster tests, by theory and permutation, for a difference between two groups of structural mr images of the brain. *IEEE Transactions on Medical Imaging*, *18*(1), 32–42. https://doi.org/10.1109/42.750253

Busche, M., & Konnerth, A. (2016). Impairments of neural circuit function in Alzheimer's disease. *Philos Trans R Soc Lond B Biol Sci*, *371*.

Busche, M., Wegmann, S., Dujardin, S., Commins, C., Schiantarelli, J., Klickstein, N., Kamath, T., Carlson, G., Nelken, I., & Hyman, B. (2019). Tau impairs neural circuits, dominating amyloid-β effects, in Alzheimer models in vivo. *Nat Neurosci*, *22*, 57–64.

Busche, M. A., Chen, X., Henning, H. A., Reichwald, J., Staufenbiel, M., Sakmann, B., & Konnerth, A. (2012). Critical role of soluble amyloid-β for early hippocampal hyperactivity in a mouse model of alzheimer's disease. *Proceedings of the National Academy of Sciences*, *109*(22), 8740–8745. https://doi.org/10.1073/pnas.1206171109

Busche, M. A., Eichhoff, G., Adelsberger, H., Abramowski, D., Wiederhold, K.-H., Haass, C., Staufenbiel, M., Konnerth, A., & Garaschuk, O. (2008). Clusters of hyperactive neurons near amyloid plaques in a mouse model of alzheimer's disease. *Science*, *321*(5896), 1686–1689. https://doi.org/10.1126/science.1162844

Busche, M. A., & Hyman, B. T. (2020). Synergy between amyloid-β and tau in Alzheimer's disease. *Nature Neuroscience*, *23*(10), 1183–1193. https://doi.org/10.1038/s41593-020-0687-6

Busche, M. A., Kekuš, M., Adelsberger, H., Noda, T., Förstl, H., Nelken, I., & Konnerth, A. (2015). Rescue of long-range circuit dysfunction in alzheimer's disease models. *Nature Neuroscience*, *18*(11), 1623–1630. https://doi.org/10.1038/nn.4137

Butz, M., & van, O. A. (2013). A simple rule for dendritic spine and axonal bouton formation can account for cortical reorganization after focal retinal lesions. *PLoS Comput Biol*, *9*, e1003259.

Buzsaaki, G., & Draguhn, A. (2004). Neuronal oscillations in cortical networks. *Science*, *304*(5679), 1926–1929. https://doi.org/10.1126/science.1099745

Buzsaki, G. (2006, August). *Rhythms of the brain*. Oxford University Press.

Buzsáki, G., & Tingley, D. (2018). Space and time: The hippocampus as a sequence generator. *Trends in Cognitive Sciences*, *22*(10), 853–869. https://doi.org/10.1016/j.tics.2018.07.006

Bystad, M., Grønli, O., Rasmussen, I. D., Gundersen, N., Nordvang, L., Wang-Iversen, H., & Aslaksen, P. M. (2016). Transcranial direct current stimulation as a memory enhancer in patients with alzheimer's disease: A randomized, placebo-controlled trial. *Alzheimer's Research & Therapy*, *8*(1). https://doi.org/10.1186/s13195-016-0180-3

Cabral, J., Hugues, E., Sporns, O., & Deco, G. (2011). Role of local network oscillations in resting-state functional connectivity. *Neuroimage*, *57*, 130–139.

Cabral, J., Luckhoo, H., Woolrich, M., Joensson, M., Mohseni, H., Baker, A., Kringelbach, M. L., & Deco, G. (2014). Exploring mechanisms of spontaneous functional connectivity in MEG: How delayed network interactions lead to structured amplitude envelopes of band-pass filtered oscillations. *Neuroimage*, *90*, 423–435.

Cabrera-Álvarez, J., Sánchez-Claros, J., Carrasco-Gómez, M., del Cerro-León, A., Gómez-Ariza, C. J., Maestú, F., Mirasso, C. R., & Susi, G. (2023). Understanding the effects of cortical gyrification in tacs: Insights from experiments and computational models. *Frontiers in Neuroscience*, *17*. https://doi.org/10.3389/fnins.2023.1223950

Canuet, L., Pusil, S., López, M. E., Bajo, R., Pineda-Pardo, J. Á., Cuesta, P., Gálvez, G., Gaztelu, J. M., Lourido, D., García-Ribas, G., & Maestú, F. (2015). Network disruption and cerebrospinal fluid amyloid-beta and phospho-tau levels in mild cognitive impairment. *J. Neurosci.*, *35*(28), 10325–10330.

Capilla, A., Arana, L., García-Huéscar, M., Melcón, M., Gross, J., & Campo, P. (2022). The natural frequencies of the resting human brain: An meg-based atlas. *NeuroImage*, *258*, 119373. https://doi.org/10.1016/j.neuroimage.2022.119373

Caporale, N., & Dan, Y. (2008). Spike timing-dependent plasticity: A hebbian learning rule. *Annu. Rev. Neurosci.*, *31*(1), 25–46.

Chan, M. M., Yau, S. S., & Han, Y. M. (2021). The neurobiology of prefrontal transcranial direct current stimulation (tdcs) in promoting brain plasticity: A systematic review and meta-analyses of human and rodent studies. *Neuroscience & Biobehavioral Reviews*, *125*, 392–416. https://doi.org/10.1016/j.neubiorev.2021.02.035

Chang, C.-H., Lane, H.-Y., & Lin, C.-H. (2018). Brain stimulation in alzheimer's disease. *Frontiers in Psychiatry*, *9*. https://doi.org/10.3389/fpsyt.2018.00201

Chen, G. F., Xu, T., Yan, Y., Zhou, Y., Jiang, Y., Melcher, K., & Xu, H. E. (2017). Amyloid beta: Structure, biology and structure-based therapeutic development. *Acta Pharmacologica Sinica*. https://doi.org/10.1038/aps.2017.28

Chen, Y., Wang, Y., Song, Z., Fan, Y., Gao, T., & Tang, X. (2023). Abnormal white matter changes in Alzheimer's disease based on diffusion tensor imaging: A systematic review. *Ageing Res Rev*, *87*, 101911.

Chertkow, H., & Bub, D. (1990). Semantic memory loss in dementia of alzheimer's type: What do various measures measure? *Brain*, *113*(2), 397–417. https://doi.org/10.1093/brain/113.2.397

Chilla, G. S., Tan, C. H., Xu, C., & Poh, C. L. (2015). Diffusion weighted magnetic resonance imaging and its recent trend-a survey. *Quant. Imaging Med. Surg.*, *5*(3), 407–422.

Christoff, K., Gordon, A. M., Smallwood, J., Smith, R., & Schooler, J. W. (2009). Experience sampling during fMRI reveals default network and executive system contributions to mind wandering. *Proceedings of the National Academy of Sciences*, *106*(21), 8719–8724. https://doi.org/10.1073/pnas.0900234106

Cirrito, J. R., Yamada, K. A., Finn, M. B., Sloviter, R. S., Bales, K. R., May, P. C., Schoepp, D. D., Paul, S. M., Mennerick, S., & Holtzman, D. M. (2005). Synaptic Activity Regulates Interstitial Fluid Amyloid-β Levels In Vivo. *Neuron*, *48*(6), 913–922. https://doi.org/10.1016/j.neuron.2005.10.028

Cocchi, L., Gollo, L., Zalesky, A., & Breakspear, M. (2017). Criticality in the brain: A synthesis of neurobiology, models and cognition. *Prog Neurobiol*, *158*, 132–152.

Cohen, J. R. (2018). The behavioral and cognitive relevance of time-varying, dynamic changes in functional connectivity. *NeuroImage*, *180*, 515–525. https://doi.org/10.1016/j.neuroimage.2017.09.036

Colclough, G., Woolrich, M., Tewarie, P., Brookes, M., Quinn, A., & Smith, S. (2016). How reliable are meg resting-state connectivity metrics? *NeuroImage*, *138*, 284–293. https://doi.org/10.1016/j.neuroimage.2016.05.070

Conti Filho, C. E., Loss, L. B., Marcolongo-Pereira, C., Rossoni Junior, J. V., Barcelos, R. M., Chiarelli-Neto, O., Silva, B. S. d., Passamani Ambrosio, R., Castro, F. C. d. A. Q., Teixeira, S. F., & Mezzomo, N. J. (2023). Advances in alzheimer's disease's pharmacological treatment. *Frontiers in Pharmacology*, *14*. https://doi.org/10.3389/fphar.2023.1101452

Cope, D. W., Di Giovanni, G., Fyson, S. J., Orbán, G., Errington, A. C., Lőrincz, M. L., Gould, T. M., Carter, D. A., & Crunelli, V. (2009). Enhanced tonic gabaa inhibition in typical absence epilepsy. *Nature Medicine*, *15*(12), 1392–1398. https://doi.org/10.1038/nm.2058

Cossart, R., Bernard, C., & Ben-Ari, Y. (2005). Multiple facets of gabaergic neurons and synapses: Multiple fates of gaba signalling in epilepsies. *Trends in Neurosciences*, *28*(2), 108–115. https://doi.org/10.1016/j.tins.2004.11.011

Costa-Klein, P., Ettinger, U., Schirner, M., Ritter, P., Falkai, P., Koutsouleris, N., & Kambeitz, J. (2020). Investigating the effect of the neuregulin-1 genotype on brain function using brain network simulations. *Biological Psychiatry*, *87*(9), S38. https://doi.org/10.1016/j.biopsych.2020.02.118

Cotelli, M., Manenti, R., Brambilla, M., Petesi, M., Rosini, S., Ferrari, C., Zanetti, O., & Miniussi, C. (2014). Anodal tdcs during face-name associations memory training in alzheimer's patients. *Frontiers in Aging Neuroscience*, *6*. https://doi.org/10.3389/fnagi.2014.00038

Courtiol, J., Guye, M., Bartolomei, F., Petkoski, S., & Jirsa, V. (2020). Dynamical Mechanisms of Interictal Resting-State Functional Connectivity in Epilepsy. *J Neurosci*, *40*, 5572–5588.

Cowan, N. (2001). The magical number 4 in short-term memory: A reconsideration of mental storage capacity. *Behavioral and Brain Sciences*, *24*(1), 87–114. https://doi.org/10.1017/s0140525x01003922

Cowan, N. (2010). The magical mystery four: How is working memory capacity limited, and why? *Current Directions in Psychological Science*, *19*(1), 51–57. https://doi.org/10.1177/0963721409359277

Cowan, N., Morey, C. C., Chen, Z., Gilchrist, A. L., & Saults, J. S. (2008). Theory and measurement of working memory capacity limits. In B. H. Ross (Ed.), *Advances in research and theory* (pp. 49–104, Vol. 49). Academic Press. https://doi.org/https://doi.org/10.1016/S0079-7421(08)00002-9

Crabtree, J. W. (2018). Functional Diversity of Thalamic Reticular Subnetworks. *Frontiers in Systems Neuroscience*, *12*. https://doi.org/10.3389/fnsys.2018.00041

Craik, F. I., & Lockhart, R. S. (1972). Levels of processing: A framework for memory research. *Journal of Verbal Learning and Verbal Behavior*, *11*(6), 671–684. https://doi.org/10.1016/s0022-5371(72)80001-x

Crunelli, V., & Hughes, S. W. (2010). The slow (<1 hz) rhythm of non-REM sleep: A dialogue between three cardinal oscillators. *Nat. Neurosci.*, *13*(1), 9–17.

Dada, J. O., & Mendes, P. (2011). Multi-scale modelling and simulation in systems biology. *Integrative Biology*, *3*(2), 86. https://doi.org/10.1039/c0ib00075b

Dai, Z., Lin, Q., Li, T., Wang, X., Yuan, H., Yu, X., He, Y., & Wang, H. (2019). Disrupted structural and functional brain networks in alzheimer's disease. *Neurobiology of Aging*, *75*, 71–82. https://doi.org/10.1016/j.neurobiolaging.2018.11.005

D'Amelio, M., Serra, L., & Bozzali, M. (2018). Ventral tegmental area in prodromal alzheimer's disease: Bridging the gap between mice and humans. *Journal of Alzheimer's Disease*, *63*(1), 181–183. https://doi.org/10.3233/jad-180094

Damoiseaux, J. S. (2012). Resting-state fmri as a biomarker for alzheimer's disease? *Alzheimer's Research & Therapy*, *4*(3), 8. https://doi.org/10.1186/alzrt106

Danet, L., Barbeau, E. J., Eustache, P., Planton, M., Raposo, N., Sibon, I., Albucher, J.-F., Bonneville, F., Peran, P., & Pariente, J. (2015). Thalamic amnesia after infarct: The role of the mammillothalamic tract and mediodorsal nucleus. *Neurology*, *85*(24), 2107–2115. https://doi.org/10.1212/wnl.0000000000002226

Dang, M., Chen, Q., Zhao, X., Chen, K., Li, X., Zhang, J., Lu, J., Ai, L., Chen, Y., & Zhang, Z. (2022). Tau as a biomarker of cognitive impairment and neuropsychiatric symptom in alzheimer's disease. *Human Brain Mapping*, *44*(2), 327–340. https://doi.org/10.1002/hbm.26043

D'Angelo, E., & Jirsa, V. (2022). The quest for multiscale brain modeling. *Trends in Neurosciences*, *45*(10), 777–790. https://doi.org/10.1016/j.tins.2022.06.007

da Silva, F. L. (2022). EEG: Origin and measurement. In C. Mulert & L. Lemieux (Eds.), *EEG - fMRI: Physiological basis, technique, and applications* (pp. 23–48). Springer International Publishing.

Datta, A., Truong, D., Minhas, P., Parra, L. C., & Bikson, M. (2012). Inter-Individual variation during transcranial direct current stimulation and normalization of dose using MRI-Derived computational models. *Front. Psychiatry*, *3*, 91.

David, O., & Friston, K. (2003). A neural mass model for MEG/EEG: coupling and neuronal dynamics. *Neuroimage*, *20*, 1743–55.

David, O., Harrison, L., & Friston, K. (2005). Modelling event-related responses in the brain. *Neuroimage*, *25*, 756–70.

Dayan, E., Censor, N., Buch, E. R., Sandrini, M., & Cohen, L. G. (2013). Noninvasive brain stimulation: From physiology to network dynamics and back. *Nat. Neurosci.*, *16*(7), 838–844.

De Marco, M., & Venneri, A. (2018). Volume and connectivity of the ventral tegmental area are linked to neurocognitive signatures of alzheimer's disease in humans. *Journal of Alzheimer's Disease*, *63*(1), 167–180. https://doi.org/10.3233/jad-171018

Deco, G., & Jirsa, V. (2012). Ongoing cortical activity at rest: criticality, multistability, and ghost attractors. *J Neurosci*, *32*, 3366–75.

Deco, G., Kringelbach, M., Jirsa, V., & Ritter, P. (2017). The dynamics of resting fluctuations in the brain: metastability and its dynamical cortical core. *Sci Rep*, *7*, 3095.

Deco, G., Cruzat, J., Cabral, J., Knudsen, G. M., Carhart-Harris, R. L., Whybrow, P. C., Logothetis, N. K., & Kringelbach, M. L. (2018). Whole-Brain Multimodal Neuroimaging Model Using Serotonin Receptor Maps Explains Non-linear Functional Effects of LSD. *Current Biology*, *28*(19), 3065–3074.e6. https://doi.org/10.1016/j.cub.2018.07.083

Deco, G., Cruzat, J., Cabral, J., Tagliazucchi, E., Laufs, H., Logothetis, N. K., & Kringelbach, M. L. (2019). Awakening: Predicting external stimulation to force transitions between different brain states. *Proc. Natl. Acad. Sci. U. S. A.*, *116*(36), 18088–18097.

Deco, G., Jirsa, V. K., Robinson, P. A., Breakspear, M., & Friston, K. (2008). The dynamic brain: From spiking neurons to neural masses and cortical fields (O. Sporns, Ed.). *PLoS Computational Biology*, *4*(8), e1000092. https://doi.org/10.1371/journal.pcbi.1000092

de Haan, W., Mott, K., van Straaten, E. C. W., Scheltens, P., & Stam, C. J. (2012). Activity dependent degeneration explains hub vulnerability in alzheimer's disease (O. Sporns, Ed.). *PLoS Computational Biology*, *8*(8), e1002582. https://doi.org/10.1371/journal.pcbi.1002582

de Haan, W., van Straaten, E. C. W., Gouw, A. A., & Stam, C. J. (2017). Altering neuronal excitability to preserve network connectivity in a computational model of alzheimer's disease (L. J. Graham, Ed.). *PLOS Computational Biology*, *13*(9), e1005707. https://doi.org/10.1371/journal.pcbi.1005707

Dehghani, N., & Wimmer, R. D. (2019). A Computational Perspective of the Role of the Thalamus in Cognition. *Neural Computation*, *31*(7), 1380–1418. https://doi.org/10.1162/neco_a_01197

de Jong, L. W., van der Hiele, K., Veer, I. M., Houwing, J. J., Westendorp, R. G. J., Bollen, E. L. E. M., de Bruin, P. W., Middelkoop, H. A. M., van Buchem, M. A., & van der Grond, J. (2008). Strongly reduced volumes of putamen and thalamus in alzheimer's disease: An mri study. *Brain*, *131*(12), 3277–3285. https://doi.org/10.1093/brain/awn278

Delbeuck, X. (2003). *Neuropsychology Review*, *13*(2), 79–92. https://doi.org/10.1023/a:1023832305702

Demirtaş, M., Falcon, C., Tucholka, A., Gispert, J., Molinuevo, J., & Deco, G. (2017). A whole-brain computational modeling approach to explain the alterations in resting-state functional connectivity during progression of Alzheimer's disease. *Neuroimage Clin*, *16*, 343–354.

Desikan, R., Ségonne, F., Fischl, B., Quinn, B., Dickerson, B., Blacker, D., Buckner, R., Dale, A., Maguire, R., Hyman, B., Albert, M., & Killiany, R. (2006). An automated labeling system for subdividing the human cerebral cortex on MRI scans into gyral based regions of interest. *Neuroimage*, *31*, 968–80.

Dewar, M., Alber, J., Butler, C., Cowan, N., & Della Sala, S. (2012). Brief wakeful resting boosts new memories over the long term. *Psychological Science*, *23*(9), 955–960. https://doi.org/10.1177/0956797612441220

Diekelmann, S., & Born, J. (2010). The memory function of sleep. *Nature Reviews Neuroscience*, *11*(2), 114–126. https://doi.org/10.1038/nrn2762

Dillen, K. N., Jacobs, H. I., Kukolja, J., Richter, N., von Reutern, B., Onur, Ö. A., Langen, K.-J., & Fink, G. R. (2017). Functional disintegration of the default mode network in prodromal alzheimer's disease (Y. Liu, Ed.). *Journal of Alzheimer's Disease*, *59*(1), 169–187. https://doi.org/10.3233/jad-161120

Dmochowski, J. P., Bikson, M., Datta, A., Richardson, J., Fridriksson, J., & Parra, L. C. (2012). On the role of electric field orientation in optimal design of transcranial current stimulation. *Conf. Proc. IEEE Eng. Med. Biol. Soc.*, *2012*, 6426–6429.

Dong, X., Yan, L., Huang, L., Guan, X., Dong, C., Tao, H., Wang, T., Qin, X., & Wan, Q. (2018). Repetitive transcranial magnetic stimulation for the treatment of alzheimer's disease: A systematic review and meta-analysis of randomized controlled trials (K. Chen, Ed.). *PLOS ONE*, *13*(10), e0205704. https://doi.org/10.1371/journal.pone.0205704

Dubois, B., & Albert, M. L. (2004). Amnestic mci or prodromal alzheimer's disease? *The Lancet Neurology*, *3*(4), 246–248. https://doi.org/10.1016/s1474-4422(04)00710-0

Dubois, B., Hampel, H., Feldman, H. H., Scheltens, P., Aisen, P., Andrieu, S., Bakardjian, H., Benali, H., Bertram, L., Blennow, K., Broich, K., Cavedo, E., Crutch, S., Dartigues, J.-F., Duyckaerts, C., Epelbaum, S., Frisoni, G. B., Gauthier, S., Genthon, R., … Jack, C. R. (2016). Preclinical alzheimer's disease: Definition, natural history, and diagnostic criteria. *Alzheimer's & Dementia*, *12*(3), 292–323. https://doi.org/10.1016/j.jalz.2016.02.002

Duquette, A., Pernègre, C., Veilleux Carpentier, A., & Leclerc, N. (2021). Similarities and differences in the pattern of tau hyperphosphorylation in physiological and pathological conditions: Impacts on the elaboration of therapies to prevent tau pathology. *Frontiers in Neurology*, *11*. https://doi.org/10.3389/fneur.2020.607680

Eichenbaum, H. (2000). A cortical–hippocampal system for declarative memory. *Nature Reviews Neuroscience*, *1*(1), 41–50. https://doi.org/10.1038/35036213

Eke, D. O., Bernard, A., Bjaalie, J. G., Chavarriaga, R., Hanakawa, T., Hannan, A. J., Hill, S. L., Martone, M. E., McMahon, A., Ruebel, O., Crook, S., Thiels, E., & Pestilli, F. (2022). International data governance for neuroscience. *Neuron*, *110*(4), 600–612. https://doi.org/10.1016/j.neuron.2021.11.017

El Houssaini, K., Bernard, C., & Jirsa, V. K. (2020). The epileptor model: A systematic mathematical analysis linked to the dynamics of seizures, refractory status epilepticus, and depolarization block. *eneuro*, *7*(2), ENEURO.0485–18.2019. https://doi.org/10.1523/eneuro.0485-18.2019

Eppler, J. M., Helias, M., Muller, E., Diesmann, M., & Gewaltig, M.-O. (2008). PyNEST: A convenient interface to the NEST simulator. *Front. Neuroinform.*, *2*, 12.

Falcon, M. I., Riley, J. D., Jirsa, V., McIntosh, A. R., Elinor Chen, E., & Solodkin, A. (2016). Functional mechanisms of recovery after chronic stroke: Modeling with the virtual brain. *eneuro*, *3*(2), ENEURO.0158–15.2016. https://doi.org/10.1523/eneuro.0158-15.2016

Falcon, M. I., Riley, J. D., Jirsa, V., McIntosh, A. R., Shereen, A. D., Chen, E. E., & Solodkin, A. (2015). The virtual brain: Modeling biological correlates of recovery after chronic stroke. *Frontiers in Neurology*, *6*. https://doi.org/10.3389/fneur.2015.00228

Fama, R., & Sullivan, E. V. (2015). Thalamic structures and associated cognitive functions: Relations with age and aging. *Neuroscience & Biobehavioral Reviews*, *54*, 29–37. https://doi.org/10.1016/j.neubiorev.2015.03.008

Fan, X., & Markram, H. (2019). A brief history of simulation neuroscience. *Frontiers in Neuroinformatics*, *13*. https://doi.org/10.3389/fninf.2019.00032

Favaretto, C., Allegra, M., Deco, G., Metcalf, N., Griffis, J., Shulman, G., Brovelli, A., & Corbetta, M. (2022). Subcortical-cortical dynamical states of the human brain and their breakdown in stroke. *Nat Commun*, *13*, 5069.

Ferguson, M. A., Lim, C., Cooke, D., Darby, R. R., Wu, O., Rost, N. S., Corbetta, M., Grafman, J., & Fox, M. D. (2019). A human memory circuit derived from brain lesions causing amnesia. *Nature Communications*, *10*(1). https://doi.org/10.1038/s41467-019-11353-z

Ferrucci, R., Mameli, F., Guidi, I., Mrakic-Sposta, S., Vergari, M., Marceglia, S., Cogiamanian, F., Barbieri, S., Scarpini, E., & Priori, A. (2008). Transcranial direct current stimulation improves recognition memory in alzheimer disease. *Neurology*, *71*(7), 493–498. https://doi.org/10.1212/01.wnl.0000317060.43722.a3

Festa, E. K., Insler, R. Z., Salmon, D. P., Paxton, J., Hamilton, J. M., & Heindel, W. C. (2005). Neocortical disconnectivity disrupts sensory integration in alzheimer's disease. *Neuropsychology*, *19*(6), 728–738. https://doi.org/10.1037/0894-4105.19.6.728

Fischl, B., Salat, D., Busa, E., Albert, M., Dieterich, M., Haselgrove, C., van der, d. K. A., Killiany, R., Kennedy, D., Klaveness, S., Montillo, A., Makris, N., Rosen, B., & Dale, A. (2002). Whole brain segmentation: automated labeling of neuroanatomical structures in the human brain. *Neuron*, *33*, 341–55.

Fjell, A. M., Sneve, M. H., Grydeland, H., Storsve, A. B., de Lange, A.-M. G., Amlien, I. K., Røgeberg, O. J., & Walhovd, K. B. (2015). Functional connectivity change across multiple cortical networks relates to episodic memory changes in aging. *Neurobiology of Aging*, *36*(12), 3255–3268. https://doi.org/10.1016/j.neurobiolaging.2015.08.020

Fogerson, P. M., & Huguenard, J. R. (2016). Tapping the Brakes: Cellular and Synaptic Mechanisms that Regulate Thalamic Oscillations. *Neuron*, *92*(4), 687–704. https://doi.org/10.1016/j.neuron.2016.10.024

Forno, G., Saranathan, M., Contador, J., Guillen, N., Falgàs, N., Tort-Merino, A., Balasa, M., Sanchez-Valle, R., Hornberger, M., & Lladó, A. (2023). Thalamic nuclei changes in early and late onset alzheimer's disease. *Current Research in Neurobiology*, *4*, 100084. https://doi.org/10.1016/j.crneur.2023.100084

Forssell, M., Goswami, C., Krishnan, A., Chamanzar, M., & Grover, P. (2021). Effect of skull thickness and conductivity on current propagation for noninvasively injected currents. *J. Neural Eng.*, *18*(4).

Franzmeier, N., Brendel, M., Beyer, L., Slemann, L., Kovacs, G. G., Arzberger, T., Kurz, C., Respondek, G., Lukic, M. J., Biel, D., Rubinski, A., Frontzkowski, L., Hummel, S., Müller, A., Finze, A., Palleis, C., Joseph, E., Weidinger, E., Katzdobler, S., ... Ewers, M. (2022). Tau deposition patterns are associated with functional connectivity in primary tauopathies. *Nature Communications*, *13*(1). https://doi.org/10.1038/s41467-022-28896-3

Franzmeier, N., Dewenter, A., Frontzkowski, L., Dichgans, M., Rubinski, A., Neitzel, J., Smith, R., Strandberg, O., Ossenkoppele, R., Buerger, K., Duering, M., Hansson, O., & Ewers, M. (2020). Patient-centered connectivity-based prediction of tau pathology spread in alzheimer's disease. *Science Advances*, *6*(48). https://doi.org/10.1126/sciadv.abd1327

Fred, A. L., Kumar, S. N., Kumar Haridhas, A., Ghosh, S., Purushothaman Bhuvana, H., Sim, W. K. J., Vimalan, V., Givo, F. A. S., Jousmäki, V., Padmanabhan, P., & Gulyás, B. (2022). A brief introduction to magnetoencephalography (meg) and its clinical applications. *Brain Sciences*, *12*(6), 788. https://doi.org/10.3390/brainsci12060788

Friston, K. (2002). Beyond phrenology: What can neuroimaging tell us about distributed circuitry? *Annual Review of Neuroscience*, *25*(1), 221–250. https://doi.org/10.1146/annurev.neuro.25.112701.142846

Friston, K. J. (1994). Functional and effective connectivity in neuroimaging: A synthesis. *Human Brain Mapping*, *2*(1-2), 56–78. https://doi.org/10.1002/hbm.460020107

Friston, K. J. (2011). Functional and Effective Connectivity: A Review. *Brain Connectivity*, *1*(1), 13–36. https://doi.org/10.1089/brain.2011.0008

Frost, B., & Diamond, M. I. (2009). Prion-like mechanisms in neurodegenerative diseases. *Nature Reviews Neuroscience*, *11*(3), 155–159. https://doi.org/10.1038/nrn2786

Fuentealba, P., & Steriade, M. (2005). The reticular nucleus revisited: Intrinsic and network properties of a thalamic pacemaker. *Progress in Neurobiology*, *75*(2), 125–141. https://doi.org/10.1016/j.pneurobio.2005.01.002

Gallagher, R., & Appenzeller, T. (1999). Beyond reductionism. *Science*, *284*(5411), 79–79. https://doi.org/10.1126/science.284.5411.79

Garcés, P., Ángel Pineda-Pardo, J., Canuet, L., Aurtenetxe, S., López, M. E., Marcos, A., Yus, M., Llanero-Luque, M., del-Pozo, F., Sancho, M., & Maestú, F. (2014). The default mode network is functionally and structurally disrupted in amnestic mild cognitive impairment — a bimodal meg–dti study. *NeuroImage: Clinical*, *6*, 214–221. https://doi.org/10.1016/j.nicl.2014.09.004

Garcés, P., López-Sanz, D., Maestú, F., & Pereda, E. (2017). Choice of magnetometers and gradiometers after signal space separation. *Sensors*, *17*(12).

Garcés, P., Vicente, R., Wibral, M., Pineda-Pardo, J. Á., López, M. E., Aurtenetxe, S., Marcos, A., de Andrés, M. E., Yus, M., Sancho, M., Maestú, F., & Fernández, A. (2013). Brain-wide slowing of spontaneous alpha rhythms in mild cognitive impairment. *Frontiers in Aging Neuroscience*, *5*. https://doi.org/10.3389/fnagi.2013.00100

Garcia-Marin, V. (2009). Diminished perisomatic GABAergic terminals on cortical neurons adjacent to amyloid plaques. *Frontiers in Neuroanatomy*, *3*. https://doi.org/10.3389/neuro.05.028.2009

Garcia-Rill, E. (2009). Reticular Activating System. In *Encyclopedia of neuroscience* (pp. 137–143). Elsevier. https://doi.org/10.1016/b978-008045046-9.01767-8

Garzón, D. N., Castillo, Y., Navas-Zuloaga, M. G., Darwin, L., Hardin, A., Culik, N., Yang, A., Castillo-Garsow, C., Ríos-Soto, K., Arriola, L., & Ghosh, A. (2021). Dynamics of prion proliferation under combined treatment of pharmacological chaperones and interferons. *Journal of Theoretical Biology*, *527*, 110797. https://doi.org/10.1016/j.jtbi.2021.110797

Gewaltig, M. O., & Diesmann, M. (2007). Nest (neural simulation tool). *Scholarpedia J.*

Giannakakis, E., Hutchings, F., Papasavvas, C., Han, C., Weber, B., Zhang, C., & Kaiser, M. (2020). Computational modelling of the long-term effects of brain stimulation on the local and global structural connectivity of epileptic patients. *PLoS One*, *15*, e0221380.

Glasser, M. F., Coalson, T. S., Robinson, E. C., Hacker, C. D., Harwell, J., Yacoub, E., Ugurbil, K., Andersson, J., Beckmann, C. F., Jenkinson, M., Smith, S. M., & Van Essen, D. C. (2016). A multi-modal parcellation of human cerebral cortex. *Nature*, *536*(7615), 171–178. https://doi.org/10.1038/nature18933

Goldstone, A., Mayhew, S. D., Hale, J. R., Wilson, R. S., & Bagshaw, A. P. (2018). Thalamic functional connectivity and its association with behavioral performance in older age. *Brain and Behavior*, *8*(4), e00943. https://doi.org/10.1002/brb3.943

Gollo, L., Mirasso, C., Sporns, O., & Breakspear, M. (2014). Mechanisms of zero-lag synchronization in cortical motifs. *PLoS Comput Biol*, *10*, e1003548.

Golob, E. J., Miranda, G. G., Johnson, J. K., & Starr, A. (2001). Sensory cortical interactions in aging, mild cognitive impairment, and alzheimer's disease. *Neurobiology of Aging*, *22*(5), 755–763. https://doi.org/10.1016/s0197-4580(01)00244-5

Gomez-Gutierrez, R., & Morales, R. (2020). The prion-like phenomenon in Alzheimer's disease: Evidence of pathology transmission in humans (S. Gilch, Ed.). *PLOS Pathogens*, *16*(10), e1009004. https://doi.org/10.1371/journal.ppat.1009004

Gómez-Isla, T., Hollister, R., West, H., Mui, S., Growdon, J. H., Petersen, R. C., Parisi, J. E., & Hyman, B. T. (1997). Neuronal loss correlates with but exceeds neurofibrillary tangles in alzheimer's disease. *Annals of Neurology*, *41*(1), 17–24. https://doi.org/10.1002/ana.410410106

Gong, C.-X., Dai, C.-L., Liu, F., & Iqbal, K. (2022). Multi-targets: An unconventional drug development strategy for alzheimer's disease. *Frontiers in Aging Neuroscience*, *14*. https://doi.org/10.3389/fnagi.2022.837649

Gonzalez-Castillo, J., Hoy, C. W., Handwerker, D. A., Robinson, M. E., Buchanan, L. C., Saad, Z. S., & Bandettini, P. A. (2015). Tracking ongoing cognition in individuals using brief, whole-brain functional connectivity patterns. *Proceedings of the National Academy of Sciences*, *112*(28), 8762–8767. https://doi.org/10.1073/pnas.1501242112

Gregory, S., Saunders, S., & Ritchie, C. W. (2022). Science disconnected: The translational gap between basic science, clinical trials, and patient care in alzheimer's disease. *The Lancet Healthy Longevity*, *3*(11), e797–e803. https://doi.org/10.1016/s2666-7568(22)00219-7

Greicius, M. D., Srivastava, G., Reiss, A. L., & Menon, V. (2004). Default-mode network activity distinguishes alzheimer's disease from healthy aging: Evidence from functional mri. *Proceedings of the National Academy of Sciences*, *101*(13), 4637–4642. https://doi.org/10.1073/pnas.0308627101

Grieder, M., Wang, D. J. J., Dierks, T., Wahlund, L.-O., & Jann, K. (2018). Default mode network complexity and cognitive decline in mild alzheimer's disease. *Frontiers in Neuroscience*, *12*. https://doi.org/10.3389/fnins.2018.00770

Grier, M. D., Zimmermann, J., & Heilbronner, S. R. (2020). Estimating brain connectivity with diffusion-weighted magnetic resonance imaging: Promise and peril. *Biological Psychiatry: Cognitive Neuroscience and Neuroimaging*, *5*(9), 846–854. https://doi.org/10.1016/j.bpsc.2020.04.009

Grimbert, F., & Faugeras, O. (2006). Bifurcation analysis of Jansen's neural mass model. *Neural Comput*, *18*, 3052–68. https://doi.org/10.1162/neco.2006.18.12.3052

Grover, V. P., Tognarelli, J. M., Crossey, M. M., Cox, I. J., Taylor-Robinson, S. D., & McPhail, M. J. (2015). Magnetic resonance imaging: Principles and techniques: Lessons for clinicians. *Journal of Clinical and Experimental Hepatology*, *5*(3), 246–255. https://doi.org/10.1016/j.jceh.2015.08.001

Guerra, A., López-Alonso, V., Cheeran, B., & Suppa, A. (2020). Variability in non-invasive brain stimulation studies: Reasons and results. *Neurosci. Lett.*, *719*, 133330.

Guillery, R., & Sherman, S. (2002). Thalamic Relay Functions and Their Role in Corticocortical Communication. *Neuron*, *33*(2), 163–175. https://doi.org/10.1016/s0896-6273(01)00582-7

Guo, T., Noble, W., & Hanger, D. P. (2017). Roles of tau protein in health and disease. *Acta Neuropathologica*, *133*(5), 665–704. https://doi.org/10.1007/s00401-017-1707-9

Gutierrez, C. E., Skibbe, H., Nakae, K., Tsukada, H., Lienard, J., Watakabe, A., Hata, J., Reisert, M., Woodward, A., Yamaguchi, Y., Yamamori, T., Okano, H., Ishii, S., & Doya, K. (2020). Optimization and validation of diffusion mri-based fiber tracking with neural tracer data as a reference. *Scientific Reports*, *10*(1). https://doi.org/10.1038/s41598-020-78284-4

Haass, C., & Selkoe, D. (2007). Soluble protein oligomers in neurodegeneration: lessons from the Alzheimer's amyloid beta-peptide. *Nat Rev Mol Cell Biol*, *8*, 101–12.

Hafkemeijer, A., Altmann-Schneider, I., Oleksik, A., van de, d. W. L., Middelkoop, H., van, B. M., van der, d. G. J., & Rombouts, S. (2013). Increased functional connectivity and brain atrophy in elderly with subjective memory complaints. *Brain Connect*, *3*, 353–62.

Halassa, M., & Sherman, S. (2019). Thalamocortical Circuit Motifs: A General Framework. *Neuron*, *103*, 762–770.

Hämäläinen, M. S., & Ilmoniemi, R. J. (1994). Interpreting magnetic fields of the brain: Minimum norm estimates. *Med. Biol. Eng. Comput.*, *32*(1), 35–42.

Hämäläinen, M., Hari, R., Ilmoniemi, R. J., Knuutila, J., & Lounasmaa, O. V. (1993). Magnetoencephalography—theory, instrumentation, and applications to noninvasive studies of the working human brain. *Rev. Mod. Phys.*, *65*(2), 413–497.

Hämäläinen, M., & Ilmoniemi, R. (1994). Interpreting magnetic fields of the brain: minimum norm estimates. *Med Biol Eng Comput*, *32*, 35–42.

Hansen, P., Kringelbach, M., & Salmelin, R. (2010, July). *MEG: An introduction to methods*. Oxford University Press.

Hausman, H. K., O'Shea, A., Kraft, J. N., Boutzoukas, E. M., Evangelista, N. D., Etten, E. J. V., Bharadwaj, P. K., Smith, S. G., Porges, E., Hishaw, G. A., Wu, S., DeKosky, S., Alexander, G. E., Marsiske, M., Cohen, R., & Woods, A. J. (2020). The Role of Resting-State Network Functional Connectivity in Cognitive Aging. *Frontiers in Aging Neuroscience*, *12*. https://doi.org/10.3389/fnagi.2020.00177

Hayne, H., & Herbert, J. (2004). Verbal cues facilitate memory retrieval during infancy. *Journal of Experimental Child Psychology*, *89*(2), 127–139. https://doi.org/10.1016/j.jecp.2004.06.002

Hebb, D. (1949). *The organization of behavior. a neuropsychological theory*. Wiley & Sons.

Helfrich, R. F., Schneider, T. R., Rach, S., Trautmann-Lengsfeld, S. A., Engel, A. K., & Herrmann, C. S. (2014). Entrainment of brain oscillations by transcranial alternating current stimulation. *Curr. Biol.*, *24*(3), 333–339.

Heneka, M. T., Carson, M. J., Khoury, J. E., Landreth, G. E., Brosseron, F., Feinstein, D. L., Jacobs, A. H., Wyss-Coray, T., Vitorica, J., Ransohoff, R. M., Herrup, K., Frautschy, S. A., Finsen, B., Brown, G. C., Verkhratsky, A., Yamanaka, K., Koistinaho, J., Latz, E., Halle, A., … Kummer, M. P. (2015). Neuroinflammation in Alzheimer's disease. *The Lancet Neurology*, *14*(4), 388–405. https://doi.org/10.1016/s1474-4422(15)70016-5

Henstridge, C., Hyman, B., & Spires-Jones, T. (2019). Beyond the neuron-cellular interactions early in Alzheimer disease pathogenesis. *Nat Rev Neurosci*, *20*, 94–108.

Herrmann, C. S., Rach, S., Neuling, T., & Strüber, D. (2013). Transcranial alternating current stimulation: A review of the underlying mechanisms and modulation of cognitive processes. *Front. Hum. Neurosci.*, *7*, 279.

Herrmann, C. S., Strüber, D., Helfrich, R. F., & Engel, A. K. (2016). Eeg oscillations: From correlation to causality. *International Journal of Psychophysiology*, *103*, 12–21. https://doi.org/10.1016/j.ijpsycho.2015.02.003

Holdefer, R. N., Sadleir, R., & Russell, M. J. (2006). Predicted current densities in the brain during transcranial electrical stimulation. *Clin. Neurophysiol.*, *117*(6), 1388–1397.

Holm, S. (1979). A simple sequentially rejective multiple test procedure. *Scand. Stat. Theory Appl.*, *6*(2), 65–70.

Holtzman, D. M., Morris, J. C., & Goate, A. M. (2011). Alzheimer's disease: The challenge of the second century. *Science Translational Medicine*, *3*(77). https://doi.org/10.1126/scitranslmed.3002369

Honey, C. J., Sporns, O., Cammoun, L., Gigandet, X., Thiran, J. P., Meuli, R., & Hagmann, P. (2009). Predicting human resting-state functional connectivity from structural connectivity. *Proceedings of the National Academy of Sciences*, *106*(6), 2035–2040. https://doi.org/10.1073/pnas.0811168106

Huang, C.-C., Rolls, E. T., Feng, J., & Lin, C.-P. (2021). An extended human connectome project multimodal parcellation atlas of the human cortex and subcortical areas. *Brain Structure and Function*, *227*(3), 763–778. https://doi.org/10.1007/s00429-021-02421-6

Huang, M., Mosher, J., & Leahy, R. (1999). A sensor-weighted overlapping-sphere head model and exhaustive head model comparison for MEG. *Phys Med Biol*, *44*, 423–40.

Huang, Y., Datta, A., Bikson, M., & Parra, L. C. (2018). ROAST: An Open-Source, Fully-Automated, realistic Volumetric-Approach-Based simulator for TES. *Conf. Proc. IEEE Eng. Med. Biol. Soc.*, *2018*, 3072–3075.

Huang, Y., Datta, A., Bikson, M., & Parra, L. C. (2019). Realistic volumetric-approach to simulate transcranial electric stimulation—roast—a fully automated open-source pipeline. *Journal of Neural Engineering*, *16*(5), 056006. https://doi.org/10.1088/1741-2552/ab208d

Huang, Y., Dmochowski, J. P., Su, Y., Datta, A., Rorden, C., & Parra, L. C. (2013). Automated mri segmentation for individualized modeling of current flow in the human head. *Journal of neural engineering*, *10*(6), 066004.

Huang, Y., Liu, A. A., Lafon, B., Friedman, D., Dayan, M., Wang, X., Bikson, M., Doyle, W. K., Devinsky, O., & Parra, L. C. (2017). Measurements and models of electric fields in the in vivo human brain during transcranial electric stimulation. *Elife*, *6*.

Huguenard, J., & McCormick, D. (2007). Thalamic synchrony and dynamic regulation of global forebrain oscillations. *Trends Neurosci*, *30*, 350–6.

Humiston, G. B., Tucker, M. A., Summer, T., & Wamsley, E. J. (2019). Resting states and memory consolidation: A preregistered replication and meta-analysis. *Scientific Reports*, *9*(1). https://doi.org/10.1038/s41598-019-56033-6

Huntley, J. D., & Howard, R. J. (2009). Working memory in early alzheimer's disease: A neuropsychological review. *International Journal of Geriatric Psychiatry*, *25*(2), 121–132. https://doi.org/10.1002/gps.2314

Huo, L., Li, R., Wang, P., Zheng, Z., & Li, J. (2018). The default mode network supports episodic memory in cognitively unimpaired elderly individuals: Different contributions to immediate recall and delayed recall. *Frontiers in Aging Neuroscience*, *10*. https://doi.org/10.3389/fnagi.2018.00006

Hutchison, R. M., Womelsdorf, T., Allen, E. A., Bandettini, P. A., Calhoun, V. D., Corbetta, M., Penna, S. D., Duyn, J. H., Glover, G. H., Gonzalez-Castillo, J., Handwerker, D. A., Keilholz, S., Kiviniemi, V., Leopold, D. A., de Pasquale, F., Sporns, O., Walter, M., & Chang, C. (2013). Dynamic functional connectivity: Promise, issues, and interpretations. *NeuroImage*, *80*, 360–378. https://doi.org/10.1016/j.neuroimage.2013.05.079

Hwang, K., Bertolero, M. A., Liu, W. B., & D'Esposito, M. (2017). The Human Thalamus Is an Integrative Hub for Functional Brain Networks. *The Journal of Neuroscience*, *37*(23), 5594–5607. https://doi.org/10.1523/jneurosci.0067-17.2017

Iaccarino, H. F., Singer, A. C., Martorell, A. J., Rudenko, A., Gao, F., Gillingham, T. Z., Mathys, H., Seo, J., Kritskiy, O., Abdurrob, F., Adaikkan, C., Canter, R. G., Rueda, R., Brown, E. N., Boyden, E. S., & Tsai, L.-H. (2016). Gamma frequency entrainment attenuates amyloid load and modifies microglia. *Nature*, *540*(7632), 230–235. https://doi.org/10.1038/nature20587

Ingala, S., Tomassen, J., Collij, L. E., Prent, N., van 't Ent, D., ten Kate, M., Konijnenberg, E., Yaqub, M., Scheltens, P., de Geus, E. J. C., Teunissen, C. E., Tijms, B., Wink, A. M., Barkhof, F., van Berckel, B. N. M., Visser, P. J., & den Braber, A. (2021). Amyloid-driven disruption of default mode network connectivity in cognitively healthy individuals. *Brain Communications*, *3*(4). https://doi.org/10.1093/braincomms/fcab201

Insel, T. R., Landis, S. C., & Collins, F. S. (2013). The nih brain initiative. *Science*, *340*(6133), 687–688. https://doi.org/10.1126/science.1239276

Ippolito, G., Bertaccini, R., Tarasi, L., Di Gregorio, F., Trajkovic, J., Battaglia, S., & Romei, V. (2022). The role of alpha oscillations among the main neuropsychiatric disorders in the adult and developing human brain: Evidence from the last 10 years of research. *Biomedicines*, *10*(12).

Iqbal, K., Liu, F., Gong, C.-X., & Grundke-Iqbal, I. (2010). Tau in alzheimer disease and related tauopathies. *Current Alzheimer Research*, *7*(8), 656–664. https://doi.org/10.2174/156720510793611592

Irwin, M. R., & Vitiello, M. V. (2019). Implications of sleep disturbance and inflammation for alzheimer's disease dementia. *Lancet Neurol.*, *18*(3), 296–306.

Iturria-Medina, Y., Canales-Rodríguez, E., Melie-García, L., Valdés-Hernández, P., Martínez-Montes, E., Alemán-Gómez, Y., & Sánchez-Bornot, J. (2007). Characterizing brain anatomical connections using diffusion weighted MRI and graph theory. *Neuroimage*, *36*, 645–60.

Jack, C. R., Knopman, D. S., Jagust, W. J., Petersen, R. C., Weiner, M. W., Aisen, P. S., Shaw, L. M., Vemuri, P., Wiste, H. J., Weigand, S. D., Lesnick, T. G., Pankratz, V. S., Donohue, M. C., & Trojanowski, J. Q. (2013). Tracking pathophysiological processes in alzheimer's disease: An updated hypothetical model of dynamic biomarkers. *The Lancet Neurology*, *12*(2), 207–216. https://doi.org/10.1016/s1474-4422(12)70291-0

Jahn, H. (2013). Memory loss in alzheimer's disease. *Dialogues in Clinical Neuroscience*, *15*(4), 445–454. https://doi.org/10.31887/dcns.2013.15.4/hjahn

Jan, J., Reiter, R., Wasdell, M., & Bax, M. (2009). The role of the thalamus in sleep, pineal melatonin production, and circadian rhythm sleep disorders. *J Pineal Res*, *46*, 1–7.

Jansen, B., & Rit, V. (1995). Electroencephalogram and visual evoked potential generation in a mathematical model of coupled cortical columns. *Biol Cybern*, *73*, 357–66.

Jeong, W.-H., Kim, W.-I., Lee, J.-W., Park, H.-K., Song, M.-K., Choi, I.-S., & Han, J.-Y. (2021). Modulation of Long-Term potentiation by gamma frequency transcranial alternating current stimulation in transgenic mouse models of alzheimer's disease. *Brain Sci*, *11*(11).

Jeremic, D., Jiménez-Díaz, L., & Navarro-López, J. D. (2021). Past, present and future of therapeutic strategies against amyloid-β peptides in alzheimer's disease: A systematic review. *Ageing Research Reviews*, *72*, 101496. https://doi.org/10.1016/j.arr.2021.101496

Jeurissen, B., Descoteaux, M., Mori, S., & Leemans, A. (2017). Diffusion mri fiber tractography of the brain. *NMR in Biomedicine*, *32*(4). https://doi.org/10.1002/nbm.3785

Jin, Y., Yang, H., Zhang, F., Wang, J., Liu, H., Yang, X., Long, H., Li, F., Gong, Q., & Lai, W. (2020). The Medial Thalamus Plays an Important Role in the Cognitive and Emotional Modulation of Orofacial Pain: A Functional Magnetic Resonance Imaging-Based Study. *Front Neurol*, *11*, 589125.

Jirsa, V., Wang, H., Triebkorn, P., Hashemi, M., Jha, J., Gonzalez-Martinez, J., Guye, M., Makhalova, J., & Bartolomei, F. (2023). Personalised virtual brain models in epilepsy. *The Lancet Neurology*, *22*(5), 443–454. https://doi.org/10.1016/s1474-4422(23)00008-x

Jirsa, V., Proix, T., Perdikis, D., Woodman, M., Wang, H., Gonzalez-Martinez, J., Bernard, C., Bénar, C., Guye, M., Chauvel, P., & Bartolomei, F. (2017). The virtual epileptic patient: Individualized whole-brain models of epilepsy spread. *NeuroImage*, *145*, 377–388. https://doi.org/10.1016/j.neuroimage.2016.04.049

Jiruska, P., de Curtis, M., Jefferys, J. G. R., Schevon, C. A., Schiff, S. J., & Schindler, K. (2013). Synchronization and desynchronization in epilepsy: controversies and hypotheses. *The Journal of Physiology*, *591*(4), 787–797. https://doi.org/10.1113/jphysiol.2012.239590

Johnson, K. A., Duffley, G., Anderson, D. N., Ostrem, J. L., Welter, M.-L., Baldermann, J. C., Kuhn, J., Huys, D., Visser-Vandewalle, V., Foltynie, T., Zrinzo, L., Hariz, M., Leentjens, A. F. G., Mogilner, A. Y., Pourfar, M. H., Almeida, L., Gunduz, A., Foote, K. D., Okun, M. S., & Butson, C. R. (2020). Structural connectivity predicts clinical outcomes of deep brain stimulation for tourette syndrome. *Brain*, *143*(8), 2607–2623. https://doi.org/10.1093/brain/awaa188

Jones, D. T., Knopman, D. S., Gunter, J. L., Graff-Radford, J., Vemuri, P., Boeve, B. F., Petersen, R. C., Weiner, M. W., & Jack, C. R. (2015). Cascading network failure across the alzheimer's disease spectrum. *Brain*, *139*(2), 547–562. https://doi.org/10.1093/brain/awv338

Jones, D., Machulda, M., Vemuri, P., McDade, E., Zeng, G., Senjem, M., Gunter, J., Przybelski, S., Avula, R., Knopman, D., Boeve, B., Petersen, R., & Jack, C. (2011). Age-related changes in the default mode network are more advanced in alzheimer disease. *Neurology*, *77*(16), 1524–1531. https://doi.org/10.1212/wnl.0b013e318233b33d

Jones, E. G. (1985). Principles of Thalamic Organization. In *The thalamus* (pp. 85–149). Springer US. https://doi.org/10.1007/978-1-4615-1749-8_3

Jones, S. R. (2016). When brain rhythms aren't 'rhythmic': Implication for their mechanisms and meaning. *Current Opinion in Neurobiology*, *40*, 72–80. https://doi.org/10.1016/j.conb.2016.06.010

Josselyn, S. A., Köhler, S., & Frankland, P. W. (2015). Finding the engram. *Nature Reviews Neuroscience*, *16*(9), 521–534. https://doi.org/10.1038/nrn4000

Jucker, M., & Walker, L. C. (2018). Propagation and spread of pathogenic protein assemblies in neurodegenerative diseases. *Nature Neuroscience*, *21*(10), 1341–1349. https://doi.org/10.1038/s41593-018-0238-6

Kabakov, A. Y., Muller, P. A., Pascual-Leone, A., Jensen, F. E., & Rotenberg, A. (2012). Contribution of axonal orientation to pathway-dependent modulation of excitatory transmission by direct current stimulation in isolated rat hippocampus. *J. Neurophysiol.*, *107*(7), 1881–1889.

Kaefer, K., Stella, F., McNaughton, B. L., & Battaglia, F. P. (2022). Replay, the default mode network and the cascaded memory systems model. *Nature Reviews Neuroscience*, *23*(10), 628–640. https://doi.org/10.1038/s41583-022-00620-6

Kaila, K., Ruusuvuori, E., Seja, P., Voipio, J., & Puskarjov, M. (2014). Gaba actions and ionic plasticity in epilepsy. *Current Opinion in Neurobiology*, *26*, 34–41. https://doi.org/10.1016/j.conb.2013.11.004

Kamenetz, F., Tomita, T., Hsieh, H., Seabrook, G., Borchelt, D., Iwatsubo, T., Sisodia, S., & Malinow, R. (2003). APP Processing and Synaptic Function. *Neuron*, *37*(6), 925–937. https://doi.org/10.1016/s0896-6273(03)00124-7

Kasten, F. H., Dowsett, J., & Herrmann, C. S. (2016). Sustained aftereffect of α-tacs lasts up to 70 min after stimulation. *Frontiers in Human Neuroscience*, *10*. https://doi.org/10.3389/fnhum.2016.00245

Kasten, F. H., Duecker, K., Maack, M. C., Meiser, A., & Herrmann, C. S. (2019). Integrating electric field modeling and neuroimaging to explain inter-individual variability of tACS effects. *Nat. Commun.*, *10*(1), 5427.

Kasten, F. H., & Herrmann, C. S. (2022). The hidden brain-state dynamics of tacs aftereffects. *NeuroImage*, *264*, 119713. https://doi.org/10.1016/j.neuroimage.2022.119713

Kato, N. (1990). Cortico-thalamo-cortical projection between visual cortices. *Brain Res*, *509*, 150–2.

Kazemi, S., & Jamali, Y. (2022). Phase synchronization and measure of criticality in a network of neural mass models. *Scientific reports*, *12*(1), 1319.

Kazim, S., Seo, J., Bianchi, R., Larson, C., Sharma, A., Wong, R., Gorbachev, K., & Pereira, A. (2021). Neuronal Network Excitability in Alzheimer's Disease: The Puzzle of Similar versus Divergent Roles of Amyloid β and Tau. *eNeuro*, *8*.

Kehler, L., Francisco, C. O., Uehara, M. A., & Moussavi, Z. (2020). The effect of transcranial alternating current stimulation (tacs) on cognitive function in older adults with dementia. *2020 42nd Annual International Conference of the IEEE Engineering in Medicine & Biology Society (EMBC)*. https://doi.org/10.1109/embc44109.2020.9175903

Kelly, S. C., He, B., Perez, S. E., Ginsberg, S. D., Mufson, E. J., & Counts, S. E. (2017). Locus coeruleus cellular and molecular pathology during the progression of alzheimer's disease. *Acta Neuropathologica Communications*, *5*(1). https://doi.org/10.1186/s40478-017-0411-2

Khedr, E. M., Gamal, N. F. E., El-Fetoh, N. A., Khalifa, H., Ahmed, E. M., Ali, A. M., Noaman, M., El-Baki, A. A., & Karim, A. A. (2014). A double-blind randomized clinical trial on the efficacy of cortical direct current stimulation for the treatment of alzheimerâ€™s disease. *Frontiers in Aging Neuroscience*, *6*. https://doi.org/10.3389/fnagi.2014.00275

Kiebel, S., Garrido, M., Moran, R., & Friston, K. (2008). Dynamic causal modelling for EEG and MEG. *Cogn Neurodyn*, *2*, 121–36.

Kirwan, C. B., Bayley, P. J., Galván, V. V., & Squire, L. R. (2008). Detailed recollection of remote autobiographical memory after damage to the medial temporal lobe. *Proceedings of the National Academy of Sciences*, *105*(7), 2676–2680. https://doi.org/10.1073/pnas.0712155105

Kitamura, T., Ogawa, S. K., Roy, D. S., Okuyama, T., Morrissey, M. D., Smith, L. M., Redondo, R. L., & Tonegawa, S. (2017). Engrams and circuits crucial for systems consolidation of a memory. *Science*, *356*(6333), 73–78. https://doi.org/10.1126/science.aam6808

Kizilirmak, J. M., Soch, J., Schütze, H., Düzel, E., Feldhoff, H., Fischer, L., Knopf, L., Maass, A., Raschick, M., Schult, A., Yakupov, R., Richter, A., & Schott, B. H. (2023). The relationship between resting-state amplitude fluctuations and memory-related deactivations of the default mode network in young and older adults. *Human Brain Mapping*, *44*(9), 3586–3609. https://doi.org/10.1002/hbm.26299

Klink, K., Peter, J., Wyss, P., & Klöppel, S. (2020). Transcranial electric current stimulation during associative memory encoding: Comparing tACS and tDCS effects in healthy aging. *Front. Aging Neurosci.*, *12*, 66.

Knight, R. G. (1998). Controlled and automatic memory process in alzheimer's disease. *Cortex*, *34*(3), 427–435. https://doi.org/10.1016/s0010-9452(08)70765-2

Knoflach, F., Hernandez, M.-C., & Bertrand, D. (2016). Gabaa receptor-mediated neurotransmission: Not so simple after all. *Biochemical Pharmacology*, *115*, 10–17. https://doi.org/10.1016/j.bcp.2016.03.014

Knopman, D. S., Amieva, H., Petersen, R. C., Chételat, G., Holtzman, D. M., Hyman, B. T., Nixon, R. A., & Jones, D. T. (2021). Alzheimer disease. *Nature Reviews Disease Primers*, *7*(1). https://doi.org/10.1038/s41572-021-00269-y

Koch, G., Casula, E. P., Bonnì, S., Borghi, I., Assogna, M., Minei, M., Pellicciari, M. C., Motta, C., D'Acunto, A., Porrazzini, F., Maiella, M., Ferrari, C., Caltagirone, C., Santarnecchi, E., Bozzali, M., & Martorana, A. (2022). Precuneus magnetic stimulation for alzheimer's disease: A randomized, sham-controlled trial. *Brain*, *145*(11), 3776–3786. https://doi.org/10.1093/brain/awac285

Koelewijn, L., Lancaster, T. M., Linden, D., Dima, D. C., Routley, B. C., Magazzini, L., Barawi, K., Brindley, L., Adams, R., Tansey, K. E., Bompas, A., Tales, A., Bayer, A., & Singh, K. (2019). Oscillatory hyperactivity and hyperconnectivity in young APOE-ε4 carriers and hypoconnectivity in alzheimer's disease. *eLife*, *8*. https://doi.org/10.7554/elife.36011

Krakauer, J. W., Ghazanfar, A. A., Gomez-Marin, A., MacIver, M. A., & Poeppel, D. (2017). Neuroscience needs behavior: Correcting a reductionist bias. *Neuron*, *93*(3), 480–490. https://doi.org/10.1016/j.neuron.2016.12.041

Krause, B., & Cohen Kadosh, R. (2014). Not all brains are created equal: The relevance of individual differences in responsiveness to transcranial electrical stimulation. *Front. Syst. Neurosci.*, *8*, 25.

Krause, M. R., Vieira, P. G., Thivierge, J.-P., & Pack, C. C. (2022). Brain stimulation competes with ongoing oscillations for control of spike timing in the primate brain. *PLoS Biol.*, *20*(5), e3001650.

Kriegeskorte, N., & Douglas, P. K. (2018). Cognitive computational neuroscience. *Nature Neuroscience*, *21*(9), 1148–1160. https://doi.org/10.1038/s41593-018-0210-5

Kringelbach, M. L., Cruzat, J., Cabral, J., Knudsen, G. M., Carhart-Harris, R., Whybrow, P. C., Logothetis, N. K., & Deco, G. (2020). Dynamic coupling of whole-brain neuronal and neurotransmitter systems. *Proceedings of the National Academy of Sciences*, *117*(17), 9566–9576. https://doi.org/10.1073/pnas.1921475117

Kronberg, G., Rahman, A., Sharma, M., Bikson, M., & Parra, L. C. (2020). Direct current stimulation boosts hebbian plasticity in vitro. *Brain Stimulation*, *13*(2), 287–301. https://doi.org/10.1016/j.brs.2019.10.014

Kukolja, J., Göreci, D. Y., Onur, Ö. A., Riedl, V., & Fink, G. R. (2016). Resting-state fmri evidence for early episodic memory consolidation: Effects of age. *Neurobiology of Aging*, *45*, 197–211. https://doi.org/10.1016/j.neurobiolaging.2016.06.004

Kuramoto, Y. (1975). Self-entrainment of a population of coupled non-linear oscillators. In *Lecture notes in physics* (pp. 420–422). Springer-Verlag. https://doi.org/10.1007/bfb0013365

Lachaux, J., Rodriguez, E., Martinerie, J., & Varela, F. (1999). Measuring phase synchrony in brain signals. *Hum Brain Mapp*, *8*, 194–208.

Lamontagne-Kam, D., Ulfat, A. K., Hervé, V., Vu, T.-M., & Brouillette, J. (2023). Implication of tau propagation on neurodegeneration in alzheimer's disease. *Frontiers in Neuroscience*, *17*. https://doi.org/10.3389/fnins.2023.1219299

Lananna, B. V., McKee, C. A., King, M. W., Del-Aguila, J. L., Dimitry, J. M., Farias, F. H. G., Nadarajah, C. J., Xiong, D. D., Guo, C., Cammack, A. J., Elias, J. A., Zhang, J., Cruchaga, C., & Musiek, E. S. (2020). Chi3l1 /ykl-40 is controlled by the astrocyte circadian clock and regulates neuroinflammation and alzheimer's disease pathogenesis. *Science Translational Medicine*, *12*(574). https://doi.org/10.1126/scitranslmed.aax3519

Landau, L. D. (1944). On the Problem of Turbulence (D. ter Haar, Ed.). *Compt. Rend. Acad. Sci. URSS*, *44*. https://doi.org/10.1016/b978-0-08-010586-4.50057-2

Lang, S., Gan, L. S., Alrazi, T., & Monchi, O. (2019). Theta band high definition transcranial alternating current stimulation, but not transcranial direct current stimulation, improves associative memory performance. *Scientific Reports*, *9*(1). https://doi.org/10.1038/s41598-019-44680-8

Langbaum, J. B., Fleisher, A. S., Chen, K., Ayutyanont, N., Lopera, F., Quiroz, Y. T., Caselli, R. J., Tariot, P. N., & Reiman, E. M. (2013). Ushering in the study and treatment of preclinical alzheimer disease. *Nature Reviews Neurology*, *9*(7), 371–381. https://doi.org/10.1038/nrneurol.2013.107

Laureys, S. (2005). The neural correlate of (un)awareness: lessons from the vegetative state. *Trends Cogn Sci*, *9*, 556–9.

Lee, J., Choi, B. H., Oh, E., Sohn, E. H., & Lee, A. Y. (2016). Treatment of alzheimer's disease with repetitive transcranial magnetic stimulation combined with cognitive training: A prospective, randomized, double-blind, placebo-controlled study. *J. Clin. Neurol.*, *12*(1), 57–64.

Lee, T.-W., & Xue, S.-W. (2018). Functional connectivity maps based on hippocampal and thalamic dynamics may account for the default-mode network. *European Journal of Neuroscience*, *47*(5), 388–398. https://doi.org/10.1111/ejn.13828

Lejko, N., Larabi, D. I., Herrmann, C. S., Aleman, A., & Ćurčić-Blake, B. (2020). Alpha power and functional connectivity in cognitive decline: A systematic review and Meta-Analysis. *J. Alzheimers. Dis.*, *78*(3), 1047–1088.

Leng, F., & Edison, P. (2020). Neuroinflammation and microglial activation in alzheimer disease: Where do we go from here? *Nature Reviews Neurology*, *17*(3), 157–172. https://doi.org/10.1038/s41582-020-00435-y

Lesourd, M., Le Gall, D., Baumard, J., Croisile, B., Jarry, C., & Osiurak, F. (2013). Apraxia and alzheimer's disease: Review and perspectives. *Neuropsychology Review*, *23*(3), 234–256. https://doi.org/10.1007/s11065-013-9235-4

Li, X., Qi, G., Yu, C., Lian, G., Zheng, H., Wu, S., Yuan, T.-F., & Zhou, D. (2021). Cortical plasticity is correlated with cognitive improvement in alzheimer's disease patients after rtms treatment. *Brain Stimulation*, *14*(3), 503–510. https://doi.org/10.1016/j.brs.2021.01.012

Li, Y.-H., Li, J.-J., Lu, Q.-C., Gong, H.-Q., Liang, P.-J., & Zhang, P.-M. (2014). Involvement of thalamus in initiation of epileptic seizures induced by pilocarpine in mice. *Neural Plasticity*, *2014*, 1–15. https://doi.org/10.1155/2014/675128

Limon, A., Reyes-Ruiz, J. M., & Miledi, R. (2012). Loss of functional gaba(a) receptors in the alzheimer diseased brain. *Proceedings of the National Academy of Sciences*, *109*(25), 10071–10076. https://doi.org/10.1073/pnas.1204606109

Lin, R. L., Douaud, G., Filippini, N., Okell, T. W., Stagg, C. J., & Tracey, I. (2017). Structural connectivity variances underlie functional and behavioral changes during pain relief induced by neuromodulation. *Scientific Reports*, *7*(1). https://doi.org/10.1038/srep41603

Liu, A., Vöröslakos, M., Kronberg, G., Henin, S., Krause, M., Huang, Y., Opitz, A., Mehta, A., Pack, C., Krekelberg, B., Berényi, A., Parra, L., Melloni, L., Devinsky, O., & Buzsáki, G. (2018). Immediate neurophysiological effects of transcranial electrical stimulation. *Nat Commun*, *9*, 5092.

Liu, A., Vöröslakos, M., Kronberg, G., Henin, S., Krause, M. R., Huang, Y., Opitz, A., Mehta, A., Pack, C. C., Krekelberg, B., Berényi, A., Parra, L. C., Melloni, L., Devinsky, O., & Buzsáki, G. (2018). Immediate neurophysiological effects of transcranial electrical stimulation. *Nat. Commun.*, *9*(1), 5092.

Liu, Y., Liu, S., Tang, C., Tang, K., Liu, D., Chen, M., Mao, Z., & Xia, X. (2023). Transcranial alternating current stimulation combined with sound stimulation improves cognitive function in patients with alzheimer's disease: Study protocol for a randomized controlled trial. *Frontiers in Aging Neuroscience*, *14*. https://doi.org/10.3389/fnagi.2022.1068175

Liu, Y., Yu, C., Zhang, X., Liu, J., Duan, Y., Alexander-Bloch, A. F., Liu, B., Jiang, T., & Bullmore, E. (2013). Impaired long distance functional connectivity and weighted network architecture in alzheimer's disease. *Cerebral Cortex*, *24*(6), 1422–1435. https://doi.org/10.1093/cercor/bhs410

Liuzzi, L., Quinn, A. J., O'Neill, G. C., Woolrich, M. W., Brookes, M. J., Hillebrand, A., & Tewarie, P. (2019). How sensitive are conventional MEG functional connectivity metrics with sliding windows to detect genuine fluctuations in dynamic functional connectivity? *Frontiers in Neuroscience*, *13*. https://doi.org/10.3389/fnins.2019.00797

Llinás, R. R. (1988). The intrinsic electrophysiological properties of mammalian neurons: Insights into central nervous system function. *Science*, *242*(4886), 1654–1664. https://doi.org/10.1126/science.3059497

Logiaco, L., Abbott, L., & Escola, S. (2021). Thalamic control of cortical dynamics in a model of flexible motor sequencing. *Cell Reports*, *35*(9), 109090. https://doi.org/10.1016/j.celrep.2021.109090

Lopes da Silva, F. (1991). Neural mechanisms underlying brain waves: from neural membranes to networks. *Electroencephalogr Clin Neurophysiol*, *79*, 81–93.

Lopes da Silva, F. (2013). Eeg and meg: Relevance to neuroscience. *Neuron*, *80*(5), 1112–1128. https://doi.org/10.1016/j.neuron.2013.10.017

López, M., Bruña, R., Aurtenetxe, S., Pineda-Pardo, J., Marcos, A., Arrazola, J., Reinoso, A., Montejo, P., Bajo, R., & Maestú, F. (2014). Alpha-band hypersynchronization in progressive mild cognitive impairment: a magnetoencephalography study. *J Neurosci*, *34*, 14551–9.

López-Cuenca, I., Nebreda, A., García-Colomo, A., Salobrar-García, E., de Frutos-Lucas, J., Bruña, R., Ramírez, A. I., Ramirez-Toraño, F., Salazar, J. J., Barabash, A., Gil, P., Maestú, F., Ramírez, J. M., & de Hoz, R. (2023). Early visual alterations in individuals at-risk of alzheimer's disease: A multidisciplinary approach. *Alzheimer's Research & Therapy*, *15*(1). https://doi.org/10.1186/s13195-023-01166-0

López-Sanz, D., Bruña, R., Garcés, P., Camara, C., Serrano, N., Rodríguez-Rojo, I. C., Delgado, M. L., Montenegro, M., López-Higes, R., Yus, M., & Maestú, F. (2016a). Alpha band disruption in the AD-continuum starts in the subjective cognitive decline stage: A MEG study. *Sci. Rep.*, *6*, 37685.

López-Sanz, D., Bruña, R., Garcés, P., Camara, C., Serrano, N., Rodríguez-Rojo, I. C., Delgado, M. L., Montenegro, M., López-Higes, R., Yus, M., & Maestú, F. (2016b). Alpha band disruption in the AD-continuum starts in the Subjective Cognitive Decline stage: a MEG study. *Scientific Reports*, *6*(1). https://doi.org/10.1038/srep37685

López-Sanz, D., Bruña, R., Garcés, P., Martín-Buro, M., Walter, S., Delgado, M., Montenegro, M., López, H. R., Marcos, A., & Maestú, F. (2017). Functional Connectivity Disruption in Subjective Cognitive Decline and Mild Cognitive Impairment: A Common Pattern of Alterations. *Front Aging Neurosci*, *9*, 109.

Lundstrom, M. S., & Alam, M. A. (2022). Moore's law: The journey ahead. *Science*, *378*(6621), 722–723. https://doi.org/10.1126/science.ade2191

Luppi, J. J., Stam, C. J., Scheltens, P., & de Haan, W. (2024). Virtual neural network-guided optimization of non-invasive brain stimulation in alzheimer's disease (M. Kaiser, Ed.). *PLOS Computational Biology*, *20*(1), e1011164. https://doi.org/10.1371/journal.pcbi.1011164

Mack, C. A. (2011). Fifty years of moore's law. *IEEE Transactions on Semiconductor Manufacturing*, *24*(2), 202–207. https://doi.org/10.1109/tsm.2010.2096437

Maestú, F., de, H. W., Busche, M., & DeFelipe, J. (2021). Neuronal excitation/inhibition imbalance: core element of a translational perspective on Alzheimer pathophysiology. *Ageing Res Rev*, *69*, 101372.

Malhotra, P. A. (2019). Impairments of attention in alzheimer's disease. *Curr. Opin. Psychol.*, *29*, 41–48.

Malotaux, V., Dricot, L., Quenon, L., Lhommel, R., Ivanoiu, A., & Hanseeuw, B. (2023). Default-mode network connectivity changes during the progression toward alzheimer's dementia: A longitudinal functional magnetic resonance imaging study. *Brain Connectivity*, *13*(5), 287–296. https://doi.org/10.1089/brain.2022.0008

Manos, T., Diaz-Pier, S., & Tass, P. (2021). Long-Term Desynchronization by Coordinated Reset Stimulation in a Neural Network Model With Synaptic and Structural Plasticity. *Front Physiol*, *12*, 716556.

Markram, H., Lübke, J., Frotscher, M., & Sakmann, B. (1997). Regulation of synaptic efficacy by coincidence of postsynaptic APs and EPSPs. *Science*, *275*, 213–5.

Martone, M. E. (2024). The past, present and future of neuroscience data sharing: A perspective on the state of practices and infrastructure for fair. *Frontiers in Neuroinformatics*, *17*. https://doi.org/10.3389/fninf.2023.1276407

Mason, M. F., Norton, M. I., Horn, J. D. V., Wegner, D. M., Grafton, S. T., & Macrae, C. N. (2007). Wandering Minds: The Default Network and Stimulus-Independent Thought. *Science*, *315*(5810), 393–395. https://doi.org/10.1126/science.1131295

Masters, C. L., Bateman, R., Blennow, K., Rowe, C. C., Sperling, R. A., & Cummings, J. L. (2015). Alzheimer's disease. *Nature Reviews Disease Primers*, *1*(1). https://doi.org/10.1038/nrdp.2015.56

Matchett, B. J., Grinberg, L. T., Theofilas, P., & Murray, M. E. (2021). The mechanistic link between selective vulnerability of the locus coeruleus and neurodegeneration in alzheimer's disease. *Acta Neuropathologica*, *141*(5), 631–650. https://doi.org/10.1007/s00401-020-02248-1

Matzen, L. E., Trumbo, M. C., Leach, R. C., & Leshikar, E. D. (2015). Effects of non-invasive brain stimulation on associative memory. *Brain Research*, *1624*, 286–296. https://doi.org/10.1016/j.brainres.2015.07.036

McCoy, E. J., Walden, A. T., & Percival, D. B. (1998). Multitaper spectral estimation of power law processes. *IEEE Trans. Signal Process.*, *46*(3), 655–668.

McDougal, R. A., Morse, T. M., Carnevale, T., Marenco, L., Wang, R., Migliore, M., Miller, P. L., Shepherd, G. M., & Hines, M. L. (2016). Twenty years of modeldb and beyond: Building essential modeling tools for the future of neuroscience. *Journal of Computational Neuroscience*, *42*(1), 1–10. https://doi.org/10.1007/s10827-016-0623-7

McGuinness, B., Barrett, S. L., Craig, D., Lawson, J., & Passmore, A. P. (2010). Attention deficits in alzheimer's disease and vascular dementia. *J. Neurol. Neurosurg. Psychiatry*, *81*(2), 157–159.

Meier, J. M., Perdikis, D., Blickensdörfer, A., Stefanovski, L., Liu, Q., Maith, O., Dinkelbach, H. Ü., Baladron, J., Hamker, F. H., & Ritter, P. (2022a). Virtual deep brain stimulation: Multiscale co-simulation of a spiking basal ganglia model and a whole-brain mean-field model with the virtual brain. *Experimental Neurology*, *354*, 114111. https://doi.org/10.1016/j.expneurol.2022.114111

Meier, J. M., Perdikis, D., Blickensdörfer, A., Stefanovski, L., Liu, Q., Maith, O., Dinkelbach, H. Ü., Baladron, J., Hamker, F. H., & Ritter, P. (2022b). Virtual deep brain stimulation: Multiscale co-simulation of a spiking basal ganglia model and a whole-brain mean-field model with the virtual brain. *Exp. Neurol.*, *354*, 114111.

Menardi, A., Dotti, L., Ambrosini, E., & Vallesi, A. (2022). Transcranial magnetic stimulation treatment in alzheimer's disease: A meta-analysis of its efficacy as a function of protocol characteristics and degree of personalization. *Journal of Neurology*, *269*(10), 5283–5301. https://doi.org/10.1007/s00415-022-11236-2

Menon, V. (2011). Large-scale brain networks and psychopathology: A unifying triple network model. *Trends in Cognitive Sciences*, *15*(10), 483–506. https://doi.org/10.1016/j.tics.2011.08.003

Merino-Serrais, P., Benavides-Piccione, R., Blazquez-Llorca, L., Kastanauskaite, A., Rábano, A., Avila, J., & DeFelipe, J. (2013). The influence of phospho-tau on dendritic spines of cortical pyramidal neurons in patients with Alzheimer's disease. *Brain*, *136*(6), 1913–1928. https://doi.org/10.1093/brain/awt088

Merlet, I., Birot, G., Salvador, R., Molaee-Ardekani, B., Mekonnen, A., Soria-Frish, A., Ruffini, G., Miranda, P. C., & Wendling, F. (2013). From oscillatory transcranial current stimulation to scalp EEG changes: A biophysical and physiological modeling study. *PLoS One*, *8*(2), e57330.

Mesulam, M.-M. (2013). Cholinergic circuitry of the human nucleus basalis and its fate in alzheimer's disease. *Journal of Comparative Neurology*, *521*(18), 4124–4144. https://doi.org/10.1002/cne.23415

Mijalkov, M., Volpe, G., Fernaud-Espinosa, I., DeFelipe, J., Pereira, J. B., & Merino-Serrais, P. (2021). Dendritic spines are lost in clusters in alzheimer's disease. *Scientific Reports*, *11*(1). https://doi.org/10.1038/s41598-021-91726-x

Milner, B., Corkin, S., & Teuber, H.-L. (1968). Further analysis of the hippocampal amnesic syndrome: 14-year follow-up study of h.m. *Neuropsychologia*, *6*(3), 215–234. https://doi.org/10.1016/0028-3932(68)90021-3

Minter, M. R., Taylor, J. M., & Crack, P. J. (2015). The contribution of neuroinflammation to amyloid toxicity in alzheimer's disease. *Journal of Neurochemistry*, *136*(3), 457–474. https://doi.org/10.1111/jnc.13411

Miranda, P. C., Lomarev, M., & Hallett, M. (2006). Modeling the current distribution during transcranial direct current stimulation. *Clin. Neurophysiol.*, *117*(7), 1623–1629.

Mishra, A. M., Bai, X., Motelow, J. E., DeSalvo, M. N., Danielson, N., Sanganahalli, B. G., Hyder, F., & Blumenfeld, H. (2013). Increased resting functional connectivity in spike-wave epilepsy in WAG/Rij rats. *Epilepsia*, *54*(7), 1214–1222. https://doi.org/10.1111/epi.12227

Modolo, J., Denoyer, Y., Wendling, F., & Benquet, P. (2018). Physiological effects of low-magnitude electric fields on brain activity: Advances from in vitro, in vivo and in silico models. *Curr Opin Biomed Eng*, *8*, 38–44.

Mofakham, S., Fry, A., Adachi, J., Stefancin, P. L., Duong, T. Q., Saadon, J. R., Winans, N. J., Sharma, H., Feng, G., Djuric, P. M., & Mikell, C. B. (2021). Electrocorticography reveals thalamic control of cortical dynamics following traumatic brain injury. *Communications Biology*, *4*(1). https://doi.org/10.1038/s42003-021-02738-2

Moliadze, V., Antal, A., & Paulus, W. (2010). Boosting brain excitability by transcranial high frequency stimulation in the ripple range. *J Physiol*, *588*, 4891–904.

Moloney, C. M., Lowe, V. J., & Murray, M. E. (2021). Visualization of neurofibrillary tangle maturity in alzheimer's disease: A clinicopathologic perspective for biomarker research. *Alzheimer's & Dementia*, *17*(9), 1554–1574. https://doi.org/10.1002/alz.12321

Momi, D., Ozdemir, R. A., Tadayon, E., Boucher, P., Shafi, M. M., Pascual-Leone, A., & Santarnecchi, E. (2021). Network-level macroscale structural connectivity predicts propagation of transcranial magnetic stimulation. *NeuroImage*, *229*, 117698. https://doi.org/10.1016/j.neuroimage.2020.117698

Mormino, E. C., Smiljic, A., Hayenga, A. O., Onami, S. H., Greicius, M. D., Rabinovici, G. D., Janabi, M., Baker, S. L., Yen, I. V., Madison, C. M., Miller, B. L., & Jagust, W. J. (2011). Relationships between beta-amyloid and functional connectivity in different components of the default mode network in aging. *Cerebral Cortex*, *21*(10), 2399–2407. https://doi.org/10.1093/cercor/bhr025

Morris, R. G., & Kopelman, M. D. (1986). The memory deficits in alzheimer-type dementia: A review. *The Quarterly Journal of Experimental Psychology Section A*, *38*(4), 575–602. https://doi.org/10.1080/14640748608401615

Murakami, S., & Okada, Y. (2006). Contributions of principal neocortical neurons to magnetoencephalography and electroencephalography signals. *The Journal of Physiology*, *575*(3), 925–936. https://doi.org/10.1113/jphysiol.2006.105379

Murphy, C. (2018). Olfactory and other sensory impairments in alzheimer disease. *Nature Reviews Neurology*, *15*(1), 11–24. https://doi.org/10.1038/s41582-018-0097-5

Musi, N., Valentine, J. M., Sickora, K. R., Baeuerle, E., Thompson, C. S., Shen, Q., & Orr, M. E. (2018). Tau protein aggregation is associated with cellular senescence in the brain. *Aging Cell*, *17*(6). https://doi.org/10.1111/acel.12840

Nakagawa, T. T., Woolrich, M., Luckhoo, H., Joensson, M., Mohseni, H., Kringelbach, M. L., Jirsa, V., & Deco, G. (2014). How delays matter in an oscillatory whole-brain spiking-neuron network model for MEG alpha-rhythms at rest. *Neuroimage*, *87*, 383–394.

Nakajima, M., & Halassa, M. M. (2017). Thalamic control of functional cortical connectivity. *Current Opinion in Neurobiology*, *44*, 127–131. https://doi.org/10.1016/j.conb.2017.04.001

Nakamura, A., Cuesta, P., Fernández, A., Arahata, Y., Iwata, K., Kuratsubo, I., Bundo, M., Hattori, H., Sakurai, T., Fukuda, K., Washimi, Y., Endo, H., Takeda, A., Diers, K., Bajo, R., Maestú, F., Ito, K., & Kato, T. (2018). Electromagnetic signatures of the preclinical and prodromal stages of Alzheimer's disease. *Brain*, *141*(5), 1470–1485. https://doi.org/10.1093/brain/awy044

Nakamura, A., Cuesta, P., Kato, T., Arahata, Y., Iwata, K., Yamagishi, M., Kuratsubo, I., Kato, K., Bundo, M., Diers, K., Fernández, A., Maestú, F., & Ito, K. (2017). Early functional network alterations in asymptomatic elders at risk for Alzheimer's disease. *Scientific Reports*, *7*(1). https://doi.org/10.1038/s41598-017-06876-8

Naud, R., Marcille, N., Clopath, C., & Gerstner, W. (2008). Firing patterns in the adaptive exponential integrate-and-fire model. *Biol. Cybern.*, *99*(4-5), 335–347.

Nebes, R. D. (1989). Semantic memory in alzheimer's disease. *Psychological Bulletin*, *106*(3), 377–394. https://doi.org/10.1037/0033-2909.106.3.377

Netoff, T. I., & Schiff, S. J. (2002). Decreased neuronal synchronization during experimental seizures. *The Journal of Neuroscience*, *22*(16), 7297–7307. https://doi.org/10.1523/jneurosci.22-16-07297.2002

Neuling, T., Rach, S., & Herrmann, C. S. (2013). Orchestrating neuronal networks: Sustained after-effects of transcranial alternating current stimulation depend upon brain states. *Frontiers in Human Neuroscience*, *7*. https://doi.org/10.3389/fnhum.2013.00161

Ng, A. S. L., Wang, J., Ng, K. K., Chong, J. S. X., Qian, X., Lim, J. K. W., Tan, Y. J., Yong, A. C. W., Chander, R. J., Hameed, S., Ting, S. K. S., Kandiah, N., & Zhou, J. H. (2021). Distinct network topology in alzheimer's disease and behavioral variant frontotemporal dementia. *Alzheimer's Research & Therapy*, *13*(1). https://doi.org/10.1186/s13195-020-00752-w

Nicoll, R. A. (2017). A brief history of long-term potentiation. *Neuron*, *93*(2), 281–290. https://doi.org/10.1016/j.neuron.2016.12.015

Nissim, N., Pham, D. V., Poddar, T., Blutt, E., & Hamilton, R. (2023). The impact of gamma transcranial alternating current stimulation (tacs) on cognitive and memory processes in patients with mild cognitive impairment or alzheimer's disease: A literature review. *Brain Stimulation*, *16*(3), 748–755. https://doi.org/10.1016/j.brs.2023.04.001

Nomura, T., Asao, A., & Kumasaka, A. (2019). Transcranial alternating current stimulation over the prefrontal cortex enhances episodic memory recognition. *Experimental Brain Research*, *237*(7), 1709–1715. https://doi.org/10.1007/s00221-019-05543-w

Novellino, F., López, M. E., Vaccaro, M. G., Miguel, Y., Delgado, M. L., & Maestu, F. (2019). Association between hippocampus, thalamus, and caudate in mild cognitive impairment apoeε4 carriers: A structural covariance mri study. *Frontiers in Neurology*, *10*. https://doi.org/10.3389/fneur.2019.01303

O'Byrne, J., & Jerbi, K. (2022). How critical is brain criticality? *Trends in Neurosciences*, *45*(11), 820–837. https://doi.org/10.1016/j.tins.2022.08.007

O'Mahony, D., Rowan, M., Feely, J., Walsh, J. B., & Coakley, D. (1994). Primary auditory pathway and reticular activating system dysfunction in alzheimer's disease. *Neurology*, *44*(11), 2089–2089. https://doi.org/10.1212/wnl.44.11.2089

Oostenveld, R., Fries, P., Maris, E., & Schoffelen, J. (2011). FieldTrip: Open source software for advanced analysis of MEG, EEG, and invasive electrophysiological data. *Comput Intell Neurosci*, *2011*, 156869.

Ossenkoppele, R., Smith, R., Ohlsson, T., Strandberg, O., Mattsson, N., Insel, P. S., Palmqvist, S., & Hansson, O. (2019). Associations between tau, $A\beta$, and cortical thickness with cognition in alzheimer disease. *Neurology*, *92*(6). https://doi.org/10.1212/wnl.0000000000006875

Palesi, F., Lorenzi, R., Casellato, C., Ritter, P., Jirsa, V., Gandini, W.-K. C., & D'Angelo, E. (2020). The Importance of Cerebellar Connectivity on Simulated Brain Dynamics. *Front Cell Neurosci*, *14*, 240.

Palmqvist, S., Schöll, M., Strandberg, O., Mattsson, N., Stomrud, E., Zetterberg, H., Blennow, K., Landau, S., Jagust, W., & Hansson, O. (2017). Earliest accumulation of β-amyloid occurs within the default-mode network and concurrently affects brain connectivity. *Nature Communications*, *8*(1). https://doi.org/10.1038/s41467-017-01150-x

Palop, J. J., Chin, J., & Mucke, L. (2006). A network dysfunction perspective on neurodegenerative diseases. *Nature*, *443*(7113), 768–773. https://doi.org/10.1038/nature05289

Palop, J. J., & Mucke, L. (2010). Amyloid-β induced neuronal dysfunction in alzheimer's disease: From synapses toward neural networks. *Nature Neuroscience*, *13*(7), 812–818. https://doi.org/10.1038/nn.2583

Palva, S., & Palva, J. M. (2007). New vistas for α-frequency band oscillations. *Trends in Neurosciences*, *30*(4), 150–158. https://doi.org/10.1016/j.tins.2007.02.001

Pariz, A., Fischer, I., Valizadeh, A., & Mirasso, C. (2021). Transmission delays and frequency detuning can regulate information flow between brain regions (D. Marinazzo, Ed.). *PLOS Computational Biology*, *17*(4), e1008129. https://doi.org/10.1371/journal.pcbi.1008129

Parvizi, J., Van Hoesen, G. W., & Damasio, A. (2001). The selective vulnerability of brainstem nuclei to alzheimer's disease. *Annals of Neurology*, *49*(1), 53–66. https://doi.org/10.1002/1531-8249(200101)49:1<53::aid-ana30>3.0.co;2-q

Payne, L., & Sekuler, R. (2014). The importance of ignoring: Alpha oscillations protect selectivity. *Curr. Dir. Psychol. Sci.*, *23*(3), 171–177.

Pekkonen, E., Hirvonen, J., Jääskeläinen, I. P., Kaakkola, S., & Huttunen, J. (2001). Auditory sensory memory and the cholinergic system: Implications for alzheimer's disease. *NeuroImage*, *14*(2), 376–382. https://doi.org/10.1006/nimg.2001.0805

Pereira, J. B., Ossenkoppele, R., Palmqvist, S., Strandberg, T. O., Smith, R., Westman, E., & Hansson, O. (2019). Amyloid and tau accumulate across distinct spatial networks and are differentially associated with brain connectivity. *eLife*, *8*. https://doi.org/10.7554/elife.50830

Perneczky, R., Jessen, F., Grimmer, T., Levin, J., Flöel, A., Peters, O., & Froelich, L. (2023). Anti-amyloid antibody therapies in alzheimer's disease. *Brain*, *146*(3), 842–849. https://doi.org/10.1093/brain/awad005

Pernet, C. R., Wilcox, R., & Rousselet, G. A. (2013). Robust correlation analyses: False positive and power validation using a new open source matlab toolbox. *Frontiers in psychology*, *3*, 606.

Petkoski, S., Ritter, P., & Jirsa, V. K. (2023). White-matter degradation and dynamical compensation support age-related functional alterations in human brain. *Cerebral Cortex*, *33*(10), 6241–6256. https://doi.org/10.1093/cercor/bhac500

Pfurtscheller, G., Neuper, C., & Mohl, W. (1994). Event-related desynchronization (ERD) during visual processing. *International Journal of Psychophysiology*, *16*(2-3), 147–153. https://doi.org/10.1016/0167-8760(89)90041-x

Philippi, C. L., Tranel, D., Duff, M., & Rudrauf, D. (2014). Damage to the default mode network disrupts autobiographical memory retrieval. *Social Cognitive and Affective Neuroscience*, *10*(3), 318–326. https://doi.org/10.1093/scan/nsu070

Polanía, R., Nitsche, M. A., & Ruff, C. C. (2018). Studying and modifying brain function with non-invasive brain stimulation. *Nat. Neurosci.*, *21*(2), 174–187.

Poo, M.-m., Du, J.-l., Ip, N. Y., Xiong, Z.-Q., Xu, B., & Tan, T. (2016). China brain project: Basic neuroscience, brain diseases, and brain-inspired computing. *Neuron*, *92*(3), 591–596. https://doi.org/10.1016/j.neuron.2016.10.050

Portas, C., Rees, G., Howseman, A., Josephs, O., Turner, R., & Frith, C. (1998). A specific role for the thalamus in mediating the interaction of attention and arousal in humans. *J Neurosci*, *18*, 8979–89.

Power, J. D., Cohen, A. L., Nelson, S. M., Wig, G. S., Barnes, K. A., Church, J. A., Vogel, A. C., Laumann, T. O., Miezin, F. M., Schlaggar, B. L., & Petersen, S. E. (2011). Functional network organization of the human brain. *Neuron*, *72*(4), 665–678. https://doi.org/10.1016/j.neuron.2011.09.006

Preston, A. R., & Eichenbaum, H. (2013). Interplay of hippocampus and prefrontal cortex in memory. *Current Biology*, *23*(17), R764–R773. https://doi.org/10.1016/j.cub.2013.05.041

Preti, M. G., Bolton, T. A., & Ville, D. V. D. (2017). The dynamic functional connectome: State-of-the-art and perspectives. *NeuroImage*, *160*, 41–54. https://doi.org/10.1016/j.neuroimage.2016.12.061

Proix, T., Jirsa, V., Bartolomei, F., Guye, M., & Truccolo, W. (2018). Predicting the spatiotemporal diversity of seizure propagation and termination in human focal epilepsy. *Nat Commun*, *9*, 1088.

Proix, T., Bartolomei, F., Guye, M., & Jirsa, V. K. (2017). Individual brain structure and modelling predict seizure propagation. *Brain*, *140*(3), 641–654. https://doi.org/10.1093/brain/awx004

Pusil, S., López, M., Cuesta, P., Bruña, R., Pereda, E., & Maestú, F. (2019). Hypersynchronization in mild cognitive impairment: the 'X' model. *Brain*, *142*, 3936–3950.

Putra, P., Thompson, T. B., Chaggar, P., & Goriely, A. (2021). Braiding Braak and Braak: Staging patterns and model selection in network neurodegeneration. *Network Neuroscience*, *5*(4), 929–956. https://doi.org/10.1162/netn_a_00208

Puzzo, D., Gulisano, W., Arancio, O., & Palmeri, A. (2015). The keystone of alzheimer pathogenesis might be sought in $A\beta$ physiology. *Neuroscience*, *307*, 26–36. https://doi.org/10.1016/j.neuroscience.2015.08.039

Qu, Z., Garfinkel, A., Weiss, J. N., & Nivala, M. (2011). Multi-scale modeling in biology: How to bridge the gaps between scales? *Progress in Biophysics and Molecular Biology*, *107*(1), 21–31. https://doi.org/10.1016/j.pbiomolbio.2011.06.004

Quevenco, F. C., van Bergen, J. M., Treyer, V., Studer, S. T., Kagerer, S. M., Meyer, R., Gietl, A. F., Kaufmann, P. A., Nitsch, R. M., Hock, C., & Unschuld, P. G. (2020). Functional brain network connectivity patterns associated with normal cognition at old-age, local β-amyloid, tau, and APOE4. *Frontiers in Aging Neuroscience*, *12*. https://doi.org/10.3389/fnagi.2020.00046

Radman, T., Ramos, R. L., Brumberg, J. C., & Bikson, M. (2009). Role of cortical cell type and morphology in subthreshold and suprathreshold uniform electric field stimulation in vitro. *Brain Stimul.*, *2*(4), 215–28, 228.e1–3.

Raichle, M. E. (2010). Two views of brain function. *Trends in Cognitive Sciences*, *14*(4), 180–190. https://doi.org/10.1016/j.tics.2010.01.008

Raichle, M. E. (2015). The Brain's Default Mode Network. *Annual Review of Neuroscience*, *38*(1), 433–447. https://doi.org/10.1146/annurev-neuro-071013-014030

Raichle, M. E., MacLeod, A. M., Snyder, A. Z., Powers, W. J., Gusnard, D. A., & Shulman, G. L. (2001). A default mode of brain function. *Proceedings of the National Academy of Sciences*, *98*(2), 676–682. https://doi.org/10.1073/pnas.98.2.676

Ramirez-Toraño, F., Bruña, R., de Frutos-Lucas, J., Rodríguez-Rojo, I. C., de Pedro, S. M., Delgado-Losada, M. L., Gómez-Ruiz, N., Barabash, A., Marcos, A., Higes, R. L., & Maestú, F. (2020). Functional Connectivity Hypersynchronization in Relatives of Alzheimer's Disease Patients: An Early E/I Balance Dysfunction? *Cerebral Cortex*, *31*(2), 1201–1210. https://doi.org/10.1093/cercor/bhaa286

Ranasinghe, K. G., Cha, J., Iaccarino, L., Hinkley, L. B., Beagle, A. J., Pham, J., Jagust, W. J., Miller, B. L., Rankin, K. P., Rabinovici, G. D., Vossel, K. A., & Nagarajan, S. S. (2020). Neurophysiological signatures in alzheimer's disease are distinctly associated with TAU, amyloid-β accumulation, and cognitive decline. *Science Translational Medicine*, *12*(534). https://doi.org/10.1126/scitranslmed.aaz4069

Ranasinghe, K. G., Hinkley, L. B., Beagle, A. J., Mizuiri, D., Dowling, A. F., Honma, S. M., Finucane, M. M., Scherling, C., Miller, B. L., Nagarajan, S. S., & Vossel, K. A. (2014). Regional functional connectivity predicts distinct cognitive impairments in alzheimer's disease spectrum. *NeuroImage: Clinical*, *5*, 385–395. https://doi.org/10.1016/j.nicl.2014.07.006

Ranasinghe, K. G., Verma, P., Cai, C., Xie, X., Kudo, K., Gao, X., Lerner, H., Mizuiri, D., Strom, A., Iaccarino, L., Joie, R. L., Miller, B. L., Gorno-Tempini, M. L., Rankin, K. P., Jagust, W. J., Vossel, K., Rabinovici, G. D., Raj, A., & Nagarajan, S. S. (2022). Altered excitatory and inhibitory neuronal subpopulation parameters are distinctly associated with tau and amyloid in alzheimer's disease. *eLife*, *11*. https://doi.org/10.7554/elife.77850

Reato, D., Rahman, A., Bikson, M., & Parra, L. C. (2013). Effects of weak transcranial alternating current stimulation on brain activity-a review of known mechanisms from animal studies. *Front. Hum. Neurosci.*, *7*, 687.

Redinbaugh, M. J., Phillips, J. M., Kambi, N. A., Mohanta, S., Andryk, S., Dooley, G. L., Afrasiabi, M., Raz, A., & Saalmann, Y. B. (2020). Thalamus Modulates Consciousness via Layer-Specific Control of Cortex. *Neuron*, *106*(1), 66–75.e12. https://doi.org/10.1016/j.neuron.2020.01.005

Reisberg, B., Doody, R., Stöffler, A., Schmitt, F., Ferris, S., & Möbius, H. J. (2003). Memantine in moderate-to-severe alzheimer's disease. *New England Journal of Medicine*, *348*(14), 1333–1341. https://doi.org/10.1056/nejmoa013128

Reisberg, B., Doody, R., Stöffler, A., Schmitt, F., Ferris, S., & Möbius, H. J. (2006). A 24-week open-label extension study of memantine in moderate to severe alzheimer disease. *Archives of Neurology*, *63*(1), 49. https://doi.org/10.1001/archneur.63.1.49

Ridder, D. D., Stöckl, T., To, W. T., Langguth, B., & Vanneste, S. (2017). Noninvasive Transcranial Magnetic and Electrical Stimulation: Working Mechanisms. In *Rhythmic stimulation procedures in neuromodulation* (pp. 193–223). Elsevier. https://doi.org/10.1016/B978-0-12-803726-3.00007-9

Ridding, M. C., & Ziemann, U. (2010). Determinants of the induction of cortical plasticity by non-invasive brain stimulation in healthy subjects. *The Journal of Physiology*, *588*(13), 2291–2304. https://doi.org/10.1113/jphysiol.2010.190314

Rigas, P., & Castro-Alamancos, M. A. (2007). Thalamocortical Up States: Differential Effects of Intrinsic and Extrinsic Cortical Inputs on Persistent Activity. *Journal of Neuroscience*, *27*(16), 4261–4272. https://doi.org/10.1523/jneurosci.0003-07.2007

Ríos, A. S., Oxenford, S., Neudorfer, C., Butenko, K., Li, N., Rajamani, N., Boutet, A., Elias, G. J. B., Germann, J., Loh, A., Deeb, W., Wang, F., Setsompop, K., Salvato, B., de Almeida, L. B., Foote, K. D., Amaral, R., Rosenberg, P. B., Tang-Wai, D. F., ... Horn, A. (2022). Optimal deep brain stimulation sites and networks for stimulation of the fornix in alzheimer's disease. *Nature Communications*, *13*(1). https://doi.org/10.1038/s41467-022-34510-3

Ritchie, H., & Roser, M. (2019). Population by age group — ourworldindata.org [[Accessed 10-01-2024]].

Rodriguez, G. A., Barrett, G. M., Duff, K. E., & Hussaini, S. A. (2020). Chemogenetic attenuation of neuronal activity in the entorhinal cortex reduces Aβ and tau pathology in the hippocampus (G. P. Bates, Ed.). *PLOS Biology*, *18*(8), e3000851. https://doi.org/10.1371/journal.pbio.3000851

Rolls, E., Joliot, M., & Tzourio-Mazoyer, N. (2015). Implementation of a new parcellation of the orbitofrontal cortex in the automated anatomical labeling atlas. *Neuroimage*, *122*, 1–5.

Rosenbaum, R. S., Priselac, S., Köhler, S., Black, S. E., Gao, F., Nadel, L., & Moscovitch, M. (2000). Remote spatial memory in an amnesic person with extensive bilateral hippocampal lesions. *Nature Neuroscience*, *3*(10), 1044–1048. https://doi.org/10.1038/79867

Roy, D. S., Park, Y.-G., Kim, M. E., Zhang, Y., Ogawa, S. K., DiNapoli, N., Gu, X., Cho, J. H., Choi, H., Kamentsky, L., Martin, J., Mosto, O., Aida, T., Chung, K., & Tonegawa, S. (2022). Brain-wide mapping reveals that engrams for a single memory are distributed across multiple brain regions. *Nature Communications*, *13*(1). https://doi.org/10.1038/s41467-022-29384-4

Rüb, U., Del Tredici, K., Schultz, C., Thal, D. R., Braak, E., & Braak, H. (2000). The evolution of alzheimer's disease-related cytoskeletal pathology in the human raphe nuclei. *Neuropathology and Applied Neurobiology*, *26*(6), 553–567. https://doi.org/10.1046/j.0305-1846.2000.00291.x

Russell, M., Goodman, T., Wang, Q., Groshong, B., & Lyeth, B. G. (2014). Gender differences in current received during transcranial electrical stimulation. *Front. Psychiatry*, *5*, 104.

Rutherford, G., Lithgow, B., & Moussavi, Z. (2015). Short and long-term effects of rtms treatment on alzheimer's disease at different stages: A pilot study. *Journal of Experimental Neuroscience*, *9*, JEN.S24004. https://doi.org/10.4137/jen.s24004

Sabbagh, M., Sadowsky, C., Tousi, B., Agronin, M. E., Alva, G., Armon, C., Bernick, C., Keegan, A. P., Karantzoulis, S., Baror, E., Ploznik, M., & Pascual-Leone, A. (2020). Effects of a combined transcranial magnetic stimulation (tms) and cognitive training intervention in patients with alzheimer's disease. *Alzheimer's & Dementia*, *16*(4), 641–650. https://doi.org/10.1016/j.jalz.2019.08.197

Sadaghiani, S., Poline, J.-B., Kleinschmidt, A., & D'Esposito, M. (2015). Ongoing dynamics in large-scale functional connectivity predict perception. *Proceedings of the National Academy of Sciences*, *112*(27), 8463–8468. https://doi.org/10.1073/pnas.1420687112

Sadeh, S., & Clopath, C. (2020). Inhibitory stabilization and cortical computation. *Nature Reviews Neuroscience*, *22*(1), 21–37. https://doi.org/10.1038/s41583-020-00390-z

Sala-Llonch, R., Bartrés-Faz, D., & Junqué, C. (2015). Reorganization of brain networks in aging: a review of functional connectivity studies. *Frontiers in Psychology*, *6*. https://doi.org/10.3389/fpsyg.2015.00663

Salobrar-García, E., de Hoz, R., Ramírez, A. I., López-Cuenca, I., Rojas, P., Vazirani, R., Amarante, C., Yubero, R., Gil, P., Pinazo-Durán, M. D., Salazar, J. J., & Ramírez, J. M. (2019). Changes in visual function and retinal structure in the progression of alzheimer's disease (S. Barnes, Ed.). *PLOS ONE*, *14*(8), e0220535. https://doi.org/10.1371/journal.pone.0220535

Sánchez-Claros, J., Pariz, A., Valizadeh, A., Canals, S., & Mirasso, C. R. (2021). Information transmission in delay-coupled neuronal circuits in the presence of a relay population. *Frontiers in Systems Neuroscience*, *15*, 705371.

Sanchez-Vives, M. V. (2020). Origin and dynamics of cortical slow oscillations [Physiology of sleep]. *Current Opinion in Physiology*, *15*, 217–223. https://doi.org/https://doi.org/10.1016/j.cophys.2020.04.005

Sandhu, Z., Tanglay, O., Young, I. M., Briggs, R. G., Bai, M. Y., Larsen, M. L., Conner, A. K., Dhanaraj, V., Lin, Y.-H., Hormovas, J., Fonseka, R. D., Glenn, C. A., & Sughrue, M. E. (2020). Parcellation-based anatomic modeling of the default mode network. *Brain and Behavior*, *11*(2). https://doi.org/10.1002/brb3.1976

Sanzeni, A., Akitake, B., Goldbach, H. C., Leedy, C. E., Brunel, N., & Histed, M. H. (2020). Inhibition stabilization is a widespread property of cortical networks. *eLife*, *9*. https://doi.org/10.7554/elife.54875

Sanz-Leon, P., Knock, S., Spiegler, A., & Jirsa, V. (2015). Mathematical framework for large-scale brain network modeling in The Virtual Brain. *Neuroimage*, *111*, 385–430.

Sanz-Leon, P., Knock, S., Woodman, M., Domide, L., Mersmann, J., McIntosh, A., & Jirsa, V. (2013). The Virtual Brain: a simulator of primate brain network dynamics. *Front Neuroinform*, *7*, 10.

Schäfer, A., Chaggar, P., Thompson, T. B., Goriely, A., & Kuhl, E. (2021). Predicting brain atrophy from tau pathology: A summary of clinical findings and their translation into personalized models. *Brain Multiphysics*, *2*, 100039. https://doi.org/10.1016/j.brain.2021.100039

Schiff, N. (2010). Recovery of consciousness after brain injury: a mesocircuit hypothesis. *Trends Neurosci*, *33*, 1–9.

Schilling, K., Gao, Y., Janve, V., Stepniewska, I., Landman, B. A., & Anderson, A. W. (2017). Can increased spatial resolution solve the crossing fiber problem for diffusion mri? *NMR in Biomedicine*, *30*(12). https://doi.org/10.1002/nbm.3787

Schilling, K. G., Daducci, A., Maier-Hein, K., Poupon, C., Houde, J.-C., Nath, V., Anderson, A. W., Landman, B. A., & Descoteaux, M. (2019). Challenges in diffusion mri tractography – lessons learned from international benchmark competitions. *Magnetic Resonance Imaging*, *57*, 194–209. https://doi.org/10.1016/j.mri.2018.11.014

Schirner, M., Rothmeier, S., Jirsa, V., McIntosh, A., & Ritter, P. (2015). An automated pipeline for constructing personalized virtual brains from multimodal neuroimaging data. *Neuroimage*, *117*, 343–57.

Schlichting, M. L., & Preston, A. R. (2014). Memory reactivation during rest supports upcoming learning of related content. *Proceedings of the National Academy of Sciences*, *111*(44), 15845–15850. https://doi.org/10.1073/pnas.1404396111

Schmitt, L., Wimmer, R., Nakajima, M., Happ, M., Mofakham, S., & Halassa, M. (2017). Thalamic amplification of cortical connectivity sustains attentional control. *Nature*, *545*, 219–223.

Schoonhoven, D. N., Briels, C. T., Hillebrand, A., Scheltens, P., Stam, C. J., & Gouw, A. A. (2022). Sensitive and reproducible MEG resting-state metrics of functional connectivity in alzheimer's disease. *Alzheimer's Research & Therapy*, *14*(1). https://doi.org/10.1186/s13195-022-00970-4

Schoonhoven, D. N., Coomans, E. M., Millán, A. P., van Nifterick, A. M., Visser, D., Ossenkoppele, R., Tuncel, H., van der Flier, W. M., Golla, S. S. V., Scheltens, P., Hillebrand, A., van Berckel, B. N. M., Stam, C. J., & Gouw, A. A. (2023). Tau protein spreads through functionally connected neurons in alzheimer's disease: A combined MEG/PET study. *Brain*, *146*(10), 4040–4054. https://doi.org/10.1093/brain/awad189

Schreiner, T., Kaufmann, E., Noachtar, S., Mehrkens, J.-H., & Staudigl, T. (2022). The human thalamus orchestrates neocortical oscillations during NREM sleep. *Nature Communications*, *13*(1). https://doi.org/10.1038/s41467-022-32840-w

Schultz, A. P., Chhatwal, J. P., Hedden, T., Mormino, E. C., Hanseeuw, B. J., Sepulcre, J., Huijbers, W., LaPoint, M., Buckley, R. F., Johnson, K. A., & Sperling, R. A. (2017). Phases of hyperconnectivity and hypoconnectivity in the default mode and salience networks track with amyloid and tau in clinically normal individuals. *The Journal of Neuroscience*, *37*(16), 4323–4331. https://doi.org/10.1523/jneurosci.3263-16.2017

Schwab, B. C., König, P., & Engel, A. K. (2021). Spike-timing-dependent plasticity can account for connectivity aftereffects of dual-site transcranial alternating current stimulation. *Neuroimage*, *237*, 118179.

Sepulcre, J., Sabuncu, M. R., Li, Q., Fakhri, G. E., Sperling, R., & Johnson, K. A. (2017). Tau and amyloid β proteins distinctively associate to functional network changes in the aging brain. *Alzheimer's & Dementia*, *13*(11), 1261–1269. https://doi.org/10.1016/j.jalz.2017.02.011

Shaheen, H., Pal, S., & Melnik, R. (2022). Multiscale co-simulation of deep brain stimulation with brain networks in neurodegenerative disorders. *Brain Multiphysics*, *3*, 100058. https://doi.org/10.1016/j.brain.2022.100058

Sherman, S. M. (2007). The thalamus is more than just a relay. *Current Opinion in Neurobiology*, *17*(4), 417–422. https://doi.org/10.1016/j.conb.2007.07.003

Sherman, S. M., & Guillery, R. W. (2005). *Exploring the Thalamus and Its Role in Cortical Function* (Second edition). MIT press.

Sherman, S. M., & Guillery, R. W. (2011). Distinct functions for direct and transthalamic corticocortical connections. *Journal of Neurophysiology*, *106*(3), 1068–1077. https://doi.org/10.1152/jn.00429.2011

Sherman, S. (2016). Thalamus plays a central role in ongoing cortical functioning. *Nat Neurosci*, *19*, 533–41.

Sheroziya, M., & Timofeev, I. (2014). Global intracellular slow-wave dynamics of the thalamocortical system. *Journal of Neuroscience*, *34*(26), 8875–8893. https://doi.org/10.1523/jneurosci.4460-13.2014

Shiffrin, R. M., & Atkinson, R. C. (1969). Storage and retrieval processes in long-term memory. *Psychological Review*, *76*(2), 179–193. https://doi.org/10.1037/h0027277

Sieveritz, B., & Raghavan, R. (2021). The Central Thalamus: Gatekeeper or Processing Hub? *J Neurosci*, *41*, 4954–4956.

Sinke, M. R. T., Otte, W. M., Christiaens, D., Schmitt, O., Leemans, A., van der Toorn, A., Sarabdjitsingh, R. A., Joëls, M., & Dijkhuizen, R. M. (2018). Diffusion mri-based cortical connectome reconstruction: Dependency on tractography procedures and neuroanatomical characteristics. *Brain Structure and Function*, *223*(5), 2269–2285. https://doi.org/10.1007/s00429-018-1628-y

Slepian, D. (1978). Prolate spheroidal wave functions, fourier analysis, and uncertainty-v: The discrete case. *Bell Syst. Tech. J.*, *57*(5), 1371–1430.

Smallwood, J., Bernhardt, B. C., Leech, R., Bzdok, D., Jefferies, E., & Margulies, D. S. (2021). The default mode network in cognition: A topographical perspective. *Nature Reviews Neuroscience*, *22*(8), 503–513. https://doi.org/10.1038/s41583-021-00474-4

Sperling, G. (1960). The information available in brief visual presentations. *Psychological Monographs: General and Applied*, *74*(11), 1–29. https://doi.org/10.1037/h0093759

Sperling, R. (2011). The potential of functional mri as a biomarker in early alzheimer's disease. *Neurobiology of Aging*, *32*, S37–S43. https://doi.org/10.1016/j.neurobiolaging.2011.09.009

Sperling, R., Mormino, E., & Johnson, K. (2014). The evolution of preclinical alzheimer's disease: Implications for prevention trials. *Neuron*, *84*(3), 608–622. https://doi.org/10.1016/j.neuron.2014.10.038

Sperling, R. A., Karlawish, J., & Johnson, K. A. (2012). Preclinical alzheimer disease—the challenges ahead. *Nature Reviews Neurology*, *9*(1), 54–58. https://doi.org/10.1038/nrneurol.2012.241

Spiegler, A., Kiebel, S., Atay, F., & Knösche, T. (2010). Bifurcation analysis of neural mass models: Impact of extrinsic inputs and dendritic time constants. *Neuroimage*, *52*, 1041–58. https://doi.org/10.1016/j.neuroimage.2009.12.081

Spinosa, V., Brattico, E., Campo, F., & Logroscino, G. (2022). A systematic review on resting state functional connectivity in patients with neurodegenerative disease and hallucinations. *NeuroImage: Clinical*, *35*, 103112. https://doi.org/10.1016/j.nicl.2022.103112

Sporns, O. (2010). *Networks of the Brain*. MIT Press.

Sporns, O. (2013). Structure and function of complex brain networks. *Dialogues in Clinical Neuroscience*, *15*(3), 247–262. https://doi.org/10.31887/dcns.2013.15.3/osporns

Sporns, O., & Betzel, R. F. (2016). Modular brain networks. *Annual Review of Psychology*, *67*(1), 613–640. https://doi.org/10.1146/annurev-psych-122414-033634

Squire, L. R. (2004). Memory systems of the brain: A brief history and current perspective. *Neurobiology of Learning and Memory*, *82*(3), 171–177. https://doi.org/10.1016/j.nlm.2004.06.005

Stam, C., Jones, B., Nolte, G., Breakspear, M., & Scheltens, P. (2006). Small-world networks and functional connectivity in alzheimer's disease. *Cerebral Cortex*, *17*(1), 92–99. https://doi.org/10.1093/cercor/bhj127

Stam, C. J., van Nifterick, A. M., de Haan, W., & Gouw, A. A. (2023). Network hyperexcitability in early alzheimer's disease: Is functional connectivity a potential biomarker? *Brain Topography*, *36*(4), 595–612. https://doi.org/10.1007/s10548-023-00968-7

Stargardt, A., Swaab, D. F., & Bossers, K. (2015). The storm before the quiet: neuronal hyperactivity and Aβ in the presymptomatic stages of Alzheimer's disease. *Neurobiology of Aging*, *36*(1), 1–11. https://doi.org/10.1016/j.neurobiolaging.2014.08.014

Stefanescu, R. A., & Jirsa, V. K. (2008). A low dimensional description of globally coupled heterogeneous neural networks of excitatory and inhibitory neurons (K. J. Friston, Ed.). *PLoS Computational Biology*, *4*(11), e1000219. https://doi.org/10.1371/journal.pcbi.1000219

Stefanovski, L., Triebkorn, P., Spiegler, A., Diaz-Cortes, M., Solodkin, A., Jirsa, V., McIntosh, A., & Ritter, P. (2019). Linking Molecular Pathways and Large-Scale Computational Modeling to Assess Candidate Disease Mechanisms and Pharmacodynamics in Alzheimer's Disease. *Front Comput Neurosci*, *13*, 54.

Stefanovski, L., Meier, J. M., Pai, R. K., Triebkorn, P., Lett, T., Martin, L., Bülau, K., Hofmann-Apitius, M., Solodkin, A., McIntosh, A. R., & Ritter, P. (2021). Bridging Scales in Alzheimer's Disease: Biological Framework for Brain Simulation With The Virtual Brain. *Frontiers in Neuroinformatics*, *15*. https://doi.org/10.3389/fninf.2021.630172

Steriade, M. (1996). Arousal–Revisiting the Reticular Activating System. *Science*, *272*(5259), 225–225. https://doi.org/10.1126/science.272.5259.225

Sterratt, D., Graham, B., Gillies, A., & Willshaw, D. (2012, June). *Principles of computational modelling in neuroscience*. Cambridge University Press.

Stuart, J. T. (1960). On the non-linear mechanics of wave disturbances in stable and unstable parallel flows part 1. the basic behaviour in plane poiseuille flow. *Journal of Fluid Mechanics*, *9*(3), 353–370. https://doi.org/10.1017/s002211206000116x

Susi, G., de Frutos-Lucas, J., Niso, G., Ye-Chen, S. M., Antón Toro, L., Chino Vilca, B. N., & Maestú, F. (2019). Healthy and pathological neurocognitive aging: Spectral and functional connectivity analyses using magnetoencephalography. In *Oxford Research Encyclopedia of Psychology* (pp. 1–46). Oxford University Press.

Tadel, F., Baillet, S., Mosher, J., Pantazis, D., & Leahy, R. (2011). Brainstorm: a user-friendly application for MEG/EEG analysis. *Comput Intell Neurosci*, *2011*, 879716.

Tadel, F., Bock, E., Niso, G., Mosher, J., Cousineau, M., Pantazis, D., Leahy, R., & Baillet, S. (2019). MEG/EEG Group Analysis With Brainstorm. *Front Neurosci*, *13*, 76.

Talamo, B. R., Rudel, R., Kosik, K. S., Lee, V. M.-Y., Neff, S., Adelman, L., & Kauer, J. S. (1989). Pathological changes in olfactory neurons in patients with alzheimer's disease. *Nature*, *337*(6209), 736–739. https://doi.org/10.1038/337736a0

Tang, S., Wang, Y., Liu, Y., Chau, S. W., Chan, J. W., Chu, W. C., Abrigo, J. M., Mok, V. C., & Wing, Y. K. (2022). Large-scale network dysfunction in α-Synucleinopathy: A meta-analysis of resting-state functional connectivity. *eBioMedicine*, *77*, 103915. https://doi.org/10.1016/j.ebiom.2022.103915

Tasserie, J., Uhrig, L., Sitt, J., Manasova, D., Dupont, M., Dehaene, S., & Jarraya, B. (2022). Deep brain stimulation of the thalamus restores signatures of consciousness in a nonhuman primate model. *Sci Adv*, *8*, eabl5547.

Taulu, S., & Hari, R. (2009). Removal of magnetoencephalographic artifacts with temporal signal-space separation: demonstration with single-trial auditory-evoked responses. *Hum Brain Mapp*, *30*, 1524–34.

Taulu, S., & Simola, J. (2006). Spatiotemporal signal space separation method for rejecting nearby interference in MEG measurements. *Phys. Med. Biol.*, *51*(7), 1759–1768.

Therriault, J., Pascoal, T. A., Lussier, F. Z., Tissot, C., Chamoun, M., Bezgin, G., Servaes, S., Benedet, A. L., Ashton, N. J., Karikari, T. K., Lantero-Rodriguez, J., Kunach, P., Wang, Y.-T., Fernandez-Arias, J., Massarweh, G., Vitali, P., Soucy, J.-P., Saha-Chaudhuri, P., Blennow, K., ... Rosa-Neto, P. (2022). Biomarker modeling of Alzheimer's disease using PET-based Braak staging. *Nature Aging*, *2*(6), 526–535. https://doi.org/10.1038/s43587-022-00204-0

Thompson, T. B., Chaggar, P., Kuhl, E., & and, A. G. (2020). Protein-protein interactions in neurodegenerative diseases: A conspiracy theory (A. Csikász-Nagy, Ed.). *PLOS Computational Biology*, *16*(10), e1008267. https://doi.org/10.1371/journal.pcbi.1008267

Tononi, G., Sporns, O., & Edelman, G. M. (1994). A measure for brain complexity: Relating functional segregation and integration in the nervous system. *Proceedings of the National Academy of Sciences*, *91*(11), 5033–5037. https://doi.org/10.1073/pnas.91.11.5033

Torrico, T., & Munakomi, S. (2021). Neuroanatomy, Thalamus. In *Statpearls [internet]*. Treasure Island (FL): StatPearls Publishing. https://www.ncbi.nlm.nih.gov/books/NBK542184/

Tounsi, H., Deweer, B., Ergis, A.-M., Van der Linden, M., Pillon, B., Michon, A., & Dubois, B. (1999). Sensitivity to semantic cuing: An index of episodic memory dysfunction in early alzheimer disease. *Alzheimer Disease & Associated Disorders*, *13*(1), 38–46. https://doi.org/10.1097/00002093-199903000-00006

Tran, H., Shirinpour, S., & Opitz, A. (2022). Effects of transcranial alternating current stimulation on spiking activity in computational models of single neocortical neurons. *Neuroimage*, *250*, 118953.

Treisman, A. M., & Gelade, G. (1980). A feature-integration theory of attention. *Cognitive Psychology*, *12*(1), 97–136. https://doi.org/10.1016/0010-0285(80)90005-5

Trevelyan, A. J. (2016). Do cortical circuits need protecting from themselves? *Trends in Neurosciences*, *39*(8), 502–511. https://doi.org/10.1016/j.tins.2016.06.002

Trevelyan, A. J., Sussillo, D., Watson, B. O., & Yuste, R. (2006). Modular propagation of epileptiform activity: Evidence for an inhibitory veto in neocortex. *The Journal of Neuroscience*, *26*(48), 12447–12455. https://doi.org/10.1523/jneurosci.2787-06.2006

Trevelyan, A. J., Sussillo, D., & Yuste, R. (2007). Feedforward inhibition contributes to the control of epileptiform propagation speed. *The Journal of Neuroscience*, *27*(13), 3383–3387. https://doi.org/10.1523/jneurosci.0145-07.2007

Tulving, E. (1985). Memory and consciousness. *Canadian Psychology / Psychologie canadienne*, *26*(1), 1–12. https://doi.org/10.1037/h0080017

Tulving, E., & Osler, S. (1968). Effectiveness of retrieval cues in memory for words. *Journal of Experimental Psychology*, *77*(4), 593–601. https://doi.org/10.1037/h0026069

Tulving, E., & Schacter, D. L. (1990). Priming and human memory systems. *Science*, *247*(4940), 301–306. https://doi.org/10.1126/science.2296719

Tzourio-Mazoyer, N., Landeau, B., Papathanassiou, D., Crivello, F., Etard, O., Delcroix, N., Mazoyer, B., & Joliot, M. (2002). Automated anatomical labeling of activations in SPM using a macroscopic anatomical parcellation of the MNI MRI single-subject brain. *Neuroimage*, *15*(1), 273–289.

Ulrich, D. (2015). Amyloid- Impairs Synaptic Inhibition via GABAA Receptor Endocytosis. *Journal of Neuroscience*, *35*(24), 9205–9210. https://doi.org/10.1523/jneurosci.0950-15.2015

Vallat, R. (2018). Pingouin: statistics in Python. *Journal of Open Source Software*, *3*(31), 1026. https://doi.org/10.21105/joss.01026

van den Heuvel, M. P., & Sporns, O. (2013). Network hubs in the human brain. *Trends in Cognitive Sciences*, *17*(12), 683–696. https://doi.org/10.1016/j.tics.2013.09.012

Van Erum, J., Van Dam, D., & De Deyn, P. P. (2019). Alzheimer's disease: Neurotransmitters of the sleep-wake cycle. *Neurosci. Biobehav. Rev.*, *105*, 72–80.

Van Regenmortel, M. H. V. (2004). Reductionism and complexity in molecular biology. scientists now have the tools to unravel biological and overcome the limitations of reductionism. *EMBO Rep.*, *5*(11), 1016–1020.

Van Veen, B. D., & Buckley, K. M. (1988). Beamforming: A versatile approach to spatial filtering. *IEEE ASSP Magazine*, *5*(2), 4–24.

van Bokhoven, P., de Wilde, A., Vermunt, L., Leferink, P. S., Heetveld, S., Cummings, J., Scheltens, P., & Vijverberg, E. G. B. (2021). The alzheimer's disease drug development landscape. *Alzheimer's Research & Therapy*, *13*(1). https://doi.org/10.1186/s13195-021-00927-z

van Dyck, C. H., Swanson, C. J., Aisen, P., Bateman, R. J., Chen, C., Gee, M., Kanekiyo, M., Li, D., Reyderman, L., Cohen, S., Froelich, L., Katayama, S., Sabbagh, M., Vellas, B., Watson, D., Dhadda, S., Irizarry, M., Kramer, L. D., & Iwatsubo, T. (2023). Lecanemab in Early Alzheimer's Disease. *New England Journal of Medicine*, *388*(1), 9–21. https://doi.org/10.1056/nejmoa2212948

van Hoesen, G. W., Hyman, B. T., & Damasio, A. R. (1991). Entorhinal cortex pathology in alzheimer's disease. *Hippocampus*, *1*(1), 1–8. https://doi.org/10.1002/hipo.450010102

van Nifterick, A. M., Gouw, A. A., van Kesteren, R. E., Scheltens, P., Stam, C. J., & de Haan, W. (2022). A multiscale brain network model links Alzheimer's disease-mediated neuronal hyperactivity to large-scale oscillatory slowing. *Alzheimer's Research & Therapy*, *14*(1). https://doi.org/10.1186/s13195-022-01041-4

Vantomme, G., Osorio-Forero, A., Lüthi, A., & Fernandez, L. (2019). Regulation of Local Sleep by the Thalamic Reticular Nucleus. *Front Neurosci*, *13*, 576.

Vartiainen, N., Perchet, C., Magnin, M., Creac'h, C., Convers, P., Nighoghossian, N., Mauguière, F., Peyron, R., & Garcia-Larrea, L. (2016). Thalamic pain: anatomical and physiological indices of prediction. *Brain*, *139*, 708–22.

Verret, L., Mann, E. O., Hang, G. B., Barth, A. M., Cobos, I., Ho, K., Devidze, N., Masliah, E., Kreitzer, A. C., Mody, I., Mucke, L., & Palop, J. J. (2012). Inhibitory interneuron deficit links altered network activity and cognitive dysfunction in alzheimer model. *Cell*, *149*(3), 708–721. https://doi.org/10.1016/j.cell.2012.02.046

Vogel, J. W., Young, A. L., Oxtoby, N. P., Smith, R., Ossenkoppele, R., Strandberg, O. T., Joie, R. L., Aksman, L. M., Grothe, M. J., Iturria-Medina, Y., Pontecorvo, M. J., Devous, M. D., Rabinovici, G. D., Alexander, D. C., Lyoo, C. H., Evans, A. C., & Hansson, O. (2021). Four distinct trajectories of tau deposition identified in alzheimer's disease. *Nature Medicine*, *27*(5), 871–881. https://doi.org/10.1038/s41591-021-01309-6

Vogeti, S., Boetzel, C., & Herrmann, C. S. (2022). Entrainment and Spike-Timing dependent plasticity - a review of proposed mechanisms of transcranial alternating current stimulation. *Front. Syst. Neurosci.*, *16*, 827353.

Vossel, K., Ranasinghe, K. G., Beagle, A. J., La, A., Pook, K. A., Castro, M., Mizuiri, D., Honma, S. M., Venkateswaran, N., Koestler, M., Zhang, W., Mucke, L., Howell, M. J., Possin, K. L., Kramer, J. H., Boxer, A. L., Miller, B. L., Nagarajan, S. S., & Kirsch, H. E. (2021). Effect of levetiracetam on cognition in patients with alzheimer disease with and without epileptiform activity. *JAMA Neurology*, *78*(11), 1345. https://doi.org/10.1001/jamaneurol.2021.3310

Vossen, A., Gross, J., & Thut, G. (2015). Alpha power increase after transcranial alternating current stimulation at alpha frequency (α-tACS) reflects plastic changes rather than entrainment. *Brain Stimul.*, *8*(3), 499–508.

Walker, L. C. (2018). Prion-like mechanisms in Alzheimer disease. In *Human prion diseases* (pp. 303–319). Elsevier. https://doi.org/10.1016/b978-0-444-63945-5.00016-7

Wamsley, E. J. (2022). Offline memory consolidation during waking rest. *Nature Reviews Psychology*, *1*(8), 441–453. https://doi.org/10.1038/s44159-022-00072-w

Wang, B., Aberra, A. S., Grill, W. M., & Peterchev, A. V. (2023). Responses of model cortical neurons to temporal interference stimulation and related transcranial alternating current stimulation modalities. *J. Neural Eng.*, *19*(6).

Wang, Y., Hou, P., Li, W., Zhang, M., Zheng, H., & Chen, X. (2022). The influence of different current-intensity transcranial alternating current stimulation on the eyes-open and eyes-closed resting-state electroencephalography. *Frontiers in Human Neuroscience*, *16*, 934382.

Warrington, E. K., & Weiskrantz, L. (1970). Amnesic syndrome: Consolidation or retrieval? *Nature*, *228*(5272), 628–630. https://doi.org/10.1038/228628a0

Warrington, E. K., & Weiskrantz, L. (1978). Further analysis of the prior learning effect in amnesic patients. *Neuropsychologia*, *16*(2), 169–177. https://doi.org/10.1016/0028-3932(78)90104-5

Watson, J. D. (2010, May). *Avoid boring people*. Random House.

Watts, D., & Strogatz, S. (1998). Collective dynamics of 'small-world' networks. *Nature*, *393*, 440–2.

Webster, K., & Ro, T. (2020). Visual modulation of resting state α oscillations. *eNeuro*, *7*(1).

Weiler, M., Stieger, K. C., Long, J. M., & Rapp, P. R. (2019). Transcranial magnetic stimulation in alzheimer's disease: Are we ready? *eneuro*, *7*(1), ENEURO.0235–19.2019. https://doi.org/10.1523/eneuro.0235-19.2019

Weinshenker, D. (2008). Functional consequences of locus coeruleus degeneration in alzheimers disease. *Current Alzheimer Research*, *5*(3), 342–345. https://doi.org/10.2174/156720508784533286

Wendling, F., Bartolomei, F., Bellanger, J., & Chauvel, P. (2002). Epileptic fast activity can be explained by a model of impaired GABAergic dendritic inhibition. *Eur J Neurosci*, *15*, 1499–508.

Wendling, F., Benquet, P., Bartolomei, F., & Jirsa, V. (2016). Computational models of epileptiform activity. *Journal of Neuroscience Methods*, *260*, 233–251. https://doi.org/10.1016/j.jneumeth.2015.03.027

Wilcoxon, F. (1945). Individual comparisons by ranking methods. *Biometrics Bulletin*, *1*(6), 80–83.

Wilson, H., & Cowan, J. (1973). A mathematical theory of the functional dynamics of cortical and thalamic nervous tissue. *Kybernetik*, *13*, 55–80.

Wilson, M. A., & McNaughton, B. L. (1994). Reactivation of hippocampal ensemble memories during sleep. *Science*, *265*(5172), 676–679. https://doi.org/10.1126/science.8036517

Wiltgen, B. J., Brown, R. A., Talton, L. E., & Silva, A. J. (2004). New circuits for old memories. *Neuron*, *44*(1), 101–108. https://doi.org/10.1016/j.neuron.2004.09.015

Wimmer, R., Schmitt, L., Davidson, T., Nakajima, M., Deisseroth, K., & Halassa, M. (2015). Thalamic control of sensory selection in divided attention. *Nature*, *526*, 705–9.

Wischnewski, M., Alekseichuk, I., & Opitz, A. (2023). Neurocognitive, physiological, and biophysical effects of transcranial alternating current stimulation. *Trends Cogn. Sci.*, *27*(2), 189–205.

Wolff, M., & Vann, S. D. (2018). The Cognitive Thalamus as a Gateway to Mental Representations. *The Journal of Neuroscience*, *39*(1), 3–14. https://doi.org/10.1523/jneurosci.0479-18.2018

Wong, K., & Wang, X. (2006). A recurrent network mechanism of time integration in perceptual decisions. *J Neurosci*, *26*, 1314–28.

Wood, E. R., Dudchenko, P. A., Robitsek, R., & Eichenbaum, H. (2000). Hippocampal neurons encode information about different types of memory episodes occurring in the same location. *Neuron*, *27*(3), 623–633. https://doi.org/10.1016/s0896-6273(00)00071-4

Wu, Y., Wu, X., Gao, L., Yan, Y., Geng, Z., Zhou, S., Zhu, W., Tian, Y., Yu, Y., Wei, L., & Wang, K. (2022). Abnormal functional connectivity of thalamic subdivisions in alzheimer's disease: A functional magnetic resonance imaging study. *Neuroscience*, *496*, 73–82. https://doi.org/10.1016/j.neuroscience.2022.06.006

Wurtz, R. H. (2009). Recounting the impact of hubel and wiesel. *The Journal of Physiology*, *587*(12), 2817–2823. https://doi.org/10.1113/jphysiol.2009.170209

Xia, X., Jiang, Q., McDermott, J., & Han, J.-D. J. (2018). Aging and alzheimer's disease: Comparison and associations from molecular to system level. *Aging Cell*, *17*(5). https://doi.org/10.1111/acel.12802

Yamamoto, K., Tanei, Z.-i., Hashimoto, T., Wakabayashi, T., Okuno, H., Naka, Y., Yizhar, O., Fenno, L. E., Fukayama, M., Bito, H., Cirrito, J. R., Holtzman, D. M., Deisseroth, K., & Iwatsubo, T. (2015). Chronic Optogenetic Activation Augments Aβ Pathology in a Mouse Model of Alzheimer Disease. *Cell Reports*, *11*(6), 859–865. https://doi.org/10.1016/j.celrep.2015.04.017

Yamamoto, T., & Hirano, A. (1985). Nucleus raphe dorsalis in alzheimer's disease: Neurofibrillary tangles and loss of large neurons. *Annals of Neurology*, *17*(6), 573–577. https://doi.org/10.1002/ana.410170608

Yamazaki, K., Vo-Ho, V.-K., Bulsara, D., & Le, N. (2022). Spiking neural networks and their applications: A review. *Brain Sciences*, *12*(7), 863. https://doi.org/10.3390/brainsci12070863

Yeh, C.-H., Jones, D. K., Liang, X., Descoteaux, M., & Connelly, A. (2020). Mapping structural connectivity using diffusion <scp>mri</scp>: Challenges and opportunities. *Journal of Magnetic Resonance Imaging*, *53*(6), 1666–1682. https://doi.org/10.1002/jmri.27188

Yeh, F.-C. (2020). Shape analysis of the human association pathways. *NeuroImage*, *223*, 117329. https://doi.org/10.1016/j.neuroimage.2020.117329

Yeh, F.-C., Liu, L., Hitchens, T. K., & Wu, Y. L. (2016). Mapping immune cell infiltration using restricted diffusion MRI. *Magnetic Resonance in Medicine*, *77*(2), 603–612. https://doi.org/10.1002/mrm.26143

Yeh, F.-C., Verstynen, T. D., Wang, Y., Fernández-Miranda, J. C., & Tseng, W.-Y. I. (2013). Deterministic Diffusion Fiber Tracking Improved by Quantitative Anisotropy (W. Zhan, Ed.). *PLoS ONE*, *8*(11), e80713. https://doi.org/10.1371/journal.pone.0080713

Yeh, F., Wedeen, V., & Tseng, W. (2010). Generalized q-sampling imaging. *IEEE Trans Med Imaging*, *29*, 1626–35.

Yu, J., Lam, C., & Lee, T. (2017). White matter microstructural abnormalities in amnestic mild cognitive impairment: A meta-analysis of whole-brain and ROI-based studies. *Neurosci Biobehav Rev*, *83*, 405–416.

Yuste, R., & Bargmann, C. (2017). Toward a global brain initiative. *Cell*, *168*(6), 956–959. https://doi.org/10.1016/j.cell.2017.02.023

Zaehle, T., Rach, S., & Herrmann, C. S. (2010). Transcranial alternating current stimulation enhances individual alpha activity in human EEG. *PLoS One*, *5*(11), e13766.

Zarubin, G., Gundlach, C., Nikulin, V., Villringer, A., & Bogdan, M. (2020). Transient amplitude modulation of Alpha-Band oscillations by Short-Time intermittent Closed-Loop tACS. *Front. Hum. Neurosci.*, *14*, 366.

Zetterberg, L. H., Kristiansson, L., & Mossberg, K. (1978). Performance of a model for a local neuron population. *Biological Cybernetics*, *31*(1), 15–26. https://doi.org/10.1007/bf00337367

Zhang, C. H., Sha, Z., Mundahl, J., Liu, S., Lu, Y., Henry, T. R., & He, B. (2015). Thalamocortical relationship in epileptic patients with generalized spike and wave discharges — a multimodal neuroimaging study. *NeuroImage: Clinical*, *9*, 117–127. https://doi.org/10.1016/j.nicl.2015.07.014

Zhang, N. K., Zhang, S. K., Zhang, L. I., Tao, H. W., & Zhang, G.-W. (2023). Sensory processing deficits and related cortical pathological changes in alzheimer's disease. *Frontiers in Aging Neuroscience*, *15*. https://doi.org/10.3389/fnagi.2023.1213379

Zhang, X.-X., Tian, Y., Wang, Z.-T., Ma, Y.-H., Tan, L., & Yu, J.-T. (2021). The epidemiology of alzheimer's disease modifiable risk factors and prevention. *The Journal of Prevention of Alzheimer's Disease*, 1–9. https://doi.org/10.14283/jpad.2021.15

Zhou, B., Liu, Y., Zhang, Z., An, N., Yao, H., Wang, P., Wang, L., Zhang, X., & Jiang, T. (2013). Impaired functional connectivity of the thalamus in alzheimer's disease and mild cognitive impairment: A resting-state fmri study. *Current Alzheimer Research*, *10*(7), 754–766. https://doi.org/10.2174/15672050113109990146

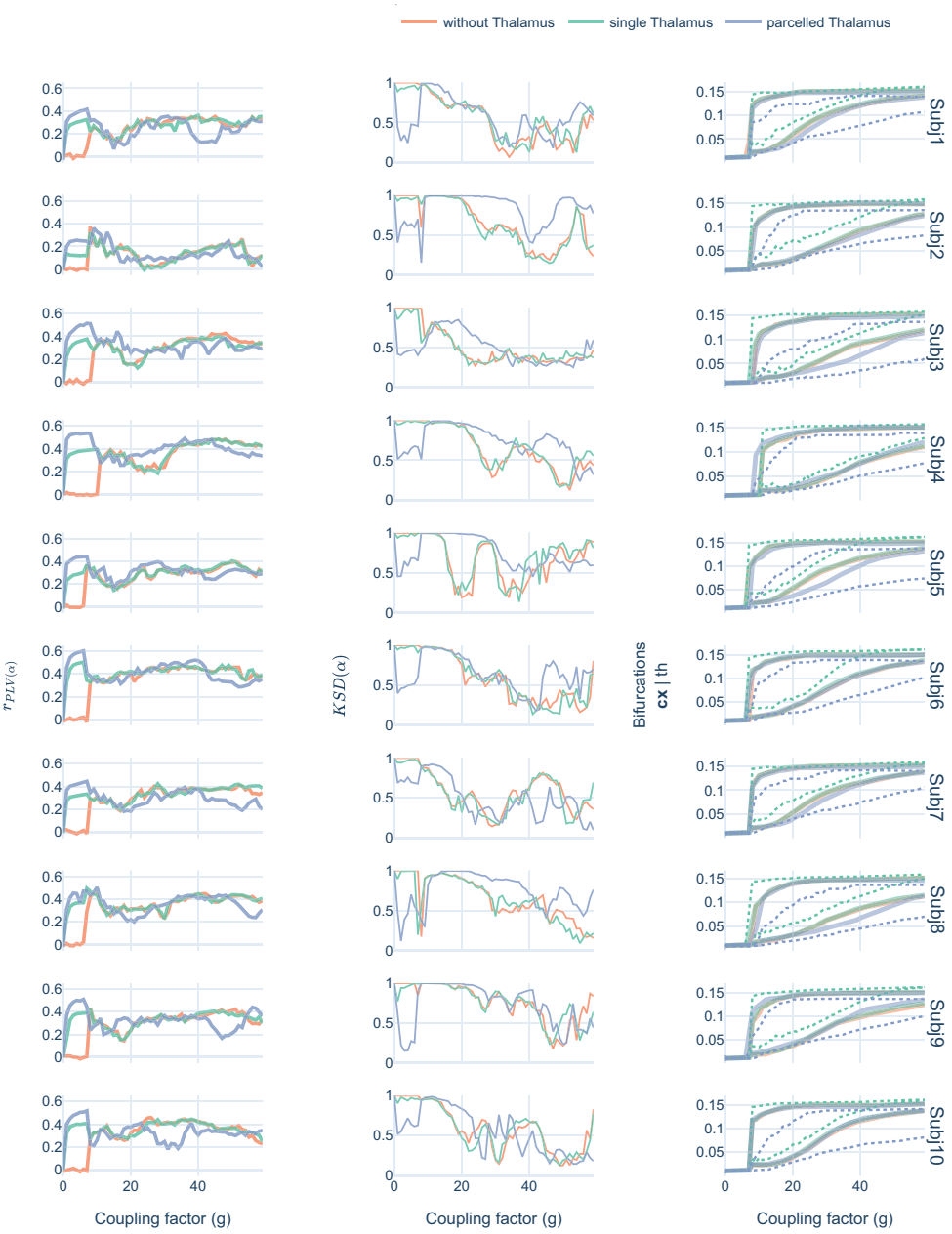
Zimmermann, J., Perry, A., Breakspear, M., Schirner, M., Sachdev, P., Wen, W., Kochan, N., Mapstone, M., Ritter, P., McIntosh, A., & Solodkin, A. (2018). Differentiation of Alzheimer's disease based on local and global parameters in personalized Virtual Brain models. *Neuroimage Clin*, *19*, 240–251.

Zott, B., Simon, M. M., Hong, W., Unger, F., Chen-Engerer, H.-J., Frosch, M. P., Sakmann, B., Walsh, D. M., & Konnerth, A. (2019). A vicious cycle of β amyloid–dependent neuronal hyperactivation. *Science*, *365*(6453), 559–565. https://doi.org/10.1126/science.aay0198

Appendix

A1 Supporting information from Chapter 2

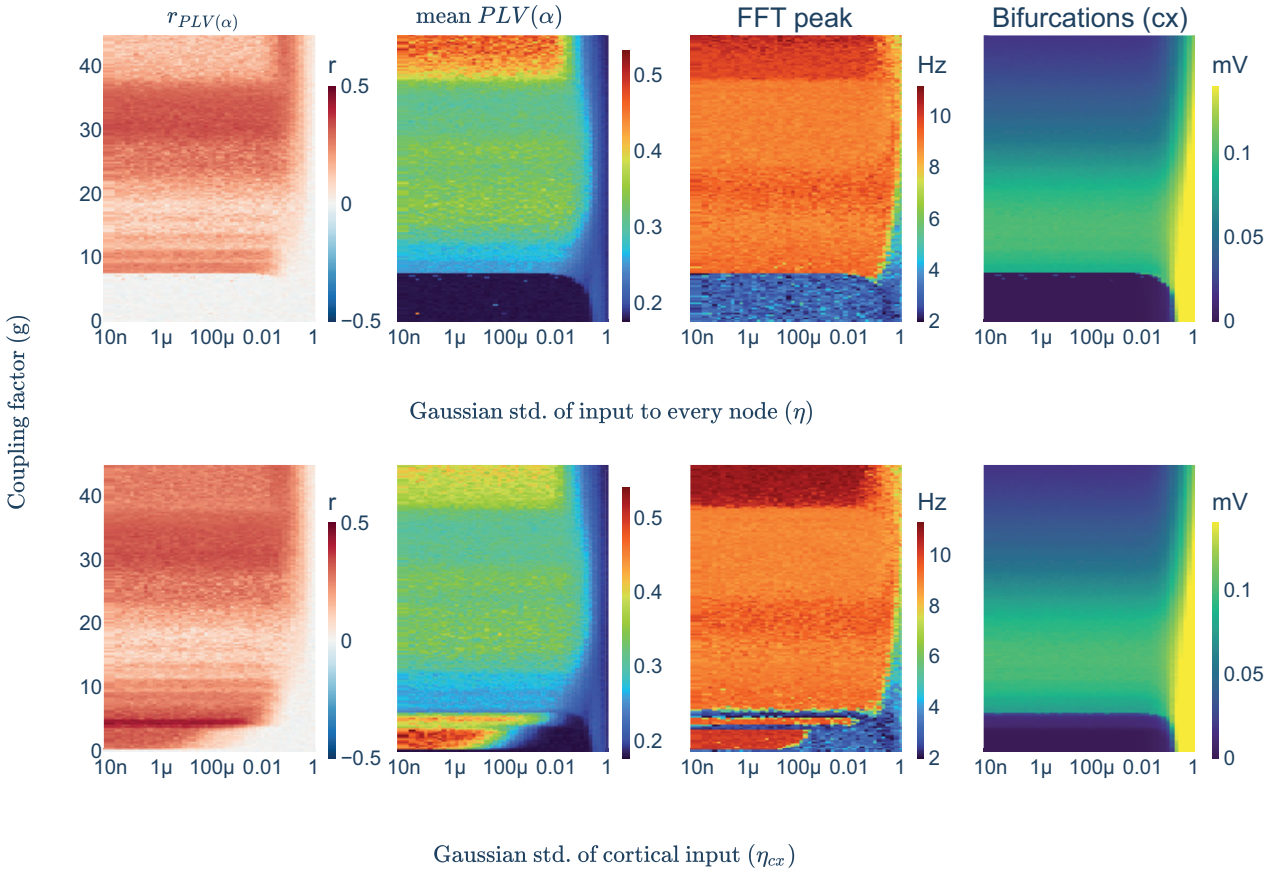
S1 Fig. **Lineplots showing $r_{PLV(\alpha)}$, KSD(α) and bifurcations per subject and SC version.** The global behavior in r_{PLV} (first column) was similar for every subject. Note slight differences for subject 2 and subject 8 in which the bifurcation does not match the highest r_{PLV} value.



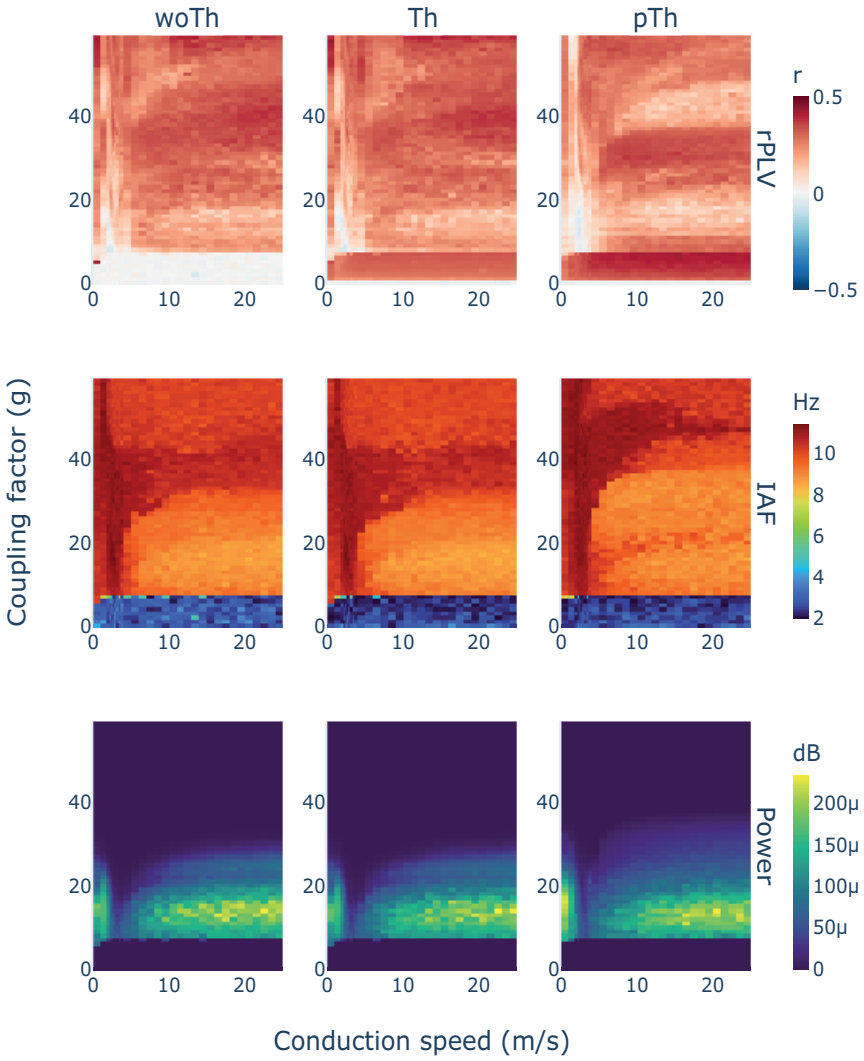
S2 Fig. **Empirical and simulated distributions of Pearson's correlation values in dFC matrices.** Simulations were performed for subject 1 with high thalamic noise (η_{th}=0.022) and in both prebifurcation (g=[3, 7]) and postbifurcation 2 (g=[9, 40]). The three thalamocortical SC (i.e., woTh, Th, pTh) versions were simulated.



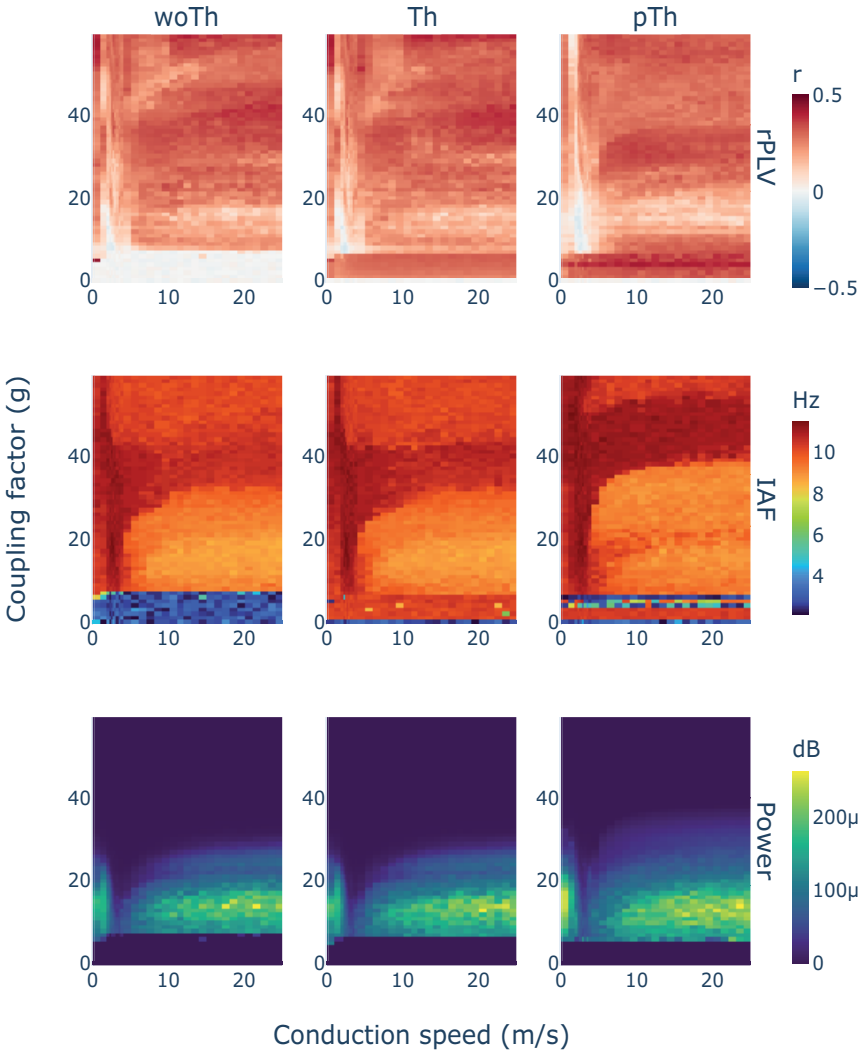
S3 Fig. **Rising cortical noise hampers $r_{PLV(\alpha)}$.** First row, showing simulations where all nodes have the same parametrization (p=0.09; η=variable). Second row, showing simulations with the thalamus in limit cycle condition p_{th}=0.15, η_{th}=0.09) and a variable noisy input to cortical nodes (p_{cx}=0.09, η_{cx}=variable).



S4 Fig. **Parameter space explorations for conduction speed and coupling factor in the BNM with initial parameters.** The model was parameterized as in the first in-silico experiment shown in Fig 2.5F (i.e., the thalamocortical experiment with high thalamic noise p_{th}=0.09, eta_{th}=0.022, p_{cx}=0.09, η_{cx}=2.2e-8). Each column shows a set of simulations with a different SC version: woTh, Th, and pTh. The three heatmaps shown per column represent different measures of the same simulation including $r_{PLV(\alpha)}$, IAF as the frequency peak of the averaged spectrum from all nodes, and the power at the frequency peak of the averaged spectrum.



S5 Fig. **Parameter space explorations for conduction speed and coupling factor in the BNM with final parameters.** The model was parameterized following the last in-silico experiments to obtain alpha in prebifurcation as shown in Fig 7 second last column (i.e., p_{th}=0.15, eta_{th}=0.09, p_{cx}=0.09, η_{cx}=2.2e-8). Each column shows a set of simulations with a different SC version: woTh, Th, and pTh. The three heatmaps shown per column represent different measures of the same simulation including $r_{PLV(\alpha)}$, IAF as the frequency peak of the averaged spectrum from all nodes, and the power at the frequency peak of the averaged spectrum.



S1 Table. **Network analysis of the regions included in the BNMs.** Degree, the number of neighbors of a region, and node strength, the average number of streamlines connecting a region to others were normalized over their respective maxima. Betweenness captures the number of shortest paths in a network that passes through a node. Path length stands for the average of the shortest paths for a node. Metrics were calculated with Networkx package in Python 3.9. The thalamus and the cerebellum are considered here in the parceled version. Note that Cingulate_Ant in AAL3 is divided in 3 parts and it was merged to match AAL2 scheme.

Region	Degree	Node strength	Betweenness	Path Length
Precentral_L	0.918367347	0.411938242	0.001546129	1.074324324
Precentral_R	0.965986395	0.335545483	0.001884953	1.027027027
Frontal_Sup_2_L	0.993197279	1	0.0023881	1
Frontal_Sup_2_R	0.993197279	0.95025204	0.002295448	1
Frontal_Mid_2_L	0.959183673	0.516657622	0.001914868	1.033783784
Frontal_Mid_2_R	0.863945578	0.3943357	0.001191249	1.128378378
Frontal_Inf_Oper_L	0.442176871	0.143038601	0.000105797	1.547297297
Frontal_Inf_Oper_R	0.578231293	0.167206469	0.000344411	1.412162162
Frontal_Inf_Tri_L	0.761904762	0.226736794	0.000721287	1.22972973
Frontal_Inf_Tri_R	0.551020408	0.191822312	0.000311354	1.439189189
Frontal_Inf_Orb_2_L	0.775510204	0.194359749	0.000820392	1.216216216
Frontal_Inf_Orb_2_R	0.795918367	0.195242561	0.000902263	1.195945946
Rolandic_Oper_L	0.721088435	0.284508522	0.000662726	1.27027027
Rolandic_Oper_R	0.591836735	0.198623849	0.000355736	1.398648649
Supp_Motor_Area_L	0.891156463	0.127450576	0.001233648	1.101351351
Supp_Motor_Area_R	0.891156463	0.16419661	0.001307158	1.101351351
Olfactory_L	0.904761905	0.060733993	0.001619367	1.087837838
Olfactory_R	0.782312925	0.06735776	0.000878651	1.209459459

Region	Degree	Node strength	Betweenness	Path Length
Frontal_Sup_Medial_L	0.925170068	0.29824941	0.001548317	1.067567568
Frontal_Sup_Medial_R	0.986394558	0.298481495	0.002225148	1.006756757
Frontal_Med_Orb_L	0.714285714	0.122914054	0.000504673	1.277027027
Frontal_Med_Orb_R	0.93877551	0.232150628	0.001739542	1.054054054
Rectus_L	0.721088435	0.076202538	0.000694964	1.27027027
Rectus_R	0.80952381	0.111050709	0.001042469	1.182432432
OFCmed_L	0.945578231	0.22522793	0.001911244	1.047297297
OFCmed_R	0.918367347	0.13301781	0.001668805	1.074324324
OFCant_L	0.952380952	0.346564442	0.001867995	1.040540541
OFCant_R	0.93877551	0.170329391	0.001741718	1.054054054
OFCpost_L	0.727891156	0.114935282	0.000719047	1.263513514
OFCpost_R	0.782312925	0.147056941	0.00071357	1.209459459
OFClat_L	0.693877551	0.067920251	0.000605943	1.297297297
OFClat_R	0.56462585	0.061913445	0.000302461	1.425675676
Insula_L	0.904761905	0.406145416	0.001414035	1.087837838
Insula_R	0.823129252	0.371356756	0.000954644	1.168918919
Cingulate_Mid_L	0.80952381	0.155997746	0.000753708	1.182432432
Cingulate_Mid_R	0.87755102	0.313251109	0.001144878	1.114864865
Cingulate_Post_L	0.761904762	0.108920912	0.000849097	1.22972973
Cingulate_Post_R	0.761904762	0.148953658	0.000952696	1.22972973
Hippocampus_L	0.972789116	0.392770992	0.002023826	1.02027027
Hippocampus_R	0.986394558	0.411021358	0.002161705	1.006756757
ParaHippocampal_L	0.986394558	0.274124781	0.002217546	1.006756757
ParaHippocampal_R	0.986394558	0.306542239	0.002216356	1.006756757
Amygdala_L	0.904761905	0.139268849	0.001423356	1.087837838
Amygdala_R	0.965986395	0.254011846	0.001922705	1.027027027

Region	Degree	Node strength	Betweenness	Path Length
Calcarine_L	0.931972789	0.265018964	0.001823924	1.060810811
Calcarine_R	0.863945578	0.336179326	0.001168752	1.128378378
Cuneus_L	0.850340136	0.203335084	0.001326773	1.141891892
Cuneus_R	0.850340136	0.247474252	0.001139246	1.141891892
Lingual_L	0.965986395	0.435293351	0.002012088	1.027027027
Lingual_R	0.911564626	0.39456641	0.001512448	1.081081081
Occipital_Sup_L	0.925170068	0.378044007	0.001686895	1.067567568
Occipital_Sup_R	0.870748299	0.390550286	0.001196135	1.121621622
Occipital_Mid_L	0.87755102	0.336411412	0.00136853	1.114864865
Occipital_Mid_R	0.714285714	0.2011457	0.000566966	1.277027027
Occipital_Inf_L	0.782312925	0.152632654	0.000874611	1.209459459
Occipital_Inf_R	0.632653061	0.105192718	0.000349623	1.358108108
Fusiform_L	0.972789116	0.57517809	0.001987875	1.02027027
Fusiform_R	0.965986395	0.62368449	0.0019321	1.027027027
Postcentral_L	0.965986395	0.407245494	0.002068254	1.027027027
Postcentral_R	0.986394558	0.44050474	0.002161705	1.006756757
Parietal_Sup_L	0.891156463	0.329406896	0.001426498	1.101351351
Parietal_Sup_R	0.918367347	0.302757437	0.001661659	1.074324324
Parietal_Inf_L	0.789115646	0.295493257	0.000957651	1.202702703
Parietal_Inf_R	0.707482993	0.2488453	0.00049724	1.283783784
SupraMarginal_L	0.428571429	0.150555341	6.14E-05	1.560810811
SupraMarginal_R	0.653061224	0.270345021	0.000453808	1.337837838
Angular_L	0.646258503	0.157167572	0.000394289	1.344594595
Angular_R	0.693877551	0.25413889	0.00059126	1.297297297
Precuneus_L	0.897959184	0.354903031	0.001603488	1.094594595
Precuneus_R	0.904761905	0.392869617	0.001439436	1.087837838

Region	Degree	Node strength	Betweenness	Path Length
Paracentral_Lobule_L	0.823129252	0.081811636	0.000767938	1.168918919
Paracentral_Lobule_R	0.56462585	0.068897105	0.0001041	1.425675676
Caudate_L	1	0.448506431	0.00247488	0.993243243
Caudate_R	0.986394558	0.525835097	0.00213861	1.006756757
Putamen_L	0.986394558	0.728753374	0.002182358	1.006756757
Putamen_R	0.986394558	0.810242625	0.002161705	1.006756757
Pallidum_L	0.979591837	0.320952799	0.002206762	1.013513514
Pallidum_R	0.986394558	0.327206359	0.002161705	1.006756757
Heschl_L	0.714285714	0.123553245	0.000710599	1.277027027
Heschl_R	0.646258503	0.08731615	0.000397898	1.344594595
Temporal_Sup_L	0.673469388	0.315444541	0.000559123	1.317567568
Temporal_Sup_R	0.714285714	0.310476315	0.00057364	1.277027027
Temporal_Pole_Sup_L	0.863945578	0.235587377	0.001271836	1.128378378
Temporal_Pole_Sup_R	0.802721088	0.242571267	0.000818947	1.189189189
Temporal_Mid_L	0.496598639	0.280075209	0.000143476	1.493243243
Temporal_Mid_R	0.496598639	0.279250914	0.000154803	1.493243243
Temporal_Pole_Mid_L	0.707482993	0.128918263	0.000550049	1.283783784
Temporal_Pole_Mid_R	0.789115646	0.231552307	0.000792529	1.202702703
Temporal_Inf_L	0.836734694	0.372036513	0.001270697	1.155405405
Temporal_Inf_R	0.802721088	0.357170032	0.000830474	1.189189189
Cerebelum_Crus1_L	0.911564626	0.417775071	0.001507644	1.081081081
Cerebelum_Crus1_R	0.931972789	0.35366002	0.001792323	1.060810811
Cerebelum_Crus2_L	0.863945578	0.23766492	0.001194357	1.128378378
Cerebelum_Crus2_R	0.870748299	0.231927862	0.001269097	1.121621622
Cerebelum_3_L	0.850340136	0.085015459	0.001175118	1.141891892
Cerebelum_3_R	0.918367347	0.138093522	0.001301984	1.074324324

Region	Degree	Node strength	Betweenness	Path Length
Cerebelum_4_5_L	0.925170068	0.361317936	0.001595558	1.067567568
Cerebelum_4_5_R	0.918367347	0.280315469	0.001562054	1.074324324
Cerebelum_6_L	0.918367347	0.414863991	0.001580167	1.074324324
Cerebelum_6_R	0.925170068	0.426231537	0.001644494	1.067567568
Cerebelum_7b_L	0.870748299	0.195382363	0.00112414	1.121621622
Cerebelum_7b_R	0.768707483	0.103823045	0.000717444	1.222972973
Cerebelum_8_L	0.87755102	0.223480258	0.001140974	1.114864865
Cerebelum_8_R	0.884353741	0.212459924	0.001378099	1.108108108
Cerebelum_9_L	0.897959184	0.122023373	0.001414779	1.094594595
Cerebelum_9_R	0.904761905	0.121993121	0.001347845	1.087837838
Cerebelum_10_L	0.795918367	0.041547033	0.000836284	1.195945946
Cerebelum_10_R	0.857142857	0.056206868	0.001094343	1.135135135
Vermis_1_2	0.680272109	0.019445478	0.000320535	1.310810811
Vermis_3	0.653061224	0.04806889	0.000204665	1.337837838
Vermis_4_5	0.789115646	0.178812136	0.000775413	1.202702703
Vermis_6	0.727891156	0.13342522	0.000533768	1.263513514
Vermis_7	0.653061224	0.098765973	0.000246492	1.337837838
Vermis_8	0.537414966	0.062579603	3.93E-05	1.452702703
Vermis_9	0.557823129	0.034807147	5.25E-05	1.432432432
Vermis_10	0.74829932	0.017687111	0.000672468	1.243243243
Thal_AV_L	0.714285714	0.051685777	0.000552927	1.277027027
Thal_AV_R	0.891156463	0.069568763	0.001255903	1.101351351
Thal_LP_L	0.68707483	0.055845676	0.000432939	1.304054054
Thal_LP_R	0.755102041	0.048958578	0.000582604	1.236486486
Thal_VA_L	1	0.297879814	0.00247488	0.993243243
Thal_VA_R	0.979591837	0.251665243	0.002004866	1.013513514

Region	Degree	Node strength	Betweenness	Path Length
Thal_VL_L	0.925170068	0.206480161	0.001593343	1.067567568
Thal_VL_R	0.959183673	0.173461709	0.001802582	1.033783784
Thal_VPL_L	0.945578231	0.208632188	0.001746287	1.047297297
Thal_VPL_R	0.93877551	0.17569502	0.001617293	1.054054054
Thal_IL_L	0.93877551	0.141914918	0.00168265	1.054054054
Thal_IL_R	0.972789116	0.134965176	0.001967677	1.02027027
Thal_Re_L	0.530612245	0.00878328	0.000109791	1.459459459
Thal_Re_R	0.43537415	0.003136444	0.000109735	1.554054054
Thal_MDm_L	0.959183673	0.151191781	0.001976765	1.033783784
Thal_MDm_R	0.952380952	0.138735005	0.001831275	1.040540541
Thal_MDl_L	0.782312925	0.072102456	0.000803595	1.209459459
Thal_MDl_R	0.857142857	0.063591674	0.001184081	1.135135135
Thal_LGN_L	0.755102041	0.048128859	0.000604553	1.236486486
Thal_LGN_R	0.775510204	0.037446723	0.000816497	1.216216216
Thal_MGN_L	0.836734694	0.083425694	0.0010506	1.155405405
Thal_MGN_R	0.857142857	0.047934894	0.001017724	1.135135135
Thal_PuA_L	0.911564626	0.088389489	0.001543893	1.081081081
Thal_PuA_R	0.891156463	0.06723148	0.001255918	1.101351351
Thal_PuM_L	0.93877551	0.191185795	0.00166836	1.054054054
Thal_PuM_R	0.93877551	0.148707821	0.00155492	1.054054054
Thal_PuL_L	0.863945578	0.118779366	0.001244586	1.128378378
Thal_PuL_R	0.918367347	0.104040845	0.001386789	1.074324324
Thal_PuI_L	0.80952381	0.081264194	0.000915122	1.182432432
Thal_PuI_R	0.80952381	0.053238873	0.000815913	1.182432432
Cingulate_Ant_L	0.714285714	0.189355694	0.000539511	1.290540541
Cingulate_Ant_R	0.73	0.260201999	0.000468661	1.277027027

Region	Degree	Node strength	Betweenness	Path Length
Global average	0.827082184	0.231314071	0.001185628	1.16517531
Thalamus average	0.851020408	0.110802257	0.001253469	1.141216216
Cerebellum average	0.882842026	0.223543432	0.001315372	1.10960961

A2 Extended data from Chapter 3

Code developed in Python 3.9 to simulate and visualize the closed-loop neurotoxicity model.

Figure 2-1. 2D representations of single node experiments varying only one parameter at a time (i.e., H_e, C_{ip}, C_{ep}, p). Dashed lines showing the default parameter value. Markers' colour scales are the same as in the heatmaps of Figure 3.2.

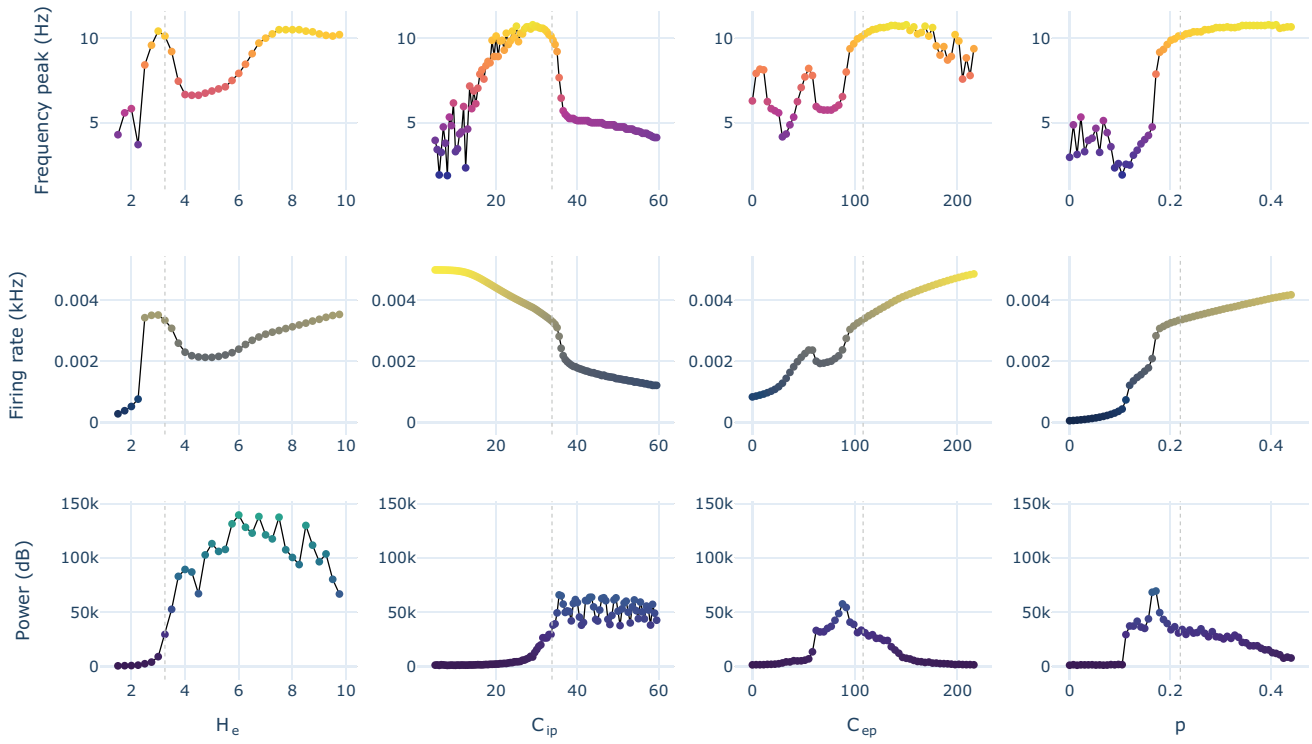


Figure 2-2. Timeseries and spectra for three different regimes shown in Figure 2: slow limit cycle, fast limit cycle and fixed point state. Two traces from independent simulations are shown.

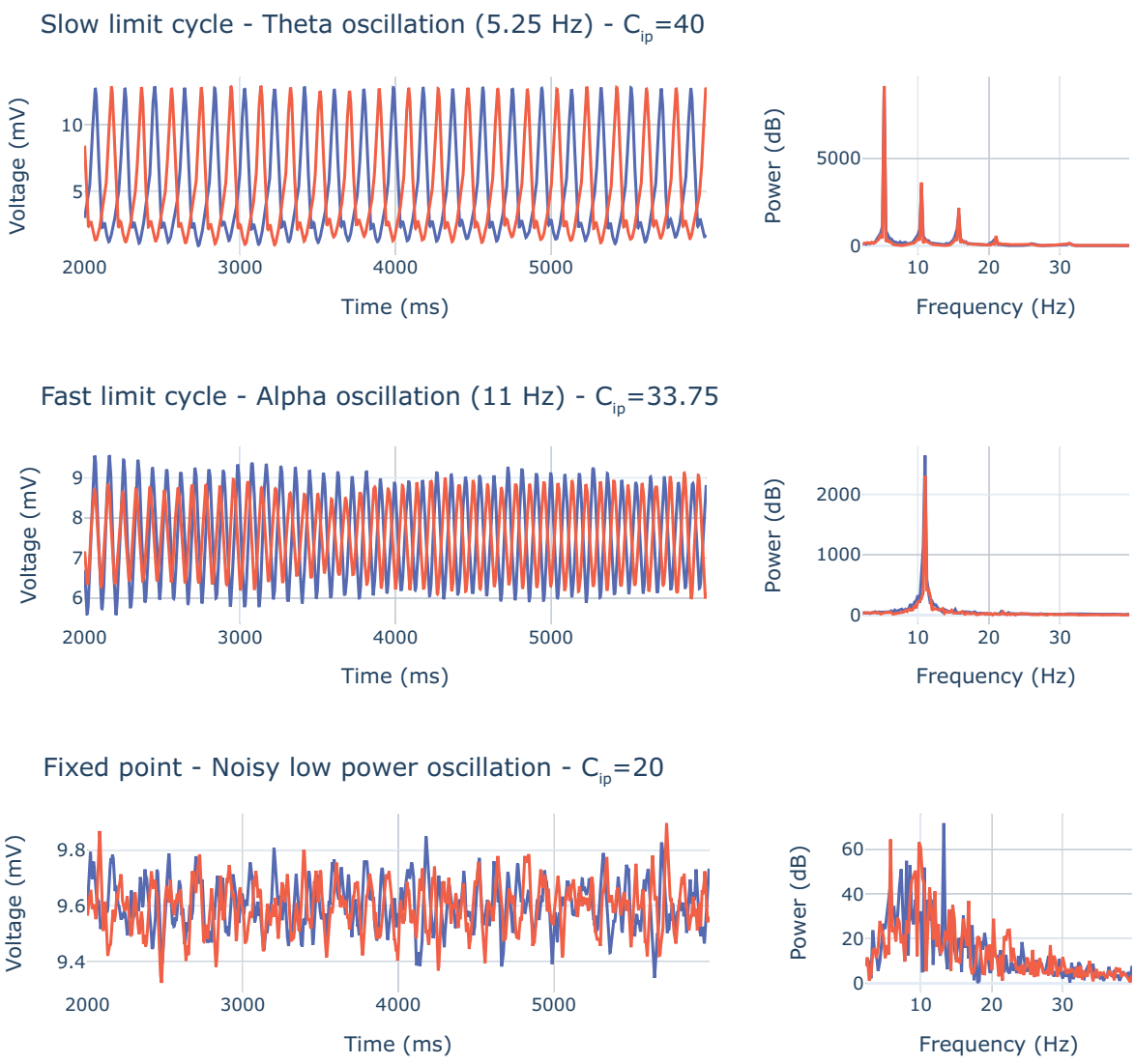


Figure 3-1. Parameter trajectories of the simulated closed-loop model with default parameters on heatmaps from single node experiments. Trajectories are represented as curves with varying colours. The colour represents time: starting in red and ending with blue. Note that heatmaps are extracted from single-node simulations in which just two parameters are varied at a time, while the trajectories imply a 4-dimensional parameter change. Therefore, the underlying heatmaps should be interpreted just as an orientation of what might happen when changing parameters in one direction.

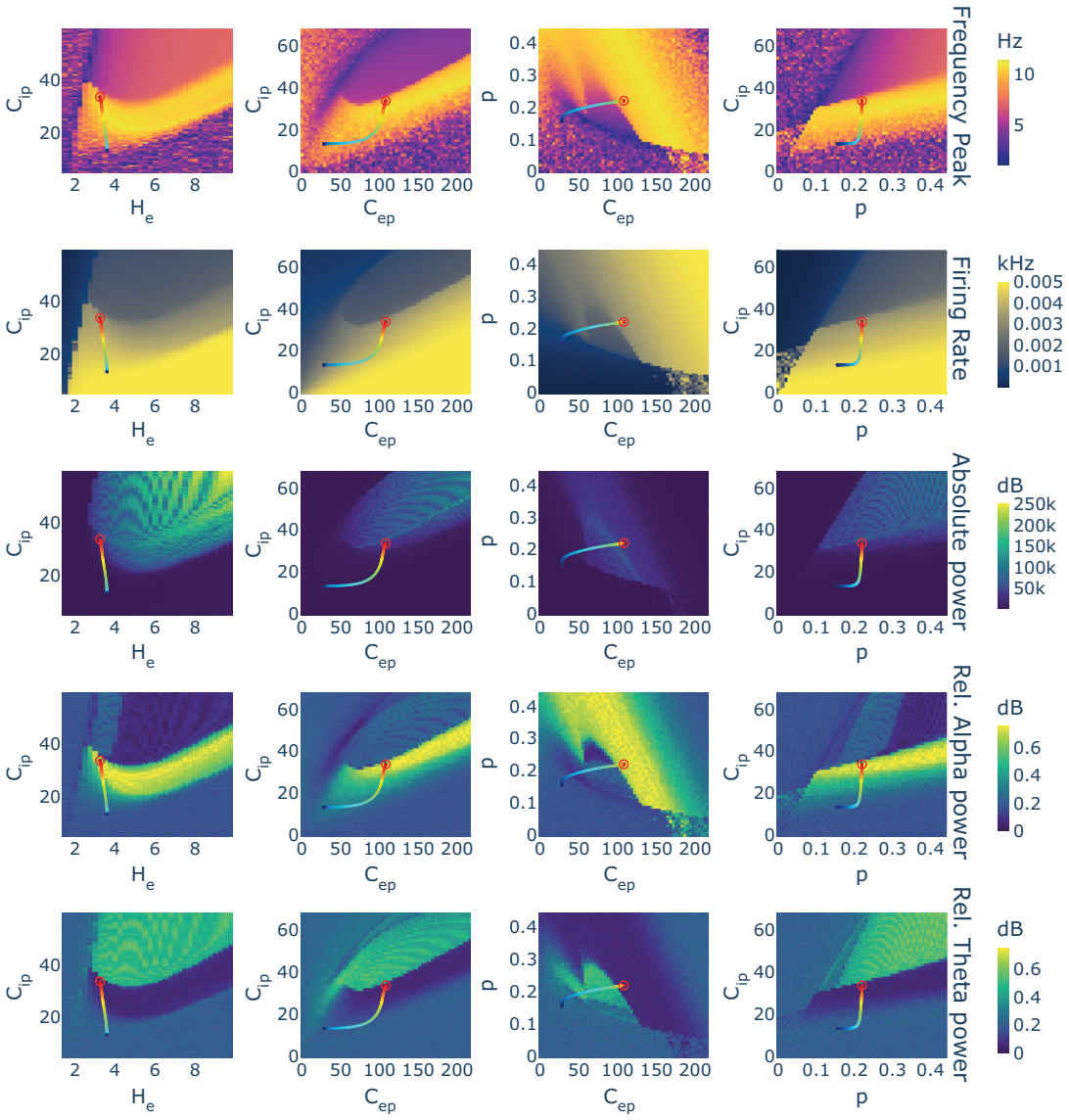


Figure 4-1. Averaged FC (PLV) of the simulated closed-loop model with default parameters for different frequency bands: delta (2 - 4 Hz), theta (4 - 8 Hz) and alpha (8 - 12 Hz).

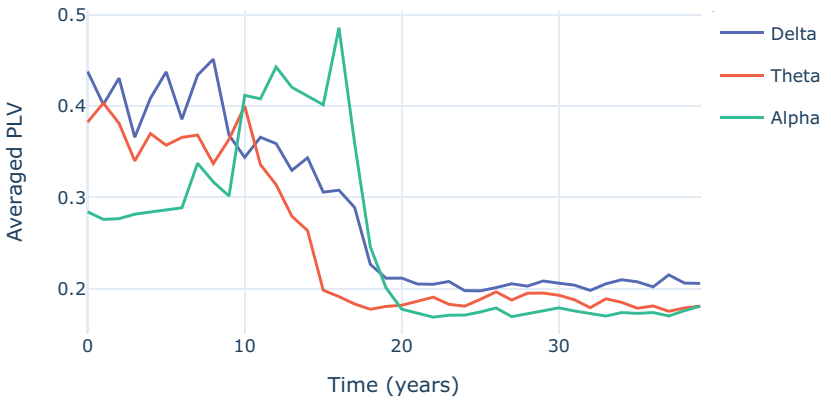


Figure 4-2. Normalized spectra per region over time (yrs.). Note the transition of all spectra to more noisy states with lower frequency peaks.

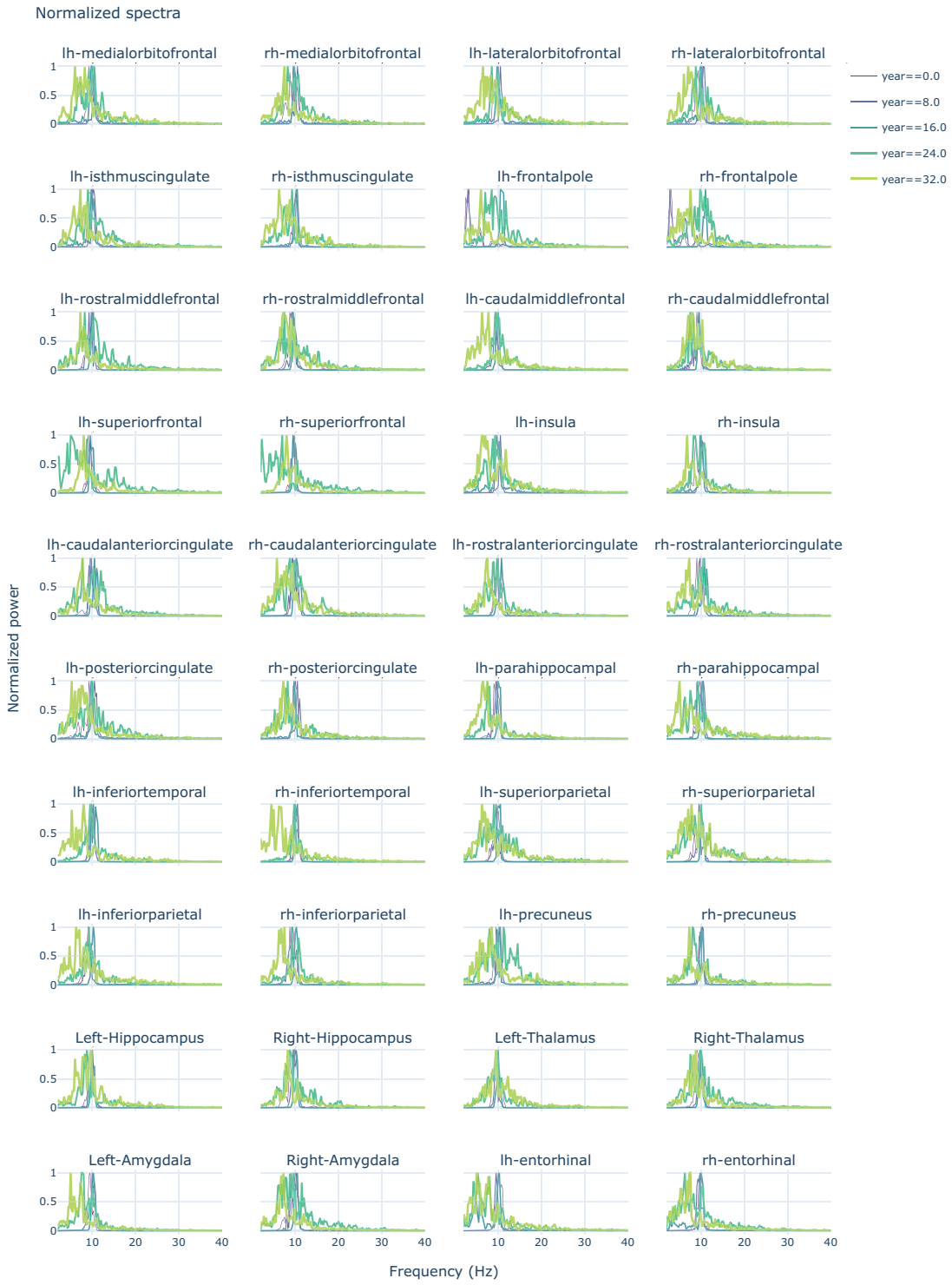


Figure 5-1. Parameter spaces to select working point. Selected parameters were g=25 and s=20 m/s (see red highlights). Note how the rising of g leads to a situation in which no FC rise is observed, similar to the reduction of s, due to high early FC levels. Also, lowering g leads to the prebifurcation regime of the JR NMMs, a situation in which the spectral frequency peak lowers towards the delta band.

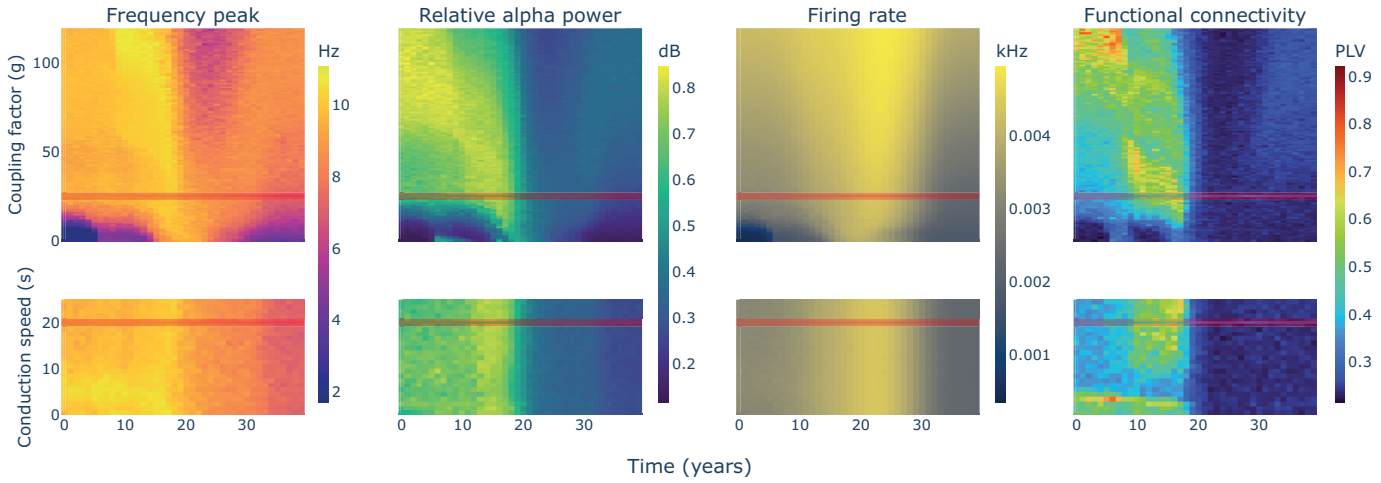
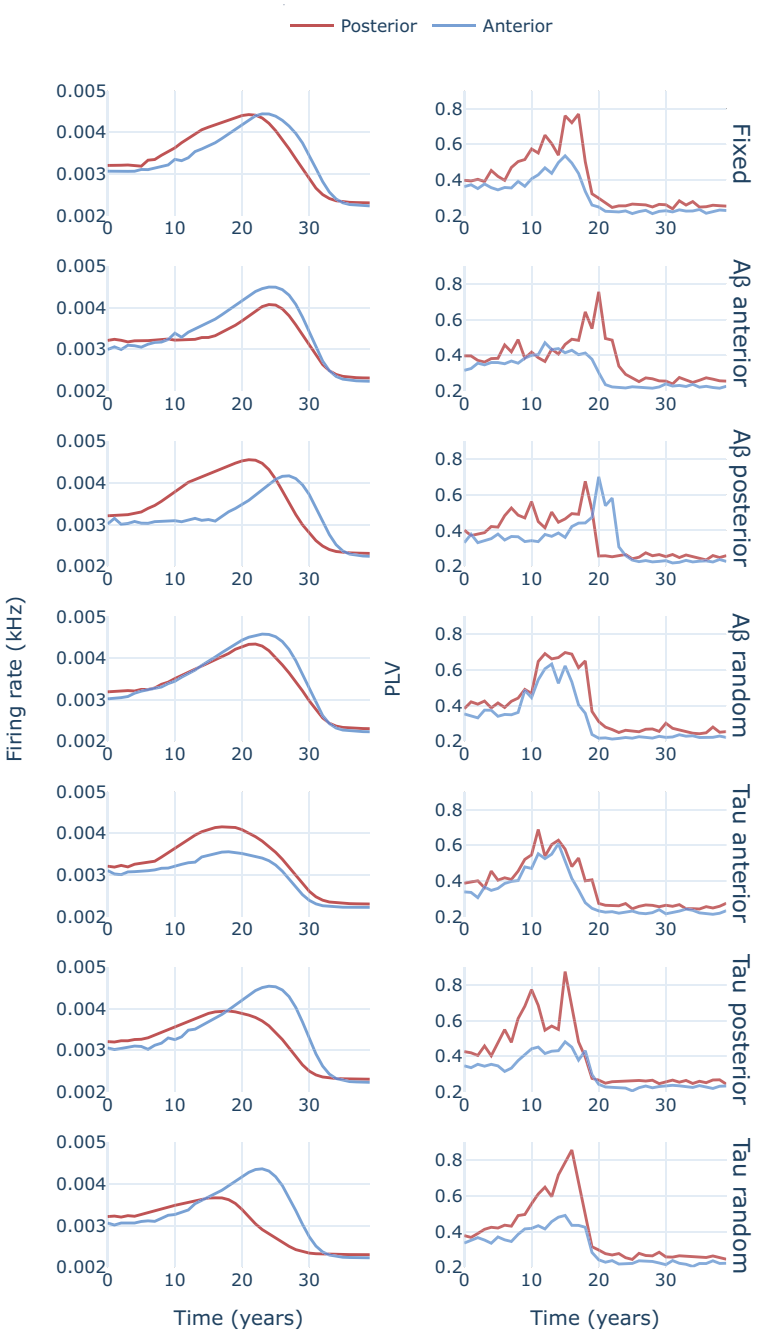


Figure 8-1. Samples of the evolution for firing rate (left column) and FC (i.e., PLV; right column) in the antero-posterior differentiation experiments. In rows, each of the four seeding implemented strategies. The effect on FC is limited to a temporal shift of the curves, however, the seeding affects the level of hyperactivity reached by the anterior or posterior regions.



A3 Supplementary data from Chapter 4

Figure SM1. Distributions of the normal components in the cortical regions of AAL.

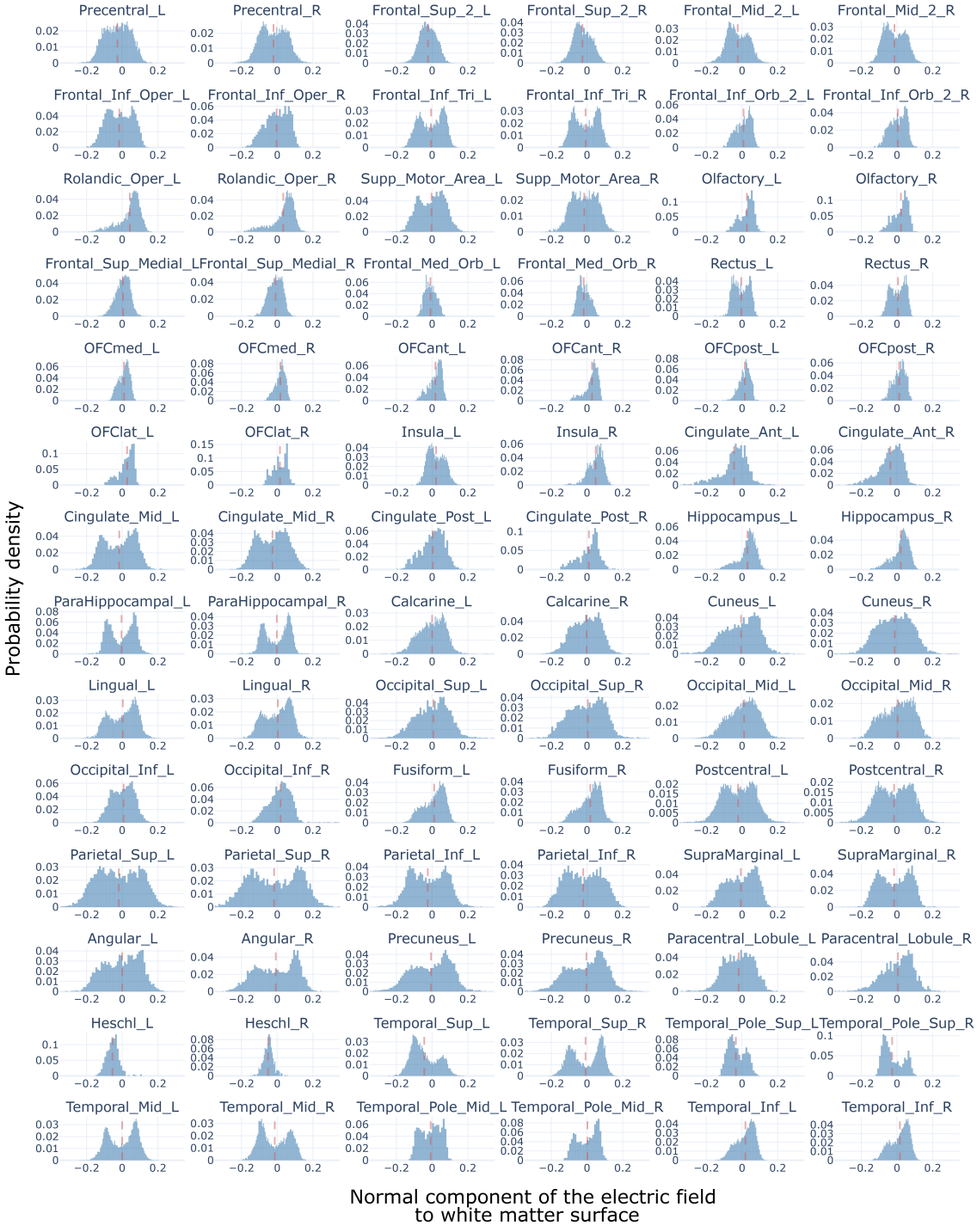


Figure SM2. Working points for the subjects in the computational sample. Simulating each virtual brain network for a range of coupling factor values [0-0.8]. In blue, the correlation between empirical and simulated PLV. In gray, the mean frequency of oscillation. Vertical dashed line corresponds to the selected working point.

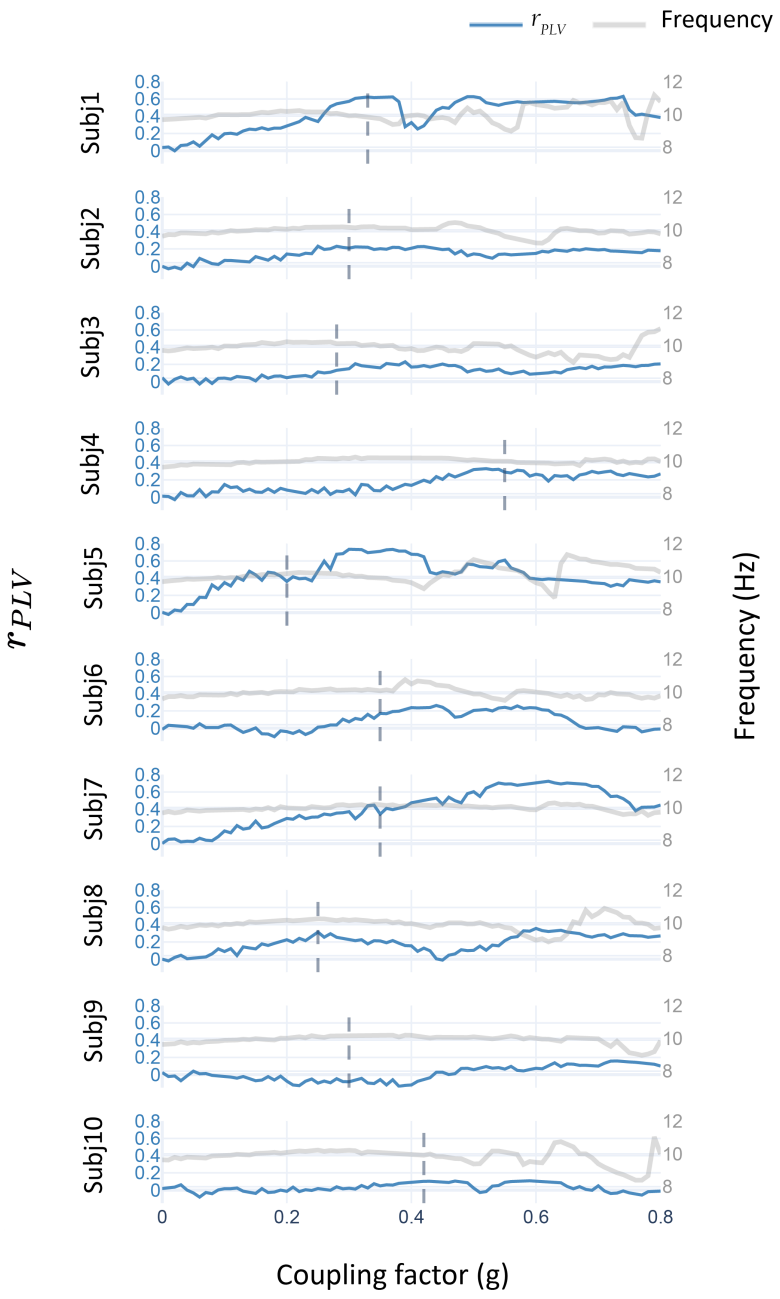


Figure SM3. Results of the SNN simulations per node included in the CBPT cluster of alpha power rise regions. Showing the oscillatory frequency of each node before and during stimulation / pre and post stimulation when $\Lambda = 35$.

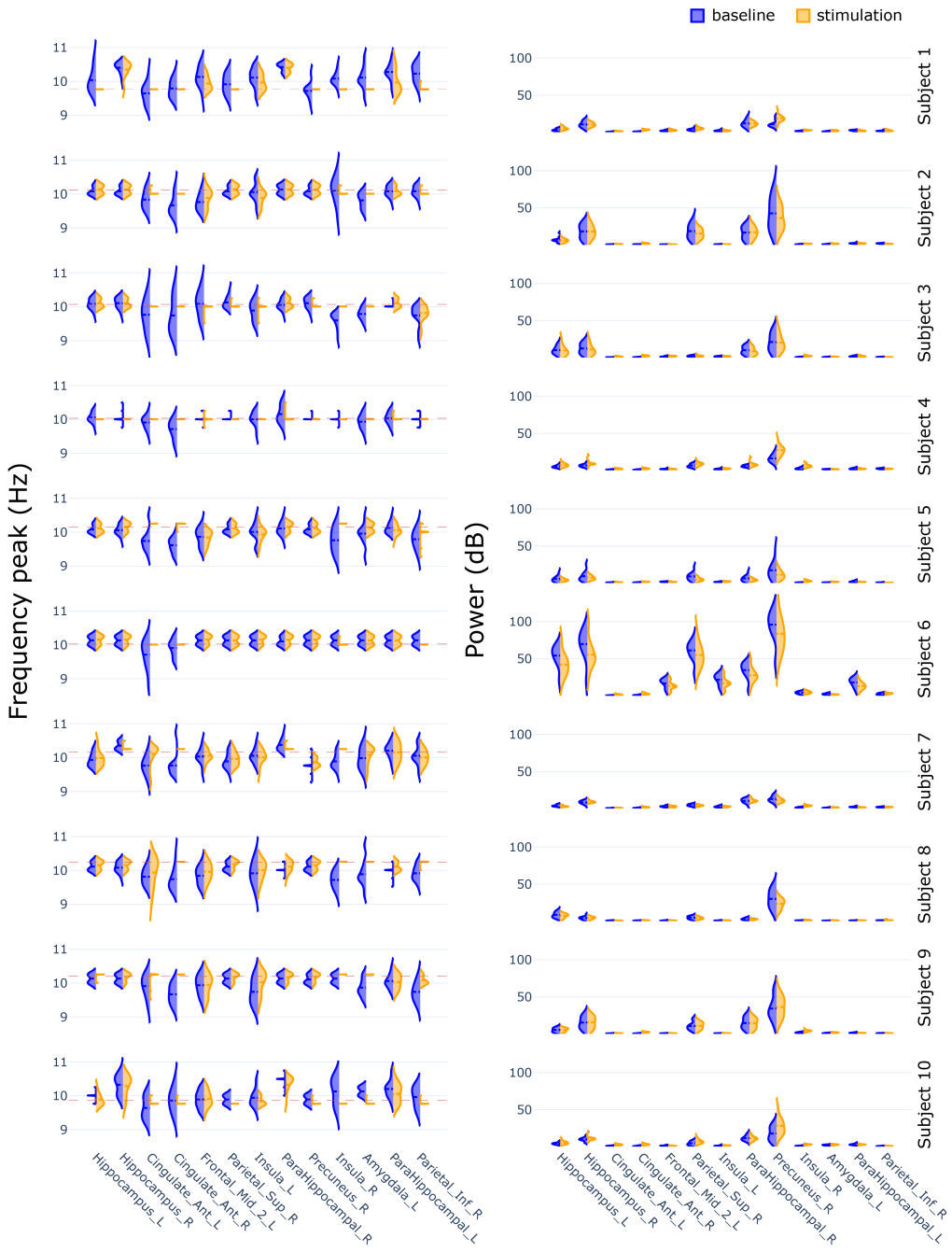


Figure SM4. Simulated LFP timeseries for subject one. Vertical dashed line separates baseline (left) and stimulation stages (right).

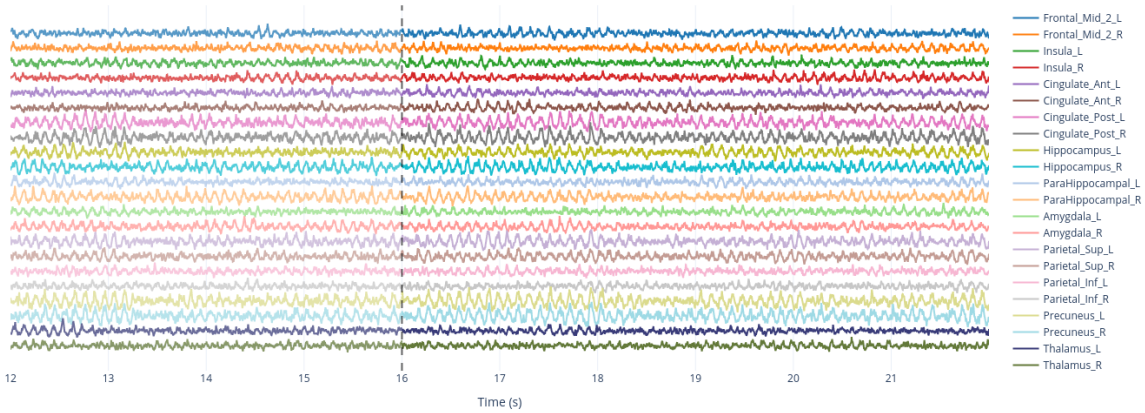


Figure SM5. Single node dynamics. Left panel represents the frequency-current curve, where to control the intensity of the incoming current we used the rate of the Poissonian spike train that every neuron receives. Right panels show different LFPs for different values of the rate.

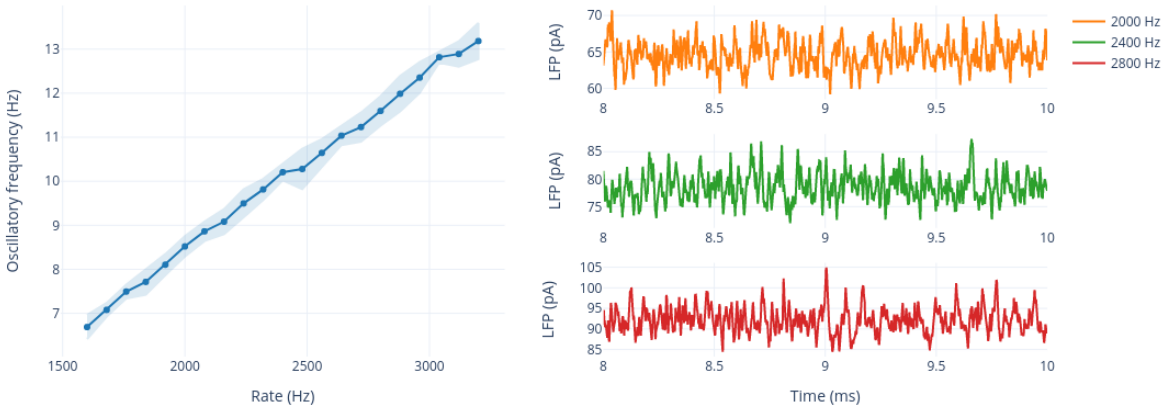


Figure SM6. Predictors of alpha lowering in simulations. Scatter plots showing the average increase in alpha power in the simulated regions that lowered the power from baseline as a function of the variables included in the multiple linear regression model. In size, the mean node strength of the region, and in colour the normal component of the electric field. PLV mean was the only significant predictor of alpha power lowering.

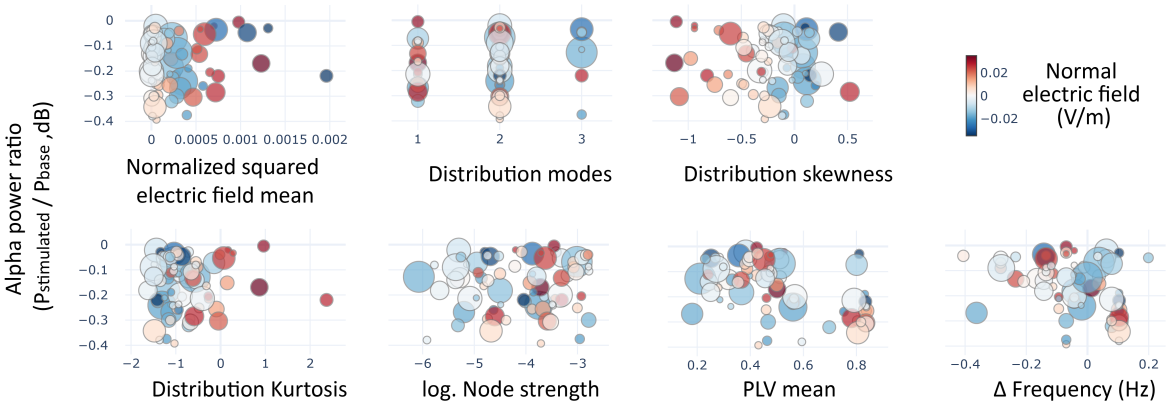


Figure SM7. Frequency peak and its power in the Precuneus_R region of the network model when only this region is stimulated (left) and when the stimulation is over the whole network (right). This is an example of how the inter-regional synaptic transmission plays a role in the alpha rise power, since the direct stimulation does not produce an effect.

